Entergy

Entergy Operations, Inc.
1340 Echelon Parkway
Jackson, MS 39213-8298
Tel 601 368 5758

Michael A. Krupa
Director
Nuclear Safety & Licensing

CNRO-2003-00042

September 18, 2003

U.S. Nuclear Regulatory Commission
ATTN: Document Control Desk
Washington, DC 20555-0001

SUBJECT: Entergy Operations, Inc.
Relaxation Request to NRC Order EA-03-009 for In-Core Instrumentation Nozzles

Waterford Steam Electric Station, Unit 3
Docket No. 50-382
License No. NPF-38

REFERENCE:
1. NRC Order EA-03-009, "Issuance of Order Establishing Interim Inspection Requirements for Reactor Pressure Vessel Heads at Pressurized Water Reactors," dated February 11, 2003
2. Entergy Operations, Inc. Letter CNRO-2003-00033 to the NRC, "Relaxation Request to NRC Order EA 03-009," dated August 27, 2003

Pursuant to Section IV.F of NRC Order EA-03-009, (Reference #1), Entergy Operations, Inc. (Entergy) requests relaxation from Section IV.C(1)(b) of the Order for Waterford Steam Electric Station, Unit 3 (Waterford 3). Specifically, Section IV.C(1)(b) of the Order requires either an ultrasonic test (UT) or a wetted surface examination using eddy current testing (ECT) or dye penetrant testing (PT) be performed on the total population of reactor pressure vessel (RPV) head penetration nozzles. Compliance with Section IV.C(1)(b) does not allow the use of a combination of inspection techniques; therefore, Entergy is requesting that a combination of techniques and supplementary analysis be allowed for determining the condition of the In-Core Instrumentation (ICI) nozzles at Waterford 3. Enclosure 1 of this letter contains Waterford 3 Relaxation Request #3. Enclosure 2 contains a copy of the fracture mechanics analysis report (Engineering Report M-EP-2003-005, Rev. 0) that supports this request.

Engineering Report M-EP-2003-005, Rev. 0 utilizes information pertaining to material properties and analytical methods provided by Dominion Engineering, Inc. via Dominion letter L-4162-00-2, "Material Properties and Modeling Methods Used in ANO Unit 2 Welding Residual Stress Analysis." Entergy provided this letter to the NRC staff via Reference #2.

A101

This letter contains new commitments as identified in Enclosure 3.

Should you have any questions, please contact Guy Davant at (601) 368-5756.

Sincerely,

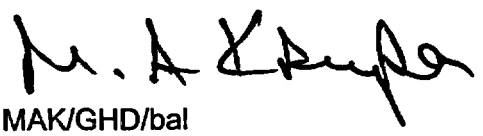

MAK/GHD/bal

Enclosure:
1. Waterford Steam Electric Station, Unit 3 Relaxation Request #3
2. Engineering Report M-EP-2003-005, Rev. 0
3. Licensee-Identified Commitments

cc: Mr. W. A. Eaton (ECH)
Mr. J. E. Venable (W3)
Mr. G. A. Williams (ECH)

Mr. T. P. Gwynn, NRC Region IV Regional Administrator
Mr. M. C. Hay, NRC Senior Resident Inspector (W3)
Mr. N. Kalyanam, NRR Project Manager (W3)

ENCLOSURE 1

CNRO-2003-00042

WATERFORD STEAM ELECTRIC STATION, UNIT 3
RELAXATION REQUEST #3

ENTERGY OPERATIONS, INC.
WATERFORD STEAM ELECTRIC STATION, UNIT 3

RELAXATION REQUEST #3 TO NRC ORDER EA-03-009

I. ASME COMPONENTS AFFECTED

Waterford Steam Electric Station, Unit 3 (Waterford 3) has one hundred-two (102) ASME Class 1 reactor pressure vessel (RPV) head penetration nozzles comprised of ninety-one (91) Control Element Drive Mechanism (CEDM) nozzles, ten (10) In-Core Instrument (ICI) nozzles, and one (1) vent line nozzle. This request pertains to the ICI nozzles only. The locations of RPV head penetrations are provided in Figure 1.

II. REQUIREMENTS

The NRC issued Order EA-03-009 (the Order) that modified the current licenses at nuclear facilities utilizing pressurized water reactors (PWRs), which includes Waterford 3. The NRC Order establishes inspection requirements for RPV head penetration nozzles. In accordance with Section IV.A of NRC Order EA-03-009, the Waterford 3 susceptibility category is "high" based on a calculated value of 16.9 effective degradation years (EDY) at the beginning of the upcoming fall refueling outage.

Section IV.C of the Order states in part:

"All Licensees shall perform inspections of the RPV head using the following techniques and frequencies:

(1) For those plants in the High category, RPV head and head penetration nozzle inspections shall be performed using the following techniques every refueling outage.

   (a) Bare metal visual examination of 100% of the RPV head surface (including 360° around each RPV head penetration nozzle), AND

   (b) Either:

      (i) Ultrasonic testing of each RPV head penetration nozzle (i.e., nozzle base material) from two (2) inches above the J-groove weld to the bottom of the nozzle and an assessment to determine if leakage has occurred into the interference fit zone, OR

      (ii) Eddy current testing or dye penetrant testing of the wetted surface of each J-groove weld and RPV head penetration nozzle base material to at least two (2) inches above the J-groove weld."

III. REASON FOR REQUEST

Section IV.F of the Order states:

"Licensees proposing to deviate from the requirements of this Order shall seek relaxation of this Order pursuant to the procedure specified below. The Director, Office of Nuclear Reactor Regulation, may, in writing, relax or rescind any of the above conditions upon demonstration by the Licensee of good cause. A request for relaxation regarding inspection of specific nozzles shall also address the following criteria:

(1) The proposed alternative(s) for inspection of specific nozzles will provide an acceptable level of quality and safety, or

(2) Compliance with this Order for specific nozzles would result in hardship or unusual difficulty without a compensating increase in the level of quality and safety.

"Requests for relaxation associated with specific penetration nozzles will be evaluated by the NRC staff using its procedure for evaluating proposed alternatives to the ASME Code in accordance with 10 CFR 50.55a(a)(3)."

Pursuant to Section IV.F(1) of the Order, Entergy Operations, Inc. (Entergy) requests relaxation from the requirements of Section IV.C(1)(b). Entergy plans to inspect RPV head ICI penetration nozzles at Waterford 3 using the ultrasonic testing (UT) method in accordance with Section IV.C(1)(b)(i) of the Order to the maximum extent possible. However, limitations due to nozzle configuration cause reduced UT inspection coverage of each nozzle. In addition, the design of the UT inspection probe introduces a limitation impacting the amount of coverage that can be obtained. These limitations are discussed below.

A. Counterbore Blind Zone

ICI nozzles are manufactured with a counterbore as shown in Figure 2. Due to lift-off of the UT transducers at the counterbore, a UT blind zone exists at the upper hillside location (180° azimuth) of each ICI nozzle. Measuring approximately 0.88 inch in axial length, the bottom of the blind zone is located 0.67 inch above the top of the J-groove weld. Centered at the upper hillside location of each nozzle, the counterbore blind zone has a circumferential extent of 135°. See Figure 6 for additional details.

It should also be noted that the blind zone associated with the counterbore does not exist at any other azimuthal locations along the circumference of the ICI nozzle within the 2-inch area above the J-groove weld. Due to the RPV head angle at the ICI locations, the counterbore is significantly closer to the J-groove weld on the upper hillside of the nozzle than on the lower hillside. Specifically, the distance from the top of the J-groove weld to the bottom of the counterbore on the lower hillside of the ICI nozzle is 9.836 inches as shown in Figure 7.

B. Blind Zone at Nozzle Bottom End

A blind zone exists along the bottom of each ICI nozzle and varies from approximately 0.20 inch to 0.70 inch. This blind zone occurs due to loss of couplant as the transducers traverse across the bottom end of the nozzle. This problem is further compounded by the configuration of the ICI nozzle bottom end which is cut to match the contour of the RPV head. See Figures 3, 4, and 5 for additional information.

IV. PROPOSED ALTERNATIVE AND BASIS FOR USE

Paragraph IV.C(1)(b)(i) of the Order requires that the UT inspection of each RPV head penetration nozzle encompass "from two (2) inches above the J-groove weld to the bottom of the nozzle." Due to the reasons stated above, Entergy requests relaxation from this requirement for Waterford 3 ICI nozzles and proposes a three-step alternative, which involves the use of analysis, UT examination, and surface examination techniques, as described below.

A. Proposed Alternative

1. Analysis

An analysis has been performed to ensure that an unidentified surface crack in the counterbore blind zone will extend along the length into an inspectable region at least one operating cycle prior to growing through-wall. The analysis, based on design information and actual UT data from a sister plant, is discussed in further detail in Section IV.B.1 below and is fully documented in Engineering Report M-EP-2003-005, Rev. 0 (Enclosure 2). Based on this analysis, no examination of the counterbore region is required.

2. UT Examination

The ID of each ICI nozzle (i.e., nozzle base material) shall be ultrasonically examined in accordance with Section IV.C(1)(b)(i) of the Order except as follows:

a) For the area of the counterbore blind zone that falls within two (2) inches above the J-groove weld on the upper hillside; and

b) For the area of the nozzle end blind zone.

In addition to the UT examination, an assessment to determine if leakage has occurred into the interference fit zone will be performed, as currently specified in Section IV.C(1)(b)(i) of the Order.

3. Augmented Inspection Plan for ICI Nozzle Bottom End

Because meaningful UT data cannot be collected at the bottom end of the ICI nozzle, Entergy will augment the UT inspection with a surface examination of the nozzle ID, OD, and weld area that falls within the blind zone at the nozzle bottom end. As previously mentioned, the nozzle end blind zone varies in length from 0.20 inch to 0.70 inch depending on probe location (see Figures 3, 4 and 5).

This augmented inspection plan will be performed on the ICI nozzles using the manual liquid penetrant testing (PT) examination method as the primary technique. Because the PT examination method cannot distinguish acceptable fabrication discontinuities from primary water stress corrosion cracking (PWSCC), PT indications are conservatively assumed to be PWSCC. Under these conditions, PT indications will be investigated by either:

(i) Supplemental inspection using the eddy current testing (ECT) examination method; or

(ii) Grinding followed by additional PT examinations.

4. Analysis Verification, Reanalysis, and Augmented Inspections of the Counterbore Blind Zone

As discussed in Section IV.B.1.a), the analysis is based on a detailed review of applicable Waterford 3 design drawings and actual UT data from a sister plant. Therefore, Entergy will take the following actions:

a) Entergy will inspect by UT each ICI nozzle to determine its actual as-built configuration and determine whether or not the configuration is bounded by the analysis.

b) For conditions determined not bounded by the current analysis, Entergy will perform supplemental analysis. The analysis must ensure that an unidentified surface crack in the counterbore blind zone will extend along the length into an inspectable region at least one operating cycle prior to growing through-wall.

(i) If the analysis meets the acceptance criterion stated in Section IV.A.4.b), no further actions will be taken.

(ii) If the analysis does not meet the acceptance criterion stated in Section IV.A.4.b), that portion of the counterbore blind zone region that falls within the 2-inch area above the J-groove weld of the ICI nozzles will be subjected to augmented inspection. The augmented inspection will utilize the PT examination method.

Entergy will include the following information in the 60-day report submitted to the NRC in accordance with Section IV.E of the Order:

- Results of the UT inspections
- Results of any required reanalysis
- Results of any required augmented inspections

B. Basis for Use

1. Analysis

The extent of the proposed alternative is established by an engineering evaluation comprised of a finite element stress analysis and fracture mechanics model of the ICI nozzle counterbore blind zone. The purpose of this engineering evaluation is to ensure that an unidentified surface crack in the counterbore blind zone will extend along the length, into an inspectable region, at least one operating cycle prior to growing through the thickness.

Only an ID fracture mechanics analysis is required for this justification. This is due to the fact that the OD surface of the nozzle is not in a reactor coolant environment which promotes PWSCC. The UT exam discussed in Section IV.A.1 confirms there is no OD crack on the nozzle creating a leak path, and the triple point examination confirms there is no leak path though the weld. Additionally, the leak assessment examination above the weld confirms there is no leak through the weld butter. Hence, PWSCC can only be initiated on the ID surface of the counterbore blind zone. Both circumferential and axial cracks were evaluated; however, detailed fracture mechanics of the circumferential crack was not required because the ID and ¼ thickness axial stress is very low tensile (< 10 ksi) or predominately compressive in the 135° arc being evaluated. Therefore, no potential exists to initiate a crack in this area.

The finite element-based stress analysis and the fracture mechanics evaluation are described below. For additional details pertaining to the engineering evaluation and its conclusions, see Engineering Report M-EP-2003-005, Rev. 0 (Enclosure 2).

a) Stress Analysis

A finite element-based stress analysis representing the ten (10) Waterford 3 ICI nozzle penetrations was performed by Dominion Engineering, Inc. (Dominion) using best estimates of as-built geometries. Since no volumetric inspections of the RPV head penetrations have been performed at Waterford 3, the nozzle dimensions were determined by a detailed review of applicable Waterford 3 design drawings and actual UT data from a sister plant. Like Waterford 3, the sister plant is of similar Combustion Engineering (CE) design rated at 3410 MWt.

UT data from the sister plant indicated that the nozzle welds are generally oversized compared to design. The finite element analysis model was adjusted for the larger weld size. The counterbore was not explicitly

modeled; rather, the elements were angled and tapered to transition from the 4.750-inch ID below the counterbore to the 4.625-inch ID above the counterbore. The actual counterbore is 0.25 inch high with a 1-to-4 (depth-to-length) taper; this transition precludes the need to evaluate stress concentrations such as required per ASME Section III, Subsection NB-3680 for transitions with less than a 1-to-3 transition.

Consideration of a Circumferential Crack in the Counterbore Blind Zone

Entergy considered a circumferential crack located on the ID surface, spanning the full 135° circumferential extent of the blind zone (see Figure 6). A circumferential crack, if propagated through-wall, could potentially lead to ejection of the associated nozzle. For this circumferential crack growth to occur, both the PWSCC environment and a conducive tensile axial stress field must exist. The Dominion axial stress finite element analysis data were reviewed for locations at the upper hillside and those angles spanning 67.5° on either side of the 180° azimuth (112.5° and 247.5°) that would encompass the circumferential extent of the counterbore blind zone.

From previous fracture mechanics evaluations for the CEDM nozzles, it was shown that no crack growth will occur for an applied hoop stress of 10 ksi; that is, the resulting applied stress intensity factor is below the threshold value of 8.19 ksi $\sqrt{in}$ needed for crack growth.

The stresses at the ID and at the 25% through-wall location, covering a 135° circumferential span around the ICI nozzle, are predominantly compressive. Hence, the initiation of a circumferential crack in the counterbore blind zone is precluded and presents no safety significance by not inspecting this region.

b) Fracture Mechanics Evaluation

Safety analyses performed by the EPRI Materials Reliability Program (MRP) have demonstrated that axial cracks in the nozzle tube material do not pose a challenge to the structural integrity of the nozzle. Axial cracks, if allowed to exist undetected for sufficient periods of time can produce a primary boundary leak that can cause damage to the reactor vessel head (carbon steel) and create a conducive environment for initiating and propagating OD circumferential cracks. These conditions challenge the pressure boundary; hence, critical importance is paid to proper periodic inspection and to the disposition of cracks that may be discovered. Therefore, proper analyses are essential to ascertain the nature of axial crack growth such that appropriate determination can be accomplished.

Several crack sizes were evaluated in the counterbore blind zone on the upper hillside. Crack aspect ratios typical of ASME Section XI (6-to-1 and 10-to-1 length-to-depth) and another aspect ratio emphasizing deep flaws (4-to-1) were evaluated to maximize through-wall growth while accommodating growth along the length of the ICI nozzle. These evaluations also considered a case in which the half-length of the crack

was less than the remaining length needed to grow to the end of the blind zone. Summaries of crack depths and lengths used to evaluate the counterbore blind zone are presented in the table below.

Crack Case ID	Description	Crack Depth. (inch)	Crack Length (inch)
1	Aspect ratio of 6-to-1 with depth initially 25% through-wall	0.1	0.6
2	Aspect ratio of 10-to-1 with an initial length of 0.4 inch	0.04	0.4
3	Aspect ratio of 4-to-1 with depth initially 25% through-wall	0.1	0.4
4	Aspect ratio of 6-to-1 with the crack spanning the length of the blind zone	0.147	0.88

In the PWSCC crack growth evaluation, the acceptability of the crack is determined by its extension outside the counterbore blind zone to a detectable length in greater than one operating cycle prior to growing through-wall. The minimum detectable crack was 0.08 inch with flaws between 0.08 inch and 0.16 inch detected based on EPRI demonstrations. For conservatism, the detectability threshold was set at 0.16 inch. That is, a crack contained within the counterbore blind zone must propagate along the length of the nozzle a distance measured from the tip of the crack to the edge of the blind zone plus an axial distance of 0.16 inch to ensure proper detection. The results of the crack growth evaluations are presented in the table below.

Crack Case ID	Propagation Length (inch)	Time to Reach Propagation Length (years)	Time to Grow Through-Wall (years)
1	0.3	5.59	7.22
2	0.4	36.68	> 40
3	0.4	10.07	11.66
4	0.16	2.02	3.68

A review of the stress output shows the through thickness and axial distribution of hoop stresses on the lower hillside (0° azimuth) of the nozzle to be higher than that of the upper hillside for the same relative distance above the J-groove weld. That is, for the length of the nozzle 0.67 inch above the top of the weld on the lower hillside, plus a region 0.88 inch beyond that (equivalent to the span of the counterbore blind zone on the upper hillside), the stress distribution was generally higher. However, the bottom of the counterbore on the lower hillside is 9.836 inches above the top of the J-groove weld and is, therefore, not subject to the requirements of the Order. Because of the higher stress field, it is reasonable to presume that under equivalent conditions, a crack could initiate in this equivalent lower hillside area more readily than on the upper hillside. However, this region is inspectable via UT; thus, the most susceptible

location based on stresses is addressed by the current inspection coverage.

c) Analysis Conclusions

The engineering evaluation supports the following conclusions:

(i) The upper hillside (180° azimuth) of the ICI nozzle above the top of the J-groove weld possesses the highest hoop stresses in the vicinity of the counterbore for which a UT blind zone exists.

(ii) The conservatisms used in the analysis (pressure applied to crack faces and high crack length-to-depth aspect ratio) provide assurance that an undetected crack in the counterbore blind zone on the upper hillside will extend along the length of the nozzle into an inspectable region at least one operating cycle prior to growing through-wall.

(iii) The area above the J-groove weld on the lower hillside of the ICI nozzle is in a higher stress field than the area on the upper hillside. Because of this, the lower hillside area is more susceptible to crack initiation than the upper hillside. However, this area is inspected by UT.

(iv) The ID surface crack on the upper hillside either did not show any potential for crack growth, or the growth in the axial direction reached a detectable area of the nozzle in at least one operating cycle prior to the crack growing through-wall. Hence, an ID surface crack in a region above the J-groove weld on the upper hillside is not significant in that it does not affect nozzle integrity.

(v) No potential exists for an ID circumferential crack to be located in the counterbore blind zone due to low tensile stress (> 10 ksi) and the predominant compressive axial stress field spanning 67.5° on either side of the upper hillside of the ICI nozzle.

This analysis incorporates a crack-growth formula different from that described in Footnote 1 of the Order, as provided in EPRI Report MRP-55. Entergy is aware that the NRC staff has not yet completed a final assessment regarding the acceptability of the EPRI report. If the NRC staff finds that the crack-growth formula in MRP-55 is unacceptable, Entergy shall revise its analysis that justifies relaxation of the Order within 30 days after the NRC informs Entergy of an NRC-approved crack-growth formula. If Entergy's revised analysis shows that the crack growth acceptance criteria are exceeded prior to the end of Operating Cycle 13 (following the upcoming refueling outage), Entergy will, within 72 hours, submit to the NRC written justification for continued operation. If the revised analysis shows that the crack growth acceptance criteria are exceeded during the subsequent operating cycle, Entergy shall, within 30 days, submit the revised analysis for NRC review. If the revised analysis shows that the crack growth acceptance criteria are not exceeded during either Operating Cycle 13 or the subsequent operating cycle, Entergy shall, within 30 days, submit a letter to the NRC confirming that its analysis has been revised. Any future crack-growth analyses performed for Operating Cycle 13 and future

cycles for RPV head penetrations will be based on an NRC-acceptable crack growth rate formula.

2. UT Examination

The UT inspection probe to be used to inspect the Waterford 3 ICI nozzles consists of seven (7) individual transducers. The configuration of the probe has been optimized for maximum coverage. UT inspection of ICI nozzles will be performed using a combination of time-of-flight diffraction (TOFD) and standard 0° pulse-echo techniques. The TOFD approach utilizes two pairs of 0.250-inch diameter, 55° refracted-longitudinal wave transducers aimed at each other. One of the transducers transmits sound into the inspection volume while the other receives the reflected and diffracted signals as they interact with the material. There will be one TOFD pair scanning in the axial direction of the penetration nozzle tube and one TOFD pair scanning in the circumferential direction of the tube. The TOFD technique is primarily used to detect and characterize planar-type defects within the full volume of the tube.

The standard 0° pulse-echo ultrasonic approach utilizes one 0.250-inch diameter straight beam transducer. The 0° technique is used to:

- Plot the penetration nozzle OD location and J-groove weld location,
- Locate and size any laminar-type defects that may be encountered, and
- Monitor the back-wall signal response to detect leakage that may occur in the interference regions of the RPV head penetration.

The UT inspection procedures and techniques to be utilized at Waterford 3 have been satisfactorily demonstrated under the EPRI Materials Reliability Program (MRP) Inspection Demonstration Program.

3. Augmented Inspection Plan of the ICI Nozzle End

Augmenting UT examination of the nozzle base material with surface examination ensures the ICI nozzle is adequately examined to determine its condition. The augmented inspection plan will only be used for those portions of the nozzles that could not be inspected by UT or excluded by analysis.

The augmented inspections will be performed using the PT examination method as the primary technique. Entergy believes the use of PT to augment UT is acceptable for ensuring that the required areas not excluded by analysis are inspected. The Order recognizes and allows the use of PT as acceptable for evaluating the condition of nozzle surfaces. Augmenting the UT examination of the nozzle base material with PT ensures the nozzle is adequately examined to determine its condition.

As discussed in Section IV.A.3 above, Entergy may use ECT to investigate indications identified by PT. ECT is also an acceptable technique for evaluating such indications. As with PT, the Order recognizes and allows the use of ECT as acceptable for evaluating the condition of nozzles and associated J-groove welds.

4. Analysis Verification, Reanalysis, and Augmented Inspections of the Counterbore Blind Zone

As addressed in Section IV.A.4 above, the stress analysis employed in the engineering evaluation utilized nozzle configuration information gleaned from design drawings and UT inspection data from a sister plant. Using UT inspection results from the upcoming fall 2003 refueling outage, Entergy will evaluate the actual as-built nozzle configurations to that assumed in the analysis. By determining each nozzle's configuration, Entergy validates the results of the analysis.

In the unlikely event a nozzle configuration is not bounded by the analysis, allowing Entergy to re-analyze the nozzle using actual configuration data and the methodology described in Engineering Report M-EP-2003-005 (Enclosure 2) will result in minimal impact on outage schedule and keep radiation exposure as low as reasonably achievable.

If a nozzle configuration does not meet the acceptance criterion of the supplemental analysis [see Section IV.A.4.b) above], Entergy will perform augmented inspections using the manual PT technique on that portion of the counterbore blind zone that falls within the 2-inch area above the J-groove weld. Entergy believes the use of PT to augment UT is acceptable for ensuring that the required areas not justified by analysis are inspected. The Order recognizes and allows the use of either technique as acceptable for evaluating the condition of nozzle surfaces. On this basis, Entergy concludes using this examination approach provides an equivalent level of quality and safety to the options allowed by the Order.

V. CONCLUSION

Section IV.F of NRC Order EA-03-009 states:

"Licensees proposing to deviate from the requirements of this Order shall seek relaxation of this Order pursuant to the procedure specified below. The Director, Office of Nuclear Reactor Regulation, may, in writing, relax or rescind any of the above conditions upon demonstration by the Licensee of good cause. A request for relaxation regarding inspection of specific nozzles shall also address the following criteria:

(1) The proposed alternative(s) for inspection of specific nozzles will provide an acceptable level of quality and safety, or

(2) Compliance with this Order for specific nozzles would result in hardship or unusual difficulty without a compensating increase in the level of quality and safety."

Section IV.C(1)(b) of the Order establishes a minimum set of RPV head penetration nozzle inspection requirements to identify the presence of cracks in penetration nozzles that could lead to leakage of reactor coolant and wastage of RPV head material.

Entergy believes the proposed alternative, described in Section IV, provides an acceptable level of quality and safety by utilizing inspections and supplemental analysis to determine the condition of the Waterford 3 ICI nozzles. The technical basis for the supplemental analysis of the proposed alternative is documented in Engineering Report M-EP-2003-005, Rev. 0, which is contained in Enclosure 2 of this letter. Therefore, Entergy requests that the proposed alternative be authorized pursuant to Section IV.F of the Order.

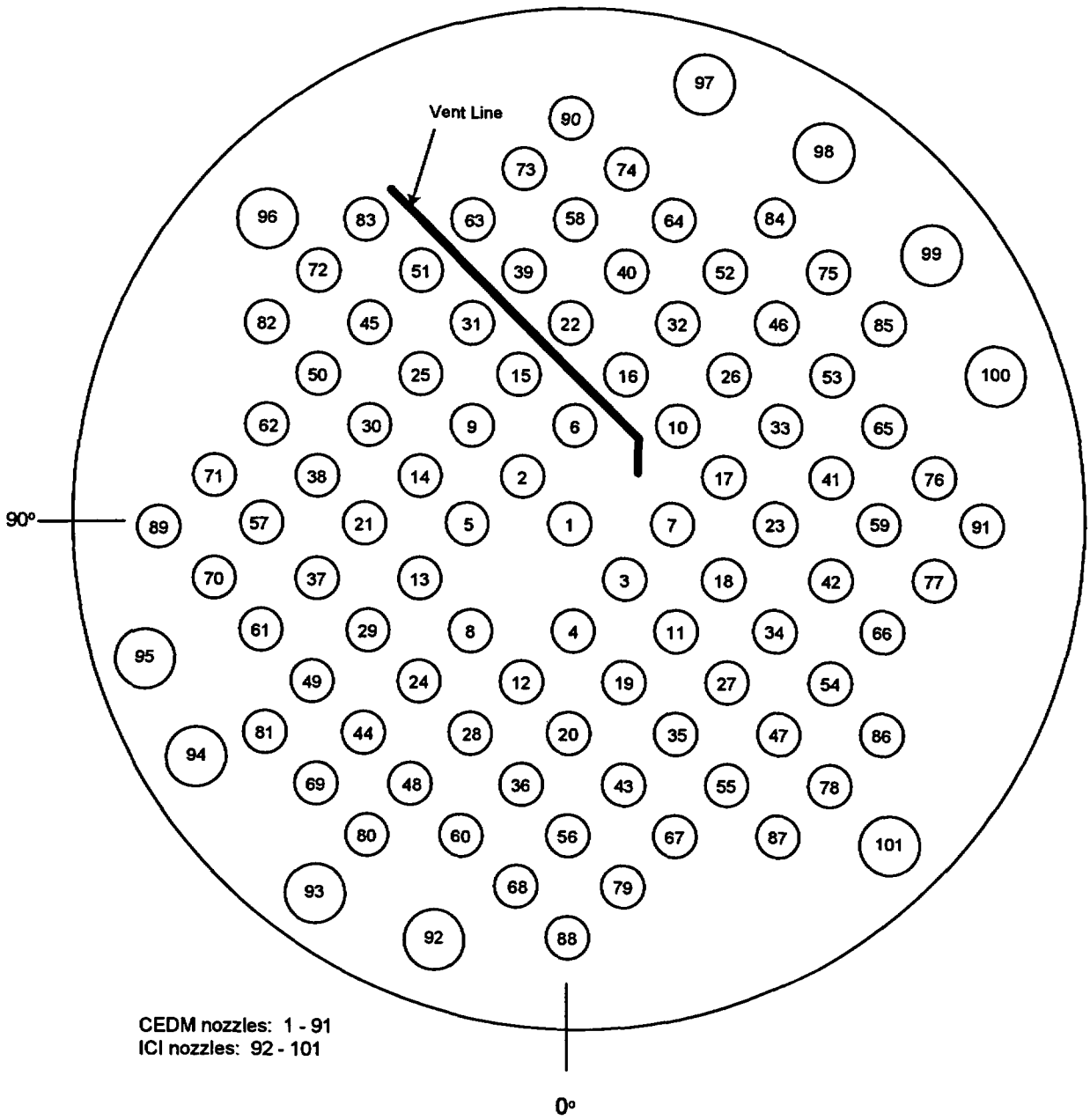

FIGURE 1
Penetration Locations in the Waterford 3 RPV Head

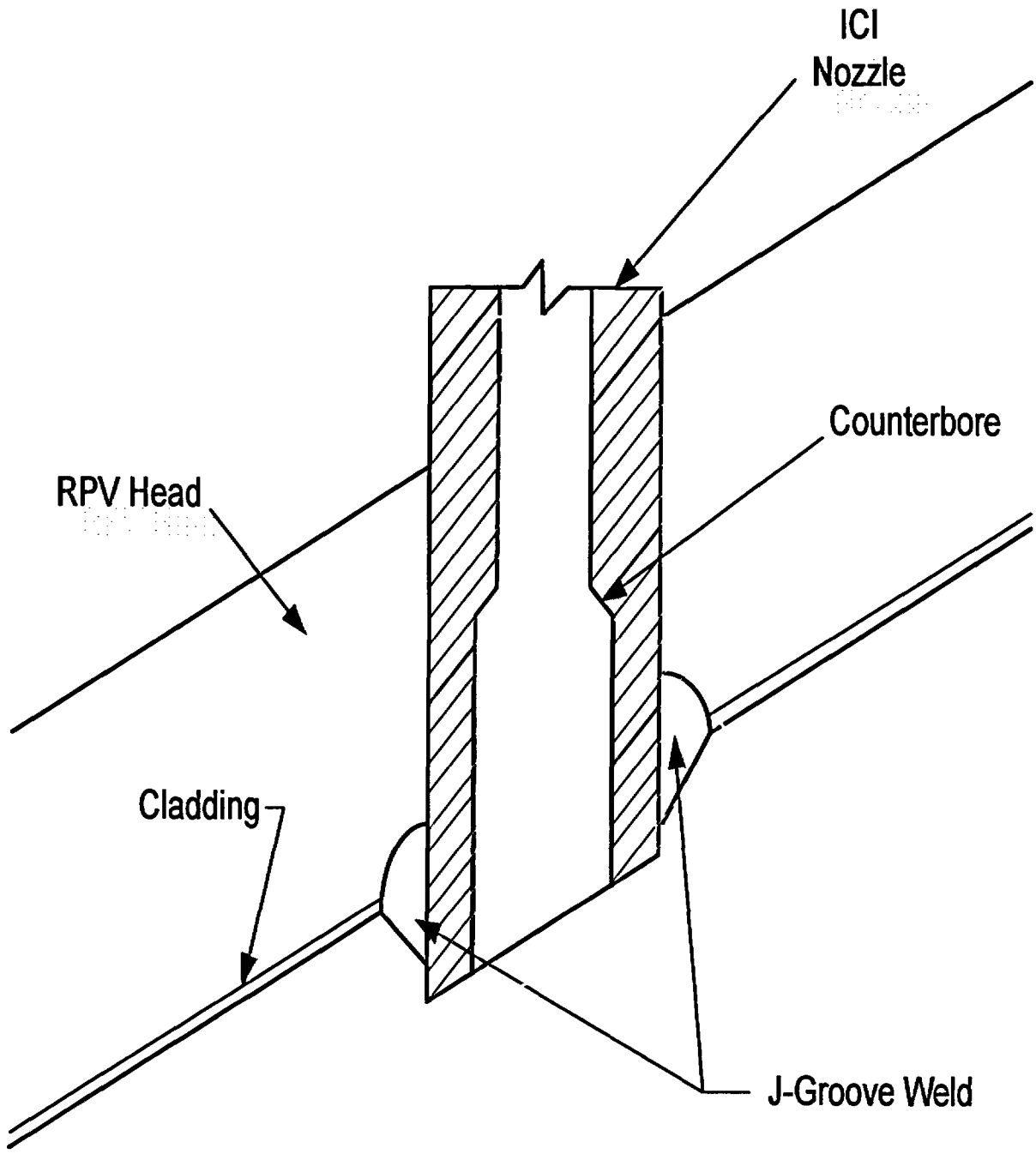

FIGURE 2
ICI NOZZLE CONFIGURATION

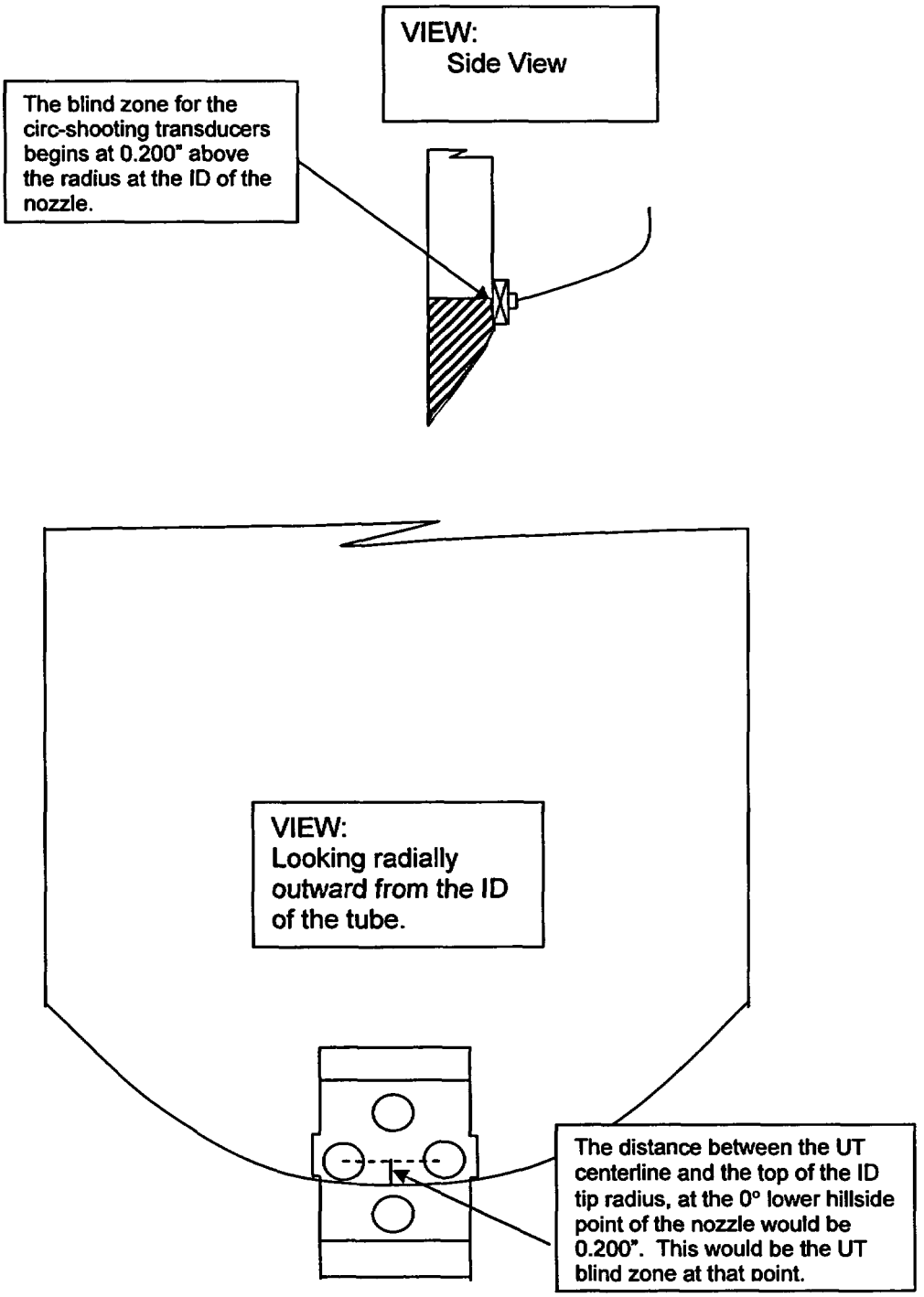

FIGURE 3
UT INSPECTION PROBE
END OF NOZZLE – LOWER HILLSIDE POSITION

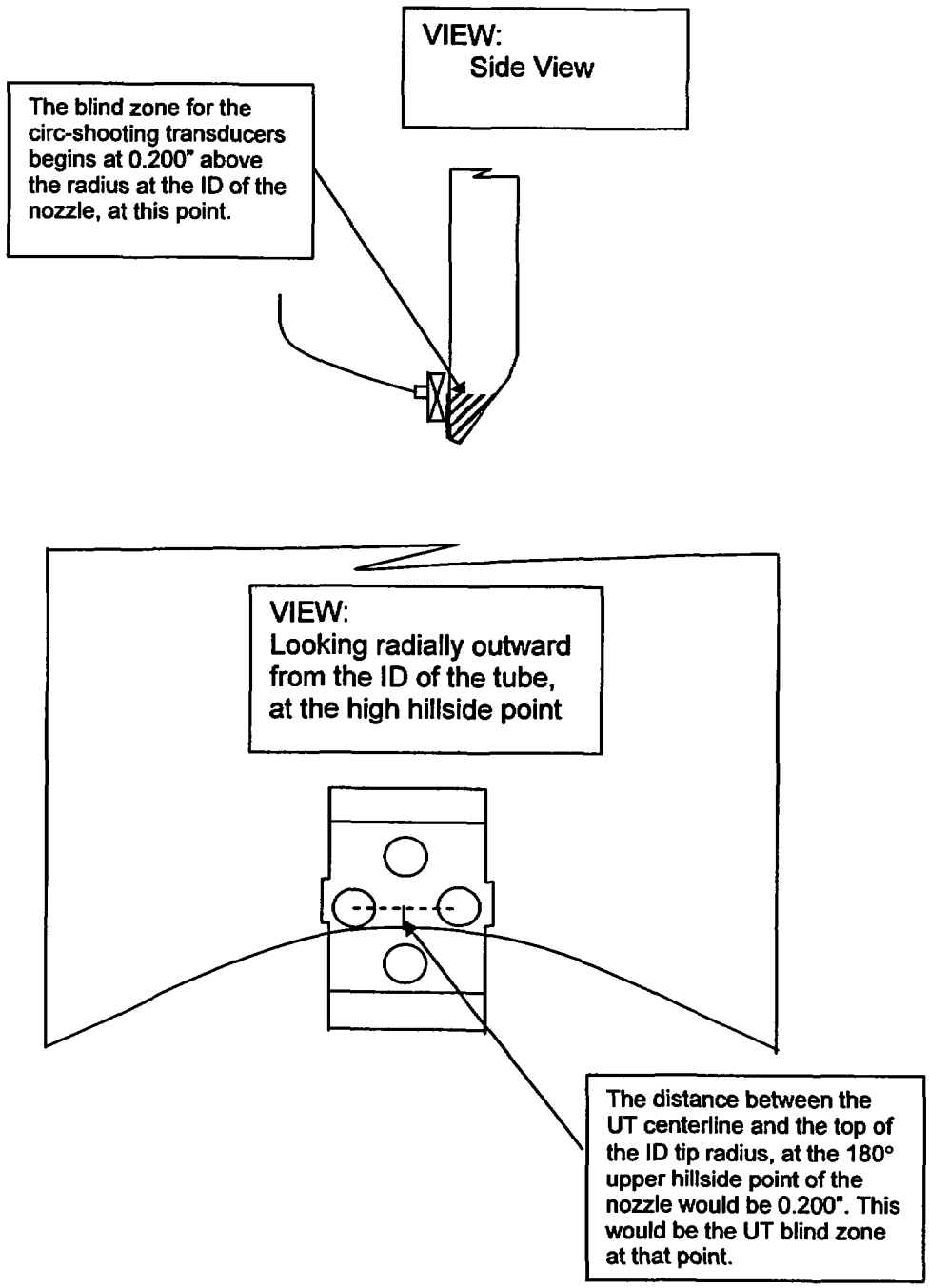

FIGURE 4
UT INSPECTION PROBE
END OF NOZZLE- UPPER HILLSIDE POSITION

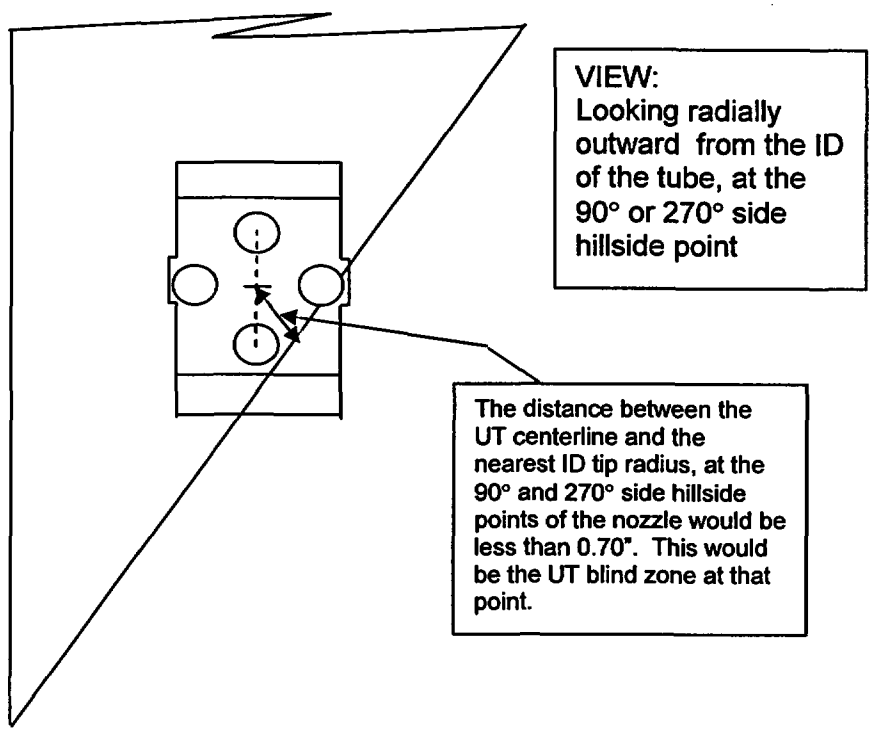

FIGURE 5
UT INSPECTION PROBE
END OF NOZZLE – SIDE VIEW @ 90° and 270°

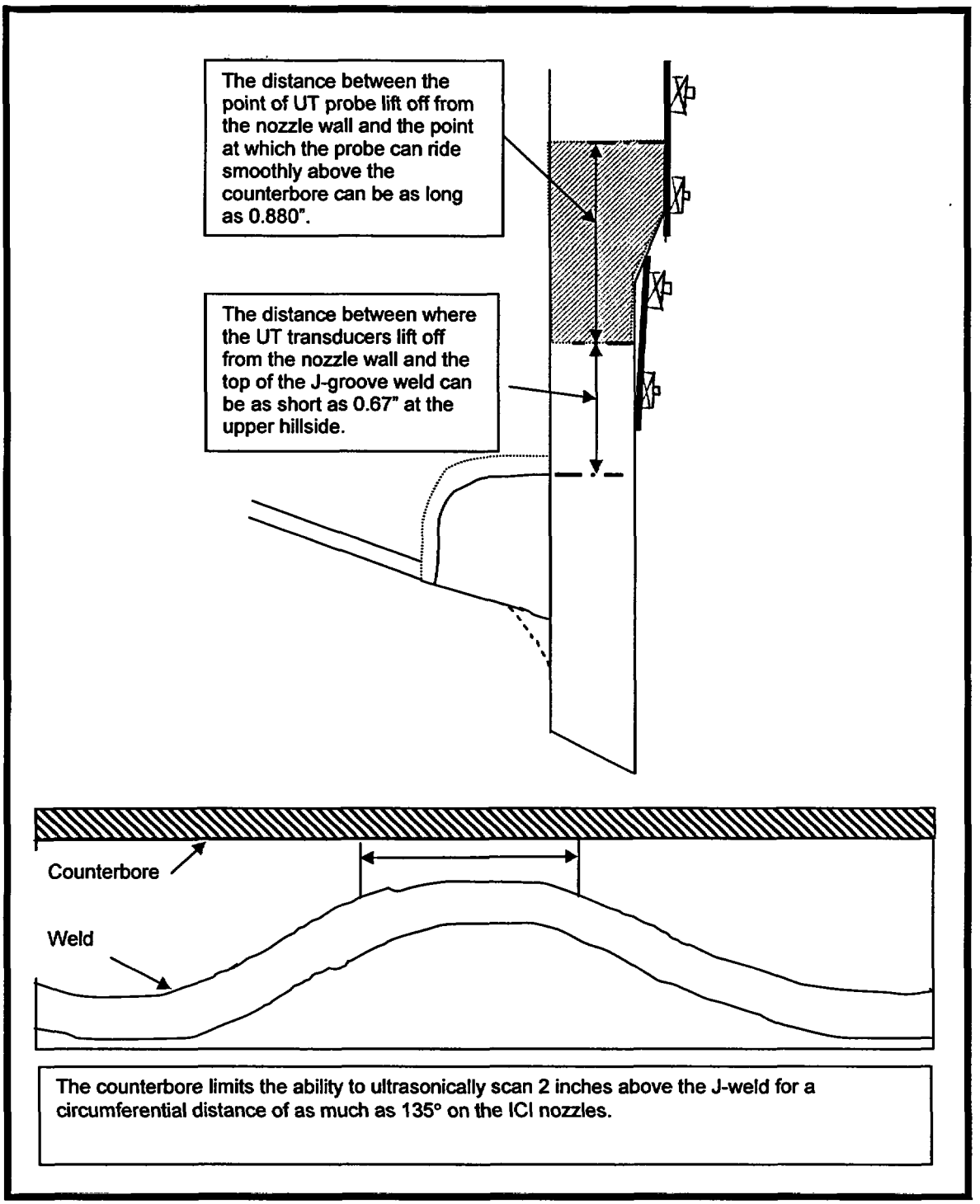

FIGURE 6
COUNTERBORE – UPPER HILLSIDE POSITION

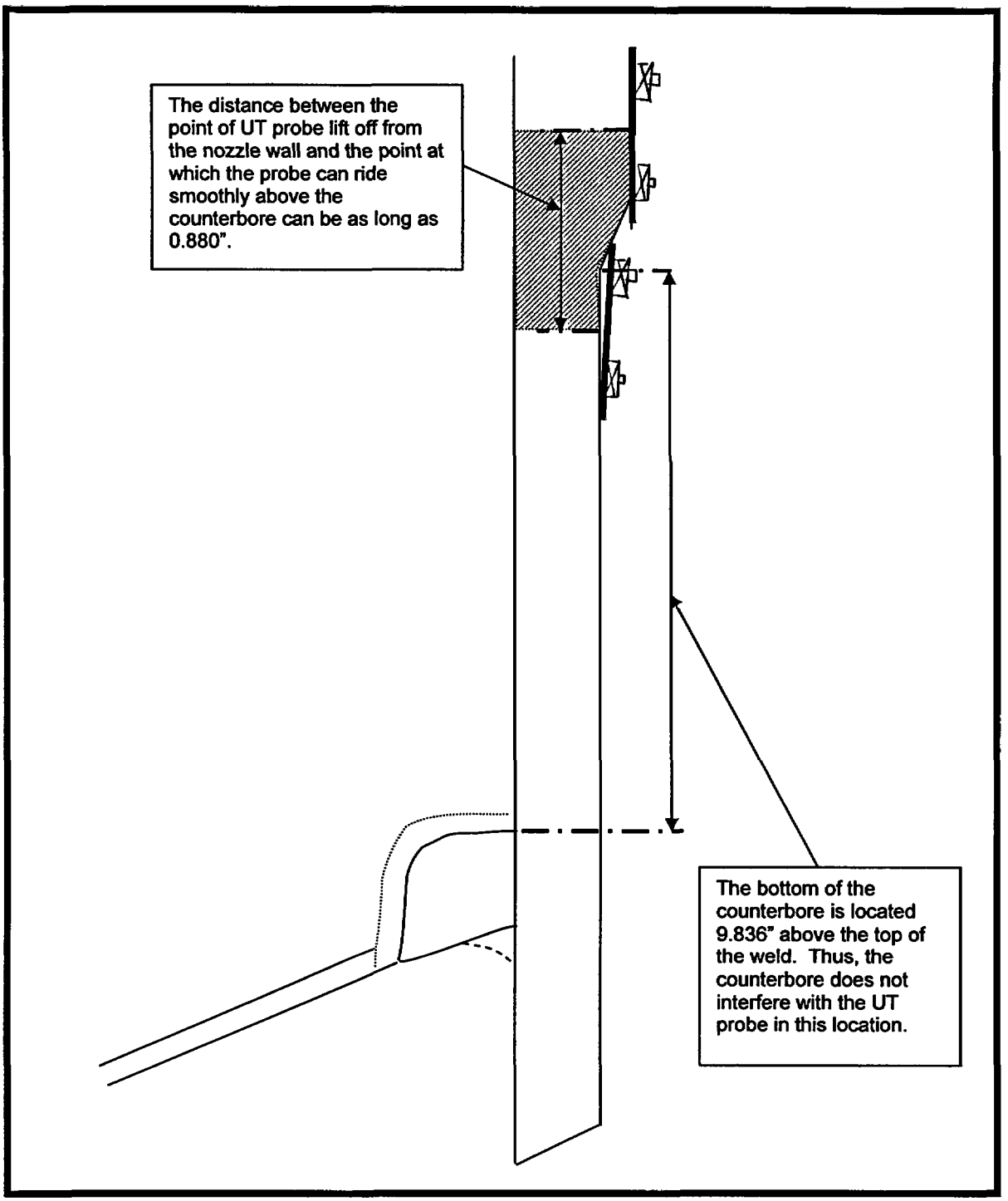

FIGURE 7
COUNTERBORE – LOWER HILLSIDE POSITION

ENCLOSURE 2

CNRO-2003-00042

ENGINEERING REPORT M-EP-2003-005, REV. 0

FRACTURE MECHANICS ANALYSIS FOR THE ASSESSMENT OF THE POTENTIAL FOR PRIMARY WATER STRESS CORROSION CRACK (PWSCC) GROWTH IN THE UNINSPECTED REGIONS OF THE IN-CORE INSTRUMENTATION (ICI) NOZZLES AT WATERFORD STEAM ELECTRIC STATION, UNIT 3

Entergy

ENTERGY NUCLEAR SOUTH
Engineering Report Coversheet

Fracture Mechanics Analysis for the Assessment of the Potential for Primary Water Stress Corrosion Crack (PWSCC) Growth in the Un-Inspected Regions of the In-Core Instrumentation (ICI) Nozzles at Waterford Steam Electric Station Unit 3

Engineering Report Type:

New ☒ Revision ☐ Deleted ☐ Superceded ☐

Applicable Site(s)

ANO ☐ Echelon ☒ GGNS ☐ RBS ☐ WF3 ☒

Report Origin: ☒ ENS ☐ Vendor **Safety-Related:** ☒ Yes ☐ No

Vendor Document No. _____

			Comments:	Attached:
Prepared by:	Brian C. Gray Responsible Engineer	Date: 9/18/03	☐ Yes ☐ No	☐ Yes ☐ No
Verified/ Reviewed by:	J. S. Bolin Design Verifier/Reviewer	Date: 9/18/03	☒ Yes ☐ No	☐ Yes ☒ No
Approved by:	R. A. R. Responsible Supervisor or Responsible Central Engineering Manager (for multiple site reports only)	Date: 9/18/03	☐ Yes ☒ No	☐ Yes ☐ No

RECOMMENDATION FOR APPROVAL FORM

			Comments:	Attached:
Prepared by:	Brian C. Gray Responsible Engineer	Date: 9/18/03	☐ Yes ☐ No	☐ Yes ☐ No
Concurrence:	Not Applicable Responsible Engineering Manager, ANO	Date:	☐ Yes ☐ No	☐ Yes ☐ No
Concurrence:	Not Applicable Responsible Engineering Manager, GGNS	Date:	☐ Yes ☐ No	☐ Yes ☐ No
Concurrence:	Not Applicable Responsible Engineering Manager, RBS	Date:	☐ Yes ☐ No	☐ Yes ☐ No
Concurrence:	Responsible Engineering Manager, WF3	Date: 9-18-03	☐ Yes ☒ No	☐ Yes ☐ No

Table of Contents

List of Attachments

Attachment Number	Content of Attachment	Number of Pages
1	Design Input Record for Waterford-3 ICI Nozzles	2
2	Determination of Over-Sized Weld Dimensions for Use in Finite Element Analysis and Fracture Mechanics Models (including transmittal e-mails)	5
3	Dominion Engineering Inc. Nodal Stress and Coordinate Data (Including Transmittal E-mails)	14
4	Mathcad Worksheet for Flaw Case 1: 25% Through-wall Flaw with an Initial Aspect Ratio of 6-to-1 (Length-to-Depth) Centered in the Blind zone	44
5	Mathcad Worksheet for Flaw Case 2: 0.4 Inch Long with an Initial Aspect Ratio of 10-to-1 (Length-to-Depth) Centered in the Blind zone	44
6	Mathcad Worksheet for Flaw Case 3: 25% Through-wall Flaw with a Initial Aspect Ratio of 4-to-1 (Length-to-Depth) Centered in the Blind zone	44
7	Mathcad Worksheet for Flaw Case 4: A Flaw Spanning the Entire 0.88-Inch Length of the Blind zone with an Initial 6-to-1 Aspect Ratio (Length-to-Depth)	44
8	Determination of Circumferential Extent of Blind Zone and Computation of Axial Stress Distribution	4

Total Pages of Attachments: 201

List of Tables

Table Number	Title	Page Number
1	Dimensions from Tangent Line Datum Plane to specified locations on the ICI Nozzle	9
2	Summary of flaw depths and lengths used to evaluate the blind zone on the uphill side above the top of the weld (blind zone begins a distance 0.67 inches above the top of the weld and extends 0.88 inch)	29
3	Results of PWSCC flaw growth evaluations in the length and depth directions	30

List of Figures

1.0 PURPOSE

The US Nuclear Regulatory Commission (NRC) issued Order EA-03-009 [Ref. 1], which modified licenses, requiring inspection of all Control Element Drive Mechanism (CEDM), In-Core Instrumentation (ICI), and vent penetration nozzles in the reactor vessel head. Paragraph IV.C.1.b of the Order requires the inspection to cover a region from the bottom of the nozzle to two (2.0) inches above the J-groove weld.

The Combustion Engineering (CE) design for the ICI nozzles consists of a 5.563-inch outside diameter (OD) nozzle, inserted into the reactor vessel head at a 55.2667° angle with the horizontal, with the portion of the nozzle extending below the inside surface of the vessel cut to the same angle. The inside diameter (ID) of the ICI nozzle is counter-bored from a diameter of 4.625 inches to 4.750 inches at a height of approximately 1.26 inches above the top of the J-groove weld on the uphill side (180° azimuth), and approximately 9.836 inches from top of the J-groove weld on the downhill side (0° azimuth), based on design drawings. (These dimensions are taken from Attachments 1 and 2 and shown in Figures 1, 2, and 3.) The ICI nozzle as-built dimensions, including the dimensions of the UT un-inspectable regions and the size of the J-groove welds, were estimated from a detailed review of applicable design drawings and UT data from a Sister Plant (Plant A), since no volumetric inspection has been performed at Waterford Steam Electric Station Unit 3 (WSES-3). These two units are of similar CE design and both are rated at 3410 MWt.

The counterbore region of the nozzle above the J-groove weld represents a challenge to interrogate the nozzle with Ultrasonic Testing (UT). Figures 1 and 2 show the typical layout and geometry of the ICI nozzle, while Figures 4 and 5 schematically depict the un-inspectable regions with UT due to the configuration of the counterbore. This un-inspectable region, hereafter referred to as the blind zone, is located a distance above the top of the weld on the uphill side, extends to an axial height above the counterbore, and spans circumferentially around the ID for a limited distance. Due to the offset distance between the downhill side (0° azimuth) and uphill side (180°) of the nozzle at the attachment J-groove weld, the blind zone is closer to the weld on the uphill side.

The UT data from Plant A was inconclusive as to the precise location of the bottom of the blind zone (as measured from the top of the weld on the uphill side), the length (or axial span) of the blind zone, and the circumferential extent of the blind zone. Weld sizes exceeding the design dimensions would suggest that the bottom of the blind zone for the Waterford-3 ICI nozzle could be closer to the top of the weld than the equivalent blind zones for ANO-2 [Ref. 2]. For analysis purposes, the minimum distance from the top of the J-groove weld to the bottom of the blind zone and the total axial length of the blind zone must be ascertained to provide assurance that future UT inspections would detect a surface flaw extending out of the blind zone, prior to it going through the nozzle thickness. Similarly, the circumferential extent of the blind zone, as centered on the uphill side (180° azimuth), is estimated from the knowledge of the distance from the top

of the weld to the bottom of the blind zone, combined with geometric data obtained from a three-dimensional finite element model of the Waterford-3 ICI nozzle. From this data, the angular distance where less than two (2.0) inches of nozzle length above the top of the J-weld is inspected can be extracted.

The unexamined region of the ICI nozzles in the counterbore region above the J-weld provides a location for surface flaws to exist with the potential to grow through the thickness of the nozzle prior to extending beyond the limits of the blind zone, into a detectable region. This is especially a concern on the uphill side of the nozzle, where the blind zone is much closer to the top of the weld and in an area subject to the accompanying high stress field of the J-weld. An ID surface flaw could exist in this somewhere in this blind zone. At the downhill location (0° azimuth), the counterbore is well removed (more than 9 inches) from the top of the weld, hence a blind zone pursuant with the NRC Order does not exist.

In order to exclude the blind zone areas above the weld in the counterbore region from the inspection campaign, a relaxation of the Order is required pursuant to the requirements prescribed in Section IV.F and footnote 2 of the order [Ref. 1].

The purpose of this engineering report is to ensure that an unidentified surface flaw in the blind zone will extend along the length, into an inspectable region, at least one operating cycle prior to growing through the thickness. Only an ID fracture mechanic analysis is required for this justification. For OD surface flaws to initiate and propagate, the existence of the necessary environment would be discovered by the bare metal visual (BMV) examination of the ICI nozzles. BMV inspection for the ICI nozzles provides conclusive evidence, since the shrink fit for the nozzles in considerably lower for the availability of a conducive environment.. Hence, PWSCC can only be initiated on the ID surface of the blind zone. ID surface axial and circumferential flaws will be considered in the analysis.

The geometric assumptions made regarding the sizing of the J-groove welds, the blind zone length, the minimum height of the blind zone above the top of the J-weld, and the circumferential extent of the blind zone will be verified during UT inspections of Waterford-3 ICI Nozzles. Adjustments to this engineering report, in the form of supplemental fracture mechanics evaluations and/or a new finite element stress analysis would be required if the as-built blind zone dimensions or weld sizes prove to be non-conservative.

2.0 GIVEN CONDITIONS AND KNOWN VALUES

2.1 ICI Nozzle Material, Operating Conditions, and Geometry:

Pipe Material: SB-167, Gr. 70 [Ref. 3]

Pipe Outside Diameter:
D_o = 5.563 in. +0.000/-0.001 in. [Ref. 3]

Pipe Inside Diameter, above counterbore:
D_{i1} = 4.625 in. ± 0.01 in. [Ref. 3]

Pipe Inside Diameter, below counterbore:
D_{i2} = 4.750 in. ± 0.01 in. [Ref. 3]

Operating Pressure = 2235 psi [Ref. 4]
Operating Temperature = 604°F [Ref. 5a gives a value of 604°F currently. Following the extended power uprate discussed in Ref 5b, the head temperature will drop to 601°F].

Figure 1: Waterford-3 ICI Geometry from the Bottom of the Nozzle
(from Ref. 3)

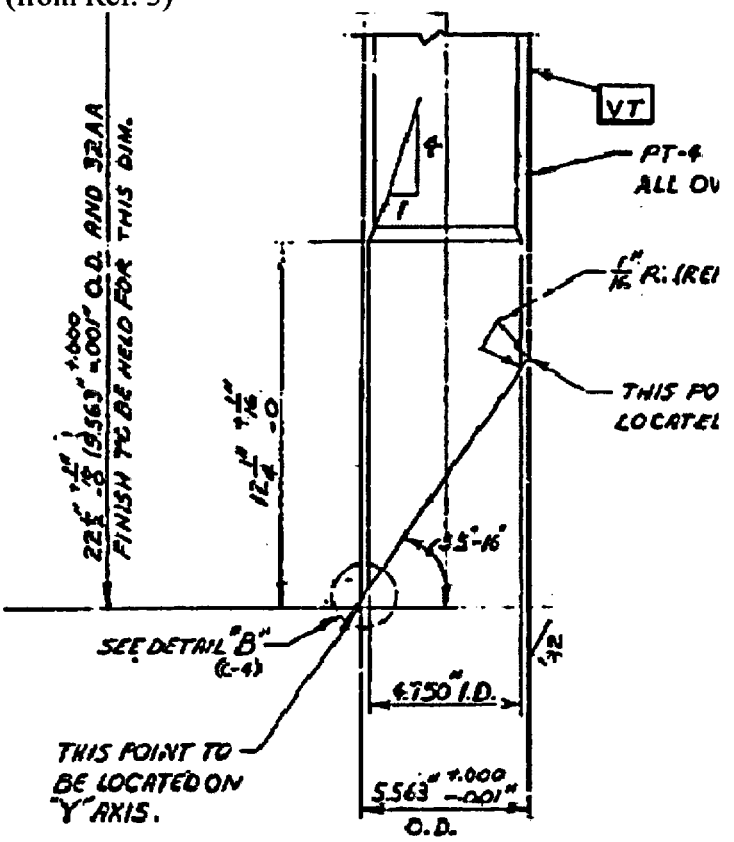

2.2 Dimensions of the Welds and Counterbore Areas:

The elevations and heights of the ICI nozzles and weld positions were obtained from design drawings and transmitted in a Design Input Record (shown Attachment 1). The figure and table below provide a summary of these inputs:

Figure 2: Measured ICI Nozzle Locations from Tangent Line Datum

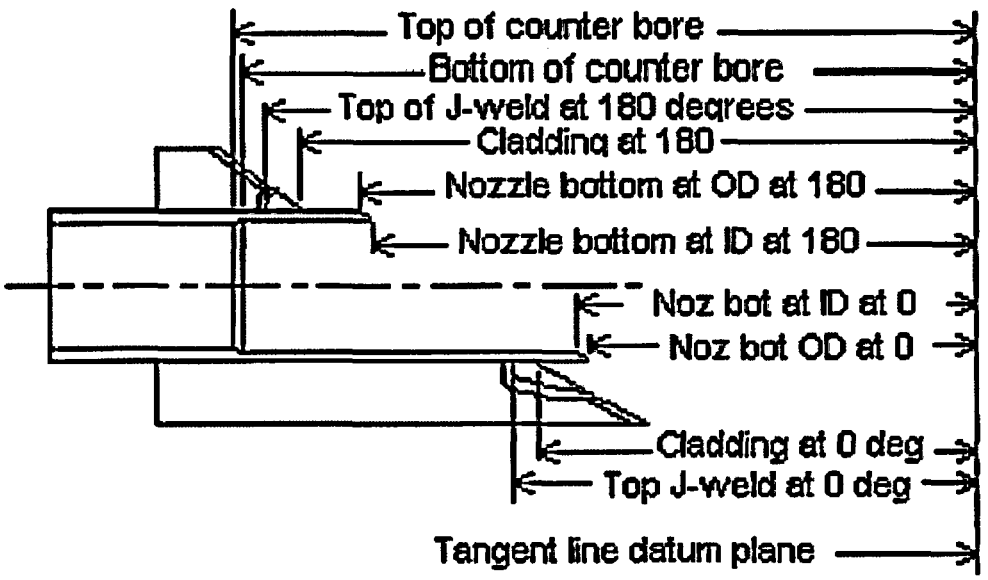

Table 1: Dimensions from Tangent Line Datum Plane to specified locations on the ICI Nozzle*

Dimension from the tangent line datum plane to:	ANO-2 (inches)	W-3 (inches)
Top of counter bore transition	48.625	55.094
Bottom of counter bore transition	48.375	54.844
Top of J-weld at the 180 degree (high hill side)azimuth location	46.998	53.440
Intersection of the projected cladding surface and the nozzle OD at the 180 degree (high hill side) azimuth location	46.211	52.655
Bottom (sharp corner) of the nozzle at the OD surface at the 180 degree (high hill side) azimuth location	44.211	50.618
Bottom (sharp corner) of the nozzle at the ID surface at the 180 degree (high hill side) azimuth location	43.602	50.031
Top of J-weld at the 0 degree (low hill side)azimuth location	38.283	45.008
Intersection of the projected cladding surface and the nozzle OD at the 0 degree (low hill side) azimuth location	37.875	44.589
Bottom (sharp corner) of the nozzle at the ID surface at the 0 degree (low hill side) azimuth location	36.484	43.180
Bottom (sharp corner) of the nozzle at the OD surface at the 0 degree (low hill side) azimuth location	35.875	42.594

*Note that the design input contained both ANO-2 and Waterford-3 data.

3.0 ASSUMPTIONS

In lieu of available UT measurements for the Waterford-3 ICI nozzles, several engineered assumptions that require verification have been considered

1.) The J-groove welds were oversized by 0.30 inch in length, and a corresponding increase in radial extent, as shown in Figure 3 below. The larger weld sizes were estimates of as-built geometry that considered the effect of accumulated tolerances and the experience gained from a review of Plant A UT data that showed a general over sizing of welds among CEDM nozzles [discussed in Ref. 6 (Jai's W-3 CEDM report)]. The larger welds as modeled in the Dominion Engineering finite element analysis will result in a higher stress field in the vicinity of the blind zone.

Figure 3: Estimated as-built ICI Nozzle configuration based on evaluation of Plant A UT data for weld sizes (for CEDMs) and the consideration of tolerances that would minimize the height between the top of the J-weld and the bottom of the counterbore.

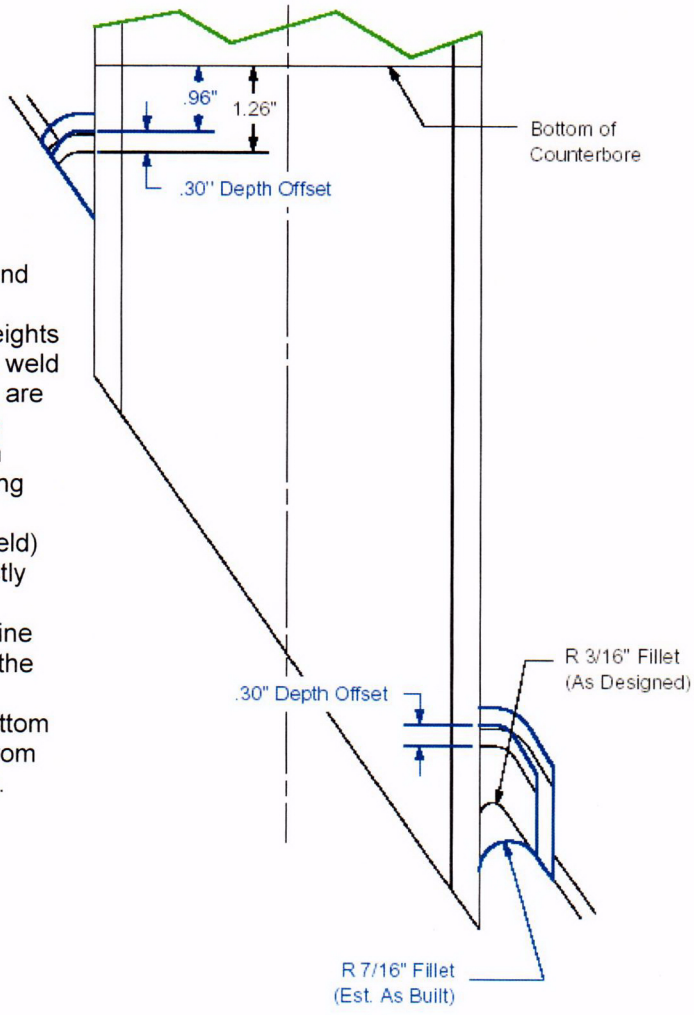

Note: The 1.26" and 0.96" dimensions provided for the heights from the top of the weld to the counterbore are typical dimensions (taken from design drawings accounting for tolerances on oversizing the J-weld) and were not directly factored into the analysis to determine the axial length of the blind zone or the elevation to the bottom of the blind zone from the top of the weld.

C01

2.) The length of the UT blind zone, that is the distance between the point at which the transducer sled starts to lift off and the point at which it can ride smoothly above the counterbore, is assumed to be 0.88 inch. This was the worst-case blind zone length as measured from the ANO-2 UT data (discussed in Ref. 2). Due to similar design dimensions in the vicinity of the counterbore region between the Waterford-3 ICI nozzles and the ANO-2 ICI nozzles, this total span of the blind zone should be similar.

3.) The distance from the top of the J-groove weld to the bottom of the blind zone is determined analytically using iterative fracture mechanics evaluations for postulated flaws in the 0.88-inch blind zone (as discussed in Assumption 2). Based on the evaluations discussed in Section 5.2 and contained in Attachments 4 through 7, this distance is 0.67 inch.

If the ICI nozzle welds are actually 0.3-inch larger than nominal design dimensions, the distance from the top of the weld to the bottom of the counterbore is 0.96 inch (from Figure 3), then the

Figure 4: Counterbore at the Uphill Side (180°) Position—the minimum UT blind zone starting point above the top of weld will be determined by analysis. The axial length of the UT blind zone is considered as 0.88 inch, based on ANO-2 UT Data.

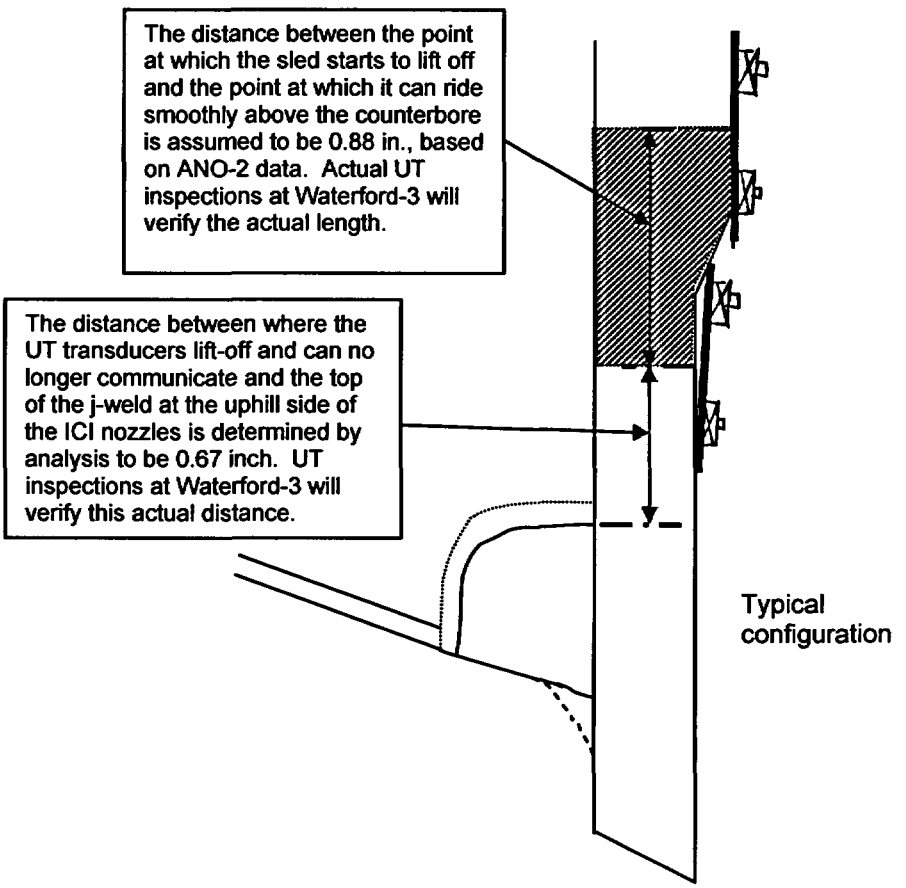

4.) Based on the 0.67-inch distance from the top of the weld to the bottom of the blind zone (Assumption 3 above), the circumferential extent of the blind zone was determined to be 135°, using geometric data from the Dominion Engineering finite element model. The derivation of this circumferential span is included in Attachment 8.

Figure 5: Circumferential Extent of the UT Blind Zone at the Uphill (180°) Position— the arc length of limitation for scanning 2.0 inches above the weld is 135° (as derived from Dominion Engineering's finite element analysis data in Attachment 8).

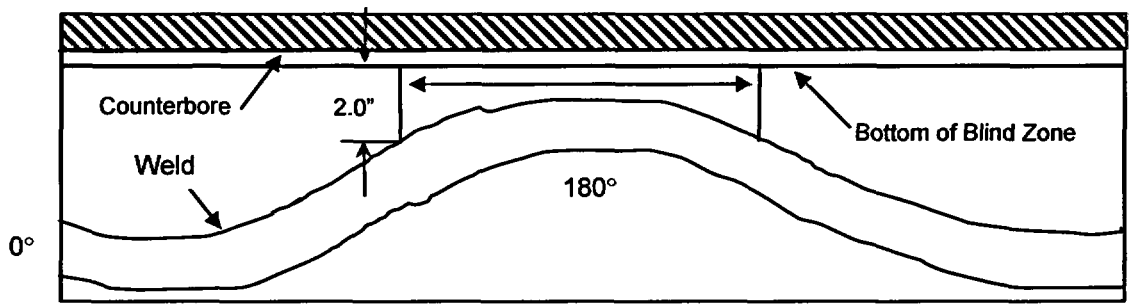

The counterbore limits the ability to ultrasonically scan 2.0 inches above the J-weld for a given circumferential distance on either side of uphill (180° azimuth). This dimension, based on assuming the blind zone bottom at 0.67 above the top of the weld on the uphill side, and on geometric data from the Dominion Engineering finite element analysis, is determined to be 135° for the Waterford-3 ICI nozzles.

4.0 METHOD OF ANALYSIS

The analysis used to determine the impact of not examining the blind zone of the ICI nozzle above the top of the weld in the counterbore region on the uphill side consists of a detailed finite element stress analysis combined with an ID surface flaw fracture mechanics model. The fracture mechanics model evaluates an ID-initiated part through-wall axial crack in a cylinder, located in the blind zone region above the top of the weld on the uphill side of the ICI nozzle. Additional consideration of an ID circumferential surface flaw is provided in Section 4.5

The following sections provide details of the finite element stress analysis and the accompanying fracture mechanics evaluation.

4.1 Finite Element Stress Analysis of Waterford-3 ICI Nozzles

A finite element-based stress analysis representing the ten (10) Waterford-3 ICI penetrations was performed by Dominion Engineering Inc. (DEI) using best estimates of as-built geometries based on the aggregate combination of tolerances and on UT data from Plant A that showed CEDM nozzle welds to be generally over-sized an average of 0.3 inch compared to design drawings. Material property data was obtained from available design information, and the material yield strength of the ten nozzles was from the same heat number. General dimensions for reactor head and ICI nozzles were obtained from Westinghouse/CE design drawings and documents. The weld height and blend radius were proportionately (appropriately) increased to accommodate the 0.3-inch higher weld prep (shown in Figure 3). A longer downhill side fillet weld was modeled by increasing the design length of 3/16 inch to 7/16 inch. The Waterford-3 ICI finite element model did not include the geometry of the ID counterbore in order to improve element refinement by adding elements in the axial direction of the nozzle, above the top of the weld. This modification will improve stress distributions required in the fracture mechanics models for the ID surface flaw in the blind zone. The counterbore is 0.25 inch high with a 1-to-4 (depth-to-length) taper; this transition precludes the need to evaluate stress concentrations such as required per ASME Section III, subsection NB-3680 [Ref. 7] for transitions with less than a 1-to-3 transition. Previous analyses [Ref. 2] showed that the inclusion of a transition region between the thinner section of the ICI nozzle (4.750-inch ID) and the thicker section (4.625-inch ID) resulted in neither a significant through-thickness stress increase nor the creation of a stress concentration. The flaw evaluation will conservatively consider the thinnest section to evaluate the propensity of the presumed flaw in the blind zone to grow through the thickness.

The finite element analysis (FEA) modeling steps using the above geometry data and assumptions to obtain the necessary stress (residual+operating) distribution in the ICI nozzle followed the process and methodology described in Reference 8a. The modeling steps were as follows:

1.) The finite element mesh consisted of three-dimensional solid (brick) elements. Four elements were used to model the tube wall and similar refinement was carried to the attaching J-weld. The elements above the top of the J-weld were refined to capture the stress field in the blind zone/counterbore region for subsequent fracture mechanics evaluations.

2.) The ICI nozzle material, possessing the same yield strength for all nozzles, resulting from a single heat of material, was modeled with a monotonic stress-strain curve. The yield strength of the nozzles was referenced to the room temperature yield strength of the stress strain curve described in Reference 8a. Temperature-dependent stress-strain curves needed to model the nonlinear welding process were obtained by indexing the temperature-dependent drop of the yield strength.

3.) The weld material was modeled as elastic-perfectly plastic for the weld simulation. This approximation is considered reasonable since most of the plastic strain in the weld metal occurs at high temperatures where metals do not work-harden significantly [Ref. 8b]. The temperature in the weld is always high during the welding process, and once the weld begins to cool, the temperatures in the weld at which strain hardening would persist are of limited duration [Ref. 8b]. This was borne out by the comparison between the analysis-based residual stress distribution and that obtained from experiments [Ref. 8c].

4.) The weld is simulated by two passes based on studies presented in Reference 8a.

5.) After completing the weld, a simulated hydro-test load step is applied to the model. The hydro-test step followed the fabrication practice.

6.) The model is then subjected to a normal operating schedule of normal heat up to steady state conditions at operating pressure. The residual plus operating stresses, once steady state has been achieved, are obtained for further analysis. The nodal stresses of interest are stored in an output file. These stresses are then transferred to an Excel spreadsheet for use in fracture mechanics analysis.

The stress contours for the ICI nozzle obtained from the finite element analysis are presented in Figures 6 through 8. The hoop stress contour color scheme is as follows:

Dark Navy blue→ from Minimum (Compression) to -10 ksi

Royal blue → from -10 to 0 ksi

Light blue → from 0 to 10 ksi

Light green → from 10 to 20 ksi

Green → from 20 to 30 ksi

Yellow green → from 30 to 40 ksi

Yellow → from 40 to 50 ksi

Red → from 50 to 100 ksi

Figure 6: Hoop stress contours for the ICI nozzle. High tensile stresses occur in the weld and adjacent tube material.

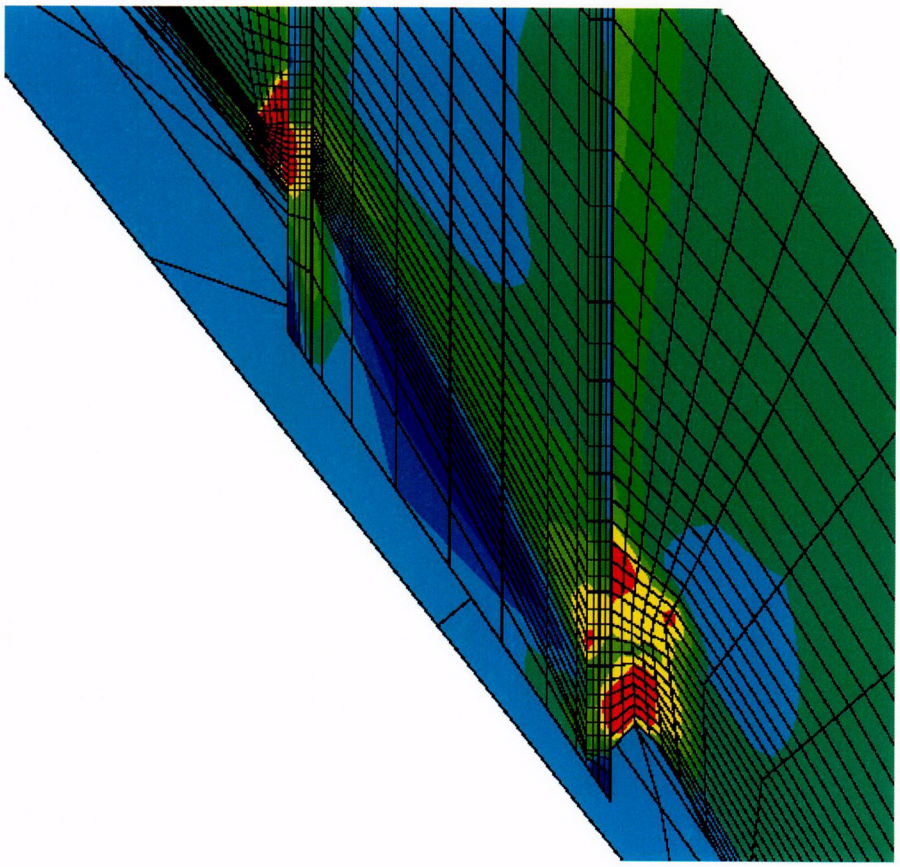

C02

Figure 7: Hoop stress contours in the upper portion (closer to the intersection with the reactor head) of the ICI nozzle

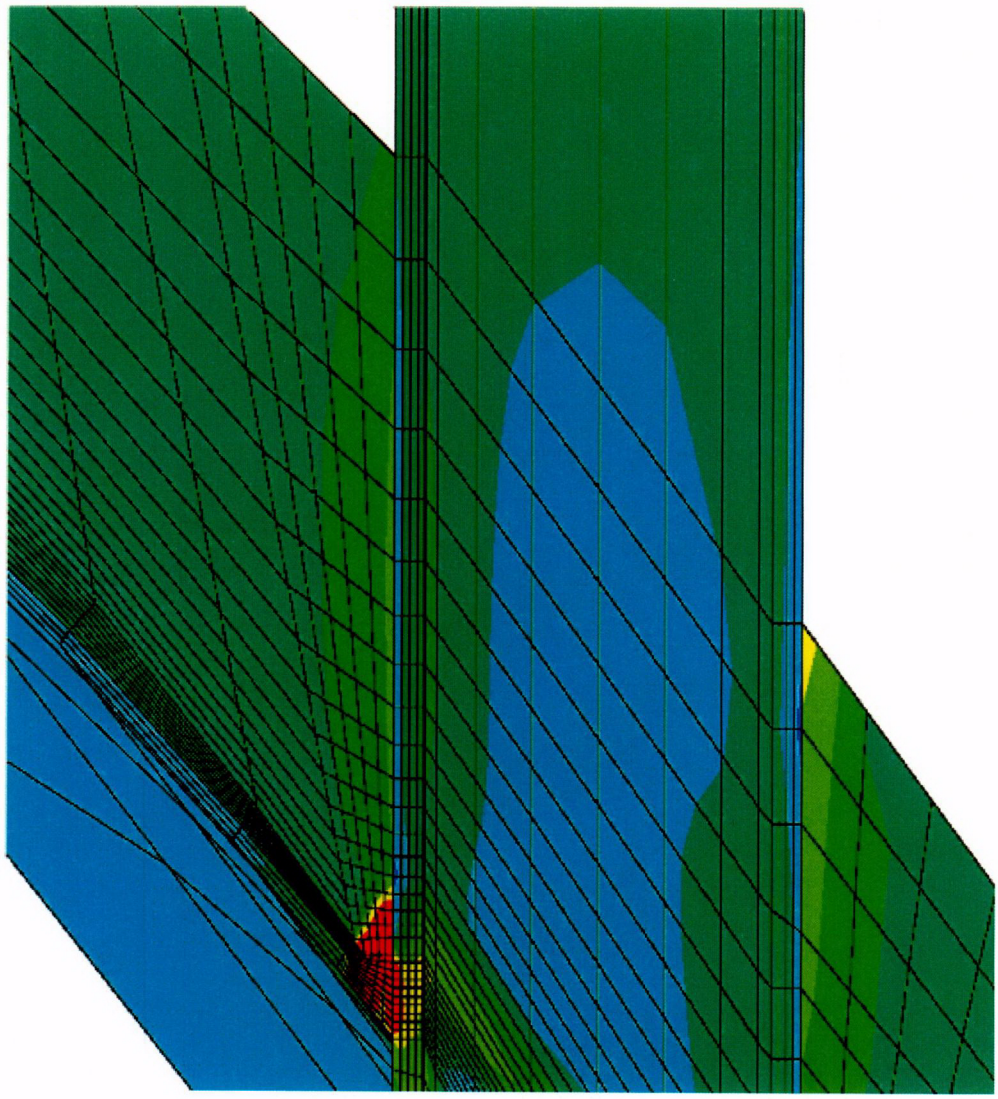

C03

Figure 8: Close-up of the uphill side (180° azimuth) hoop stress in the vicinity of the J-groove weld and counterbore region

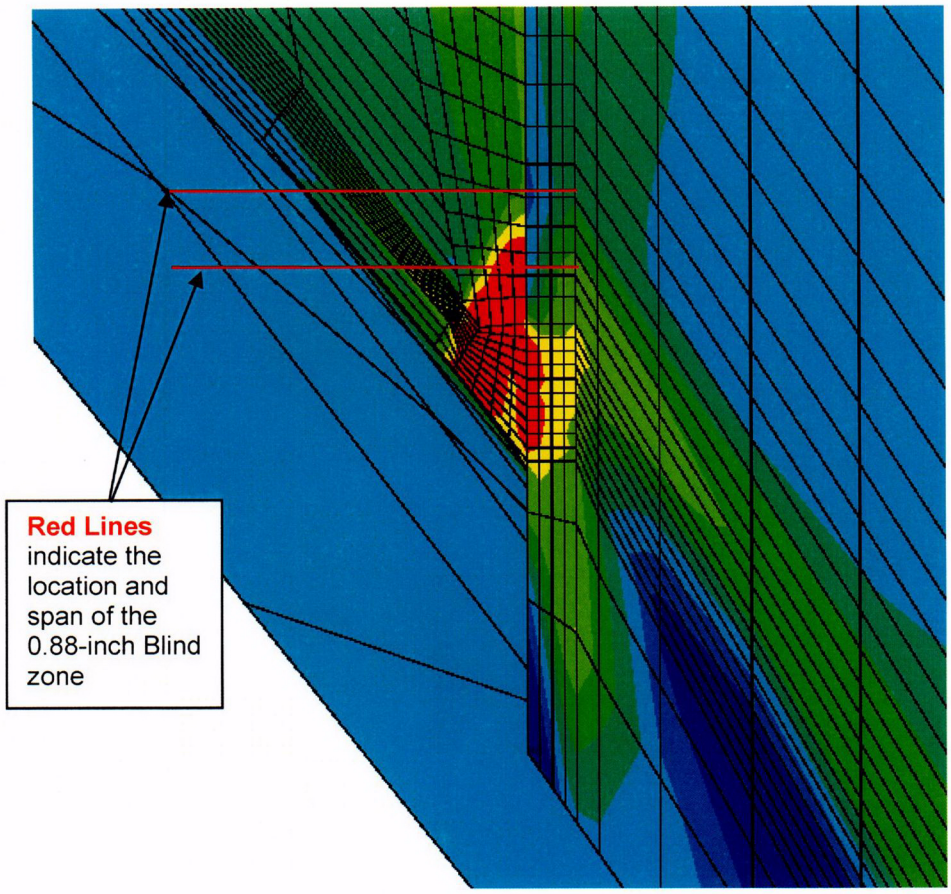

The nodal stresses for locations of interest were provided by DEI and were tabulated in Reference 8d. (This data is also shown in Attachment 3.) The location of the weld bottom at each azimuth was maintained at the node row ending with "601", while the top of the weld at each azimuth was the node row ending with "1301". The blind zone is shown on Figure 8 as an overlay to the stress contours.

From the stress data in Attachment 3, the uphill side (the 80000 series nodes from the stress data) hoop stresses are the second highest in the ICI nozzle above the weld; the downhill side above the weld has higher hoop stresses, and these will be addressed in Section 5.2. Additionally, axial stresses used to evaluate circumferentially flaws were tabulated in Reference 9d and contained in Attachment 3. These stresses and the potential of circumferential flaws in the blind zone will be discussed in more detail in Section 4.5.

The nodal stress data from the DEI analyses are imported into the respective Mathcad worksheet (discussed later) for further processing to obtain the pertinent

stress distributions required for the fracture mechanics analysis described in Section 4.2. Additional processing of the nodal stress data is described in Section 4.4.2.

4.2 ID Surface Flaw Fracture Mechanics Model

The model used to evaluate an ID surface flaw contained in the 0.88-inch Blind zone above the top of the weld is described in detail in Reference 6, and was originally presented in a NASA Publication, Reference 9. This model evaluates an axial, part through-wall flaw on the ID surface of a cylinder, subject to an arbitrary stress distribution (up to a cubic polynomial fit). This model is valid for a ratio of mean radius (R_{mean})-to-thickness (t) between 1.0 and 300. Since the ICI nozzle has R_m/t equal to 6.4, this model is considered applicable.

The fracture mechanics model [Ref. 9] gives the equation for the stress intensity factor (SIF) for both deepest point of the crack and the tip of the flaw along the surface, as follows:

$$K_I = \left(\frac{\pi}{Q}a\right)^{0.5} * \left(\sum_{i=0}^{3}\sigma_i G_{ai}\right)$$ for the SIF at the deepest point of the flaw

$$K_I = \left(\frac{\pi}{Q}c\right)^{0.5} * \left(\sum_{i=0}^{3}\sigma_i G_{ci}\right)$$ for the SIF at the tip of the flaw on the surface

where:

K_I is the applied Stress Intensity Factor, or SIF $\{ ksi\sqrt{in} \}$

Q = Crack shape factor; defined as

$$Q = 1 + 1.464 \cdot \left(\frac{a}{c}\right)^{1.65}$$ when a/c ≤ 1.0 and,

$$Q = 1 + 1.464 \cdot \left(\frac{c}{a}\right)^{1.65}$$ when a/c > 1.0

a = Crack depth {inch}

c = Crack half flaw length {inch}

σ_i = Coefficients of the stress polynomial describing the hoop stress variation through the crack depth. Describes the power loading on the crack face.

$G_{a,i}$ = Stress Intensity Correction Factors (SICF) for the deepest point, which are provided in tables in Reference 9.

$G_{c,i}$ = Stress Intensity Correction Factors (SICF) for the surface tip, which are provided in tables in Reference 9.

In Reference 9, SICFs are presented for both the depth-point of the crack ("a-tip") and for the surface point of the crack ("c-tip"). Separate tables are provided for internal (ID) and external (OD) surface cracks. In addition, the values are provided in association with the R_m/t ratio, a/c ratio (flaw aspect ratio), and a/t ratio (normalized crack depth). The SICF tables are large, and a suitable interpolation scheme is necessary to obtain proper coefficients dependent on crack size and shape for a given cylindrical geometry. Selected SICFs from the tables for internal cracks for two different R_m/t ratios and a/c ratios are presented in Figure 9 below.

Figure 9: SICF shown as a function of normalized crack depth for the "a-tip" (left figure) and the "c-tip" (right figure). These figures show that simple linear interpolation would not provide accurate coefficients. These figures also show that a proper R_m/t is essential to provide a reasonably accurate estimate of the SIF

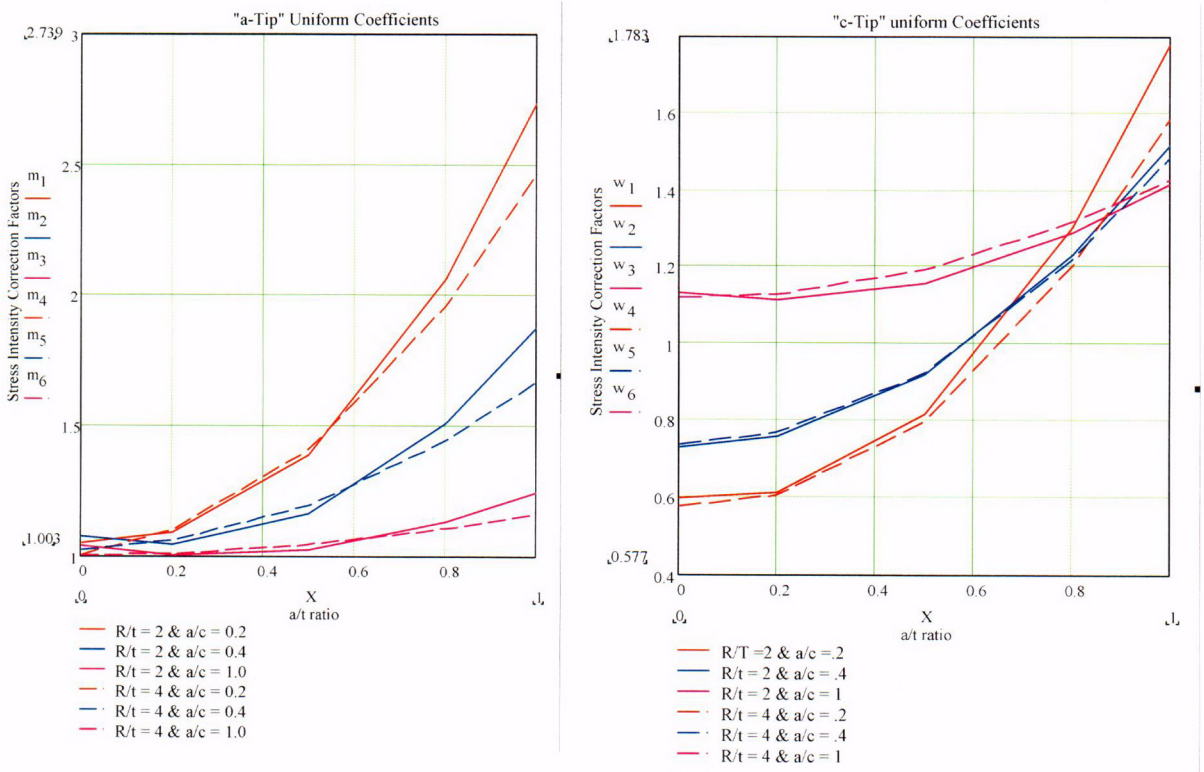

The figure above shows two features that are significant:

C05

1.) The interpolation used to obtain the SICF must be carefully performed such that the value accurately represents the crack geometry. This is accommodated by selecting a suitable order for the curve-fitting polynomial prior to performing an interpolation to obtain the specific value. This aspect is discussed in further detail below;

2.) The correct R_m/t ratio is essential for obtaining a reasonably accurate estimate of the SIF. Using a higher ratio will tend to underestimate the SIF and hence under predict the crack growth.

Both these features have been considered in the development of the analysis model such that a reasonable, yet conservative, estimate of the SIF is obtained. This SIF is the critical input to determine the rate of PWSCC growth in the ICI nozzle. The growth model is discussed in Section 4.3.

4.3 PWSCC Growth Model

To evaluate the potential for crack growth due to PWSCC, the crack growth rate equation from EPRI Report MRP-55 [Ref. 10] was used. The crack growth rate as a function of the SIF with a correction for temperature effects is given as [Ref. 10]:

$$\frac{da}{dt} = \exp\left[-\frac{Q_g}{R}\left(\frac{1}{T}-\frac{1}{T_{ref}}\right)\right]\cdot\alpha\cdot(K-K_{th})^{\beta}$$

Where:

da/dt = crack growth rate at temperature T {meters/second}

Q_g = thermal activation energy for crack growth {31.0 kcal/mole}

R = universal gas constant $\{1.103\times10^{-3}$ kcal/mole-°R$\}$

T = absolute operating temperature at crack tip {°R}; the value used was the 604°F operating temperature of the head, per Section 2.1

T = absolute reference temperature for data normalization {1076.67 °R}

α = crack growth amplitude of 2.67×10^{-12}

K = crack tip SIF $\{\text{MPa}\sqrt{m}\}$

K_{th} = threshold SIF for crack growth $\{\text{MPa}\sqrt{m}\}$

β = exponent of 1.16

The above equation represents the seventy-fifth (75^{th}) percentile curve. Since the PWSCC crack growth of interest is in the primary water, this model would provide a reasonably conservative crack growth.

4.4 Iterative Mathcad Model for Stress Curve-Fitting and Flaw Growth Evaluation

4.4.1 Mathcad Worksheet Format

The analytical scheme was developed using Mathcad [Ref. 11] which facilitates calculations (including recursive) in a logical manner. Reference 6, Appendix B, provides an annotated version of the ID surface crack worksheet used in the current analysis. In the paragraphs below the general approach used to develop the worksheet is presented. The three (3) parts of the Mathcad worksheet requiring user input is discussed in detail.

The first part of the Mathcad worksheet contains a section of imported FEA stress and elevation data for the ID, OD, and other locations through the thickness of the ICI nozzle. This section highlights the significant difference between the methodology used in Reference 6 for the CEDM nozzle evaluations and the current fracture mechanics evaluation for the counterbore region in the ICI nozzles: the "reversal" of the elevations obtained from the nodal stress and location data from DEI's FEA models. For the CEDM nozzles, the reference point and "0"-elevation point is the bottom of the nozzle, since the bottom is level. For the ICI models, DEI indexed their data from the lowest part of the nozzle for each azimuth. For example, the ID corner on the uphill side represents the zero 0-elevation; due to the nozzle cut angle, the OD corner is at a higher elevation. DEI provided data for locations and stresses from the bottom to the top of the nozzle (as shown in Attachment 3). The CEDM evaluations and iterative loops considered a surface flaw in the nozzle below the weld growing axially upwards in the length direction. However, for a flaw in the counterbore region above the top of the weld in the ICI nozzles, due to the stress field being much higher axially down toward the weld, the flaw growth would be in the opposite direction. In order to avoid changes to the loop structure used for the CEDM analyses [Ref. 6] and definitions, the elevations referenced from the bottom of the ICI nozzle were modified to reference from the top of the nozzle as given in the FEA output data.

The second part of the worksheet requires the proper identification for the analysis being performed. In this region the component and the reference location in that component are identified. Immediately below the identification entry are the geometric landmark entries. For an ID surface crack, three entries are required and these are:

1.) The location of a reference line (for example, the blind zone location) referenced to the top of the ICI nozzle from the FEA data (not the true top of the ICI nozzle from Reference 3 $\{\mathbf{Ref_{Point}}\}$.

2.) The location of the crack with respect to the reference line (Upper crack tip at the reference line, center of crack at the reference line or lower crack tip at the reference line) {**Val**}

3.) The distance to the top of the weld, measured downward from the nozzle bottom {$\mathbf{Elev_{Strs.Dist}}$}.

The third part of each Mathcad worksheet contains the inputs for crack dimensions, tube geometry, internal pressure, years of operation, iteration limit, operating temperature, constants for the PWSCC crack growth parameters, and the flaw geometry. It should be noted that the crack growth is performed using metric units; hence, those constants are required to be in metric units. The remainder of this sheet does not require user input. The calculation shown is simple arithmetic to determine the values necessary for the analysis. The remaining parts of the Mathcad worksheet involving the regression of the stress data and the iterative analysis for flaw growth are discussed in Sections 4.4.2 and 4.4.3, respectively.

4.4.2 Regression Analysis of Axial and Through-Wall Stress Distributions

A regression analysis on the FEA stress data is required to obtain the appropriate stress distribution to be used in the determination of the SIF. Regression (that is, curve-fitting) of the stresses is needed because the SIF formulation is based on use of a uniform stress distribution along the length of the tube. However, the stress field in the nozzle above the weld, starting at the top of the nozzle where it intersects the reactor head, increases in magnitude as the top of the weld is approached. Consequently, if an assumed crack located in the vicinity of the reference line (in the blind zone) were to grow by PWSCC, it would be subjected to an increasing stress field. Thus, to use the stress distribution at the initial crack location would lead to an underestimate of the SIF, since the SIF is directly proportional to the applied stress. In order to obtain a reasonably representative SIF under the prevailing stress field variation, a moving average scheme was developed. This scheme is as follows:

1.) For the initial crack location, the stress distribution at the two crack tips (lower and upper) and the crack center are averaged to produce an average stress field that is applied to the crack. It is this stress distribution that is used to ascertain whether there exists a potential for PWSCC crack growth. This method is considered reasonable since it is similar to the superposition principle used in finite element-based SICF determination.

2.) The remaining portion of the nozzle extending from the lower crack tip to the top of the weld is divided into twenty (20) equal segments.

3.) The stress distribution in the first segment, below the lower crack tip, is an arithmetic average of the first three initial crack region distributions (the lower tip, center of crack and the upper tip) plus the distribution in the first segment. Thus, when the crack enters the first segment the magnitude of the stress distribution is appropriately increased to account for the increased applied stress. Similarly, as the crack progresses downward, out of the blind zone and toward the top of the weld through the various segments, the applied stress distribution is adjusted accordingly. The small extent of the length between the reference line and the top of the weld can be sufficiently accommodated by the twenty-segment characterization.

To accomplish this averaging scheme, the nodal stresses at the five (5) nodal locations through the nozzle thickness and the variation along the length of are individually regressed with a polynomial curve-fit. For the nodal stresses along the length of the nozzle, a third-order polynomial was used to curve fit these stresses in the region of interest (that is, starting with the length of nozzle above the top of the flaw and extending down toward the top of the weld). The distance chosen for the axial curve-fit was evaluated for each set of stresses through the thickness to provide for precision in the area of interest and to avoid either under predicting or highly overshooting the stresses with the resulting polynomial. Reference 6 provides details on the importance of selecting a limited region for regression. Significant variation in stresses might produce errors in the determination of the SIF, which in turn could lead to an inaccurate estimate in crack growth. The regression is performed along the nozzle axis at each of the five (5) locations individually. The result of the regression provides the spatial coefficients required to describe the stress distribution. The nodal stress data representing the region of interest, from the top of the nozzle (elevation "0") to an elevation just below the top of the weld, is selected. In this manner, it is expected that proper representation of the stress distribution, pertinent to crack initiation and growth, can be accurately described. For the through-thickness stress distribution, a third-order polynomial was used to fit the stresses at each axial elevation. The results of the regression are contained in the Mathcad worksheets in Attachments 4 through 7. From these curves, it is evident that in the regions of interest, the fourth-order regression of the stresses along the length of the ICI nozzle provides an adequate representation of the stress distribution.

In the through-thickness regression, the nozzle thickness was assumed to be equal to the minimum section thickness to simplify application to the fracture mechanics iterative loop; that is, the nozzle below the counterbore with a minimum thickness (factoring in tolerances) of [(5.563-0.001)-(4.750+0.010)]/2 = 0.401 inch was used. To simplify the computations for the fracture mechanics loop, it was assumed that that thickness of the entire

nozzle above the weld was 0.401 inch. This is conservative, since the thickness above the counterbore (0.4635 inch), which is 13.5% thicker than the thinner section, has lower stresses (owing to it being further removed from the highly stressed weld region) and a greater thickness through which a similarly sized flaw can propagate. Thus, the five (5) nodal stresses for the thicker section were assumed to be the equivalent nodal stresses for a thinner section in that region. As discussed previously, the 1-to-4 taper on the counterbore is sufficient to not incur any stress concentrations or significant variations in through-thickness stress distributions in the model, hence it was not explicitly modeled. Furthermore, the residual stress effects in this region are muted, and the applied stresses from the operating pressure govern above the counterbore around the full circumference, as shown in Figure 7.

Following the determination of the five polynomial equations for the axial distribution of stresses, the through-wall stress distribution for the three locations defined by the crack and the twenty segments are established. The distributions at the twenty-three locations are subjected to a third-order polynomial regression to obtain the coefficients describing the through-wall distributions. These coefficients are used within the recursive loop to assign the coefficients based on the current depth and crack location. The five axial distributions are used for the ID surface crack.

4.4.3 Iterative Analysis to Determine Stress Intensity Correction Factors (SICFs)

For the ID surface crack, the SICF coefficients were incorporated in two data tables. The first table contains the geometry data (R_m/t, a/c and a/t) and the second table consists of the SICF data for the appropriate cylinder and crack geometry. The values for the data were obtained from Reference 9 and were subsequently used in Reference 6 for the CEDM nozzle flaw evaluation. The data contained in the two tables were regressed into function statements with an appropriate polynomial order. The data for cylindrical geometries with R_m/t ratios ranging from one (1) to four (4) were regressed with a third-order polynomial, and for those above four, a second-order polynomial was used. The selection of the polynomial order was based on matching the value in the table given, for a selected set of independent variables, with that obtained from the interpolation performed using the regressed coefficients. In this manner the accuracy of the regression-interpolation method was established. The interpolation equation was defined outside the recursive loop and function call was made inside the loop using the pertinent variables at the time of the call.

The recursive loop starts the calculation scheme to determine the crack growth for a specified time period under the prevailing conditions of applied stress. The first few statements are the initialization parameters. The calculation algorithm begins with the assignment of the through-wall stress

coefficients based on the current crack location. Once the four coefficients (uniform, linear, quadratic and cubic) are assigned, the through-wall stress distribution is used as the basis to establish the stress distribution along the crack face in the crack depth direction. That is, the stresses through the thickness are used to determine the stress along the crack face for application in the determination of the SIF in accordance with Reference 9. Once again, five locations along the crack depth were used to define the crack face distribution. The stresses representing the crack face values were regressed with a third-order polynomial to obtain the stress coefficients that would be used in the determination. At this point, the internal pressure is added to the SICF coefficient for the uniform term. Therefore, the crack face is subjected to an additional stress representing the internal pressure.

Following the determination of the stress coefficients, the function call to obtain the four SICF coefficients is made. In this case the two function calls were necessary to account for the "a-tip" and the "c-tip". The crack shape factor ("Q") was then computed using the appropriate crack dimensions. The SIF is calculated separately for the "a-tip" and the "c-tip" using the stress coefficients, appropriate SICFs and crack dimensions. The calculated SIFs were converted to metric units for the computation of crack growth. The crack growth rate, based on the prevailing SIF was computed in metric units. Once this was done, a conditional branch statement was used to calculate the crack growth within the prescribed time increment. The crack growth was computed in English units by converting the calculated crack growth rate in meters-per-second to inches-per-hour. Thus, the crack growth extent was obtained in inches for the specified time period. Since the operating time was selected to be forty (40) years and the number of iterations chosen at eight thousand (8000), the time increment for each crack growth block was approximately forty-four (44) hours. After the calculations were performed, all necessary information (crack growth, SIFs etc.) was assigned to an output variable such that it is stored in an array. The last step of the recursive loop consisted of updating the essential parameters (namely, the index, crack length, time increment etc.). This loop was annotated in Appendix B of Reference 6 to show the various steps.

Graphical displays of the results for flaw size in the depth direction, flaw growth in the length direction, the total flaw half length, and the SIFs for the number of operating years complete the work sheet. The Mathcad plots are used to determine whether or not the crack in the blind zone will grow through the thickness prior to extending beyond the blind zone and into an inspectable region. Tabular results of this analysis are shown in Table 3 of Section 5.2.

4.5 Consideration of a Circumferential Flaw in the Un-Inspectable Region

With the location of the blind zone above the top of the weld, the safety concerns of a circumferential flaw are significant. A circumferential flaw located on the ID surface, spanning the full 135° circumferential extent of the blind zone (from Figure 5), has the potential to grow through thickness and around the length of the ICI nozzle, thus creating an ejection mechanism leading to a loss of coolant accident. For this circumferential flaw growth to occur, both the PWSCC environment and a conducive tensile axial stress field must exist. The DEI axial stress FEA data in Attachment 3 were reviewed for locations at the uphill side and those angles spanning 67.5° on either side of the 180° azimuth that would encompass the circumferential extent of the blind zone; these angular positions include the 180°, 157.5°, 135°, and 112.5° azimuths.

From previous fracture mechanics evaluations for the CEDM nozzles [Ref. 6], it was shown that no flaw growth will occur for an applied hoop stress of 10 ksi; that is, the resulting applied stress intensity factor is below the threshold value of 8.19 ksi $\sqrt{in}$ needed for flaw growth. With this premise applied to the axial stress distributions for growth of a circumferential flaw, Figures 10 and 11, below, show the axial curve-fits of the stress distribution for the 112.5° to 247.5° azimuths.

Figure 10: ID Axial Stress Distribution Spanning 67.5° on Either Side (135° Total) of Uphill

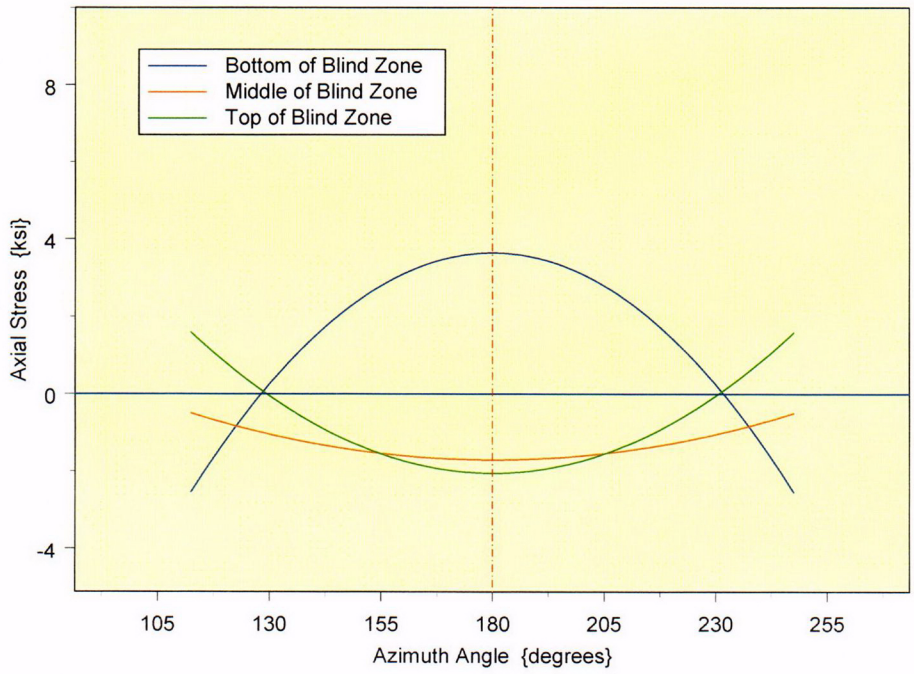

C06

Figure 11: 25% Through-Wall Position Axial Stress Distribution Spanning 67.5° on Either Side (135° Total) of Uphill

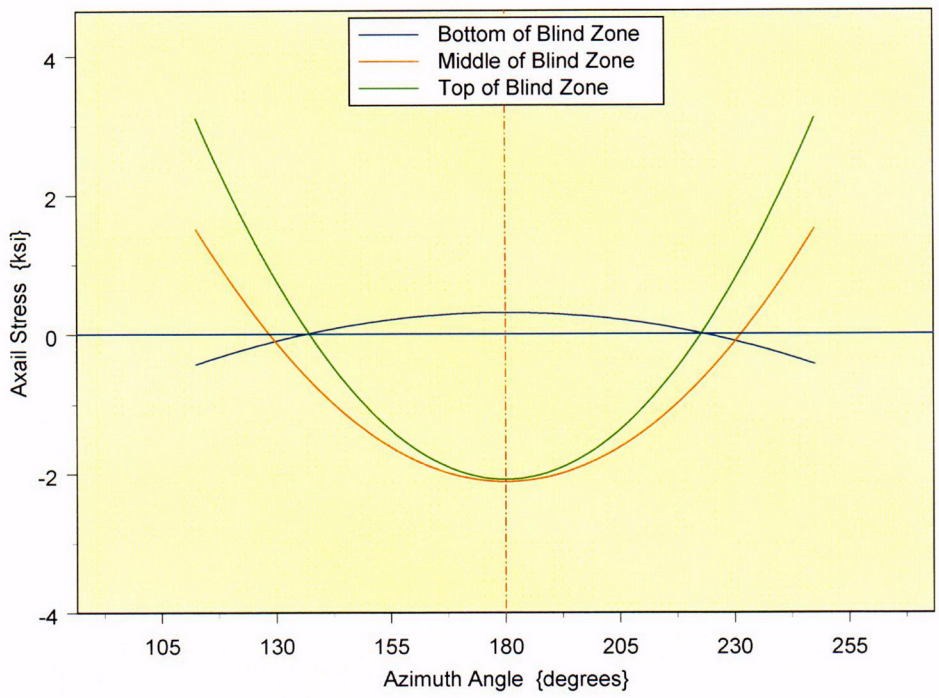

From Figures 10 and 11, the stresses at the ID and at the 25% through-wall locations, covering a 135° circumferential span around the ICI nozzle, are predominantly compressive or very low tensile (< 10 ksi). Hence, the initiation of a circumferential flaw in the blind zone above the top of the weld on the uphill side (180° azimuth) is precluded, thus presenting no safety significance by not inspecting this region.

5.0 DISCUSSION AND RESULTS

5.1 Discussion

The goal of the inspection program designed for the reactor vessel head penetrations is to ensure that the postulated crack in the vicinity of the blind zone does not reach the weld or propagate through-wall during the upcoming operating cycle following the refueling outage when the inspections are performed. Safety analyses performed by the MRP have demonstrated that axial cracks in the nozzle tube material do not pose a challenge to the structural integrity of the nozzle. Axial cracks, if allowed to exist undetected for sufficient periods of time can produce a primary pressure boundary leak that can cause damage to the reactor vessel head (carbon steel) and create a conducive environment for initiating and propagating OD circumferential cracks. These conditions challenge the pressure boundary; hence, critical importance is paid to proper periodic inspection and to the disposition of cracks that may be discovered. Therefore, proper analyses are essential to ascertain the nature of axial crack growth such that appropriate determination can be accomplished.

The analyses performed in this report were designed to capture the behavior of postulated ID part through-wall flaws that might exist in the blind zone region of the ICI nozzle, above the top of the weld, in the vicinity of the counterbore, on the uphill side. These would tend to grow along the tube ID, into the high stress field at the top of the weld, and through the thickness above the top of the weld.

The design review of the reactor vessel head construction, the detailed residual stress analyses, selection of representative fracture mechanics models, and the application of a suitable crack growth law has provided the bases for arriving at a comprehensive and prudent decision.

The axial crack geometry is selected for evaluation because this crack has the potential for propagation into the pressure boundary weld (the J-groove weld and the ICI nozzle). At all locations above the weld, the ID and the interior are in tension. The OD of the nozzle experiences slight compression in the counterbore transition region and low tension just below this region before ramping to a high tensile stress field at the top of the weld; this is due to the complex, three-dimensional ovalization of the ICI nozzle resulting from the welding process.

The fracture mechanics evaluation considered the crack face to be subjected to the operating reactor coolant system (RCS) pressure. This is accomplished by arithmetically adding the RCS pressure to the uniform stress coefficient in the ID surface crack. In this manner, the stress imposed on the crack is accurately and conservatively modeled. The moving average technique was previously verified (in Appendix D of Reference 6) to be an accurate yet conservative depiction of stress application to the crack face. In this evaluation, the axial distribution of the stresses along the axis was kept constant. In this manner, the moving average method should provide results that have the same distribution at all locations along the tube axis.

This implies the through-wall distribution is invariant along the length of the tube. The results of the analysis showed that the stress distribution across the wall remained unchanged along the axis of the tube. Therefore, the moving stress averaging method is validated for the ID surface crack model.

5.2 Results of the ID Surface Flaw Evaluation

As discussed in Section 3.0, Assumption 3, an iterative fracture mechanics evaluation was performed to determine the minimum blind zone elevation above the top of the weld from which a flaw would propagate along the length into a detectable region at least one operating cycle (1.5 years) prior to growing through the ICI nozzle thickness. Several flaw sizes were evaluated in the blind zone region above the weld on the uphill side. Flaw aspect ratios typical of ASME Section XI (6-to-1 and 10-to-1 on length-to-depth) and another emphasizing deep flaws (4-to-1 aspect ratio) were evaluated that sought to maximize growth through-wall while accommodating growth along the length of the ICI nozzle. These evaluations also considered a case where the half length ("c") of the flaw was less than the remaining length needed to grow to the end of the blind zone. Additionally, for those low aspect ratios (4-to-1 and 6-to-1), a conservative depth of 25% of the wall thickness (0.100 inch) was assumed. With this depth, a flaw need only propagate 0.3 inch through the thickness to reach through-wall, whereas the flaw along the length must extend either 0.3 inch or 0.4 inch (measured from the tip of the flaw on the ID surface to the edge of the blind zone, plus an additional 0.16 inch in order to become detectable).

The iterative analysis shown in Attachments 4 through 7 confirmed the minimum distance to the bottom blind zone from the top of the weld to be 0.67 inch, assuming a blind zone length (axial span) of 0.88 inch. Table 2 below shows the assumed flaw sizes based on these aspect ratios and blind zone dimensions.

Table 2: Summary of flaw depths and lengths used to evaluate the blind zone on the uphill side above the top of the weld (blind zone begins a distance 0.67 inch above the top of the weld and extends axially 0.88 inch)

Flaw Case No.	Description	Flaw Depth (in.)	Flaw length (in.)
1	Aspect ratio of 6-to-1 with depth initially 25% through-wall	0.1	0.6
2	Aspect ratio of 10-to-1 with an initial length of 0.4 inch	0.04	0.4
3	Aspect ratio of 4-to-1 with depth initially 25% through-wall	0.1	0.4
4	Flaw spanning the length of the Blind zone with 6-to-1 aspect ratio	0.147	0.88

In the PWSCC flaw growth evaluation, the acceptability of the flaw is determined by its extension outside of the blind zone region, to a detectable length, prior to growing through the thickness, with at least one fuel cycle (1.5 years) between the length and depth growths reaching these values. From Reference 12, the minimum detectable length of a flaw was 2 mm (0.08 inch), with all flaws in the EPRI demonstration between 2 mm and 4 mm (0.16 inch) being detected. Thus, the detectability threshold in the Mathcad worksheets in Attachments 4 through 7 was set to 0.16 inch (or 4 mm). That is, a flaw contained within the 0.88-inch blind zone must propagate along the length of the nozzle a distance measured from the tip of the flaw to the edge of the blind zone (mathematically, this is BZ_length/2 – c_0, where BZ_length is the blind zone length and c_0 is the initial half flaw length), plus an additional axial distance of 0.16 to ensure proper detection. This length is defined as the Propagation Length, **Prop_Length**, in the Mathcad worksheets shown in Attachments 4 through 7. At the same time, the growth through the thickness is limited to reaching through-wall from the initial depth, a_0. Table 3 below provides the results of the flaw growth evaluation for each of the four (4) flaw cases given in Table 2. The detailed Mathcad worksheets are contained in Attachments 4 through 7.

Table 3: Results of PWSCC flaw growth evaluations in the length and depth directions.

Flaw Case ID	Prop_Length {in.} (BZ_length/2 – c_0 + 0.16 in.)	Time to reach Prop_Length (years)	Time to go Through-wall (in.)
1	0.3	5.59	7.22
2	0.4	36.68	> 40
3	0.4	10.07	11.66
4	0.16	2.02	3.68

These results suggest that a sufficiently deep flaw in the 0.88-inch blind zone above the top of the weld on the uphill side (180° azimuth) would grow to a detectable length at least one fuel cycle (1.5 years) prior to growing through-wall. Graphical details of the depth and length flaw growth are shown in Figures 12 through 15.

Figure 12: Flaw Case 1—Depth Growth (top) and Length Growth (bottom) versus number of operating years. For Flaw Case 1, the growth through-wall occurs in 7.22 years. The length growth into an inspectable region occurs in 5.59 years.

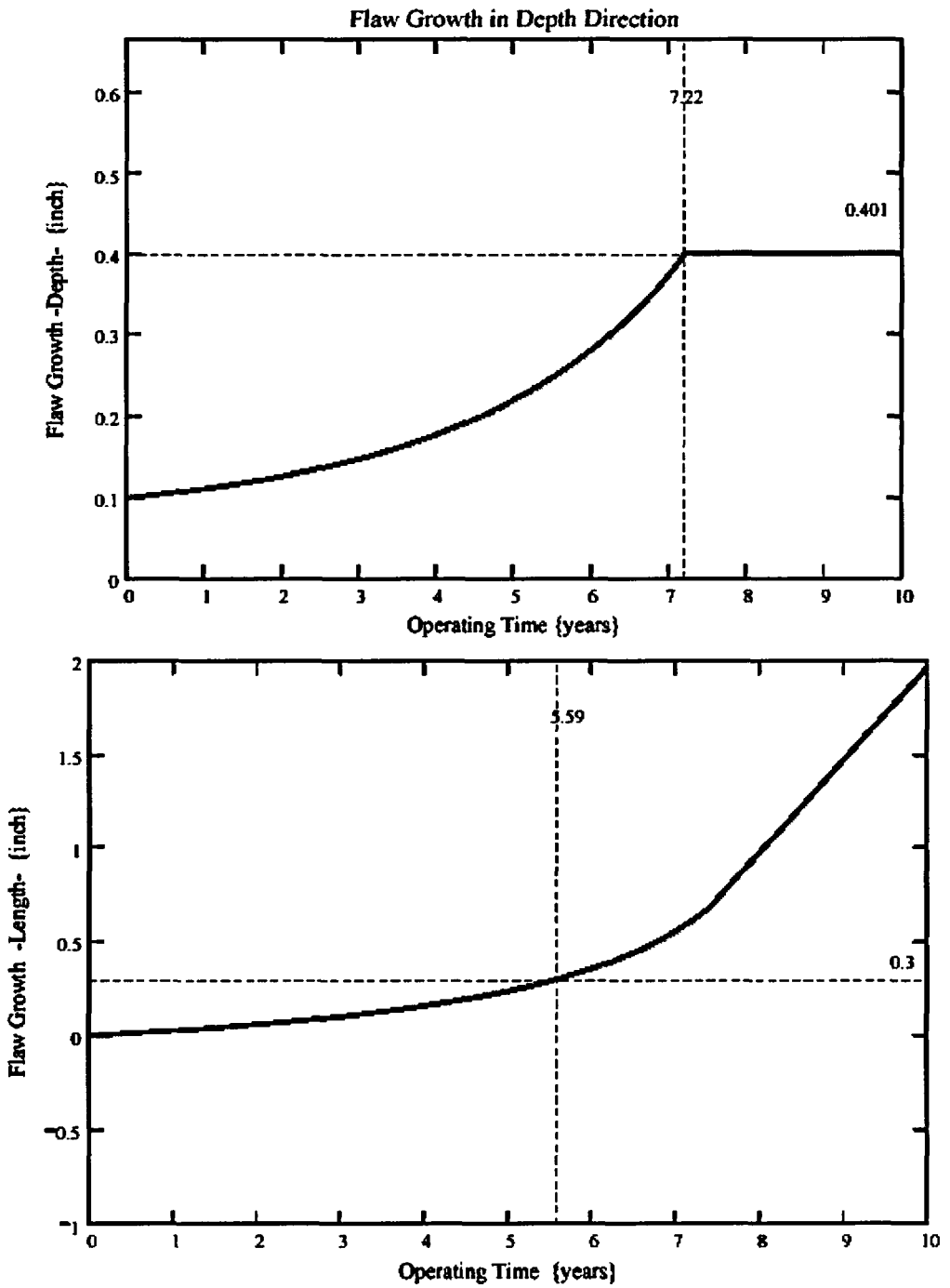

Figure 13: Flaw Case 2—Depth Growth (top) and Length Growth (bottom) versus number of operating years. For Flaw Case 2, the flaw will not grow through-wall in 40 years. The length growth into an inspectable region occurs in 36.68 years.

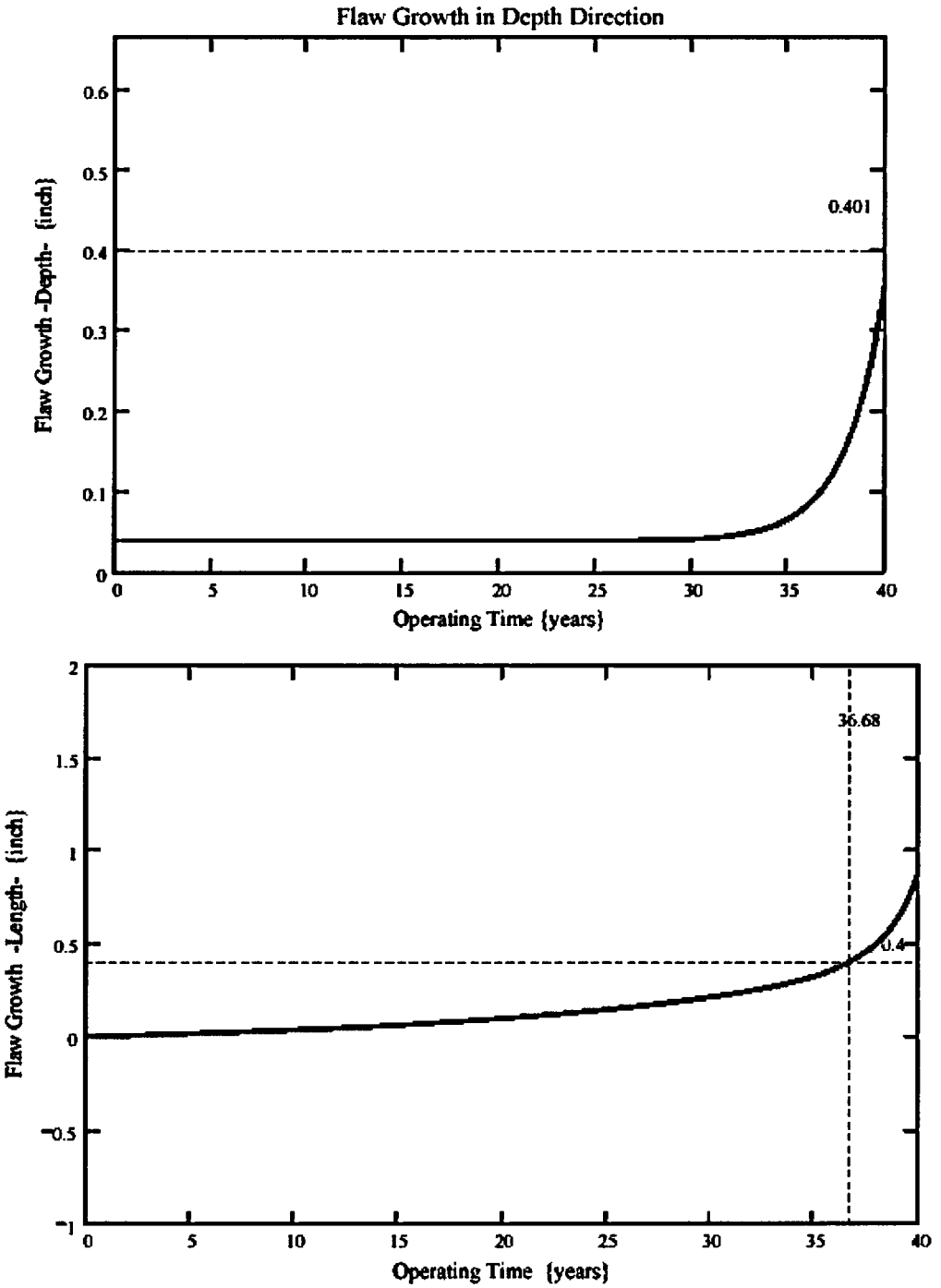

Figure 14: Flaw Case 3—Depth Growth (top) and Length Growth (bottom) versus number of operating years. For Flaw Case 3, the growth through-wall occurs in 11.66 years. The length growth into an inspectable region occurs in 10.07 years.

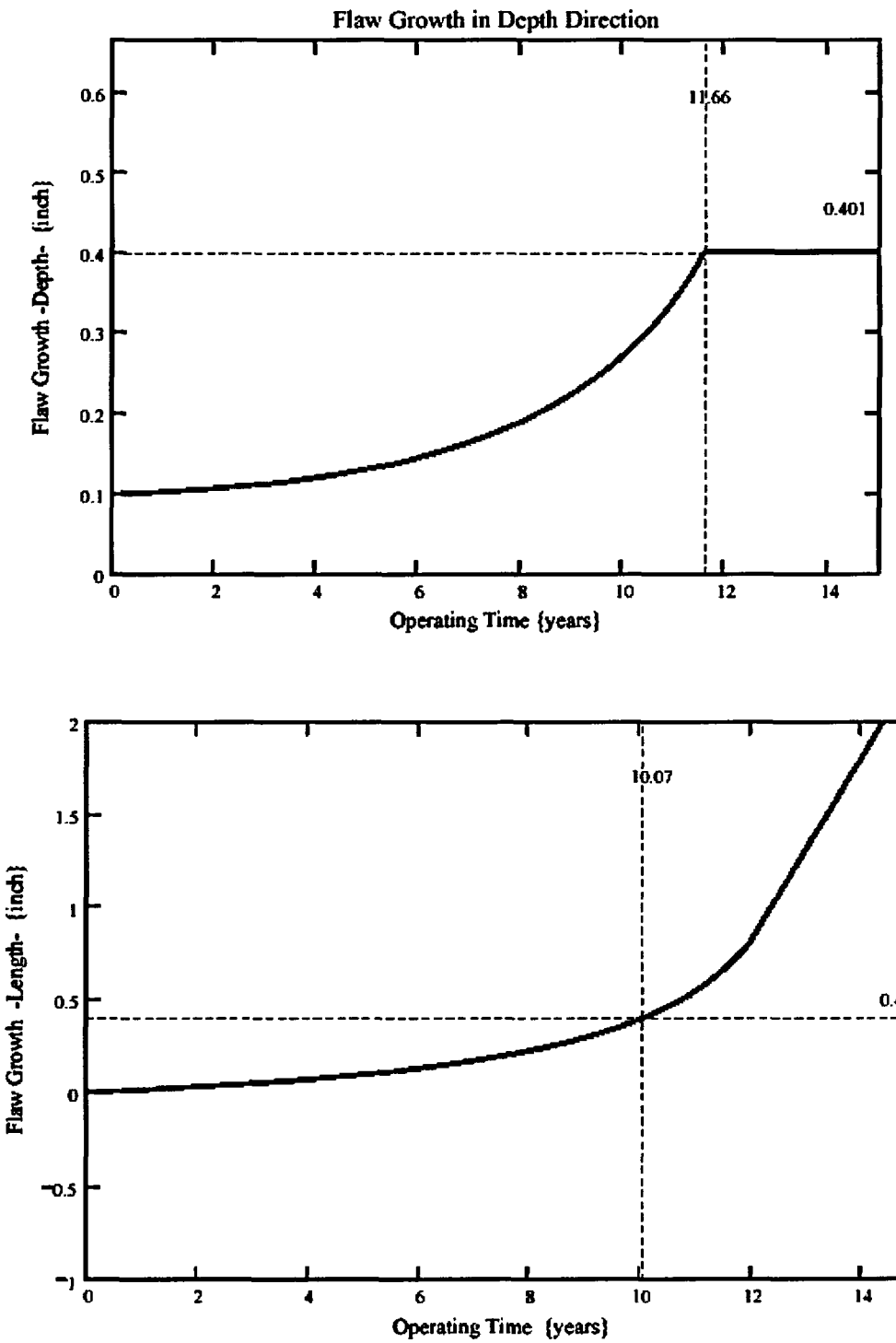

Figure 15: Flaw Case 4—Depth Growth (top) and Length Growth (bottom) versus number of operating years. For Flaw Case 4, the growth through-wall occurs in 3.68 years. The length growth into an inspectable region occurs in 2.02 years.

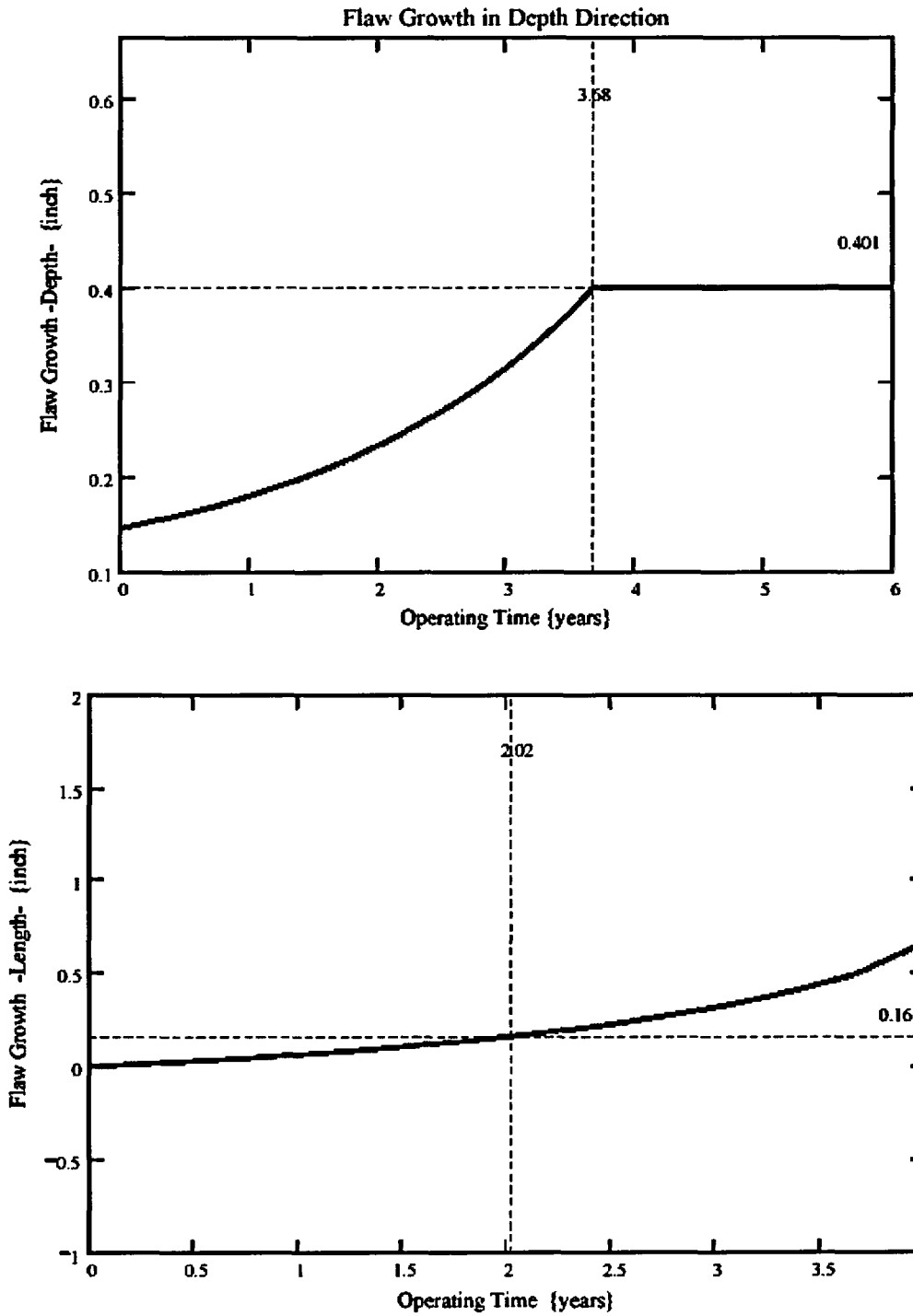

A review of DEI's FEA stress output shows the through thickness and axial distribution of hoop stresses on the downhill side (0° azimuth) of the nozzle to be higher than that for the uphill side for the same relative distance above the weld. That is, for the length of the nozzle 0.67 inch above the top of the weld on the downhill side, plus a region 0.88 inch beyond that (equivalent to the axial span of the blind zone on the uphill side), the stress distribution was similar in through-wall behavior but generally higher in magnitude. The counterbore region on the downhill side, as measured from nominal design dimensions given in Section 2.2, is 54.844 in. – 45.008 in. = 9.836 inches above the top of the weld and not subject to the requirements of the Order. Because of the higher stress field, it is reasonable to presume that under equivalent conditions, a flaw could initiate in this equivalent downhill side area more readily than on the uphill side. However, this region is inspected via UT; thus, the most susceptible location based on stresses is addressed by the current inspection coverage.

6.0 CONCLUSIONS

The evaluation performed and presented in the preceding sections support the following conclusions:

1) The uphill side (180° azimuth) of the ICI nozzle above the top of the weld possesses the highest (hoop) stresses in the vicinity of the counterbore for which a UT blind zone exists.
2) Several key assumptions that require verification were made to provide for the potential of over-sized welds on the ICI nozzles, the axial length of the blind zone, the location of the bottom of the blind zone above the top of the weld, and the circumferential extent of the blind zone.
3) The developed fracture mechanics model, incorporating a method to account for applied stress distribution variation along the ICI nozzle length, has been shown to be a reasonably realistic yet conservative representation of the expected crack growth and morphology.
4) The conservatisms used in the analysis (pressure applied to crack faces and high flaw length-to-depth aspect ratio) provide assurance that an undetected crack in a 0.88-inch blind zone region above the top of the weld on the uphill side (180° azimuth) will extend out of the blind zone and into an inspectable region at least one operating cycle (1.5 years) prior to growth through the thickness.
5) Though the downhill side (0° azimuth) of the ICI nozzle at an equivalent distance above the top of the weld is in a higher stress field and more susceptible to crack initiation, it is inspected by UT.
6) For the ID surface crack on the uphill, with the bottom of the blind zone located 0.67 inch above the top of the weld, the crack growth in the axial direction reached a detectable area at least one operating cycle prior to the crack growing through-wall. Hence, an ID surface crack at least in a region above the weld on the uphill side is not significant.
7) No potential exists for an ID circumferential crack to be located in the 135° circumferential extent of the blind zone due to the low tensile (< 10 ksi) and compressive axial stress field spanning 67.5° on either side of the uphill side (180° azimuth) of the ICI nozzle.
8) The results of this engineering report on contingent on verification of the weld and blind zone geometry for the Waterford-3 ICI Nozzles. Adjustments to this engineering report, in the form of supplemental fracture mechanics evaluations, additional finite element analyses, or alternative surface examinations would be required if the as-built weld sizes or blind zone dimensions prove to be non-conservative.

7.0 REFERENCES

1) NRC Order; Issued by letter EA-03-009 addressed to "Holders of Licenses for Operating Pressurized Water Reactors"; dated February 11, 2003.

2) Entergy Nuclear South/Central Engineering Programs Engineering Report No. M-EP-2003-003, Rev. 00, "Fracture Mechanics Analysis for the Assessment of the Potential for Primary Water Stress Corrosion Crack (PWSCC) Growth in the Un-Inspected Regions of the In-Core Instrumentation (ICI) Nozzles at Arkansas Nuclear One Unit 2"; dated September 3, 2003. [Previously sent to the NRC under Relaxation Request transmittal CNRO-2003-00035, dated September 3, 2003.]

3) Waterford-3 Drawing No. 1564-508 "Instrument Nozzles"

4) Waterford-3 Calculation No. EC-M96-021 "Analytical Report for Louisiana-Waterford Unit No. 3 Reactor Vessel"; prepared by Combustion Engineering, Inc.; dated June 1976 (CE Calc. No. CENC-1259).

5) a) "Engineering Report to Support 1.5 percent Power Uprate at Waterford 3 Steam Electric Station"; ER-WS-ST-0001, Rev. 3; September 2001.

   b) "Waterford 3 Extended Power Uprate Report"; (Draft); August 2003.

6) Entergy Nuclear South/Central Engineering Programs Engineering Report No. M-EP-2003-002, Rev. 01, "Fracture Mechanics Analysis for the Assessment of the Potential for Primary Water Stress Corrosion Crack (PWSCC) Growth in the Un-Inspected Regions of the Control Element Drive Mechanism (CEDM) Nozzles at Waterford Steam Electric Station Unit 3"; dated September 15, 2003. [Previously sent to the NRC under Relaxation Request transmittal CNRO-2003-00038, dated September 15, 2003.]

7) ASME Boiler and Pressure Vessel Code, Section III NB, 1992 Edition.

8) a) "PWSCC of Alloy 600 Materials in PWR Primary System Penetrations"; EPRI TR-103696; Electric Power Research Institute, Palo Alto, CA; July 1994.

   b) "BWR Vessel and Internals Project – Evaluation of crack growth in BWR Stainless Steel RPV Internals (BWRVIP-14)"; EPRI TR-105873; Electric Power Research Institute, Palo Alto, CA; March 1996.

   c) "BWR Vessel and Internals Project – Evaluation of crack growth in BWR Nickel Base Austenitic Alloys in RPV Internals (BWRVIP-59)"; EPRI TR-108710; Electric Power Research Institute, Palo Alto, CA; December 1998.

   d) Dominion Engineering Inc. e-mails E-4162-00-12 and E-4162-00-13, containing the nodal elevations, hoop and axial stress data, and stress plots for the Waterford-3 ICI Analysis; J. Broussard (DEI) to B. Gray (Entergy); dated September 12 and 16, 2003.

9) "Stress Intensity Factors for Part-Through Surface Cracks in Hollow Cylinders": S. R. Mettu et al; NASA TM-111707; Prepared by Lockheed Engineering & Science Services; Houston, Texas; July 1992.

10) "Materials Reliability Program (MRP) Crack Growth Rates for Evaluating Primary Water Stress Corrosion cracking (PWSCC) of Thick Wall Alloy 600 Material": MRP-55, Revision 1; Electric Power Research Institute (EPRI); dated November 13, 2002.

11) Mathcad – 11; Data Analysis Products Division; Mathsoft Inc.; Seattle WA; November 2002.

12) EPRI NDE Demonstration Report; "MRP Inspection Demonstration Program – Wesdyne Qualification": Transmitted by e-mail from B. Rassler (EPRI) to K. C. Panther (Entergy); Dated March 27, 2003.

Page 1 of 1
Design Input Revision 0

DESIGN INPUT RECORD

Document Type: _____

Document Number: _____ Document Revision: _____

Design Objective: (Attach additional sheets as required)

The purpose of this Design Input Record is to establish the applicable design inputs associated with the In-Core Instrument (ICI) nozzle configurations at ANO-2 and Waterford-3. This information will be used as input to fracture mechanics evaluations being prepared in accordance with ASME Section XI, part IWB-3600 to evaluate flaw propagation associated with potential future nozzle repairs due to PWSCC cracking in Alloy 600 material.

Design Inputs: (Identify requirement and how it is applied. Ref. DC-141, Sec. 5.1.2)
See attached sheets

Contributing Disciplines:
NOTE 1

Mechanical	_____	_____
I & C	_____	_____
Electrical	_____	_____
Civil	_____	_____
Piping	_____	_____
Structures	_____	_____
Engineering programs	_____	_____
Other	_____	_____

NOTE 1: The contributing discipline engineer shall provide his/her name beside the appropriate block.

-Lead Discipline Mechanical

-Prepared by (DA)	Jamie GoBell Jamie GoBell	Date	07/21/03
Lead Design/Responsible Engineer	JAI BRIHMADESAM	Date	
Lead Discipline Reviewer	Nara Ray Nara Ray	Date	7-24-03
-Lead Discipline Supervisor	William Sims William Sims	Date	7-30-03

The dimensions of the ICI nozzles relative to the J-groove welds and cladding surface inside the head were calculated relative to the "tangent line" that defines the radius of curvature of the head. These dimensional references are depicted in the sketch below.

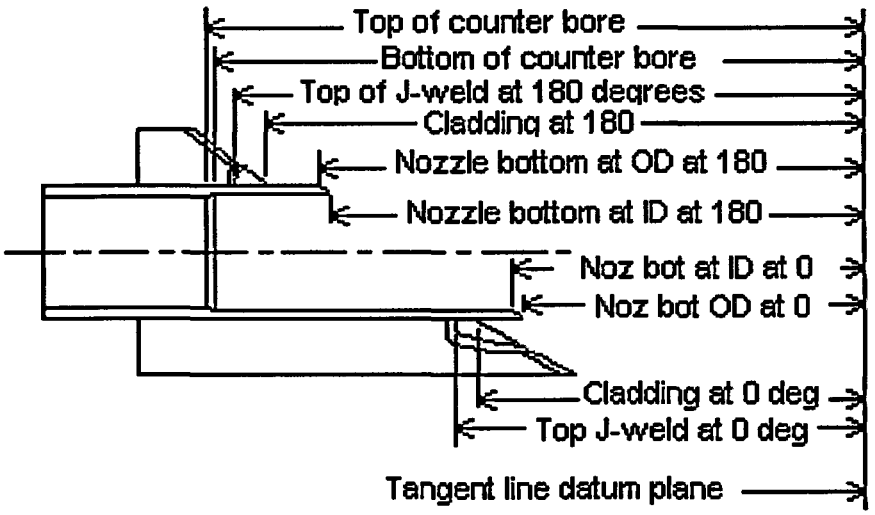

Because there is a slight variation in the location of the ICI nozzles at Waterford 3 relative to the centerline of the head, there is a very slight variation in the values calculated from nozzle to nozzle. Because the variation is very small, only one set of values is reported in the tabulated data. If desired, the specific values for a specific nozzle can be extracted from the Excel spreadsheet that calculated the values. The values for ANO-2 and Waterford 3 were calculated using Excel spreadsheets, and the results are summarized in the table below.

Dimension from the tangent line datum plane to:	ANO-2 (inches)	W-3 (inches)
Top of counter bore transition	48.625	55.094
Bottom of counter bore transition	48.375	54.844
Top of J-weld at the 180 degree (high hill side)azimuth location	46.998	53.440
Intersection of the projected cladding surface and the nozzle OD at the 180 degree (high hill side) azimuth location	46.211	52.655
Bottom (sharp corner) of the nozzle at the OD surface at the 180 degree (high hill side) azimuth location	44.211	50.618
Bottom (sharp corner) of the nozzle at the ID surface at the 180 degree (high hill side) azimuth location	43.602	50.031
Top of J-weld at the 0 degree (low hill side)azimuth location	38.283	45.008
Intersection of the projected cladding surface and the nozzle OD at the 0 degree (low hill side) azimuth location	37.875	44.589
Bottom (sharp corner) of the nozzle at the ID surface at the 0 degree (low hill side) azimuth location	36.484	43.180
Bottom (sharp corner) of the nozzle at the OD surface at the 0 degree (low hill side) azimuth location	35.875	42.594

GRAY, BRIAN C

From: John Broussard [jbroussard@domeng.com]
Sent: Tuesday, September 16, 2003 8:04 AM
To: GOBELL, JAMIE N; GRAY, BRIAN C
Subject: RE: FW: ICI As Built Figure

Jamie reasons this all out very well. I agree with all the points he makes in his last e-mail. The one thing to remember is that the location of the counterbore relative to the top of the weld is for Brian's modelling only, since this latest version of the FEA model ignores the counterbore. The dimensional components that do matter, then, for the FEA model are the ones concerning J-groove depth. The 0.256" vertical offset I described earlier does not affect this depth; in fact, the FEA model has the curvature of the head built in so the J-groove is located appropriately relative to the nozzle.

I'll get you stress plots of the ICI nozzle this morning, Brian.

John Broussard.

At 05:29 PM 9/15/2003 -0500, GOBELL, JAMIE N wrote:

>I changed my mind! After thinking about this a little more, it started
>making sense:
>
>1. I had been providing nominal dimensions relative to the weld and
>counter bore, ignoring tolerances. This resulted in a nominal distance
>from the top of the J-weld up to the bottom of the counter bore of 1.4
>inches.
>
>2. Based on NED examination data, Jai wanted to increase the weld size
>to a point where the top of the J-weld was 0.3 inches closer to the
>counter bore than I had been calling out as the "design" value.
>
>3. If I stack up the tolerances in that direction, the "design" would
>allow the top of the J-weld to be 0.994 inches below the counter bore
>as the absolute minimum and still be within the design drawing.
>
>4. Based on this, it appears that during installation, they typically
>ate into those tolerance values. This makes sense: If I tell a
>craftsman that anything between 1 and 2 is acceptable, he will shoot
>for 1.5.
>
>So what should we (dominion) model? They should model a weld that is
>the worst case. In this case, the worst case design puts the top of
>the J-weld at 0.994 inches below the bottom of the counter bore. The
>latest Dominion model that uses 1.261 inches nominal, then increases
>the size by 0.3 inches gives a model where the top of the J-weld is
>0.96 inches below the bottom of the counter bore. The 0.96 bounds the
>worst case design configuration, therefore, your SHOULD use the latest
>model (1.261") to predict the residual stress distributions. The first
>model (that ended up with 0.71" from the weld to the counter bore)
>would be overly conservative. The only advantage that you would get
>from using the 0.71" model is that you would have less chance of
>discovering a configuration that was not bounded by the analysis.
>However, examinations at ANO would indicate that it is not likely that
>the welds exceed the worst case design tolerance.
>
>Ok, that's my last $0.02 worth.
>
>Jamie
>
>
>-----Original Message-----

>From: GOBELL, JAMIE N
>Sent: Monday, September 15, 2003 4:57 PM
>To: GRAY, BRIAN C
>Cc: 'jbroussard@domeng.com'
>Subject: RE: FW: ICI As Built Figure
>
>
>Brian,
>
>I think you can use the first figure that John sent (with 1.01 inches
>from the top of the J-weld up to the bottom of the counter bore) if
>your analysis will pass. My basis for this is that if you use the
>numbers that were used to get to the 1.261" dimension below, except
>that you use the whole tolerance for the depth of the J-weld prep and
>the minimum cladding thickness, you get:
>
>89-46.40625+12.25 = 54.84375" (tangent line to bottom of counter bore)
>52.895+1.0-0.125 = 53.77" (tangent line to top of J-weld) 54.84375 -
>53.77 = 1.07375"
>
>Pretty close the John's original 1.01, and 1.01 is pretty close to my
>0.994" worst case. There is no need for John to do any extra work to
>change their analysis model from 1.01 to 1.261. The 1.01" model would
>be more conservative, but since we are going to have to validate either
>one with the actual field examinations, you can go with whichever one
>passes. If this doesn't make sense, give me a call.
>
>Jamie
>
>
>-----Original Message-----
>From: GRAY, BRIAN C
>Sent: Monday, September 15, 2003 4:02 PM
>To: GOBELL, JAMIE N
>Subject: FW: FW: ICI As Built Figure
>
>
>
>
>-----Original Message-----
>From: John Broussard [mailto:jbroussard@domeng.com]
>Sent: Monday, September 15, 2003 3:45 PM
>To: GRAY, BRIAN C
>Subject: Re: FW: ICI As Built Figure
>
>
>Brian,
>
>Attached is a corrected figure to account for the 0.256" difference in
>elevation that arises from using a straight 55.3 degree line for the
>head inside radius as opposed to the actual radius of curvature at the
>working point for the uphill side J-groove at the ICI nozzle.
>
>When it comes to splitting tolerances, I should have been more
>specific. We really only split the difference on tolerances in setting
>up the J-groove weld cavity. We did not split the difference on
>tolerances for the buttering thickness, the nozzle length, and the
>height of the ICI counterbore. That is probably the reason why we
>stopped splitting the difference on tolerances - too many things to
>split the difference on.
>
>The 0.256" should be the major source of discrepancy. Jamie can check
>it and let me know, but I agree with the rest of his numbers. If you
>remove the splits for the buttering thickness, nozzle length, and ICI
>counterbore height, I calculate 1.26" for the height as follows:
>

>89-46.40625+12.25 = 54.84375" (tangent line to bottom of counterbore)
>52.895+0.9375-0.25 = 53.5825" (tangent line to top of J-weld) 54.84375
>- 53.5825 = 1.261"
>
>
>
>At 02:10 PM 9/15/2003 -0500, you wrote:
>
>>Jamie Gobell gets a value of 1.355", from the top of the weld to the
>>bottom of the counterbore, by splitting the difference in the
>>tolerances, the same as you did. He used the following drawings (CE
>>drawing numbers):
>>
>>74170-108-001
>>74170-101-005
>>74170-101-002
>>E-9270-160X (I can not read the last digit, if there is one, of this
>>document)
>>
>>Can you help troubleshoot the discrepancies between your numbers and
>>his?
>>
>>If you have any questions, let me know.
>>
>>Thanks,
>>
>>
>>Brian C. Gray
>>Central Engineering Programs
>>M-ECH-36
>>Phone: 601-368-5419 (internal: 8-433-5419)
>>Fax: 601-368-5394 (internal: 8-433-5394)
>>Email: bgray1@entergy.com
>>
>>
>>-----Original Message-----
>>From: GOBELL, JAMIE N
>>Sent: Monday, September 15, 2003 1:50 PM
>>To: GRAY, BRIAN C
>>Subject: RE: ICI As Built Figure
>>
>>
>>No, I get 1.355 if I split the difference between ALL the tolerances
>>(see basis below).
>>
>>Working from the tangent line datum, the drawing shows the following
>>dimensions:
>>
>>Top of ICI nozzles: 8+81(+1/4", -0.0") split the tolerance = 89.125"
>>Cladding intersection with 5-13/16" dia. Working point - the 5-13/16"
>>diameter could be as large as 5-5/16" + [2 X 1/4" (+1/8", -0.0")]:
>>split the 1/8" = 52.895" Working point up to J-weld prep in base metal:
>>7/8" (+1/8", -0.0") split = 0.9375" Cladding nominal is 1/4", minimum is 1/8" per note
>>1: split = 0.187 5" Length of nozzle: 46.40625 (no tolerance specified Bottom of nozzle
to bottom
>>of counterbore: 12.25 (+1/16",-0.0") split = 12.28125"
>>
>>Addition: 89.125-46.40625+12.28125 = 55" (tangent line to bottom of
>>counterbore
>> 52.895+0.9375-0.1875 = 53.645" (tangent line to top of J-weld)
>> 55 - 53.645 = 1.355"
>>
>>If I remove the 1/16" tolerance on the bottom of nozzle to bottom of
>>counterbore, and remove half of the 1/4" to the top of the nozzle, I'm
>>still 0.1575" different from what Dominion got.
>>

>>Jamie
>>
>>
>>-----Original Message-----
>>From: GRAY, BRIAN C
>>Sent: Monday, September 15, 2003 12:21 PM
>>To: GOBELL, JAMIE N
>>Subject: FW: ICI As Built Figure
>>
>>
>>This is what I was referring to on my phone message. Can you concur
>>with Dominion's sketch? (John Broussard said for the W-3 ICI, they
>>split the difference on most of the tolerances to give them this 1.01"
>>dimension. It is close to your 0.996" dimension that you mentioned
>>about 2 weeks ago.)
>>
>>Brian C. Gray
>>Central Engineering Programs
>>M-ECH-36
>>Phone: 601-368-5419 (internal: 8-433-5419)
>>Fax: 601-368-5394 (internal: 8-433-5394)
>>Email: bgray1@entergy.com
>>
>>
>>-----Original Message-----
>>From: John Broussard [mailto:jbroussard@domeng.com]
>>Sent: Monday, September 15, 2003 12:18 PM
>>To: GRAY, BRIAN C
>>Subject: ICI As Built Figure
>>
>>
>>Brian,
>>
>>As we discussed, attached is a figure for the ICI As Built model, with
>>the additional J-groove weld depth shown as well as the location of the
>>bottom of the counterbore. As I mentioned, these models are based on
>>nominal plus "split the difference" on tolerances, so the distance from
>>the top of the weld to the bottom of the counterbore is lower than what
>>one would calculate using purely nominal dimensions.
>>
>>
>>John Broussard, P.E.
>>Dominion Engineering, Inc.
>>E-mail: jbroussard@domeng.com
>>Phone : 703-437-7826 x236
>>Fax : 703-437-0780
>
>
>John Broussard, P.E.
>Dominion Engineering, Inc.
>E-mail: jbroussard@domeng.com
>Phone : 703-437-7826 x236
>Fax : 703-437-0780

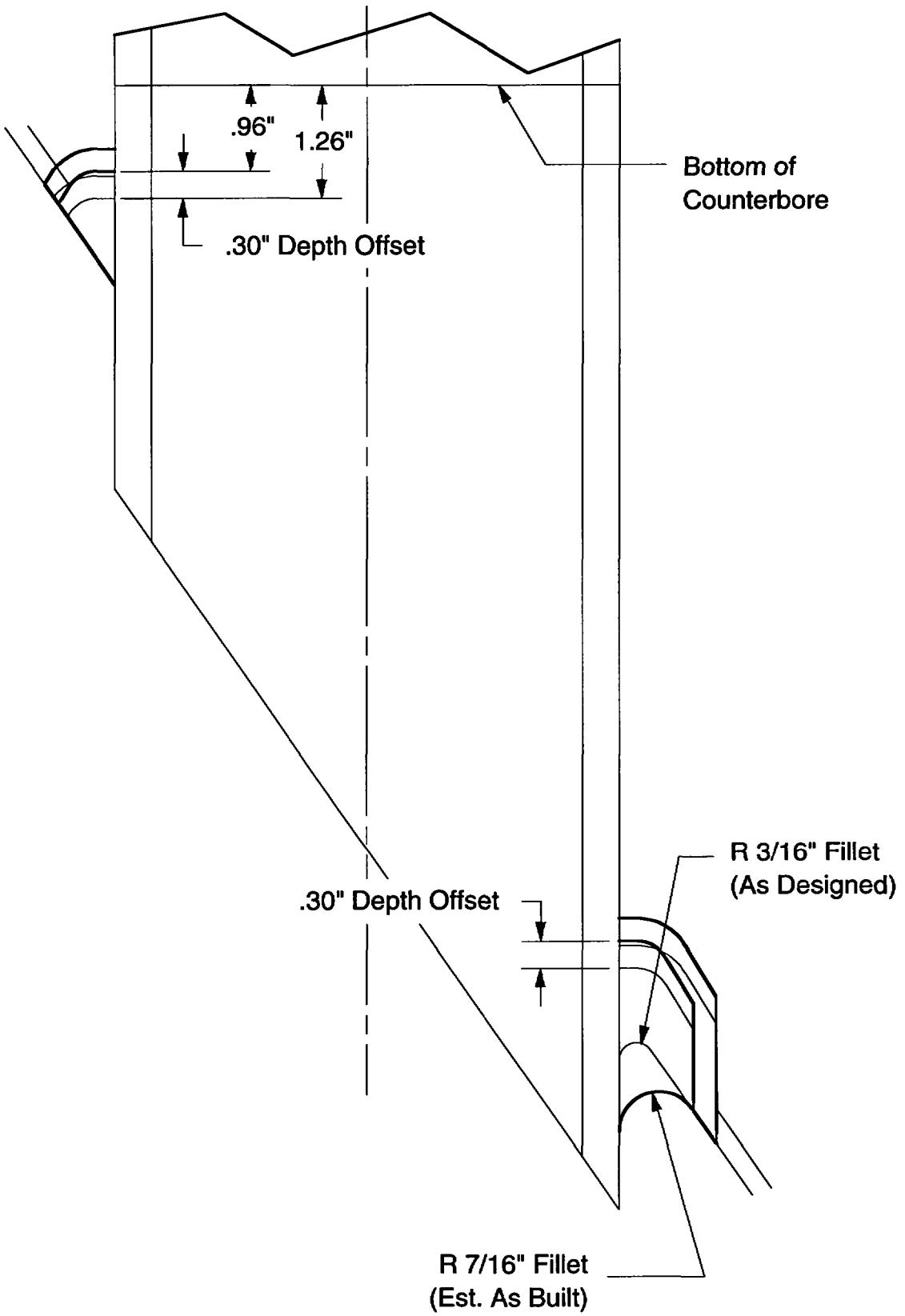
.96"
1.26"
Bottom of
Counterbore
.30" Depth Offset
R 3/16" Fillet
(As Designed)
.30" Depth Offset
R 7/16" Fillet
(Est. As Built)

GRAY, BRIAN C

From: John Broussard [jbroussard@domeng.com]
Sent: Friday, September 12, 2003 2:26 PM
To: GRAY, BRIAN C
Subject: E-4162-00-12, Waterford 3 ICI Alternate As-Built Results

Waterford As Built ICI Data - ...

Brian,

Attached is an Excel spreadsheet with the analysis data for the Waterford 3 "alternate" as-built ICI nozzle model. This model has a straight 4.75" ID (no internal counterbore) and has a 0.3" inch deeper J-groove weld along with the 7/16" fillet radius used for the previous as-built model. Additionally, this model has much greater refinement in the nozzle above the top of the weld. The following data are included:

1. Through-wall hoop stress data for the nodes from the bottom of the nozzle to the top of the weld, on the tab labeled "Waterford 3 ICI - Below Weld". Also included on this tab are detailed elevations for the nozzle nodes below the weld, which are not straight across the nozzle wall. Data are presented for every circumferential plane in the model.

2. Through-wall hoop and axial stress data for the nodes from the top of the weld to the top of the nozzle, on the tab labeled "Waterford 3 ICI - Above Weld". Because the nozzle mesh is much more uniform without the presence of the ID counterbore, there is only one elevation listed per nodal row.

If you have any questions or require further information, do not hesitate to call or e-mail.

John Broussard, P.E.
Dominion Engineering, Inc.
E-mail: jbroussard@domeng.com
Phone : 703-437-7826 x236
Fax : 703-437-0780

ALL STRESSES REPORTED IN KSI

HOOP STRESS

	Row	Height	ID	25%	50%	75%	OD
Weld Top	1301	3.286	44.221	45.032	48.733	49.561	48.079
	1401	3.592	41.671	40.559	39.665	37.353	34.993
	1501	3.853	38.853	34.912	30.504	28.733	29.337
	1601	4.140	35.919	31.936	29.285	25.975	18.897
Downhill Plane	1701	4.459	31.758	29.037	26.431	20.174	5.330
	1801	4.811	28.233	26.014	22.414	13.028	-2.972
	1901	5.201	25.205	22.192	18.089	7.566	-4.826
	2001	5.632	20.631	18.677	15.063	5.132	-3.623
	2101	6.108	18.170	16.794	12.949	5.372	-0.679
	2201	6.636	17.232	16.081	11.799	6.921	2.986
	2301	7.219	16.904	15.414	11.539	8.255	5.406
	2401	7.864	17.103	15.375	11.897	9.076	6.544
	2501	8.577	17.902	16.181	12.578	9.648	6.841
	2601	9.367	18.979	17.317	13.396	10.108	6.929
	2701	10.240	19.881	18.050	13.639	10.044	6.665
	2801	11.206	19.958	17.783	13.038	9.105	5.204
	2901	12.274	20.433	17.618	13.358	9.639	5.775
	3001	13.456	19.070	14.964	10.322	6.073	2.015
	3101	14.763	16.038	10.144	5.153	0.397	-4.322
	3201	16.209	15.986	11.462	7.372	3.463	-0.242
	3301	25.504	15.244	14.522	13.836	13.239	12.788
Weld Top	11301	3.370	39.524	40.400	42.160	42.921	47.857
	11401	3.669	36.958	34.783	33.402	32.908	35.007
	11501	3.917	33.499	30.584	27.797	27.501	29.405
	11601	4.192	30.816	28.153	25.531	21.820	15.863
22.5° From	11701	4.498	28.698	25.974	22.702	16.480	6.335
Downhill Plane	11801	4.837	26.621	22.770	19.308	11.386	0.098
	11901	5.213	23.730	19.499	16.215	7.568	-2.187
	12001	5.631	20.395	17.145	14.084	5.963	-1.401
	12101	6.095	18.468	15.850	12.623	6.213	0.710
	12201	6.609	17.169	15.318	11.671	7.554	3.853
	12301	7.181	16.330	14.741	11.455	8.750	6.122
	12401	7.815	16.171	14.459	11.863	9.666	7.568
	12501	8.518	16.830	14.952	12.493	10.388	8.319
	12601	9.299	17.581	15.676	12.979	10.615	8.364
	12701	10.166	18.996	16.889	13.922	11.247	8.672
	12801	11.129	18.309	16.165	13.073	10.435	7.974
	12901	12.197	16.910	14.523	11.591	9.189	6.941
	13001	13.382	15.240	12.315	9.154	6.399	3.963
	13101	14.698	13.092	8.920	5.386	2.119	-1.043
	13201	16.158	13.686	10.132	7.091	4.212	1.347
	13301	25.198	15.026	14.378	13.783	13.270	12.885
Weld Top	21301	3.479	29.801	29.619	28.235	27.749	31.862
	21401	3.767	28.755	27.231	25.489	26.468	28.811
	21501	4.002	27.050	25.010	21.007	18.587	20.222
	21601	4.263	25.618	23.576	19.145	14.836	14.986

HOOP STRESS

	Row	Height	ID	25%	50%	75%	OD
45° From Downhill Plane	21701	4.554	24.224	21.549	17.299	11.875	9.676
	21801	4.877	22.106	18.553	15.192	9.442	4.856
	21901	5.238	20.193	16.484	13.639	7.995	2.983
	22001	5.639	18.757	15.038	12.867	8.101	3.645
	22101	6.086	17.463	13.917	11.778	8.368	5.117
	22201	6.583	15.219	13.115	11.235	9.274	7.207
	22301	7.138	13.018	12.275	11.121	10.216	9.065
	22401	7.755	12.270	11.882	11.483	11.160	10.710
	22501	8.442	12.492	12.144	11.967	11.793	11.640
	22601	9.207	13.478	13.102	12.717	12.395	12.224
	22701	10.059	13.954	13.034	12.306	11.633	10.845
	22801	11.007	13.583	12.477	11.607	10.833	10.017
	22901	12.064	12.289	11.358	10.688	10.112	9.472
	23001	13.240	9.417	8.741	8.113	7.578	7.185
	23101	14.550	8.447	7.438	6.492	5.671	5.083
	23201	16.009	10.108	8.736	7.745	6.866	5.896
	23301	24.328	14.606	14.125	13.827	13.570	13.279
Weld Top	31301	3.575	27.740	23.680	19.201	18.134	17.153
	31401	3.852	27.255	24.756	18.835	16.225	13.456
	31501	4.072	25.790	24.354	17.188	11.235	9.737
	31601	4.318	24.216	22.876	16.208	10.352	10.905
67.5° From Downhill Plane	31701	4.593	22.611	20.935	15.346	9.743	8.868
	31801	4.901	20.373	18.329	14.405	9.686	7.276
	31901	5.244	17.718	15.910	13.048	9.416	7.228
	32001	5.627	14.868	13.422	11.565	9.588	8.053
	32101	6.055	11.844	11.347	10.855	10.307	9.953
	32201	6.533	8.888	9.510	10.290	11.087	12.018
	32301	7.067	6.561	8.623	10.471	12.194	13.939
	32401	7.664	5.858	8.559	10.939	13.187	15.306
	32501	8.330	7.428	9.386	11.697	13.927	15.634
	32601	9.074	7.592	9.744	11.792	13.690	15.344
	32701	9.906	8.125	9.622	11.161	12.528	13.456
	32801	10.834	8.372	9.542	10.832	11.991	12.860
	32901	11.871	6.930	8.197	9.587	10.782	11.575
	33001	13.030	5.797	7.198	8.660	9.968	10.878
	33101	14.324	6.054	7.372	8.600	9.726	10.737
	33201	15.769	8.109	8.719	9.519	10.348	10.995
	33301	23.024	14.757	14.217	14.095	13.970	13.568
Weld Top	41301	3.628	23.140	17.964	14.076	14.236	10.827
	41401	3.892	24.976	22.067	15.699	11.580	8.258
	41501	4.099	25.962	23.843	15.408	8.651	3.411
	41601	4.331	25.837	23.334	15.281	8.539	8.014
90° From Downhill Plane	41701	4.591	24.176	21.194	14.718	8.701	8.306
	41801	4.882	20.813	18.189	14.158	10.047	8.136
	41901	5.208	15.689	14.235	12.014	9.901	8.744
	42001	5.573	9.236	9.828	9.911	9.871	10.079
	42101	5.983	4.977	7.359	9.210	10.965	12.813
	42201	6.441	2.342	6.172	9.414	12.471	15.615

HOOP STRESS

	Row	Height	ID	25%	50%	75%	OD
	42301	6.955	1.259	5.828	9.935	13.837	17.454
	42401	7.530	0.914	6.145	10.528	14.636	18.818
	42501	8.174	2.508	6.833	10.939	14.833	18.631
	42601	8.896	3.397	7.445	11.060	14.489	17.921
	42701	9.705	3.489	7.379	10.907	14.259	17.484
	42801	10.611	2.525	6.383	9.959	13.397	16.593
	42901	11.625	2.278	6.098	9.674	13.134	16.392
	43001	12.762	3.065	6.451	9.760	12.960	15.807
	43101	14.036	5.242	7.913	10.459	12.912	15.110
	43201	15.462	7.981	9.487	11.056	12.612	13.966
	43301	21.487	15.165	14.274	14.012	13.736	13.012
Weld Top	51301	3.857	22.674	18.118	15.774	15.755	13.226
	51401	4.109	27.811	22.485	16.839	13.071	11.121
	51501	4.304	29.289	24.341	15.836	9.079	2.421
	51601	4.523	28.042	23.833	15.463	8.394	5.757
112.5° From	51701	4.769	24.680	20.913	14.452	8.848	7.773
Downhill Plane	51801	5.046	18.448	15.790	12.318	9.757	8.338
	51901	5.356	9.843	9.631	9.125	8.585	8.517
	52001	5.705	5.166	6.720	8.082	9.267	10.511
	52101	6.097	3.035	5.889	8.668	11.301	13.594
	52201	6.537	2.139	6.009	9.556	12.969	16.217
	52301	7.031	2.710	6.688	10.492	14.085	17.466
	52401	7.587	3.429	7.413	11.142	14.753	18.085
	52501	8.211	3.962	7.717	11.233	14.626	17.652
	52601	8.912	4.219	7.746	11.202	14.556	17.475
	52701	9.699	4.079	7.587	10.997	14.297	17.196
	52801	10.584	4.166	7.693	11.101	14.409	17.321
	52901	11.578	4.719	8.126	11.288	14.352	17.177
	53001	12.694	6.085	8.948	11.607	14.189	16.622
	53101	13.948	7.931	10.082	11.966	13.794	15.625
	53201	15.356	10.144	11.216	12.192	13.153	14.131
	53301	20.175	15.163	13.945	13.324	12.723	11.760
Weld Top	61301	4.023	31.328	27.117	23.901	20.399	23.262
	61401	4.266	33.266	27.991	20.765	13.425	4.287
	61501	4.450	32.145	27.397	17.847	8.494	0.811
	61601	4.659	29.542	25.239	16.545	9.285	5.294
135° From	61701	4.893	24.037	20.162	14.069	8.281	5.624
Downhill Plane	61801	5.157	15.389	12.993	10.167	7.307	5.394
	61901	5.454	9.004	8.511	7.453	6.656	5.946
	62001	5.789	8.288	8.552	8.618	8.745	8.767
	62101	6.166	8.870	9.399	9.933	10.440	11.076
	62201	6.591	9.843	10.548	11.196	11.860	12.592
	62301	7.069	10.750	11.293	11.893	12.520	13.054
	62401	7.608	11.439	11.766	12.292	12.846	13.213
	62501	8.215	11.668	11.942	12.399	12.899	13.243
	62601	8.899	11.769	12.055	12.436	12.851	13.220
	62701	9.669	11.946	12.214	12.519	12.838	13.163
	62801	10.536	12.255	12.396	12.591	12.770	12.949

HOOP STRESS

	Row	Height	ID	25%	50%	75%	OD
	62901	11.513	12.539	12.555	12.617	12.658	12.675
	63001	12.614	12.792	12.667	12.599	12.508	12.385
	63101	13.853	13.019	12.807	12.654	12.514	12.342
	63201	15.249	13.448	13.114	12.790	12.495	12.275
	63301	19.062	14.379	13.299	12.575	11.913	11.128
Weld Top	71301	4.135	39.971	35.691	31.194	24.423	31.864
	71401	4.370	37.873	31.506	23.824	15.247	3.376
	71501	4.546	35.659	30.545	21.503	9.919	6.000
	71601	4.746	30.497	26.887	18.780	8.848	2.036
167.5° From	71701	4.971	24.142	20.896	14.750	7.911	3.201
Downhill Plane	71801	5.224	16.550	13.221	8.291	3.527	-0.036
	71901	5.511	14.982	12.319	8.190	4.420	1.182
	72001	5.835	16.107	13.897	10.198	6.869	3.846
	72101	6.201	17.136	15.401	11.947	8.811	5.852
	72201	6.614	18.124	16.422	12.990	9.842	6.794
	72301	7.080	18.871	17.112	13.616	10.381	7.242
	72401	7.606	19.330	17.427	13.788	10.451	7.264
	72501	8.201	19.572	17.477	13.731	10.336	7.107
	72601	8.872	19.713	17.369	13.592	10.217	6.996
	72701	9.630	19.738	17.098	13.432	10.193	7.089
	72801	10.486	19.413	16.660	13.240	10.246	7.385
	72901	11.453	19.000	16.000	13.034	10.411	7.889
	73001	12.544	18.041	15.280	12.915	10.704	8.607
	73101	13.776	16.937	14.718	12.907	11.230	9.572
	73201	15.168	15.717	14.214	12.949	11.773	10.647
	73301	18.318	13.049	12.531	12.153	11.845	11.554
Weld Top	81301	4.205	39.763	38.158	34.368	27.002	41.729
	81401	4.435	37.068	33.351	25.957	16.947	6.333
	81501	4.605	34.079	32.268	24.632	11.934	5.354
	81601	4.798	29.820	28.465	21.515	10.551	3.714
Uphill Plane	81701	5.015	23.668	21.543	14.530	5.734	0.010
	81801	5.262	18.722	14.133	7.280	0.963	-4.004
	81901	5.541	18.383	15.071	8.650	3.277	-1.652
	82001	5.857	18.876	17.269	11.236	6.243	1.578
	82101	6.214	19.527	18.517	12.761	7.898	3.319
	82201	6.619	20.331	19.550	13.998	9.088	4.422
	82301	7.077	20.976	20.149	14.467	9.428	4.629
	82401	7.596	21.408	20.378	14.437	9.275	4.330
	82501	8.183	21.667	20.400	14.263	9.100	4.150
	82601	8.847	21.792	20.133	13.976	8.964	4.177
	82701	9.599	21.742	19.395	13.664	8.987	4.508
	82801	10.451	21.550	18.466	13.362	9.158	5.143
	82901	11.415	21.213	17.311	13.126	9.525	6.042
	83001	12.505	19.876	16.176	13.009	10.038	7.179
	83101	13.740	18.311	15.380	12.983	10.759	8.539
	83201	15.138	16.442	14.525	12.960	11.508	10.066
	83301	18.057	12.330	12.146	12.033	11.987	11.973

AXIAL STRESS

Row	ID	25%	50%	75%	OD
1301	21.367	23.522	27.990	30.088	28.153
1401	25.075	27.101	30.256	31.662	31.873
1501	30.831	29.895	28.592	25.383	18.260
1601	33.877	31.596	29.533	22.278	12.158
1701	32.217	30.780	29.125	20.505	4.789
1801	29.163	28.845	27.823	20.207	1.605
1901	26.353	26.128	26.180	19.766	5.658
2001	23.203	23.796	25.037	18.750	11.254
2101	20.935	22.617	23.744	20.003	16.633
2201	20.095	22.016	22.289	21.252	20.448
2301	20.177	21.611	21.980	22.009	22.230
2401	20.331	21.330	21.790	22.151	22.599
2501	20.018	21.026	21.412	21.660	21.873
2601	19.161	20.195	20.484	20.626	20.657
2701	18.185	18.960	18.812	18.693	18.594
2801	17.225	17.542	16.989	16.426	15.678
2901	14.927	14.974	15.038	14.897	14.494
3001	12.576	11.841	11.185	10.449	9.765
3101	12.269	9.291	6.780	4.188	1.462
3201	10.326	7.838	5.757	3.731	1.486
3301	6.783	6.620	6.165	5.681	5.540
11301	25.367	27.041	29.878	32.478	34.514
11401	29.113	28.940	29.338	30.300	33.952
11501	32.152	30.442	28.152	25.407	22.922
11601	32.626	30.581	27.180	19.887	14.318
11701	31.602	29.719	26.505	18.653	8.435
11801	29.481	27.677	25.834	18.835	6.073
11901	26.277	25.378	25.139	18.312	7.791
12001	22.875	23.561	24.250	18.124	11.795
12101	20.705	22.466	22.610	18.805	15.280
12201	20.342	21.699	21.017	19.426	17.889
12301	20.509	20.939	20.438	19.893	19.324
12401	20.144	20.316	20.253	20.225	20.177
12501	19.491	19.780	19.981	20.244	20.406
12601	18.307	18.811	19.181	19.627	20.023
12701	17.887	18.126	18.150	18.203	18.222
12801	16.185	16.101	15.718	15.454	15.200
12901	13.206	13.176	13.165	13.249	13.343
13001	11.612	11.012	10.406	9.898	9.477
13101	11.686	9.343	7.354	5.374	3.298
13201	9.250	7.336	5.856	4.418	2.713
13301	6.391	6.283	5.976	5.645	5.555
21301	36.782	34.907	32.722	31.141	29.639
21401	38.331	36.099	34.269	35.553	39.175
21501	38.069	34.882	31.059	27.404	25.881
21601	36.150	33.503	29.267	23.421	20.833

AXIAL STRESS

Row	ID	25%	50%	75%	OD
21701	33.410	30.944	27.362	20.745	16.667
21801	29.153	26.889	24.964	18.255	11.631
21901	25.103	24.273	23.197	16.609	10.451
22001	22.302	22.862	21.396	16.148	11.096
22101	21.068	21.492	19.076	15.302	11.661
22201	20.236	19.772	17.723	15.368	12.963
22301	18.734	18.186	17.088	16.083	14.869
22401	16.878	17.011	17.128	17.287	17.314
22501	15.063	15.915	16.871	17.783	18.686
22601	14.499	15.396	16.289	17.178	18.074
22701	13.589	14.083	14.727	15.383	15.880
22801	12.399	12.741	13.256	13.793	14.234
22901	11.101	11.152	11.368	11.598	11.708
23001	9.809	9.397	9.027	8.691	8.369
23101	9.274	8.354	7.525	6.750	5.999
23201	6.918	6.186	5.770	5.362	4.749
23301	5.939	5.925	5.928	5.929	5.943
31301	40.712	36.624	31.839	29.336	24.868
31401	40.467	36.965	31.793	29.971	28.628
31501	38.123	35.238	29.668	24.531	22.195
31601	34.914	33.110	28.793	23.480	22.673
31701	32.254	30.543	26.748	20.991	18.615
31801	28.468	26.670	23.707	18.275	14.477
31901	24.689	23.032	19.600	14.074	10.116
32001	22.310	19.865	16.285	11.970	8.167
32101	19.696	17.468	14.768	11.867	9.145
32201	16.213	15.018	13.729	12.658	11.621
32301	12.716	13.196	13.581	14.040	14.519
32401	10.122	11.729	13.210	14.667	16.070
32501	9.809	11.310	13.002	14.696	16.154
32601	8.938	10.489	12.051	13.524	14.839
32701	8.484	9.413	10.406	11.304	11.931
32801	8.734	9.090	9.546	9.933	10.160
32901	8.035	8.220	8.491	8.690	8.731
33001	7.285	7.624	7.975	8.245	8.384
33101	6.356	6.721	7.102	7.490	7.821
33201	5.049	5.309	5.741	6.148	6.403
33301	6.097	5.973	6.052	6.173	6.136
41301	35.781	31.149	26.847	25.721	21.956
41401	35.163	31.569	25.495	22.407	21.126
41501	33.477	30.510	22.914	16.858	12.683
41601	31.365	28.485	22.514	17.036	16.157
41701	28.841	25.651	20.349	14.370	13.240
41801	25.073	22.135	17.560	12.577	10.379
41901	19.771	16.873	12.680	8.787	6.459
42001	13.343	11.432	9.020	6.664	4.671
42101	9.530	9.081	8.409	7.774	7.216
42201	6.470	7.540	8.390	9.233	10.231

AXIAL STRESS

Row	ID	25%	50%	75%	OD
42301	4.312	6.405	8.331	10.286	12.142
42401	3.107	5.780	8.151	10.475	12.904
42501	3.622	5.614	7.665	9.787	11.995
42601	4.501	5.914	7.286	8.622	9.906
42701	5.337	6.457	7.549	8.643	9.612
42801	5.173	6.382	7.570	8.770	9.858
42901	5.067	6.521	7.971	9.473	10.859
43001	4.775	6.149	7.593	9.037	10.292
43101	4.782	5.742	6.737	7.781	8.674
43201	4.614	5.188	5.838	6.440	6.922
43301	6.392	6.023	5.997	6.022	5.777
51301	27.885	22.921	19.570	19.035	18.997
51401	29.346	23.198	16.672	13.493	12.681
51501	27.985	22.121	12.804	6.387	-0.197
51601	25.775	20.643	11.897	4.884	2.342
51701	22.691	17.895	10.184	3.569	1.950
51801	16.797	12.717	7.223	2.658	0.090
51901	8.348	6.091	3.020	-0.262	-2.337
52001	3.662	2.805	1.525	0.057	-0.871
52101	0.738	1.300	1.764	2.229	2.665
52201	-0.905	0.803	2.397	4.048	5.741
52301	-0.998	0.998	2.953	4.908	6.845
52401	0.277	2.015	3.764	5.529	7.121
52501	1.785	3.148	4.533	5.923	7.077
52601	2.940	4.174	5.478	6.792	7.876
52701	3.587	4.914	6.277	7.660	8.871
52801	3.987	5.463	6.974	8.505	9.852
52901	4.244	5.654	7.028	8.427	9.719
53001	4.589	5.663	6.748	7.835	8.813
53101	4.820	5.586	6.306	7.045	7.750
53201	4.983	5.443	5.891	6.301	6.699
53301	6.532	6.054	5.951	5.864	5.497
61301	14.755	10.447	7.863	5.612	13.262
61401	18.633	12.317	4.486	-2.346	-13.240
61501	19.332	13.278	1.575	-8.530	-16.853
61601	18.594	12.174	0.801	-7.926	-11.657
61701	14.376	8.026	-0.901	-8.143	-11.408
61801	6.427	2.592	-2.446	-7.071	-10.102
61901	-0.372	-1.870	-4.146	-6.224	-7.738
62001	-2.571	-2.732	-3.147	-3.461	-3.591
62101	-3.335	-2.555	-1.860	-1.188	-0.371
62201	-2.598	-1.416	-0.275	0.857	2.008
62301	-0.743	0.183	1.196	2.190	3.054
62401	1.170	1.760	2.514	3.259	3.836
62501	2.642	3.130	3.744	4.370	4.886
62601	3.787	4.248	4.803	5.372	5.875
62701	4.606	5.051	5.566	6.076	6.532
62801	5.216	5.556	5.988	6.392	6.722

AXIAL STRESS

Row	ID	25%	50%	75%	OD
62901	5.683	5.915	6.226	6.499	6.693
63001	5.972	6.070	6.277	6.454	6.529
63101	5.877	6.000	6.202	6.373	6.464
63201	5.909	5.974	6.071	6.168	6.250
63301	6.529	6.172	6.080	5.973	5.692
71301	15.587	9.545	0.755	-7.993	9.427
71401	17.536	11.038	-2.904	-15.957	-28.954
71501	17.133	11.806	-3.420	-16.260	-20.185
71601	13.997	8.010	-3.685	-14.140	-20.637
71701	9.020	4.106	-2.721	-9.294	-13.697
71801	2.200	-0.009	-3.774	-7.378	-9.981
71901	-1.798	-2.074	-3.345	-4.703	-5.555
72001	-2.840	-2.580	-2.515	-2.529	-2.368
72101	-2.123	-1.696	-1.219	-0.839	-0.441
72201	-0.462	-0.298	-0.032	0.162	0.284
72301	1.392	1.282	1.147	0.950	0.672
72401	3.064	2.777	2.306	1.806	1.259
72501	4.450	4.029	3.326	2.609	1.845
72601	5.529	4.997	4.169	3.359	2.479
72701	6.344	5.760	4.929	4.131	3.271
72801	6.942	6.319	5.575	4.884	4.118
72901	7.348	6.652	6.060	5.485	4.846
73001	7.438	6.764	6.308	5.874	5.373
73101	7.044	6.602	6.373	6.127	5.790
73201	6.686	6.411	6.279	6.160	5.975
73301	6.495	6.311	6.211	6.109	5.988
81301	14.771	8.648	-3.028	-14.071	16.338
81401	16.076	11.973	-5.026	-21.660	-34.201
81501	13.669	10.741	-5.491	-19.718	-24.580
81601	10.540	6.703	-3.299	-12.556	-20.874
81701	7.137	3.174	-3.158	-9.735	-14.060
81801	2.418	0.451	-2.775	-5.861	-8.341
81901	-0.431	-1.304	-2.396	-3.401	-4.052
82001	-0.839	-1.692	-1.824	-1.808	-1.656
82101	0.071	-0.799	-1.068	-1.008	-0.927
82201	1.667	0.644	-0.087	-0.445	-0.858
82301	3.357	2.207	0.983	0.185	-0.677
82401	4.846	3.634	2.044	0.860	-0.418
82501	5.990	4.794	3.020	1.629	0.154
82601	6.850	5.723	3.982	2.581	1.106
82701	7.421	6.402	4.832	3.555	2.219
82801	7.797	6.886	5.559	4.488	3.358
82901	8.019	7.050	6.090	5.215	4.283
83001	7.986	7.052	6.372	5.707	4.980
83101	7.510	6.855	6.458	6.048	5.537
83201	6.964	6.566	6.366	6.177	5.889
83301	6.497	6.379	6.252	6.142	6.090

GRAY, BRIAN C

From: John Broussard [jbroussard@domeng.com]
Sent: Tuesday, September 16, 2003 8:55 AM
To: GRAY, BRIAN C
Subject: E-4162-00-13, ICI model stress plots

Wat3 ICI Stress Plots.pdf (137...

Brian,

Attached in PDF format are stress plots for the ICI as-built model with the 0.3" deeper J-groove weld. All stress plots are for operating hoop stress in the nozzle-centered cylindrical coordinate system. Call or e-mail with any questions or if you need further information.

John Broussard, P.E.
Dominion Engineering, Inc.
E-mail: jbroussard@domeng.com
Phone : 703-437-7826 x236
Fax : 703-437-0780

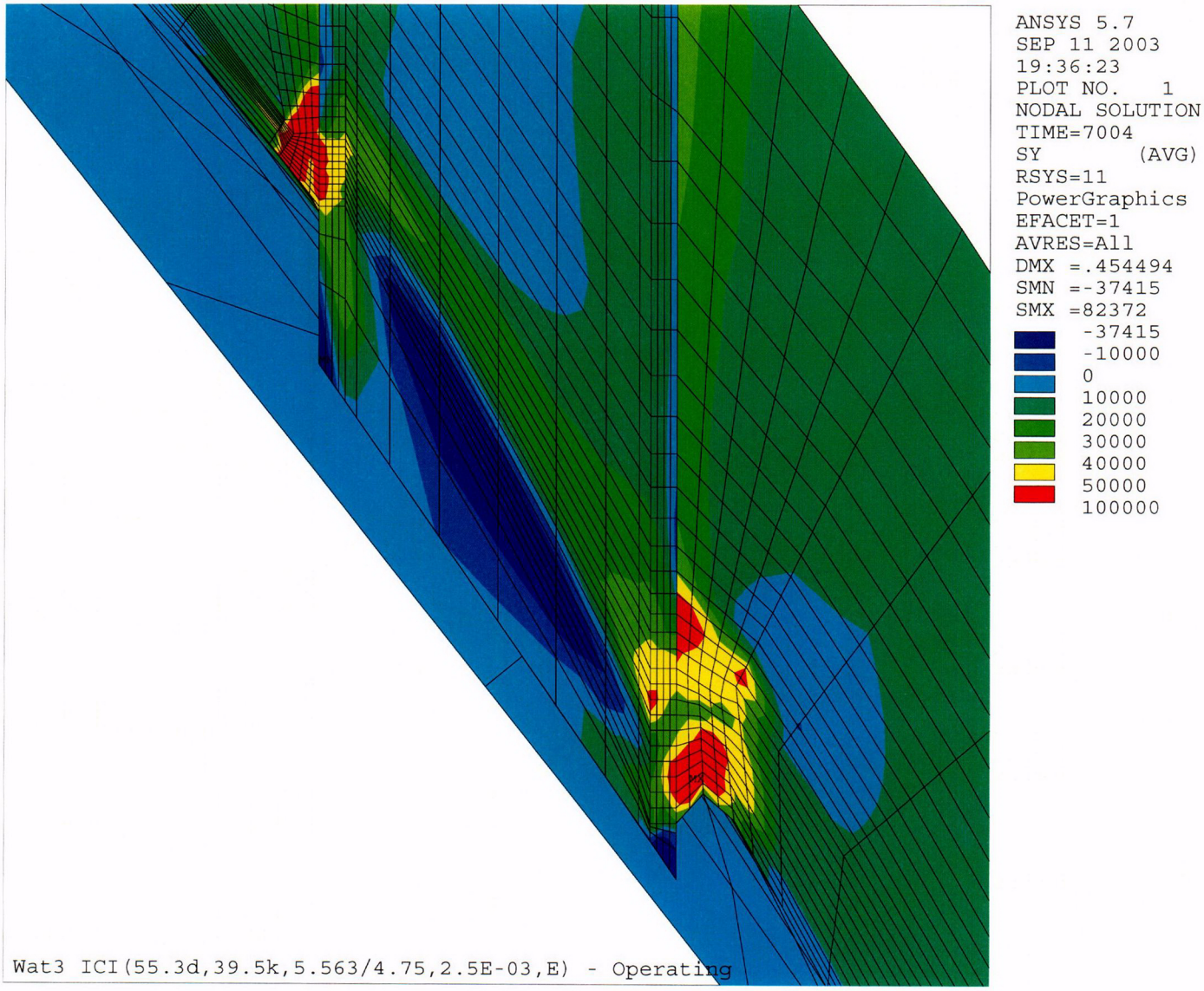
ANSYS 5.7
SEP 11 2003
19:36:23
PLOT NO. 1
NODAL SOLUTION
TIME=7004
SY (AVG)
RSYS=11
PowerGraphics
EFACET=1
AVRES=All
DMX =.454494
SMN =-37415
SMX =82372
-37415
-10000
0
10000
20000
30000
40000
50000
100000
Wat3 ICI(55.3d,39.5k,5.563/4.75,2.5E-03,E) - Operating

C08

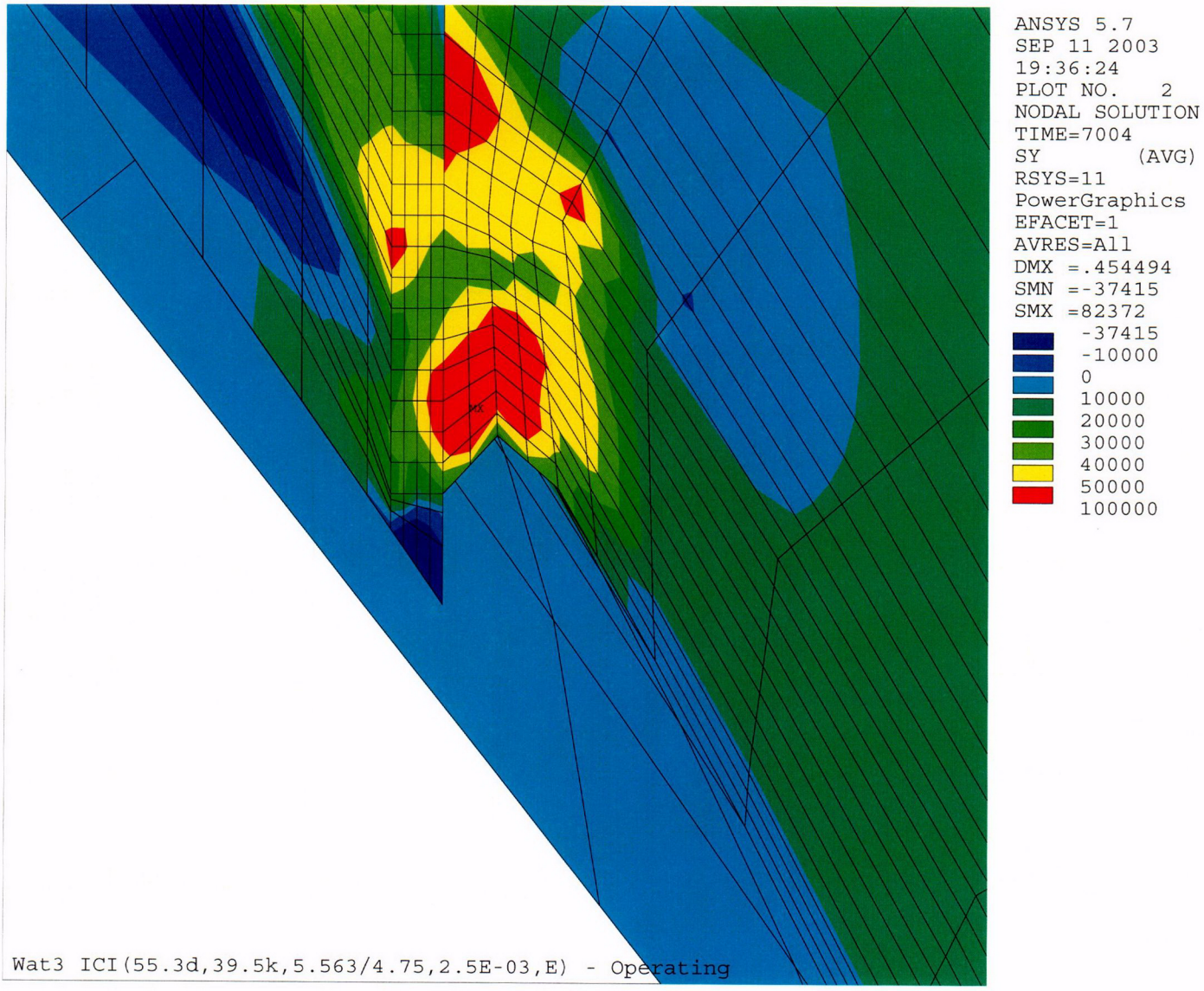
ANSYS 5.7
SEP 11 2003
19:36:24
PLOT NO. 2
NODAL SOLUTION
TIME=7004
SY (AVG)
RSYS=11
PowerGraphics
EFACET=1
AVRES=All
DMX =.454494
SMN =-37415
SMX =82372
-37415
-10000
0
10000
20000
30000
40000
50000
100000
Wat3 ICI(55.3d,39.5k,5.563/4.75,2.5E-03,E) - Operating

C09

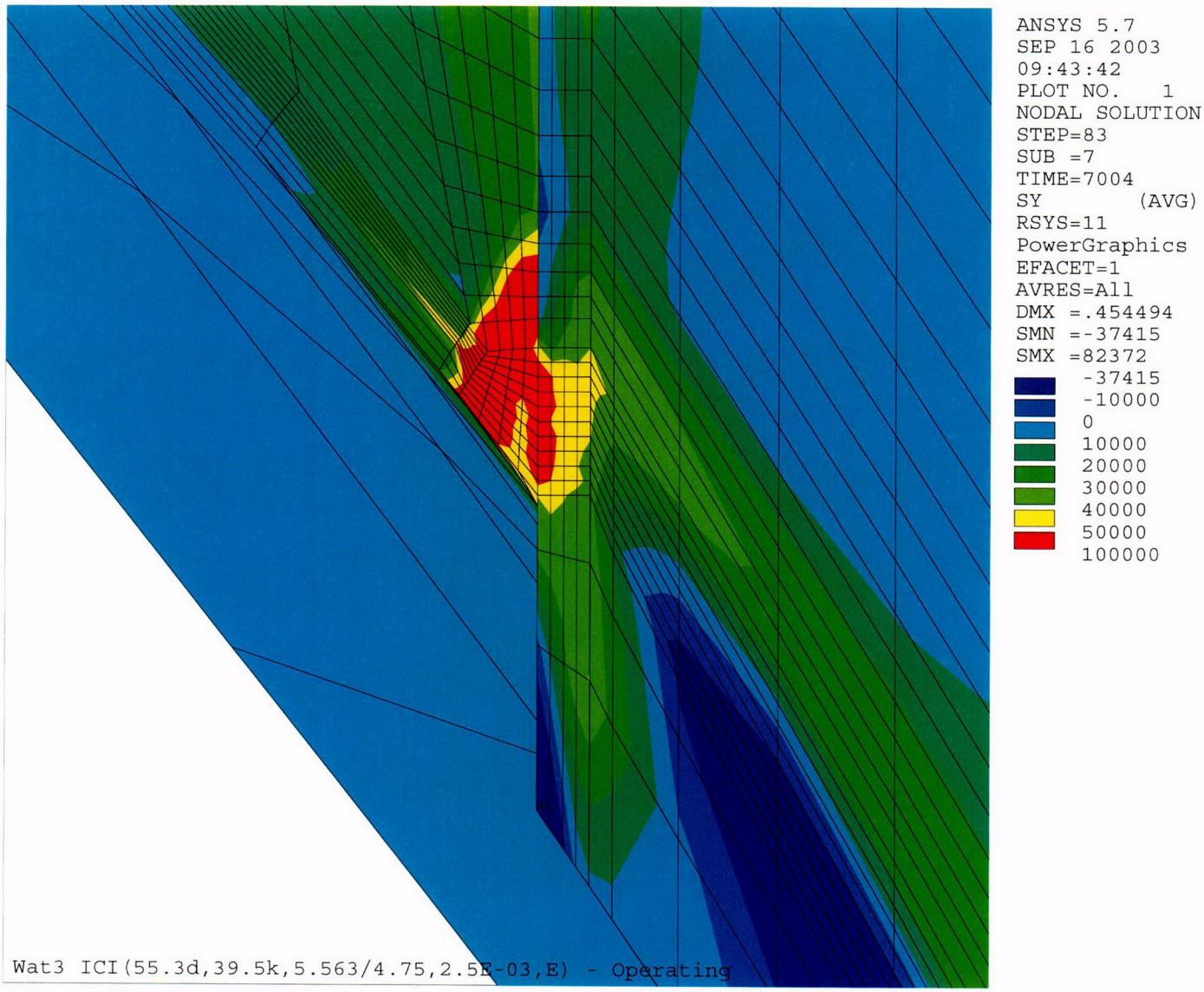
ANSYS 5.7
SEP 16 2003
09:43:42
PLOT NO. 1
NODAL SOLUTION
STEP=83
SUB =7
TIME=7004
SY (AVG)
RSYS=11
PowerGraphics
EFACET=1
AVRES=All
DMX =.454494
SMN =-37415
SMX =82372
-37415
-10000
0
10000
20000
30000
40000
50000
100000
Wat3 ICI(55.3d,39.5k,5.563/4.75,2.5E-03,E) - Operating

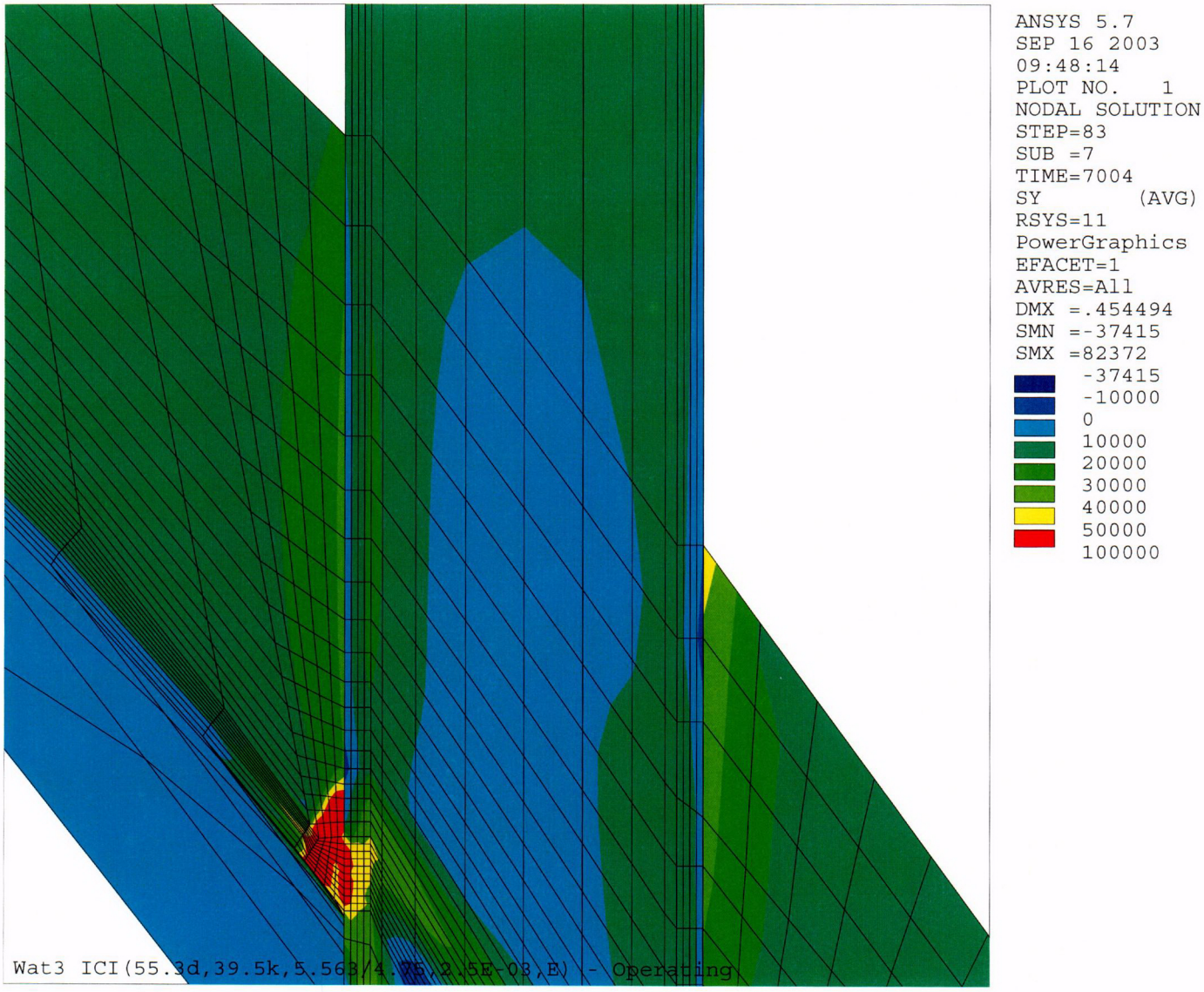
ANSYS 5.7
SEP 16 2003
09:48:14
PLOT NO. 1
NODAL SOLUTION
STEP=83
SUB =7
TIME=7004
SY (AVG)
RSYS=11
PowerGraphics
EFACET=1
AVRES=All
DMX =.454494
SMN =-37415
SMX =82372
-37415
-10000
0
10000
20000
30000
40000
50000
100000
Wat3 ICI(55.3d,39.5k,5.563/4.75,2.5E-03,E) - Operating

C11

Waterford Steam Electric Station Unit 3

Primary Water Stress Corrosion Crack Growth Analysis for an ICI ID Surface Flaw Uphill (180°), in the Blind Zone above the Top of the J-Groove Weld
Developed by Central Engineering Programs, Entergy Operations Inc.

Flaw Case 1: 25% Through-Wall Flaw with a 6-to-1 Flaw Length-to-Depth Aspect Ratio, Located at the Center of the Blind Zone

Calculation Basis: MRP 75 th Percentile and Flaw Face Pressurized

Mean Radius -to- Thickness Ratio:- "R_m/t" -- between 1.0 and 300.0

Note : ***The Metric form of the equation from EPRI MRP was used 55-Rev. 1*** *. A correction factor is applied in the determination of the crack extension to convert the units of meters per second to the value in inches per hour .*

ID Surface Flaw

User Input:

The Dominion Engineering Inc. (DEI) finite element model nodal elevations and hoop stresses for the uphill side (180° azimuth) of the ICI nozzle are brought into the Mathcad worksheet from data supplied in Reference 8d. The data are composed of the nodal elevations (in inches), along with the ID, 25% through-wall (tw), 50% tw, 75% tw, and OD hoop stresses, beginning two nodal lines below (nodal line 81101) the top of the weld (nodal line 81301) and extending to the top of the nozzle in the FEA model (nodal line 83301), which is at the point where the nozzle intersects the reactor vessel head.

The DEI FEA data has elevation referenced from the bottom of the ICI nozzle. The elevations of the node points in the DEI FEA model, beginning below the top of the weld, at nodal line 81101, and the corresponding hoop stresses are as follows:

Note the following terms used throughout this evaluation:

ID-inside diameter of ICI nozzle
QT-25% tw position
MD-50% tw, or mid-wall, position
TQ-75% tw position
OD-outside diameter of ICI nozzle

$i := 0..20$

Node_line :=	Elev_fea :=	ID_stress_fea :=	QT_stress_fea :=
81101	3.973	43.347	41.640
81201	4.089	42.799	39.703
81301	4.205	39.763	38.158
81401	4.435	37.068	33.351
81501	4.605	34.079	32.268
81601	4.798	29.820	28.465
81701	5.015	23.668	21.543
81801	5.262	18.722	14.133
81901	5.541	18.383	15.071
82001	5.857	18.876	17.269
82101	6.214	19.527	18.517
82201	6.619	20.331	19.550
82301	7.077	20.976	20.149
82401	7.596	21.408	20.378
82501	8.183	21.667	20.400
82601	8.847	21.792	20.133
82701	9.599	21.742	19.395
82801	10.451	21.550	18.466
82901	11.415	21.213	17.311
83001	12.505	19.876	16.176
83101	13.740	18.311	15.380
83201	15.138	16.442	14.525
83301	18.057	12.330	12.146

$$MD\_stress\_fea := \begin{pmatrix} 43.666 \\ 41.445 \\ 34.368 \\ 25.957 \\ 24.632 \\ 21.515 \\ 14.530 \\ 7.280 \\ 8.650 \\ 11.236 \\ 12.761 \\ 13.998 \\ 14.467 \\ 14.437 \\ 14.263 \\ 13.976 \\ 13.664 \\ 13.362 \\ 13.126 \\ 13.009 \\ 12.983 \\ 12.960 \\ 12.033 \end{pmatrix}$$

$$TQ\_stress\_fea := \begin{pmatrix} 50.638 \\ 40.722 \\ 27.002 \\ 16.947 \\ 11.934 \\ 10.551 \\ 5.734 \\ 0.963 \\ 3.277 \\ 6.243 \\ 7.898 \\ 9.088 \\ 9.428 \\ 9.275 \\ 9.100 \\ 8.964 \\ 8.987 \\ 9.158 \\ 9.525 \\ 10.038 \\ 10.759 \\ 11.508 \\ 11.987 \end{pmatrix}$$

$$OD\_stress\_fea := \begin{pmatrix} 59.979 \\ 51.289 \\ 41.729 \\ 6.333 \\ 5.354 \\ 3.714 \\ 0.010 \\ -4.004 \\ -1.652 \\ 1.578 \\ 3.319 \\ 4.422 \\ 4.629 \\ 4.330 \\ 4.150 \\ 4.177 \\ 4.508 \\ 5.143 \\ 6.042 \\ 7.179 \\ 8.539 \\ 10.066 \\ 11.973 \end{pmatrix}$$

Blind Zone and Counterbore Reference dimensions:

From design drawings (Ref. 3) and the design details of **Attachment 1**, the following dimensions are used to locate the counterbore bottom and blind zone locations (bottom, top, and middle) as referenced from the nodal coordinates of the DEI FEA model.

$Actual\_cbore\_bottom\_elev := Elev\_fea_2 + 1.01$

$Actual\_cbore\_bottom\_elev = 5.215$

Primary Assumptions on blind zone dimensions:

$topweld\_to\_bottom\_BZ := 0.67$ This is the distance from top of the J-weld, on the uphill side, to the bottom of the blind zone. Without UT data to verify this dimension, this value be iterated to determine the MINIMUM height above the top of the weld for which the blind zone can begin and yield an acceptable fracture mechanics solution.

$BZ\_length = 0.88$ This value is based on the longest blind zone seen in the ANO-2 ICI nozzles. Both Waterford-3 and ANO-2 ICI nozzles have similar geometries above the top of the weld. Thus, a reasonable engineered assumption is that the largest blind zone for ANO-2 is assumed for the Waterford-3 ICI nozzles.

$$elev\_to\_mid\_BZ := Elev\_fea_2 + topweld\_to\_bottom\_BZ + \frac{BZ\_length}{2}$$

$elev\_to\_mid\_BZ = 5.315$

$bottom\_of\_BZ := Elev\_fea_2 + topweld\_to\_bottom\_BZ$

$bottom\_of\_BZ = 4.875$

$top\_of\_BZ := Elev\_fea_2 + topweld\_to\_bottom\_BZ + BZ\_length$

$top\_of\_BZ = 5.755$

For stress averaging and fracture mechanics purposes, the reference coordinate system--with a "0" elevation at the bottom of the nozzle, at the ID corner--must be converted into a new coordinate system with the top of the nozzle (nodal line 83301) as the new "0" elevation.. The positive direction along this new coordinate system will be towards nodal line 81101, which is the just below the top of the weld. This modification facilitates a fracture mechanics model more ammenable to the surface flaw loop structure previously developed in Reference 6.

The following iterative loop converts the five (5) through-wall stress components--ID, 25% tw (QT), 50% tw (MD), 75% tw (TQ), and OD--and the associated elevation, initially given in the DEI FEA model, into the "new" coordinate system, referenced from the top of the nozzle where it meets the reactor vessel head.

$$
\begin{aligned}
\text{Conv} := \;& n \leftarrow 20 \\
& \text{Top} \leftarrow \text{Elev\_fea}_n \\
& j \leftarrow n \\
& i \leftarrow 0 \\
& \text{while } j \geq 0 \\
& \quad \text{Elev\_conv}_i \leftarrow \text{Top} - \text{Elev\_fea}_j \\
& \quad \text{ID\_stress}_i \leftarrow \text{ID\_stress\_fea}_j \\
& \quad \text{QT\_stress}_i \leftarrow \text{QT\_stress\_fea}_j \\
& \quad \text{MD\_stress}_i \leftarrow \text{MD\_stress\_fea}_j \\
& \quad \text{TQ\_stress}_i \leftarrow \text{TQ\_stress\_fea}_j \\
& \quad \text{OD\_stress}_i \leftarrow \text{OD\_stress\_fea}_j \\
& \quad \text{output}_{(i,0)} \leftarrow \text{Elev\_conv}_i \\
& \quad \text{output}_{(i,1)} \leftarrow \text{ID\_stress}_i \\
& \quad \text{output}_{(i,2)} \leftarrow \text{QT\_stress}_i \\
& \quad \text{output}_{(i,3)} \leftarrow \text{MD\_stress}_i \\
& \quad \text{output}_{(i,4)} \leftarrow \text{TQ\_stress}_i \\
& \quad \text{output}_{(i,5)} \leftarrow \text{OD\_stress}_i \\
& \quad j \leftarrow j - 1 \\
& \quad i \leftarrow i + 1 \\
& \text{output}
\end{aligned}
$$

$Elev := Conv^{\langle 0 \rangle}$

$ID\_stress := Conv^{\langle 1 \rangle}$

$QT\_stress := Conv^{\langle 2 \rangle}$

$MD\_stress := Conv^{\langle 3 \rangle}$

$TQ\_stress := Conv^{\langle 4 \rangle}$

$OD\_stress := Conv^{\langle 5 \rangle}$

$Elev_i$ =	ID_stress_i =	QT_stress_i =	MD_stress_i =	TQ_stress_i =	OD_stress_i =
0	18.311	15.38	12.983	10.759	8.539
1.235	19.876	16.176	13.009	10.038	7.179
2.325	21.213	17.311	13.126	9.525	6.042
3.289	21.55	18.466	13.362	9.158	5.143
4.141	21.742	19.395	13.664	8.987	4.508
4.893	21.792	20.133	13.976	8.964	4.177
5.557	21.667	20.4	14.263	9.1	4.15
6.144	21.408	20.378	14.437	9.275	4.33
6.663	20.976	20.149	14.467	9.428	4.629
7.121	20.331	19.55	13.998	9.088	4.422
7.526	19.527	18.517	12.761	7.898	3.319
7.883	18.876	17.269	11.236	6.243	1.578
8.199	18.383	15.071	8.65	3.277	-1.652
8.478	18.722	14.133	7.28	0.963	-4.004
8.725	23.668	21.543	14.53	5.734	0.01
8.942	29.82	28.465	21.515	10.551	3.714
9.135	34.079	32.268	24.632	11.934	5.354
9.305	37.068	33.351	25.957	16.947	6.333
9.535	39.763	38.158	34.368	27.002	41.729
9.651	42.799	39.703	41.445	40.722	51.289
9.767	43.347	41.64	43.666	50.638	59.979

The five arrays given above include the elevation measured from the top of the ICI nozzle from the FEA model down to the top of the J-weld and the corresponding hoop stresses in the modified coordinate system (MCS).

Additional Geometry in Modified Coordinate System

The top of the J-groove weld in the MCS is equal to entry 18 in the "Elev" array:

$Top\_Jweld := Elev_{18}$

$Top\_Jweld = 9.535$

The location of the top of the UT blind zone (BZ) in the MCS (as measured from the ID surface) is

$BZ\_top := Top\_Jweld - (topweld\_to\_bottom\_BZ + BZ\_length)$

$BZ\_top = 7.985$

The midpoint of the BZ in the MCS is

$$BZ\_mid := BZ\_top + \frac{BZ\_length}{2}$$

$BZ\_mid = 8.425$

The bottom of the BZ in the MCS is

$BZ\_bottom := BZ\_top + BZ\_length$

$BZ\_bottom = 8.865$

The location of the actual counterbore (from design drawings) in the MCS:

$cbore\_elev := Top\_Jweld - 1.377$

$cbore\_elev = 8.158$

From the MCS, the stress distribution from elevation 0 (the top of the ICI nozzle where it intersects the RV head) to the top of the weld is graphically shown below.

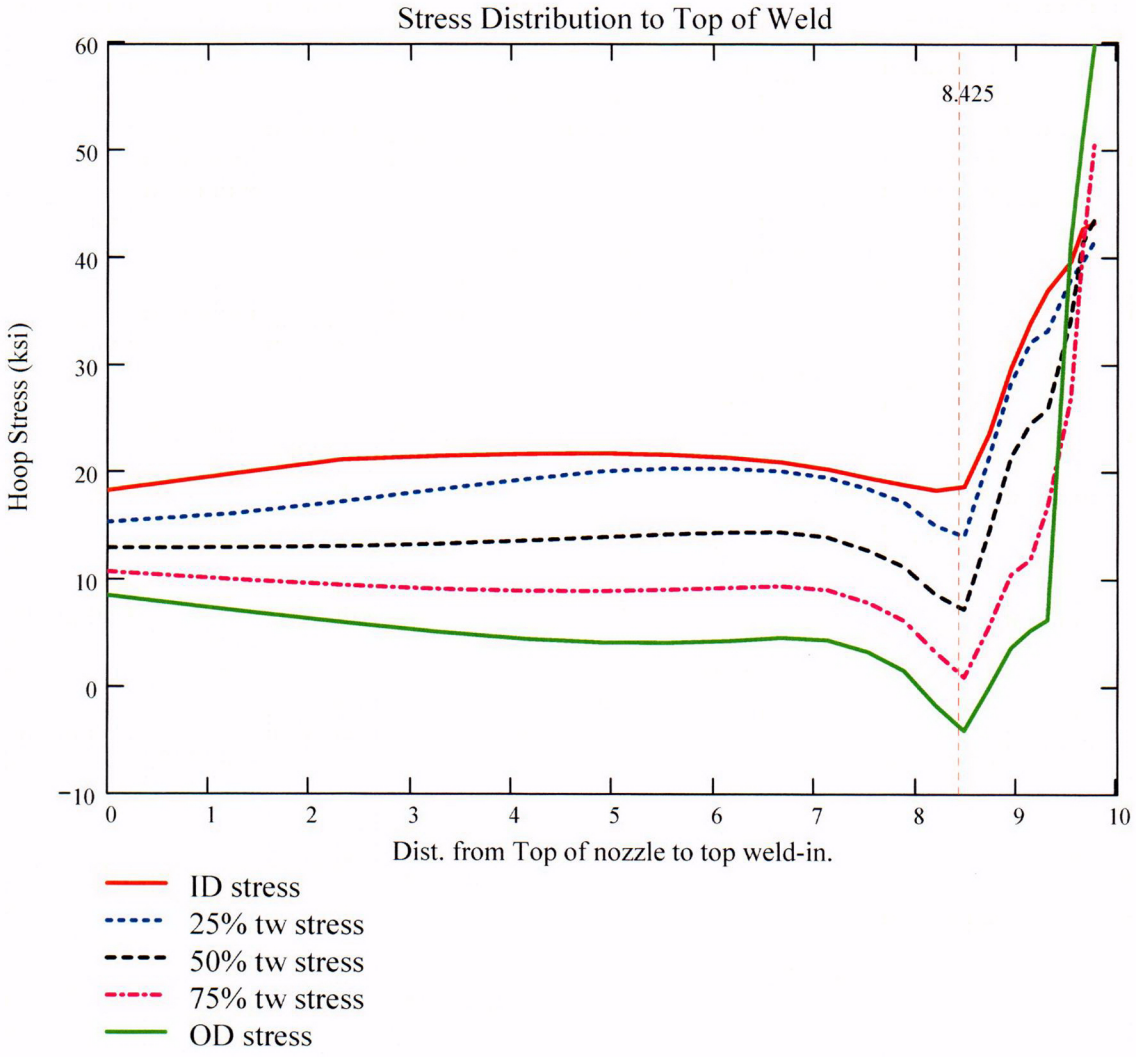

For the ID surface flaw model, the reference point is the location along the axis of the nozzle used to locate the flaw. For this analysis, the reference point is considered at the mid-height of the blind zone.

$Ref_{Point} := BZ\_mid$

C12

To place the flaw with respect to the reference point, the flaw tips and center can be located as follows:

1) The Upper "c- tip" located at the reference point (Enter 1)
2) The Center of the flaw at the reference point (Enter 2)
3) The lower "c- tip" located at the reference point (Enter 3).

$Val := 2$

The Input Below is the point below the blind zone region where stresses will be considered for curve-fitting. This point is taken as the top of the weld, since the stress distribution changes drastically within the weld region Enter this dimension or variable below.

$Elev_{Strs.Dist} := Elev_{20}$ The elevation to the point of maximum stress to consider (Axial distance from elevation 0 in the MCS).

ICI Nozzle Geometry Input Data:

$od := 5.563 - 0.001$ Tube OD, in inches (The value from Ref. 3, is 5.563" +0.00/-0.001)

$id1 := 4.625 + 0.01$ Maximum Tube ID above counterbore, in inches (The value from Ref. 3 is 4.625" +/- 0.010")

$id2 := 4.750 + 0.01$ Maximum Tube ID below counterbore, in inches (The value from Ref. 3 is 4.750" +/- 0.010")

$t1 := \frac{(od - id1)}{2}$

Minmum wall thickness above the counterbore, in inches

$t1 = 0.4635$

$t2 := \frac{(od - id2)}{2}$

Minimum wall thickness below the counterbore, in inches

$t2 = 0.401$

$R_o := \frac{od}{2}$ $R_o = 2.781$

$R_{id1} := \frac{id1}{2}$ $R_{id1} = 2.3175$

$R_{id2} := \frac{id2}{2}$ $R_{id2} = 2.38$

$R_{m1} := R_{id1} + \frac{t1}{2}$ $R_{m1} = 2.54925$

$R_{m2} := R_{id2} + \frac{t2}{2}$ $R_{m2} = 2.5805$

$R_t := \frac{R_{m2}}{t2}$ $R_t = 6.43516$

$\frac{R_o}{t2} = 6.93516$

Flaw Geometry Input Data:

A postulated flaw could exist in the **0.88"** UT Blindzone that occurs **0.67"** above the top of the J-weld at the uphill (180°) location. The flaw length (c) and depth (a) constitute the input parameters. This flaw represents an internal surface crack in a cylinder, as described in Reference 9.

$AR_0 := 6$ The flaw length-to-depth aspect ratio. This is a ratio common to ASME Section XI, and one sufficient to promote flaw growth through the thickness.

$t2 \cdot .25 = 0.10025$

$a_0 := 0.1$ Initial Flaw Depth of the ID surface flaw in the blind zone above the top of the weld on the uphill side. The minimum detectable depth of a surface flaw from UT demonstrations [Ref. 12] was 8% throughwall. Conservatively, a 25% throughwall flaw is assumed. This flaw is sufficiently deep to see the stress field developed through the thickness.

$L := a_0 \cdot AR_0$ Initial Flaw Length of an ID surface flaw in the counterbore region, in inches. The length was determined by assuming a 6-to-1 flaw length-to-depth aspect ratio. Half the flaw length (0.3 inch) was placed the below the mid-height of the blind zone, while the other half was placed above the mid-height.

$L = 0.6$

$c_0 := \frac{L}{2}$ The half flaw length used in the fracture mechanics model

Additional Input Data:

$P_{Int} := 2.235$ Design Operating Pressure (internal) [Ref. 4]

$Years := 40$ Number of Operating Years

$I_{lim} := 8000$ Iteration limit for Crack Growth loop

$T := 604$ Operating Temperature for the head, in °F. Reference 5b gives a value of 601°F after the Extended Power Uprate (EPU), and 604°F currently. Thus, the temperature of the head will be taken as 604°F.

$\alpha_{0c} := 2.67 \cdot 10^{-12}$ Constant in MRP-55 PWSCC Model for I-600 Wrought @ 617 deg. F [Ref. 10]

$Q_g := 31.0$ Thermal activation Energy for Crack Growth {MRP) [Ref. 10]

$T_{ref} := 617$ Reference Temperature for normalizing Data deg. F [Ref. 10]

$Tim_{opr} := 365.2422 \cdot 24 \cdot Years$ Numer of operating hours in a year

$CF_{inhr} := 1.417 \cdot 10^{5}$ Correction factor to convert meters per second to inches per hour

$$C_{blk} := \frac{Tim_{opr}}{I_{lim}}$$ Calculation block size for the crack growth iteration loop

$C_{blk} = 43.82906$

$$Prnt_{blk} := \left| \frac{I_{lim}}{50} \right|$$

$$C_{01} := e^{\left[\frac{-Q_g}{1.103 \cdot 10^{-3}} \cdot \left(\frac{1}{T+459.67} - \frac{1}{T_{ref}+459.67} \right) \right] \cdot \alpha_{0c}}$$ Temperature Correction for Coefficient Alpha from EPRI MRP-55, Revision 1 [Ref. 10]

$C_0 := 1.0 C_{01}$ 75 th percentile from MRP-55 Revision 1 [Ref. 10]

The flaw model used for a postulated flaw within the counterbore region on the uphill side of the ICI nozzle is an internal surface flaw in a cylinder, subject to an arbitrary stress distribution.

To allow for a "moving average" of through-thickness stress values as the flaw extends along the length of the ICI ID surface, the length from the bottom tip of the of the initial flaw in the blind zone to the stress distribution upper limit--$Elev_{Strs.Dist}$--is broken into 20 equal segments. Note that due to the MCS used, with a 0 elevation occurring at the TOP of the nozzle, the term "U_{Tip}" (implying the upper tip of the flaw) is actually the physical bottom tip of the flaw, closer to the top of the weld. U_{Tip} is the term used in Reference 6 for the CEDM nozzles, and thus it will continue to be used in the ICI nozzle evaluation.

$$FL_{Cntr} := \begin{cases} Ref_{Point} - c_0 & \text{if } Val = 1 \\ Ref_{Point} & \text{if } Val = 2 \\ Ref_{Point} + c_0 & \text{otherwise} \end{cases}$$

Flaw center Location at the mid-point of the blind zone region

$$U_{Tip} := FL_{Cntr} + c_0$$

$$U_{Tip} = 8.725$$

$$Inc_{Strs.avg} := \frac{Elev_{Strs.Dist} - U_{Tip}}{20}$$

$$Inc_{Strs.avg} = 0.0521$$

$$Ref_{Point} = 8.425$$

No User Input is required beyond this Point

Regression of Through-Thickness Stresses as a Function of Axial Elevation

Because of the minor variation in stresses occuring at the top of the nozzle where it intersects the reactor head and the need to accurately curve fit stresses in the region of interest in the BZ, the entire range of stresses is not appropriate to curve fit. To accomodate an area below and above the BZ region, the first two data points in each of the elevation and stress arrays were removed from consideration in the curve fitting equations. This is a reasonable assumption, given that in the completely through-wall tensile stress field that exists in the nozzle above the top of the J-weld, a flaw centered in the BZ region is likely to grow through the thickness entirely (in addition to growth along the surface of the nozzle) rather than grow very long into an area close to the top of the head or below the top of the J-weld (i.e., elevation ranges not included in the stress polynomial curve fit). Initially, a **third (3rd)** order polynomial was chosen for axial stress regression. After regression, the stress at the mid-height of the blind zone (8.445 inches in the MCS) is checked.

Regression for ID stresses:

$k := 0..5$

$$ID\_elev\_cf := \begin{pmatrix} 7.883 \\ 8.199 \\ 8.478 \\ 8.725 \\ 8.942 \\ 9.135 \end{pmatrix} \qquad ID\_stress\_cf := \begin{pmatrix} 18.876 \\ 18.383 \\ 18.722 \\ 23.668 \\ 29.82 \\ 34.079 \end{pmatrix}$$

$R_{ID} := regress(ID\_elev\_cf, ID\_stress\_cf, 3)$

$$R_{ID} = \begin{pmatrix} 3 \\ 3 \\ 3 \\ 3578.38988 \\ -1136.79548 \\ 118.13463 \\ -3.95831 \end{pmatrix}$$

$z_{ID} := 7.883, 7.884.. 9.135$

$f_{ID}(z_{ID}) := interp(R_{ID}, ID\_elev\_cf, ID\_stress\_cf, z_{ID})$

$Elev_i$ =	ID_stress_i =
0	18.311
1.235	19.876
2.325	21.213
3.289	21.55
4.141	21.742
4.893	21.792
5.557	21.667
6.144	21.408
6.663	20.976
7.121	20.331
7.526	19.527
7.883	18.876
8.199	18.383
8.478	18.722
8.725	23.668
8.942	29.82
9.135	34.079
9.305	37.068
9.535	39.763
9.651	42.799
9.767	43.347

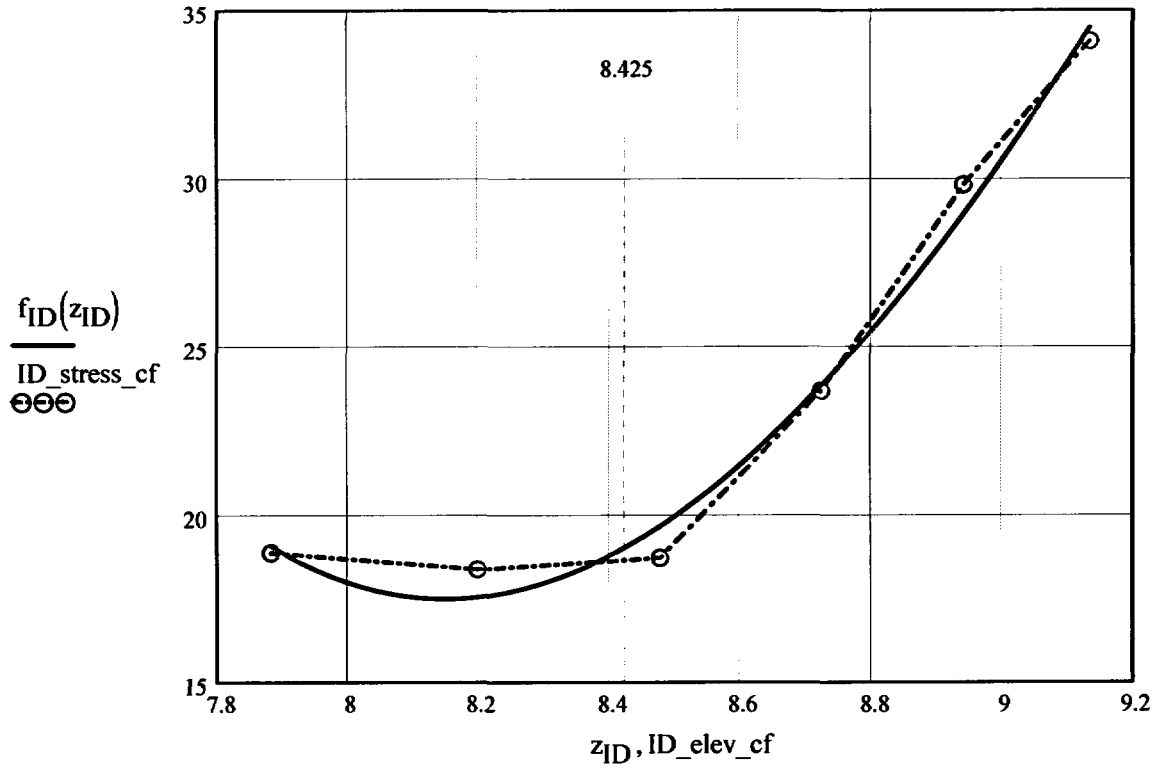

$f_{ID}(8.425) = 19.03958$

Regression for 25% throughwall stresses:

$$QT\_elev\_cf := \begin{pmatrix} 7.883 \\ 8.199 \\ 8.478 \\ 8.725 \\ 8.942 \\ 9.135 \end{pmatrix} \qquad QT\_stress\_cf := \begin{pmatrix} 17.269 \\ 15.071 \\ 14.133 \\ 21.543 \\ 28.465 \\ 32.268 \end{pmatrix}$$

$R_{QT} := regress(QT\_elev\_cf, QT\_stress\_cf, 3)$

$z_{QT} := 7.883, 7.884 .. 9.135$

$$R_{QT} = \begin{pmatrix} 3 \\ 3 \\ 3 \\ 10745.64054 \\ -3630.8401 \\ 406.73522 \\ -15.0681 \end{pmatrix}$$

$f_{QT}(z_{QT}) := interp(R_{QT}, QT\_elev\_cf, QT\_stress\_cf, z_{QT})$

$Elev_i =$	$QT\_stress_i =$
0	15.38
1.235	16.176
2.325	17.311
3.289	18.466
4.141	19.395
4.893	20.133
5.557	20.4
6.144	20.378
6.663	20.149
7.121	19.55
7.526	18.517
7.883	17.269
8.199	15.071
8.478	14.133
8.725	21.543
8.942	28.465
9.135	32.268
9.305	33.351
9.535	38.158
9.651	39.703
9.767	41.64

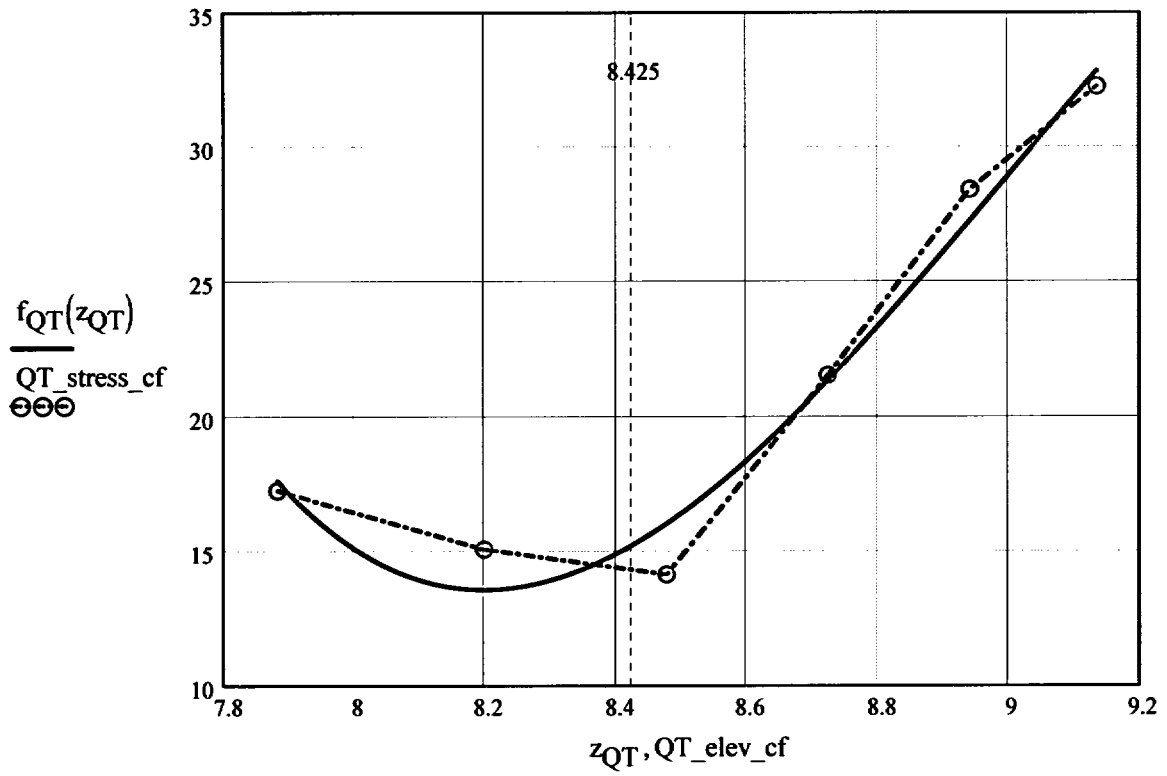

$f_{QT}(8.425) = 15.22949$

Regression for 50% throughwall stresses:

$$MD\_elev\_cf := \begin{pmatrix} 7.883 \\ 8.199 \\ 8.478 \\ 8.725 \\ 8.942 \\ 9.135 \end{pmatrix} \qquad MD\_stress\_cf := \begin{pmatrix} 11.236 \\ 8.65 \\ 7.28 \\ 14.53 \\ 21.515 \\ 24.632 \end{pmatrix}$$

$R_{MD} := regress(MD\_elev\_cf, MD\_stress\_cf, 3)$

$z_{MD} := 7.883, 7.884 .. 9.135$

$$R_{MD} = \begin{pmatrix} 3 \\ 3 \\ 3 \\ 11819.16519 \\ -4010.84838 \\ 451.35824 \\ -16.8173 \end{pmatrix}$$

$f_{MD}(z_{MD}) := interp(R_{MD}, MD\_elev\_cf, MD\_stress\_cf, z_{MD})$

$Elev_i$ =	MD_stress_i =
0	12.983
1.235	13.009
2.325	13.126
3.289	13.362
4.141	13.664
4.893	13.976
5.557	14.263
6.144	14.437
6.663	14.467
7.121	13.998
7.526	12.761
7.883	11.236
8.199	8.65
8.478	7.28
8.725	14.53
8.942	21.515
9.135	24.632
9.305	25.957
9.535	34.368
9.651	41.445
9.767	43.666

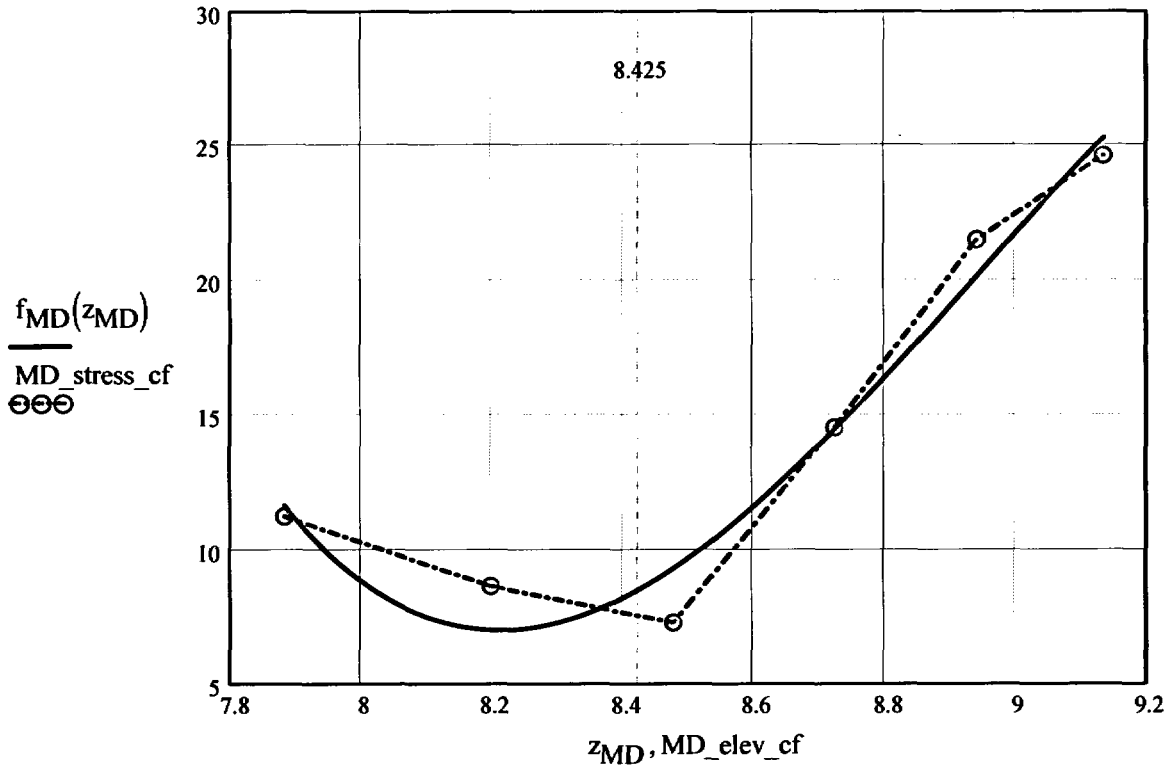

$f_{MD}(8.425) = 8.51122$

Regression for 75% throughwall stresses:

$$TQ\_elev\_cf := \begin{pmatrix} 7.883 \\ 8.199 \\ 8.478 \\ 8.725 \\ 8.942 \\ 9.135 \end{pmatrix} \qquad TQ\_stress\_cf := \begin{pmatrix} 6.243 \\ 3.277 \\ 0.963 \\ 5.734 \\ 10.551 \\ 11.934 \end{pmatrix}$$

$R_{TQ} := regress(TQ\_elev\_cf, TQ\_stress\_cf, 3)$

$z_{TQ} := 7.883, 7.884 .. 9.135$

$$R_{TQ} = \begin{pmatrix} 3 \\ 3 \\ 3 \\ 9313.45524 \\ -3159.012 \\ 355.56516 \\ -13.2686 \end{pmatrix}$$

$f_{TQ}(z_{TQ}) := \text{interp}(R_{TQ}, TQ\_elev\_cf, TQ\_stress\_cf, z_{TQ})$

$Elev_i =$	$TQ\_stress_i =$
0	10.759
1.235	10.038
2.325	9.525
3.289	9.158
4.141	8.987
4.893	8.964
5.557	9.1
6.144	9.275
6.663	9.428
7.121	9.088
7.526	7.898
7.883	6.243
8.199	3.277
8.478	0.963
8.725	5.734
8.942	10.551
9.135	11.934
9.305	16.947
9.535	27.002
9.651	40.722
9.767	50.638

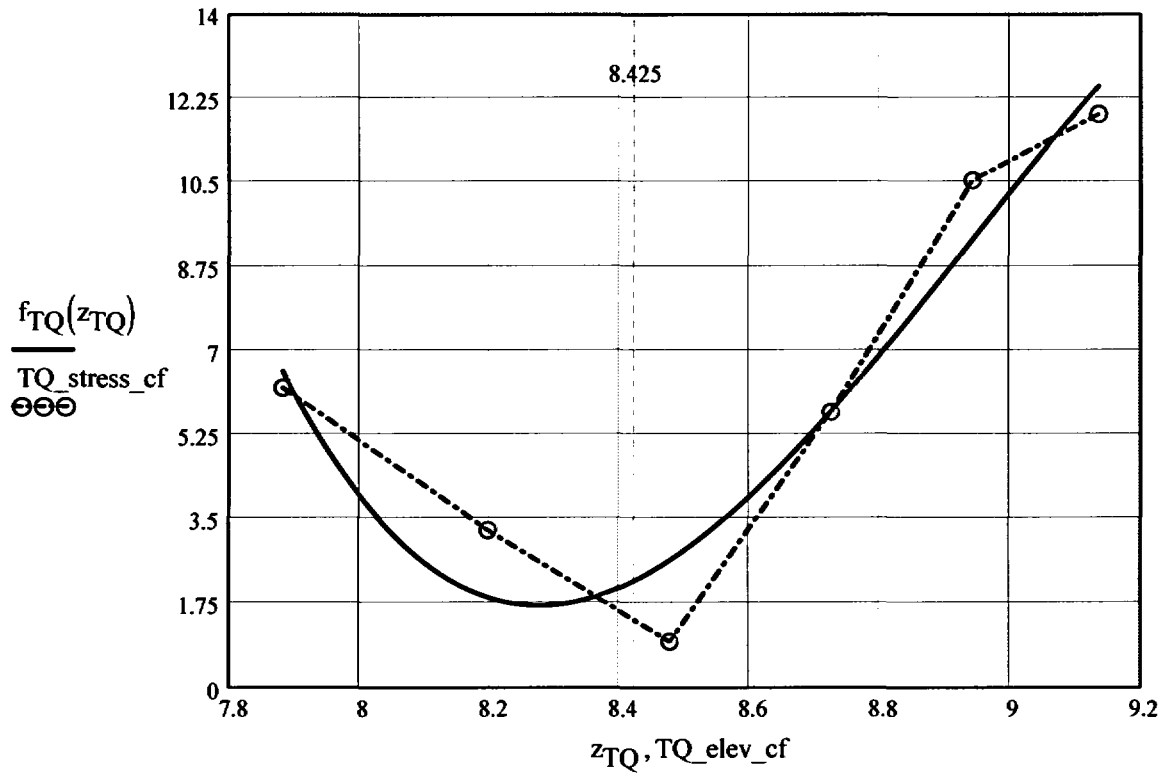

$f_{TQ}(8.425) = 2.2362$

Regression for OD stresses:

$kk := 0..5$

$$OD\_elev\_cf := \begin{pmatrix} 7.883 \\ 8.199 \\ 8.478 \\ 8.725 \\ 8.942 \\ 9.135 \end{pmatrix} \qquad OD\_stress\_cf := \begin{pmatrix} 1.578 \\ -1.652 \\ -4.004 \\ 0.01 \\ 3.714 \\ 5.354 \end{pmatrix}$$

$R_{OD} := regress(OD\_elev\_cf, OD\_stress\_cf, 3)$

$z_{OD} := 7.883, 7.884 .. 9.135$

$$R_{OD} = \begin{pmatrix} 3 \\ 3 \\ 3 \\ 7570.62763 \\ -2550.59622 \\ 284.86761 \\ -10.54291 \end{pmatrix}$$

$f_{OD}(z_{OD}) := interp(R_{OD}, OD\_elev\_cf, OD\_stress\_cf, z_{OD})$

$Elev_i =$	$OD\_stress_i =$
0	8.539
1.235	7.179
2.325	6.042
3.289	5.143
4.141	4.508
4.893	4.177
5.557	4.15
6.144	4.33
6.663	4.629
7.121	4.422
7.526	3.319
7.883	1.578
8.199	-1.652
8.478	-4.004
8.725	0.01
8.942	3.714
9.135	5.354
9.305	6.333
9.535	41.729
9.651	51.289
9.767	59.979

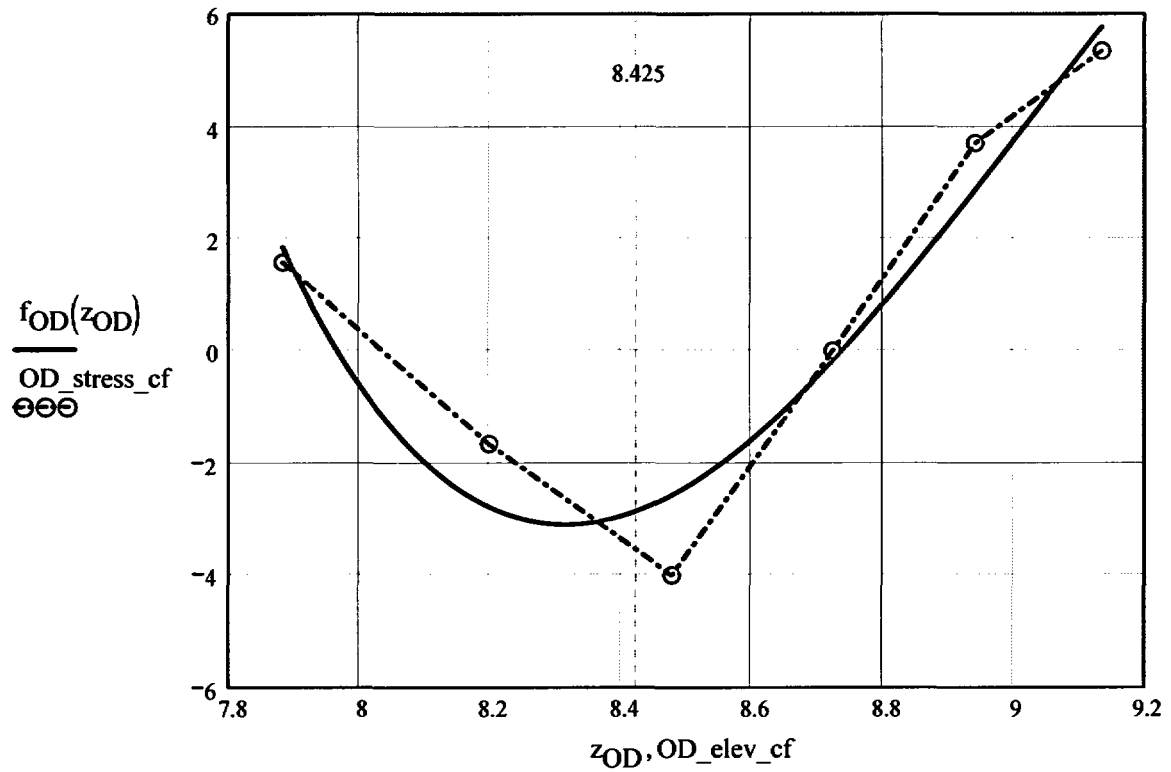

$f_{OD}(8.425) = -2.84902$

Calculation to develop Stress Profiles for Analysis

This analysis for the axial stress regression and the through-wall stress regression is the same as that used for the CEDM Nozzles (in Ref. 6); that is, the axial stresses are fit with a third-order polynomial.

$N := 20$ *Number of locations for stress profiles*

$Loc_0 := FL_{Cntr} - L$

$FL_{Cntr} = 8.425$

$L = 0.6$

$j := 1..N + 3$

$$Incr_i := \begin{cases} c_0 & \text{if } i < 4 \\ Inc_{Strs.avg} & \text{otherwise} \end{cases}$$

$Loc_i := Loc_{i-1} + Incr_i$

$SID_i := R_{ID_3} + R_{ID_4} \cdot Loc_i + R_{ID_5} \cdot (Loc_i)^2 + R_{ID_6} \cdot (Loc_i)^3$

$SQT_i := R_{QT_3} + R_{QT_4} \cdot Loc_i + R_{QT_5} \cdot (Loc_i)^2 + R_{QT_6} \cdot (Loc_i)^3$

$SMD_i := R_{MD_3} + R_{MD_4} \cdot Loc_i + R_{MD_5} \cdot (Loc_i)^2 + R_{MD_6} \cdot (Loc_i)^3$

$STQ_i := R_{TQ_3} + R_{TQ_4} \cdot Loc_i + R_{TQ_5} \cdot (Loc_i)^2 + R_{TQ_6} \cdot (Loc_i)^3$

$SOD_i := R_{OD_3} + R_{OD_4} \cdot Loc_i + R_{OD_5} \cdot (Loc_i)^2 + R_{OD_6} \cdot (Loc_i)^3$

$j := 1..N$

$$S_{id_j} := \begin{cases} \dfrac{SID_j + SID_{j+1} + SID_{j+2}}{3} & \text{if } j = 1 \\ \dfrac{S_{id_{j-1}} \cdot (j+1) + SID_{j+2}}{j+2} & \text{otherwise} \end{cases}$$

$$S_{qt_j} := \begin{cases} \dfrac{SQT_j + SQT_{j+1} + SQT_{j+2}}{3} & \text{if } j = 1 \\ \dfrac{S_{qt_{(j-1)}} \cdot (j+1) + SQT_{j+2}}{j+2} & \text{otherwise} \end{cases}$$

$$S_{md_j} := \begin{cases} \dfrac{SMD_j + SMD_{j+1} + SMD_{j+2}}{3} & \text{if } j = 1 \\ \dfrac{S_{md_{j-1}} \cdot (j+1) + SMD_{j+2}}{j+2} & \text{otherwise} \end{cases}$$

$$S_{tq_j} := \begin{cases} \dfrac{STQ_j + STQ_{j+1} + STQ_{j+2}}{3} & \text{if } j = 1 \\ \dfrac{S_{tq_{j-1}} \cdot (j+1) + STQ_{j+2}}{j+2} & \text{otherwise} \end{cases}$$

$$S_{od_j} := \begin{cases} \dfrac{SOD_j + SOD_{j+1} + SOD_{j+2}}{3} & \text{if } j = 1 \\ \dfrac{S_{od_{j-1}} \cdot (j+1) + SOD_{j+2}}{j+2} & \text{otherwise} \end{cases}$$

Through-Wall Stress Distribution for ID Flaws (i.e. ID to OD Stress distribution)

$u_0 := 0.000$ $u_1 := 0.25$ $u_2 := 0.50$ $u_3 := 0.75$ $u_4 := 1.00$

$$Y := \text{stack}(u_0, u_1, u_2, u_3, u_4)$$

$SIG_1 := \text{stack}(S_{id_1}, S_{qt_1}, S_{md_1}, S_{tq_1}, S_{od_1})$ $SIG_2 := \text{stack}(S_{id_2}, S_{qt_2}, S_{md_2}, S_{tq_2}, S_{od_2})$

$SIG_3 := \text{stack}(S_{id_3}, S_{qt_3}, S_{md_3}, S_{tq_3}, S_{od_3})$ $SIG_4 := \text{stack}(S_{id_4}, S_{qt_4}, S_{md_4}, S_{tq_4}, S_{od_4})$

$SIG_5 := \text{stack}(S_{id_5}, S_{qt_5}, S_{md_5}, S_{tq_5}, S_{od_5})$ $SIG_6 := \text{stack}(S_{id_6}, S_{qt_6}, S_{md_6}, S_{tq_6}, S_{od_6})$

$SIG_7 := \text{stack}(S_{id_7}, S_{qt_7}, S_{md_7}, S_{tq_7}, S_{od_7})$ $SIG_8 := \text{stack}(S_{id_8}, S_{qt_8}, S_{md_8}, S_{tq_8}, S_{od_8})$

$SIG_9 := \text{stack}(S_{id_9}, S_{qt_9}, S_{md_9}, S_{tq_9}, S_{od_9})$ $SIG_{10} := \text{stack}(S_{id_{10}}, S_{qt_{10}}, S_{md_{10}}, S_{tq_{10}}, S_{od_{10}})$

$SIG_{11} := \text{stack}(S_{id_{11}}, S_{qt_{11}}, S_{md_{11}}, S_{tq_{11}}, S_{od_{11}})$ $SIG_{12} := \text{stack}(S_{id_{12}}, S_{qt_{12}}, S_{md_{12}}, S_{tq_{12}}, S_{od_{12}})$

$SIG_{13} := \text{stack}(S_{id_{13}}, S_{qt_{13}}, S_{md_{13}}, S_{tq_{13}}, S_{od_{13}})$ $SIG_{14} := \text{stack}(S_{id_{14}}, S_{qt_{14}}, S_{md_{14}}, S_{tq_{14}}, S_{od_{14}})$

$SIG_{15} := \text{stack}(S_{id_{15}}, S_{qt_{15}}, S_{md_{15}}, S_{tq_{15}}, S_{od_{15}})$ $SIG_{16} := \text{stack}(S_{id_{16}}, S_{qt_{16}}, S_{md_{16}}, S_{tq_{16}}, S_{od_{16}})$

$SIG_{17} := \text{stack}(S_{id_{17}}, S_{qt_{17}}, S_{md_{17}}, S_{tq_{17}}, S_{od_{17}})$ $SIG_{18} := \text{stack}(S_{id_{18}}, S_{qt_{18}}, S_{md_{18}}, S_{tq_{18}}, S_{od_{18}})$

$SIG_{19} := \text{stack}(S_{id_{19}}, S_{qt_{19}}, S_{md_{19}}, S_{tq_{19}}, S_{od_{19}})$ $SIG_{20} := \text{stack}(S_{id_{20}}, S_{qt_{20}}, S_{md_{20}}, S_{tq_{20}}, S_{od_{20}})$

Regression of Through-Wall Stress distribution to Obtain Stress Coefficients Using a Third Order Polynomial

$IDRG_1 := regress(Y, SIG_1, 3)$

$IDRG_2 := regress(Y, SIG_2, 3)$

$IDRG_3 := regress(Y, SIG_3, 3)$

$IDRG_4 := regress(Y, SIG_4, 3)$

$IDRG_5 := regress(Y, SIG_5, 3)$

$IDRG_6 := regress(Y, SIG_6, 3)$

$IDRG_7 := regress(Y, SIG_7, 3)$

$IDRG_8 := regress(Y, SIG_8, 3)$

$IDRG_9 := regress(Y, SIG_9, 3)$

$IDRG_{10} := regress(Y, SIG_{10}, 3)$

$IDRG_{11} := regress(Y, SIG_{11}, 3)$

$IDRG_{12} := regress(Y, SIG_{12}, 3)$

$IDRG_{13} := regress(Y, SIG_{13}, 3)$

$IDRG_{14} := regress(Y, SIG_{14}, 3)$

$IDRG_{15} := regress(Y, SIG_{15}, 3)$

$IDRG_{16} := regress(Y, SIG_{16}, 3)$

$IDRG_{17} := regress(Y, SIG_{17}, 3)$

$IDRG_{18} := regress(Y, SIG_{18}, 3)$

$IDRG_{19} := regress(Y, SIG_{19}, 3)$

$IDRG_{20} := regress(Y, SIG_{20}, 3)$

Stress Distribution in the tube. ***Stress influence coefficients obtained from thrid-order polynomial curve fit to the throughwall stress distribution***

Data Files for Flaw Shape Factors from NASA SC04 Model [Ref. 9]

{NO INPUT Required}

Mettu Raju Newman Sivakumar Forman Solution of ID Part throughwall Flaw in Cyinder

Jsb :=

	0	1	2
0	1.000	0.200	0.000
1	1.000	0.200	0.200
2	1.000	0.200	0.500
3	1.000	0.200	0.800
4	1.000	0.200	1.000
5	1.000	0.400	0.000
6	1.000	0.400	0.200
7	1.000	0.400	0.500
8	1.000	0.400	0.800
9	1.000	0.400	1.000
10	1.000	1.000	0.000
11	1.000	1.000	0.200
12	1.000	1.000	0.500
13	1.000	1.000	0.800
14	1.000	1.000	1.000
15	2.000	0.200	0.000
16	2.000	0.200	0.200
17	2.000	0.200	0.500
18	2.000	0.200	0.800
19	2.000	0.200	1.000
20	2.000	0.400	0.000
21	2.000	0.400	0.200
22	2.000	0.400	0.500
23	2.000	0.400	0.800
24	2.000	0.400	1.000
25	2.000	1.000	0.000
26	2.000	1.000	0.200
27	2.000	1.000	0.500
28	2.000	1.000	0.800
29	2.000	1.000	1.000
30	4.000	0.200	0.000
31	4.000	0.200	0.200
32	4.000	0.200	0.500
33	4.000	0.200	0.800
34	4.000	0.200	1.000
35	4.000	0.400	0.000
36	4.000	0.400	0.200

37	4.000	0.400	0.500
38	4.000	0.400	0.800
39	4.000	0.400	1.000
40	4.000	1.000	0.000
41	4.000	1.000	0.200
42	4.000	1.000	0.500
43	4.000	1.000	0.800
44	4.000	1.000	1.000
45	10.000	0.200	0.000
46	10.000	0.200	0.200
47	10.000	0.200	0.500
48	10.000	0.200	0.800
49	10.000	0.200	1.000
50	10.000	0.400	0.000
51	10.000	0.400	0.200
52	10.000	0.400	0.500
53	10.000	0.400	0.800
54	10.000	0.400	1.000
55	10.000	1.000	0.000
56	10.000	1.000	0.200
57	10.000	1.000	0.500
58	10.000	1.000	0.800
59	10.000	1.000	1.000
60	300.000	0.200	0.000
61	300.000	0.200	0.200
62	300.000	0.200	0.500
63	300.000	0.200	0.800
64	300.000	0.200	1.000
65	300.000	0.400	0.000
66	300.000	0.400	0.200
67	300.000	0.400	0.500
68	300.000	0.400	0.800
69	300.000	0.400	1.000
70	300.000	1.000	0.000
71	300.000	1.000	0.200
72	300.000	1.000	0.500
73	300.000	1.000	0.800
74	300.000	1.000	1.000

Sambi :=

	0	1	2	3	4	5	6	7
0	1.076	0.693	0.531	0.434	0.608	0.083	0.023	0.009
1	1.056	0.647	0.495	0.408	0.615	0.085	0.027	0.013
2	1.395	0.767	0.557	0.446	0.871	0.171	0.069	0.038
3	2.53	1.174	0.772	0.58	1.554	0.363	0.155	0.085
4	3.846	1.615	0.995	0.716	2.277	0.544	0.233	0.127
5	1.051	0.689	0.536	0.444	0.74	0.112	0.035	0.015
6	1.011	0.646	0.504	0.421	0.745	0.119	0.041	0.02
7	1.149	0.694	0.529	0.435	0.916	0.181	0.073	0.04
8	1.6	0.889	0.642	0.51	1.334	0.307	0.132	0.073
9	2.087	1.093	0.761	0.589	1.752	0.421	0.183	0.101
10	0.992	0.704	0.534	0.506	1.044	0.169	0.064	0.032
11	0.987	0.701	0.554	0.491	1.08	0.182	0.067	0.034
12	1.01	0.709	0.577	0.493	1.116	0.2	0.078	0.041
13	1.07	0.73	0.623	0.523	1.132	0.218	0.095	0.051
14	1.128	0.75	0.675	0.556	1.131	0.229	0.11	0.06
15	1.049	0.673	0.519	0.427	0.6	0.078	0.021	0.008
16	1.091	0.661	0.502	0.413	0.614	0.083	0.025	0.012
17	1.384	0.764	0.556	0.446	0.817	0.15	0.058	0.031
18	2.059	1.033	0.708	0.545	1.3	0.291	0.123	0.067
19	2.739	1.301	0.858	0.643	1.783	0.421	0.18	0.099
20	1.075	0.674	0.527	0.436	0.73	0.072	0.044	0.021
21	1.045	0.659	0.511	0.425	0.76	0.122	0.043	0.021
22	1.16	0.71	0.536	0.441	0.919	0.197	0.064	0.034
23	1.51	0.854	0.623	0.498	1.231	0.271	0.114	0.062
24	1.876	0.995	0.71	0.555	1.519	0.317	0.161	0.089
25	1.037	0.732	0.594	0.505	1.132	0.192	0.07	0.035
26	1.003	0.707	0.577	0.493	1.113	0.19	0.071	0.036
27	1.023	0.714	0.58	0.495	1.155	0.207	0.08	0.042
28	1.129	0.774	0.619	0.521	1.286	0.247	0.098	0.052
29	1.242	0.84	0.661	0.549	1.416	0.285	0.115	0.061
30	1.003	0.649	0.511	0.43	0.577	0.07	0.015	0.005
31	1.097	0.666	0.511	0.426	0.606	0.079	0.023	0.01
32	1.405	0.776	0.567	0.46	0.797	0.141	0.054	0.028
33	1.959	0.996	0.692	0.542	1.201	0.262	0.108	0.059
34	2.461	1.197	0.808	0.619	1.586	0.37	0.154	0.085
35	1.024	0.668	0.528	0.451	0.737	0.11	0.033	0.015
36	1.057	0.666	0.52	0.439	0.77	0.123	0.042	0.021
37	1.193	0.715	0.545	0.454	0.924	0.174	0.068	0.036
38	1.443	0.828	0.614	0.509	1.219	0.263	0.109	0.059
39	1.665	0.934	0.681	0.565	1.487	0.339	0.143	0.078

40	1.005	0.72	0.597	0.518	1.119	0.188	0.068	0.034
41	1.009	0.713	0.588	0.511	1.128	0.194	0.072	0.037
42	1.041	0.726	0.594	0.515	1.191	0.214	0.082	0.043
43	1.105	0.768	0.623	0.536	1.316	0.248	0.097	0.05
44	1.162	0.81	0.653	0.558	1.428	0.277	0.109	0.055
45	0.973	0.635	0.499	0.446	0.579	0.07	0.016	0.005
46	1.115	0.673	0.514	0.438	0.607	0.079	0.023	0.01
47	1.427	0.783	0.571	0.462	0.791	0.138	0.052	0.027
48	1.872	0.96	0.671	0.529	1.179	0.253	0.104	0.056
49	2.23	1.108	0.757	0.594	1.548	0.356	0.149	0.081
50	0.992	0.656	0.52	0.443	0.733	0.109	0.032	0.014
51	1.072	0.672	0.523	0.441	0.777	0.125	0.043	0.021
52	1.217	0.723	0.549	0.456	0.936	0.176	0.069	0.036
53	1.393	0.806	0.601	0.493	1.219	0.259	0.106	0.056
54	1.521	0.875	0.647	0.528	1.469	0.328	0.135	0.071
55	0.994	0.715	0.59	0.518	1.114	0.187	0.068	0.035
56	1.015	0.715	0.588	0.512	1.14	0.197	0.074	0.038
57	1.05	0.729	0.596	0.515	1.219	0.221	0.085	0.044
58	1.09	0.76	0.618	0.532	1.348	0.255	0.099	0.051
59	1.118	0.788	0.639	0.55	1.456	0.282	0.109	0.056
60	0.936	0.62	0.486	0.405	0.582	0.068	0.015	0.005
61	1.145	0.681	0.514	0.42	0.613	0.081	0.024	0.011
62	1.459	0.79	0.569	0.454	0.79	0.138	0.051	0.026
63	1.774	0.917	0.641	0.501	1.148	0.239	0.096	0.051
64	1.974	1.008	0.696	0.537	1.482	0.328	0.134	0.07
65	0.982	0.651	0.512	0.427	0.721	0.103	0.031	0.013
66	1.095	0.677	0.52	0.431	0.782	0.127	0.045	0.022
67	1.244	0.727	0.546	0.446	0.946	0.18	0.071	0.037
68	1.37	0.791	0.585	0.473	1.201	0.253	0.102	0.054
69	1.438	0.838	0.618	0.496	1.413	0.31	0.126	0.066

$\underset{\sim}{W} := Jsb^{\langle 0 \rangle}$ $\quad X := Jsb^{\langle 1 \rangle}$ $\quad Y := Jsb^{\langle 2 \rangle}$

$a_U := Sambi^{\langle 0 \rangle}$ $\quad a_L := Sambi^{\langle 1 \rangle}$ $\quad a_Q := Sambi^{\langle 2 \rangle}$ $\quad a_C := Sambi^{\langle 3 \rangle}$

$c_U := Sambi^{\langle 4 \rangle}$ $\quad c_L := Sambi^{\langle 5 \rangle}$ $\quad c_Q := Sambi^{\langle 6 \rangle}$ $\quad c_C := Sambi^{\langle 7 \rangle}$

$$n := \begin{cases} 3 & \text{if } R_t \le 4.0 \\ 2 & \text{otherwise} \end{cases}$$

"a-Tip" Uniform Term

$M_{aU} := \text{augment}(W, X, Y)$ $V_{aU} := a_U$ $R_{aU} := \text{regress}(M_{aU}, V_{aU}, n)$

$$f_{aU}(W, X, Y) := \text{interp}\left[R_{aU}, M_{aU}, V_{aU}, \begin{pmatrix} W \\ X \\ Y \end{pmatrix}\right]$$

$f_{aU}(4, .4, .8) = 1.7089$ *Check Calculation*

Linear Term

$M_{aL} := \text{augment}(W, X, Y)$ $V_{aL} := a_L$ $R_{aL} := \text{regress}(M_{aL}, V_{aL}, n)$

$$f_{aL}(W, X, Y) := \text{interp}\left[R_{aL}, M_{aL}, V_{aL}, \begin{pmatrix} W \\ X \\ Y \end{pmatrix}\right]$$

$f_{aL}(4, .4, .8) = 0.93393$ *Check Calculation*

Quadratic Term

$M_{aQ} := \text{augment}(W, X, Y)$ $V_{aQ} := a_Q$ $R_{aQ} := \text{regress}(M_{aQ}, V_{aQ}, n)$

$$f_{aQ}(W, X, Y) := \text{interp}\left[R_{aQ}, M_{aQ}, V_{aQ}, \begin{pmatrix} W \\ X \\ Y \end{pmatrix}\right]$$

$f_{aQ}(4,.4,.8) = 0.67668$ *Check Calculation*

Cubic Term

$M_{aC} := \text{augment}(W,X,Y)$ $V_{aC} := a_C$ $R_{aC} := \text{regress}(M_{aC}, V_{aC}, n)$

$$f_{aC}(W,X,Y) := \text{interp}\left[R_{aC}, M_{aC}, V_{aC}, \begin{pmatrix} W \\ X \\ Y \end{pmatrix}\right]$$

$f_{aC}(4,.4,.8) = 0.54151$ *Check Calculation*

"C" Tip Coefficients

Uniform Term

$M_{cU} := \text{augment}(W,X,Y)$ $V_{cU} := c_U$ $R_{cU} := \text{regress}(M_{cU}, V_{cU}, n)$

$$f_{cU}(W,X,Y) := \text{interp}\left[R_{cU}, M_{cU}, V_{cU}, \begin{pmatrix} W \\ X \\ Y \end{pmatrix}\right]$$

$f_{cU}(4,.4,.8) = 1.31015$ *Check Calculation*

Linear Term

$M_{cL} := \text{augment}(W,X,Y)$ $V_{cL} := c_L$ $R_{cL} := \text{regress}(M_{cL}, V_{cL}, n)$

$$f_{cL}(W,X,Y) := \text{interp}\left[R_{cL}, M_{cL}, V_{cL}, \begin{pmatrix} W \\ X \\ Y \end{pmatrix}\right]$$

$f_{cL}(2,.4,.8) = 0.28509$ *Check Calculation*

Quadratic Term

$M_{cQ} := \text{augment}(W,X,Y)$ $V_{cQ} := c_Q$ $R_{cQ} := \text{regress}(M_{cQ}, V_{cQ}, n)$

$$f_{cQ}(W,X,Y) := \text{interp}\left[R_{cQ}, M_{cQ}, V_{cQ}, \begin{pmatrix} W \\ X \\ Y \end{pmatrix}\right]$$

$f_{cQ}(4,.4,.8) = 0.11797$ *Check Calculation*

Cubic Term

$M_{cC} := \text{augment}(W,X,Y)$ $V_{cC} := c_C$ $R_{cC} := \text{regress}(M_{cC}, V_{cC}, n)$

$$f_{cC}(W,X,Y) := \text{interp}\left[R_{cC}, M_{cC}, V_{cC}, \begin{pmatrix} W \\ X \\ Y \end{pmatrix}\right]$$

$f_{cC}(4,.4,.8) = 0.06384$ *Check Calculation*

Calculations : Recursive calculations to estimate flaw growth

Recursive Loop for Calculation of PWSCC Crack Growth

$CGR_{sambi} :=$ | $j \leftarrow 0$

$a_0 \leftarrow a_0$

$c_0 \leftarrow c_0$

$t \leftarrow t2$

$NCB_0 \leftarrow C_{blk}$

while $j \le I_{lim}$

$\sigma_0 \leftarrow$ | $IDRG_{1_3}$ if $c_j \le c_0$

$IDRG_{2_3}$ if $c_0 < c_j \le c_0 + Inc_{Strs.avg}$

$IDRG_{3_3}$ if $c_0 + Inc_{Strs.avg} < c_j \le c_0 + 2 \cdot Inc_{Strs.avg}$

$IDRG_{4_3}$ if $c_0 + 2 \cdot Inc_{Strs.avg} < c_j \le c_0 + 3 \cdot Inc_{Strs.avg}$

$IDRG_{5_3}$ if $c_0 + 3 \cdot Inc_{Strs.avg} < c_j \le c_0 + 4 \cdot Inc_{Strs.avg}$

$IDRG_{6_3}$ if $c_0 + 4 \cdot Inc_{Strs.avg} < c_j \le c_0 + 5 \cdot Inc_{Strs.avg}$

$IDRG_{7_3}$ if $c_0 + 5 \cdot Inc_{Strs.avg} < c_j \le c_0 + 6 \cdot Inc_{Strs.avg}$

$IDRG_{8_3}$ if $c_0 + 6 \cdot Inc_{Strs.avg} < c_j \le c_0 + 7 \cdot Inc_{Strs.avg}$

$IDRG_{9_3}$ if $c_0 + 7 \cdot Inc_{Strs.avg} < c_j \le c_0 + 8 \cdot Inc_{Strs.avg}$

$IDRG_{10_3}$ if $c_0 + 8 \cdot Inc_{Strs.avg} < c_j \le c_0 + 9 \cdot Inc_{Strs.avg}$

$IDRG_{11_3}$ if $c_0 + 9 \cdot Inc_{Strs.avg} < c_j \le c_0 + 10 \cdot Inc_{Strs.avg}$

$IDRG_{12_3}$ if $c_0 + 10 \cdot Inc_{Strs.avg} < c_j \le c_0 + 11 \cdot Inc_{Strs.avg}$

$IDRG_{13_3}$ if $c_0 + 11 \cdot Inc_{Strs.avg} < c_j \le c_0 + 12 \cdot Inc_{Strs.avg}$

$IDRG_{14_3}$ if $c_0 + 12 \cdot Inc_{Strs.avg} < c_j \le c_0 + 13 \cdot Inc_{Strs.avg}$

$IDRG$ if $c_0 + 13 \cdot Inc$ $< c_j \le c_0 + 14 \cdot Inc$

$$\begin{cases} \text{IDRG}15_3 & \text{if } c_0 + 13\cdot\text{Inc}_{\text{Strs.avg}} < c_j \le c_0 + 14\cdot\text{Inc}_{\text{Strs.avg}} \\ \text{IDRG}16_3 & \text{if } c_0 + 14\cdot\text{Inc}_{\text{Strs.avg}} < c_j \le c_0 + 15\cdot\text{Inc}_{\text{Strs.avg}} \\ \text{IDRG}17_3 & \text{if } c_0 + 15\cdot\text{Inc}_{\text{Strs.avg}} < c_j \le c_0 + 16\cdot\text{Inc}_{\text{Strs.avg}} \\ \text{IDRG}18_3 & \text{if } c_0 + 16\cdot\text{Inc}_{\text{Strs.avg}} < c_j \le c_0 + 17\cdot\text{Inc}_{\text{Strs.avg}} \\ \text{IDRG}19_3 & \text{if } c_0 + 17\cdot\text{Inc}_{\text{Strs.avg}} < c_j \le c_0 + 18\cdot\text{Inc}_{\text{Strs.avg}} \\ \text{IDRG}20_3 & \text{otherwise} \end{cases}$$

$$\sigma_1 \leftarrow \begin{cases} \text{IDRG}1_4 & \text{if } c_j \le c_0 \\ \text{IDRG}2_4 & \text{if } c_0 < c_j \le c_0 + \text{Inc}_{\text{Strs.avg}} \\ \text{IDRG}3_4 & \text{if } c_0 + \text{Inc}_{\text{Strs.avg}} < c_j \le c_0 + 2\cdot\text{Inc}_{\text{Strs.avg}} \\ \text{IDRG}4_4 & \text{if } c_0 + 2\cdot\text{Inc}_{\text{Strs.avg}} < c_j \le c_0 + 3\cdot\text{Inc}_{\text{Strs.avg}} \\ \text{IDRG}5_4 & \text{if } c_0 + 3\cdot\text{Inc}_{\text{Strs.avg}} < c_j \le c_0 + 4\cdot\text{Inc}_{\text{Strs.avg}} \\ \text{IDRG}6_4 & \text{if } c_0 + 4\cdot\text{Inc}_{\text{Strs.avg}} < c_j \le c_0 + 5\cdot\text{Inc}_{\text{Strs.avg}} \\ \text{IDRG}7_4 & \text{if } c_0 + 5\cdot\text{Inc}_{\text{Strs.avg}} < c_j \le c_0 + 6\cdot\text{Inc}_{\text{Strs.avg}} \\ \text{IDRG}8_4 & \text{if } c_0 + 6\cdot\text{Inc}_{\text{Strs.avg}} < c_j \le c_0 + 7\cdot\text{Inc}_{\text{Strs.avg}} \\ \text{IDRG}9_4 & \text{if } c_0 + 7\cdot\text{Inc}_{\text{Strs.avg}} < c_j \le c_0 + 8\cdot\text{Inc}_{\text{Strs.avg}} \\ \text{IDRG}10_4 & \text{if } c_0 + 8\cdot\text{Inc}_{\text{Strs.avg}} < c_j \le c_0 + 9\cdot\text{Inc}_{\text{Strs.avg}} \\ \text{IDRG}11_4 & \text{if } c_0 + 9\cdot\text{Inc}_{\text{Strs.avg}} < c_j \le c_0 + 10\cdot\text{Inc}_{\text{Strs.avg}} \\ \text{IDRG}12_4 & \text{if } c_0 + 10\cdot\text{Inc}_{\text{Strs.avg}} < c_j \le c_0 + 11\cdot\text{Inc}_{\text{Strs.avg}} \\ \text{IDRG}13_4 & \text{if } c_0 + 11\cdot\text{Inc}_{\text{Strs.avg}} < c_j \le c_0 + 12\cdot\text{Inc}_{\text{Strs.avg}} \\ \text{IDRG}14_4 & \text{if } c_0 + 12\cdot\text{Inc}_{\text{Strs.avg}} < c_j \le c_0 + 13\cdot\text{Inc}_{\text{Strs.avg}} \\ \text{IDRG}15_4 & \text{if } c_0 + 13\cdot\text{Inc}_{\text{Strs.avg}} < c_j \le c_0 + 14\cdot\text{Inc}_{\text{Strs.avg}} \\ \text{IDRG}16_4 & \text{if } c_0 + 14\cdot\text{Inc}_{\text{Strs.avg}} < c_j \le c_0 + 15\cdot\text{Inc}_{\text{Strs.avg}} \end{cases}$$

$IDRG17_4$ if $c_0 + 15 \cdot Inc_{Strs.avg} < c_j \le c_0 + 16 \cdot Inc_{Strs.avg}$

$IDRG18_4$ if $c_0 + 16 \cdot Inc_{Strs.avg} < c_j \le c_0 + 17 \cdot Inc_{Strs.avg}$

$IDRG19_4$ if $c_0 + 17 \cdot Inc_{Strs.avg} < c_j \le c_0 + 18 \cdot Inc_{Strs.avg}$

$IDRG20_4$ otherwise

$\sigma_2 \leftarrow$

$IDRG1_5$ if $c_j \le c_0$

$IDRG2_5$ if $c_0 < c_j \le c_0 + Inc_{Strs.avg}$

$IDRG3_5$ if $c_0 + Inc_{Strs.avg} < c_j \le c_0 + 2 \cdot Inc_{Strs.avg}$

$IDRG4_5$ if $c_0 + 2 \cdot Inc_{Strs.avg} < c_j \le c_0 + 3 \cdot Inc_{Strs.avg}$

$IDRG5_5$ if $c_0 + 3 \cdot Inc_{Strs.avg} < c_j \le c_0 + 4 \cdot Inc_{Strs.avg}$

$IDRG6_5$ if $c_0 + 4 \cdot Inc_{Strs.avg} < c_j \le c_0 + 5 \cdot Inc_{Strs.avg}$

$IDRG7_5$ if $c_0 + 5 \cdot Inc_{Strs.avg} < c_j \le c_0 + 6 \cdot Inc_{Strs.avg}$

$IDRG8_5$ if $c_0 + 6 \cdot Inc_{Strs.avg} < c_j \le c_0 + 7 \cdot Inc_{Strs.avg}$

$IDRG9_5$ if $c_0 + 7 \cdot Inc_{Strs.avg} < c_j \le c_0 + 8 \cdot Inc_{Strs.avg}$

$IDRG10_5$ if $c_0 + 8 \cdot Inc_{Strs.avg} < c_j \le c_0 + 9 \cdot Inc_{Strs.avg}$

$IDRG11_5$ if $c_0 + 9 \cdot Inc_{Strs.avg} < c_j \le c_0 + 10 \cdot Inc_{Strs.avg}$

$IDRG12_5$ if $c_0 + 10 \cdot Inc_{Strs.avg} < c_j \le c_0 + 11 \cdot Inc_{Strs.avg}$

$IDRG13_5$ if $c_0 + 11 \cdot Inc_{Strs.avg} < c_j \le c_0 + 12 \cdot Inc_{Strs.avg}$

$IDRG14_5$ if $c_0 + 12 \cdot Inc_{Strs.avg} < c_j \le c_0 + 13 \cdot Inc_{Strs.avg}$

$IDRG15_5$ if $c_0 + 13 \cdot Inc_{Strs.avg} < c_j \le c_0 + 14 \cdot Inc_{Strs.avg}$

$IDRG16_5$ if $c_0 + 14 \cdot Inc_{Strs.avg} < c_j \le c_0 + 15 \cdot Inc_{Strs.avg}$

$IDRG17_5$ if $c_0 + 15 \cdot Inc_{Strs.avg} < c_j \le c_0 + 16 \cdot Inc_{Strs.avg}$

$$\begin{aligned}
&\left|\begin{array}{ll}
\mathrm{IDRG}_{18_5} & \text{if } c_0 + 16\cdot \mathrm{Inc}_{\mathrm{Strs.avg}} < c_j \le c_0 + 17\cdot \mathrm{Inc}_{\mathrm{Strs.avg}} \\
\mathrm{IDRG}_{19_5} & \text{if } c_0 + 17\cdot \mathrm{Inc}_{\mathrm{Strs.avg}} < c_j \le c_0 + 18\cdot \mathrm{Inc}_{\mathrm{Strs.avg}} \\
\mathrm{IDRG}_{20_5} & \text{otherwise}
\end{array}\right. \\
\sigma_3 \leftarrow &\left|\begin{array}{ll}
\mathrm{IDRG}_{1_6} & \text{if } c_j \le c_0 \\
\mathrm{IDRG}_{2_6} & \text{if } c_0 < c_j \le c_0 + \mathrm{Inc}_{\mathrm{Strs.avg}} \\
\mathrm{IDRG}_{3_6} & \text{if } c_0 + \mathrm{Inc}_{\mathrm{Strs.avg}} < c_j \le c_0 + 2\cdot \mathrm{Inc}_{\mathrm{Strs.avg}} \\
\mathrm{IDRG}_{4_6} & \text{if } c_0 + 2\cdot \mathrm{Inc}_{\mathrm{Strs.avg}} < c_j \le c_0 + 3\cdot \mathrm{Inc}_{\mathrm{Strs.avg}} \\
\mathrm{IDRG}_{5_6} & \text{if } c_0 + 3\cdot \mathrm{Inc}_{\mathrm{Strs.avg}} < c_j \le c_0 + 4\cdot \mathrm{Inc}_{\mathrm{Strs.avg}} \\
\mathrm{IDRG}_{6_6} & \text{if } c_0 + 4\cdot \mathrm{Inc}_{\mathrm{Strs.avg}} < c_j \le c_0 + 5\cdot \mathrm{Inc}_{\mathrm{Strs.avg}} \\
\mathrm{IDRG}_{7_6} & \text{if } c_0 + 5\cdot \mathrm{Inc}_{\mathrm{Strs.avg}} < c_j \le c_0 + 6\cdot \mathrm{Inc}_{\mathrm{Strs.avg}} \\
\mathrm{IDRG}_{8_6} & \text{if } c_0 + 6\cdot \mathrm{Inc}_{\mathrm{Strs.avg}} < c_j \le c_0 + 7\cdot \mathrm{Inc}_{\mathrm{Strs.avg}} \\
\mathrm{IDRG}_{9_6} & \text{if } c_0 + 7\cdot \mathrm{Inc}_{\mathrm{Strs.avg}} < c_j \le c_0 + 8\cdot \mathrm{Inc}_{\mathrm{Strs.avg}} \\
\mathrm{IDRG}_{10_6} & \text{if } c_0 + 8\cdot \mathrm{Inc}_{\mathrm{Strs.avg}} < c_j \le c_0 + 9\cdot \mathrm{Inc}_{\mathrm{Strs.avg}} \\
\mathrm{IDRG}_{11_6} & \text{if } c_0 + 9\cdot \mathrm{Inc}_{\mathrm{Strs.avg}} < c_j \le c_0 + 10\cdot \mathrm{Inc}_{\mathrm{Strs.avg}} \\
\mathrm{IDRG}_{12_6} & \text{if } c_0 + 10\cdot \mathrm{Inc}_{\mathrm{Strs.avg}} < c_j \le c_0 + 11\cdot \mathrm{Inc}_{\mathrm{Strs.avg}} \\
\mathrm{IDRG}_{13_6} & \text{if } c_0 + 11\cdot \mathrm{Inc}_{\mathrm{Strs.avg}} < c_j \le c_0 + 12\cdot \mathrm{Inc}_{\mathrm{Strs.avg}} \\
\mathrm{IDRG}_{14_6} & \text{if } c_0 + 12\cdot \mathrm{Inc}_{\mathrm{Strs.avg}} < c_j \le c_0 + 13\cdot \mathrm{Inc}_{\mathrm{Strs.avg}} \\
\mathrm{IDRG}_{15_6} & \text{if } c_0 + 13\cdot \mathrm{Inc}_{\mathrm{Strs.avg}} < c_j \le c_0 + 14\cdot \mathrm{Inc}_{\mathrm{Strs.avg}} \\
\mathrm{IDRG}_{16_6} & \text{if } c_0 + 14\cdot \mathrm{Inc}_{\mathrm{Strs.avg}} < c_j \le c_0 + 15\cdot \mathrm{Inc}_{\mathrm{Strs.avg}} \\
\mathrm{IDRG}_{17_6} & \text{if } c_0 + 15\cdot \mathrm{Inc}_{\mathrm{Strs.avg}} < c_j \le c_0 + 16\cdot \mathrm{Inc}_{\mathrm{Strs.avg}} \\
\mathrm{IDRG}_{18_6} & \text{if } c_0 + 16\cdot \mathrm{Inc}_{\mathrm{Strs.avg}} < c_j \le c_0 + 17\cdot \mathrm{Inc}_{\mathrm{Strs.avg}} \\
\mathrm{IDRG} & \text{if } c_0 + 17\cdot \mathrm{Inc}_{\mathrm{Strs.avg}} < c_j \le c_0 + 18\cdot \mathrm{Inc}
\end{array}\right.
\end{aligned}$$

$IDRG19_6$ if $c_0 + 17 \cdot inc_{Strs.avg} < c_j \le c_0 + 18 \cdot inc_{Strs.avg}$

$IDRG20_6$ otherwise

$\xi_0 \leftarrow \sigma_0$

$\xi_1 \leftarrow \sigma_0 + \sigma_1 \cdot \left(\frac{0.25 \cdot a_j}{t}\right) + \sigma_2 \cdot \left(\frac{0.25 \cdot a_j}{t}\right)^2 + \sigma_3 \cdot \left(\frac{0.25 \cdot a_j}{t}\right)^3$

$\xi_2 \leftarrow \sigma_0 + \sigma_1 \cdot \left(\frac{0.5 \cdot a_j}{t}\right) + \sigma_2 \cdot \left(\frac{0.5 \cdot a_j}{t}\right)^2 + \sigma_3 \cdot \left(\frac{0.5 \cdot a_j}{t}\right)^3$

$\xi_3 \leftarrow \sigma_0 + \sigma_1 \cdot \left(\frac{0.75 \cdot a_j}{t}\right) + \sigma_2 \cdot \left(\frac{0.75 \cdot a_j}{t}\right)^2 + \sigma_3 \cdot \left(\frac{0.75 \cdot a_j}{t}\right)^3$

$\xi_4 \leftarrow \sigma_0 + \sigma_1 \cdot \left(\frac{1.0 \cdot a_j}{t}\right) + \sigma_2 \cdot \left(\frac{1.0 \cdot a_j}{t}\right)^2 + \sigma_3 \cdot \left(\frac{1.0 \cdot a_j}{t}\right)^3$

$x_0 \leftarrow 0.0$

$x_1 \leftarrow 0.25$

$x_2 \leftarrow 0.5$

$x_3 \leftarrow 0.75$

$x_4 \leftarrow 1.0$

$X \leftarrow \text{stack}(x_0, x_1, x_2, x_3, x_4)$

$ST \leftarrow \text{stack}(\xi_0, \xi_1, \xi_2, \xi_3, \xi_4)$

$RG \leftarrow \text{regress}(X, ST, 3)$

$\sigma_{00} \leftarrow RG_3 + P_{Int}$

$\sigma_{10} \leftarrow RG_4$

$\sigma_{20} \leftarrow RG_5$

$\sigma_{30} \leftarrow RG_6$

$AR_j \leftarrow \frac{a_j}{c_j}$

$AT_j \leftarrow \frac{a_j}{t}$

$$G_{au_j} \leftarrow f_{aU}(R_t, AR_j, AT_j)$$

$$G_{al_j} \leftarrow f_{aL}(R_t, AR_j, AT_j)$$

$$G_{aq_j} \leftarrow f_{aQ}(R_t, AR_j, AT_j)$$

$$G_{ac_j} \leftarrow f_{aC}(R_t, AR_j, AT_j)$$

$$G_{cu_j} \leftarrow f_{cU}(R_t, AR_j, AT_j)$$

$$G_{cl_j} \leftarrow f_{cL}(R_t, AR_j, AT_j)$$

$$G_{cq_j} \leftarrow f_{cQ}(R_t, AR_j, AT_j)$$

$$G_{cc_j} \leftarrow f_{cC}(R_t, AR_j, AT_j)$$

$$Q_j \leftarrow \begin{cases} 1 + 1.464 \cdot \left(\frac{a_j}{c_j}\right)^{1.65} & \text{if } c_j \geq a_j \\ 1 + 1.464 \cdot \left(\frac{c_j}{a_j}\right)^{1.65} & \text{otherwise} \end{cases}$$

$$K_{a_j} \leftarrow \left(\frac{\pi \cdot a_j}{Q_j}\right)^{0.5} \cdot \left(\sigma_{00} \cdot G_{au_j} + \sigma_{10} \cdot G_{al_j} + \sigma_{20} \cdot G_{aq_j} + \sigma_{30} \cdot G_{ac_j}\right)$$

$$K_{c_j} \leftarrow \left(\frac{\pi \cdot c_j}{Q_j}\right)^{0.5} \cdot \left(\sigma_{00} \cdot G_{cu_j} + \sigma_{10} \cdot G_{cl_j} + \sigma_{20} \cdot G_{cq_j} + \sigma_{30} \cdot G_{cc_j}\right)$$

$$K_{\alpha_j} \leftarrow K_{a_j} \cdot 1.099$$

$$K_{\gamma_j} \leftarrow K_{c_j} \cdot 1.099$$

$$K_{\alpha_j} \leftarrow \begin{cases} 9.0 & \text{if } K_{\alpha_j} \leq 9.0 \\ K_{\alpha_j} & \text{otherwise} \end{cases}$$

$$K_{\gamma_j} \leftarrow \begin{cases} 9.0 & \text{if } K_{\gamma_j} \leq 9.0 \\ K_{\gamma_j} & \text{otherwise} \end{cases}$$

$$D_{a_i} \leftarrow C_0 \cdot \left(K_{\alpha_i} - 9.0\right)^{1.16}$$

$$D_{ag_j} \leftarrow \begin{cases} D_{a_j} \cdot CF_{inhr} \cdot C_{blk} & \text{if } K_{\alpha_j} < 80.0 \\ 4 \cdot 10^{-10} \cdot CF_{inhr} \cdot C_{blk} & \text{otherwise} \end{cases}$$

$$D_{c_j} \leftarrow C_0 \cdot \left(K_{\gamma_j} - 9.0\right)^{1.16}$$

$$D_{cg_j} \leftarrow \begin{cases} D_{c_j} \cdot CF_{inhr} \cdot C_{blk} & \text{if } K_{\gamma_j} < 80.0 \\ 4 \cdot 10^{-10} \cdot CF_{inhr} \cdot C_{blk} & \text{otherwise} \end{cases}$$

$$output_{(j,0)} \leftarrow j$$

$$output_{(j,1)} \leftarrow a_j$$

$$output_{(j,2)} \leftarrow c_j - c_0$$

$$output_{(j,3)} \leftarrow D_{ag_j}$$

$$output_{(j,4)} \leftarrow D_{cg_j}$$

$$output_{(j,5)} \leftarrow K_{a_j}$$

$$output_{(j,6)} \leftarrow K_{c_j}$$

$$output_{(j,7)} \leftarrow \frac{NCB_j}{365 \cdot 24}$$

$$output_{(j,8)} \leftarrow G_{au_j}$$

$$output_{(j,9)} \leftarrow G_{al_j}$$

$$output_{(j,10)} \leftarrow G_{aq_j}$$

$$output_{(j,11)} \leftarrow G_{ac_j}$$

$$output_{(j,12)} \leftarrow G_{cu_j}$$

$$output_{(j,13)} \leftarrow G_{cl_j}$$

$$output_{(j,14)} \leftarrow G_{cq_j}$$

$$output_{(j,15)} \leftarrow G_{cc_j}$$

$$j \leftarrow j + 1$$

$$a_j \leftarrow a_{j-1} + D_{ag_{j-1}}$$

$$c_j \leftarrow c_{j-1} + D_{cg_{j-1}}$$

$$a_j \leftarrow \begin{cases} t & \text{if } a_j \geq t \\ a_j & \text{otherwise} \end{cases}$$

$$NCB_j \leftarrow NCB_{j-1} + C_{blk}$$

output

$k := 0 .. I_{lim}$

The curve below shows the flaw growth through-wall and the operating time (in years) it takes for the initial flaw in the blind zone to go through-wall.

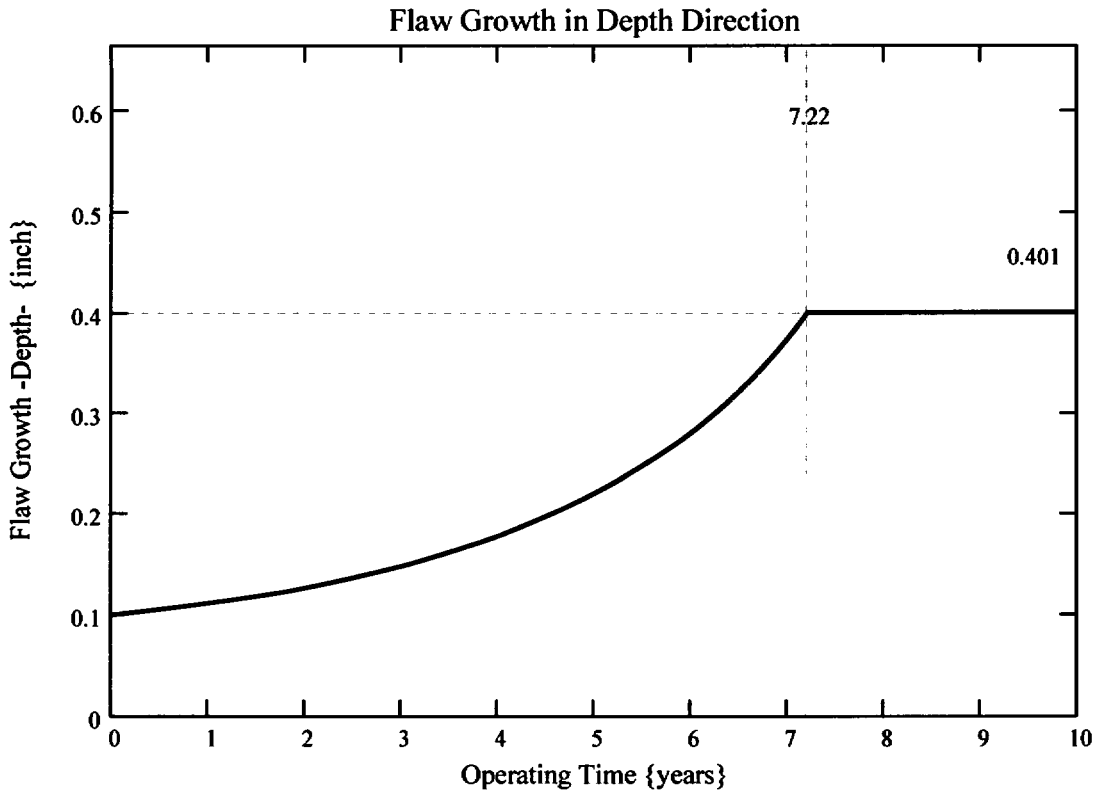

The propagation length for the ICI nozzles is defined as the length for which the initial flaw in the blind zone would extend out of the blind zone and grow to a detectable flaw. Reference 12 gives the minimum detectable flaw size of 4 mm (0.16) in length; thus, 0.16 inch was considered as this minimum detectable flaw length. This dimension is added to the end of the blind zone.

$$\text{Prop\_Length} := \frac{\text{BZ\_length}}{2} - c_0 + 0.16$$

$$\text{Prop\_Length} = 0.3$$

This implies that a flaw initially within the blindzone must grow 0.3 inch to become detectable via UT.

The curve below shows the flaw growth along the length of the ICI nozzle and the operating time (in years) it takes to reach the Prop_Length value defined above.

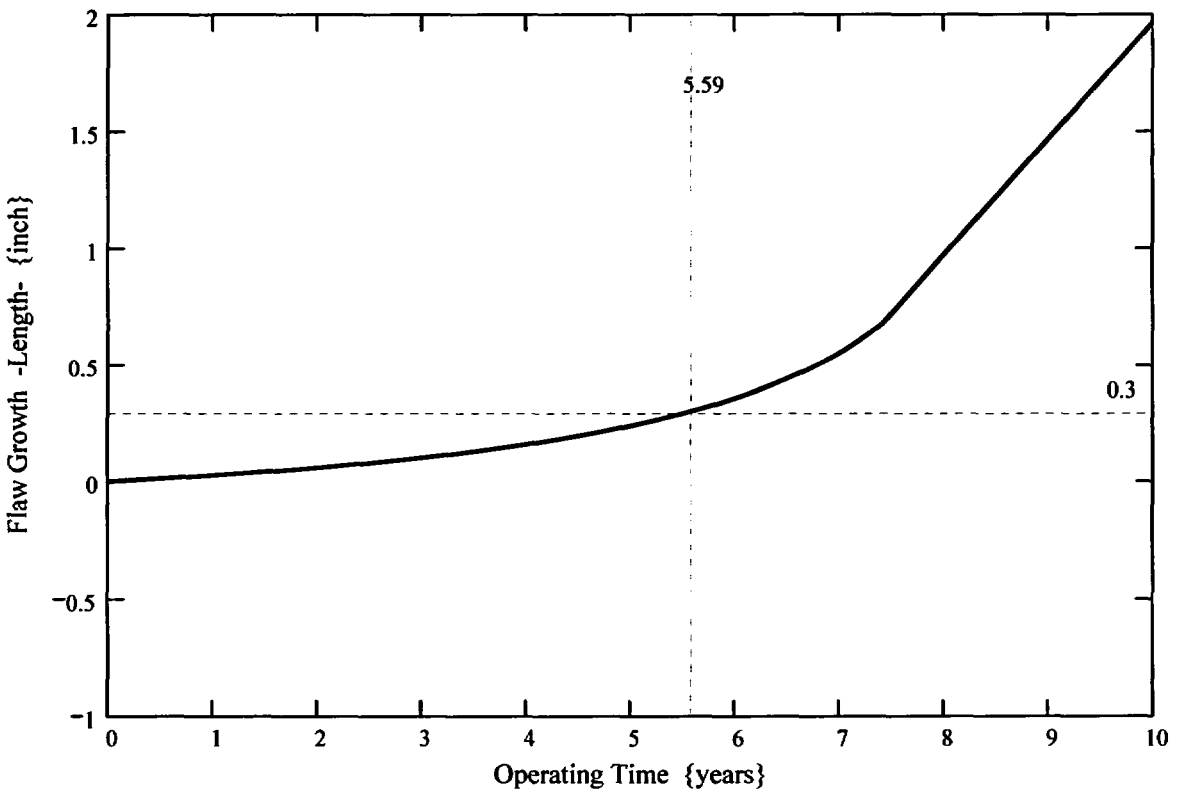

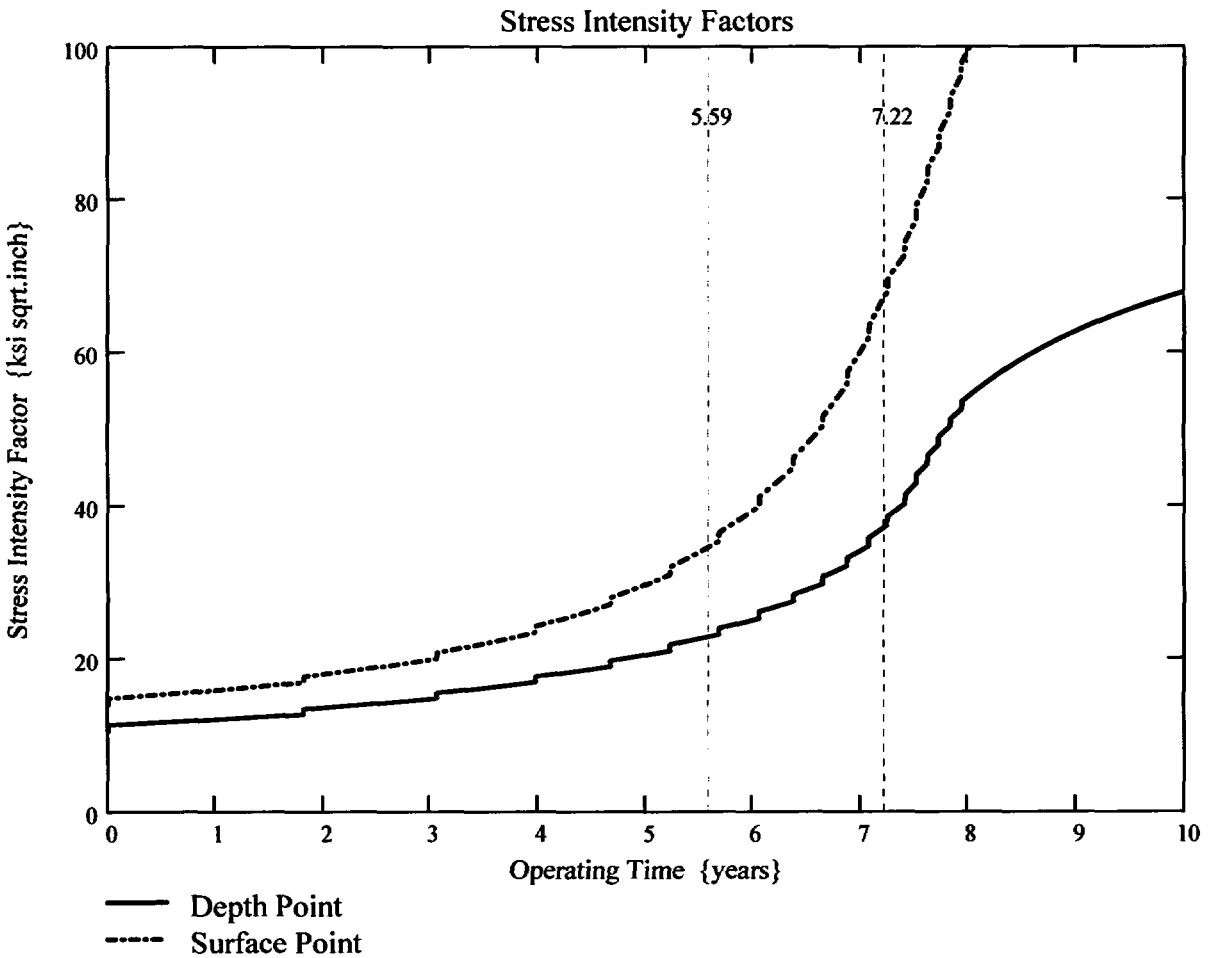
Stress Intensity Factors
Stress Intensity Factor {ksi sqrt.inch}
Operating Time {years}
5.59
7.22
0
20
40
60
80
100
0
1
2
3
4
5
6
7
8
9
10
Depth Point
Surface Point

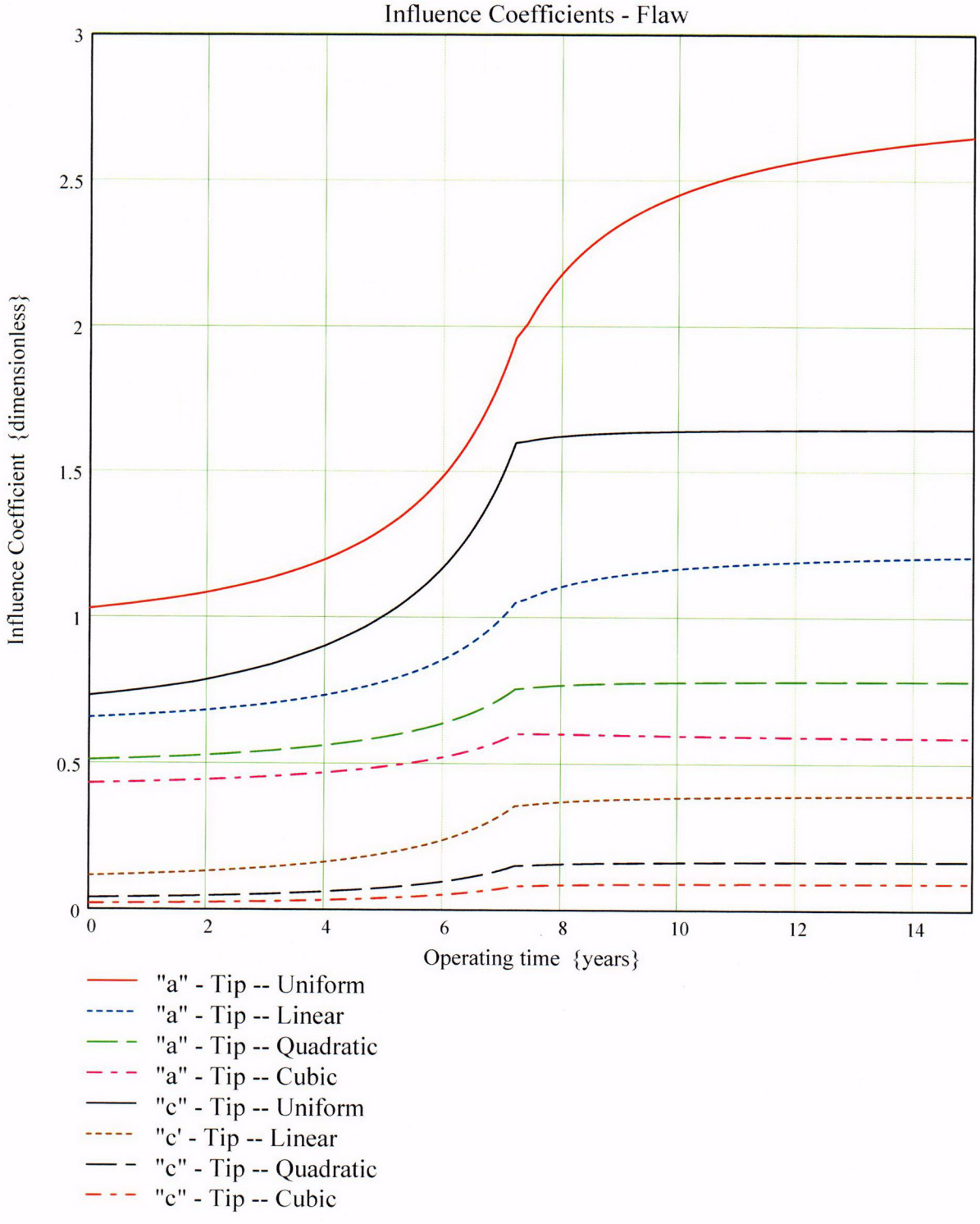
Influence Coefficients - Flaw
Influence Coefficient {dimensionless}
Operating time {years}
0
0.5
1
1.5
2
2.5
3
0
2
4
6
8
10
12
14
"a" - Tip -- Uniform
"a" - Tip -- Linear
"a" - Tip -- Quadratic
"a" - Tip -- Cubic
"c" - Tip -- Uniform
"c' - Tip -- Linear
"c" - Tip -- Quadratic
"c" - Tip -- Cubic

C13

Waterford Steam Electric Station Unit 3

Primary Water Stress Corrosion Crack Growth Analysis for an ICI ID Surface Flaw Uphill (180°), in the Blind Zone above the Top of the J-Groove Weld
Developed by Central Engineering Programs, Entergy Operations Inc.

Flaw Case 2: 0.4-inch Long Flaw with a 10-to-1 Flaw Length-to-Depth Aspect Ratio, Located at the Center of the Blind Zone

Calculation Basis: MRP 75 th Percentile and Flaw Face Pressurized

Mean Radius -to- Thickness Ratio:- "R_m/t" -- between 1.0 and 300.0

Note : ***The Metric form of the equation from EPRI MRP was used 55-Rev. 1*** *. A correction factor is applied in the determination of the crack extension to convert the units of meters per second to the value in inches per hour .*

ID Surface Flaw

User Input:

The Dominion Engineering Inc. (DEI) finite element model nodal elevations and hoop stresses for the uphill side (180° azimuth) of the ICI nozzle are brought into the Mathcad worksheet from data supplied in Reference 8d. The data are composed of the nodal elevations (in inches), along with the ID, 25% through-wall (tw), 50% tw, 75% tw, and OD hoop stresses, beginning two nodal lines below (nodal line 81101) the top of the weld (nodal line 81301) and extending to the top of the nozzle in the FEA model (nodal line 83301), which is at the point where the nozzle intersects the reactor vessel head.

The DEI FEA data has elevation referenced from the bottom of the ICI nozzle. The elevations of the node points in the DEI FEA model, beginning below the top of the weld, at nodal line 81101, and the corresponding hoop stresses are as follows:

Note the following terms used throughout this evaluation:

ID-inside diameter of ICI nozzle
QT-25% tw position
MD-50% tw, or mid-wall, position
TQ-75% tw position
OD-outside diameter of ICI nozzle

$i := 0..20$

Node_line :=	Elev_fea :=	ID_stress_fea :=	QT_stress_fea :=
81101	3.973	43.347	41.640
81201	4.089	42.799	39.703
81301	4.205	39.763	38.158
81401	4.435	37.068	33.351
81501	4.605	34.079	32.268
81601	4.798	29.820	28.465
81701	5.015	23.668	21.543
81801	5.262	18.722	14.133
81901	5.541	18.383	15.071
82001	5.857	18.876	17.269
82101	6.214	19.527	18.517
82201	6.619	20.331	19.550
82301	7.077	20.976	20.149
82401	7.596	21.408	20.378
82501	8.183	21.667	20.400
82601	8.847	21.792	20.133
82701	9.599	21.742	19.395
82801	10.451	21.550	18.466
82901	11.415	21.213	17.311
83001	12.505	19.876	16.176
83101	13.740	18.311	15.380
83201	15.138	16.442	14.525
83301	18.057	12.330	12.146

$$MD\_stress\_fea := \begin{pmatrix} 43.666 \\ 41.445 \\ 34.368 \\ 25.957 \\ 24.632 \\ 21.515 \\ 14.530 \\ 7.280 \\ 8.650 \\ 11.236 \\ 12.761 \\ 13.998 \\ 14.467 \\ 14.437 \\ 14.263 \\ 13.976 \\ 13.664 \\ 13.362 \\ 13.126 \\ 13.009 \\ 12.983 \\ 12.960 \\ 12.033 \end{pmatrix}$$

$$TQ\_stress\_fea := \begin{pmatrix} 50.638 \\ 40.722 \\ 27.002 \\ 16.947 \\ 11.934 \\ 10.551 \\ 5.734 \\ 0.963 \\ 3.277 \\ 6.243 \\ 7.898 \\ 9.088 \\ 9.428 \\ 9.275 \\ 9.100 \\ 8.964 \\ 8.987 \\ 9.158 \\ 9.525 \\ 10.038 \\ 10.759 \\ 11.508 \\ 11.987 \end{pmatrix}$$

$$OD\_stress\_fea := \begin{pmatrix} 59.979 \\ 51.289 \\ 41.729 \\ 6.333 \\ 5.354 \\ 3.714 \\ 0.010 \\ -4.004 \\ -1.652 \\ 1.578 \\ 3.319 \\ 4.422 \\ 4.629 \\ 4.330 \\ 4.150 \\ 4.177 \\ 4.508 \\ 5.143 \\ 6.042 \\ 7.179 \\ 8.539 \\ 10.066 \\ 11.973 \end{pmatrix}$$

Blind Zone and Counterbore Reference dimensions:

From design drawings (Ref. 3) and the design details of Attachment 1, the following dimensions are used to locate the counterbore bottom and blind zone locations (bottom, top, and middle) as referenced from the nodal coordinates of the DEI FEA model.

Actual_cbore_bottom_elev := $Elev\_fea_2$ + 1.01

Actual_cbore_bottom_elev = 5.215

Primary Assumptions on blind zone dimensions:

topweld_to_bottom_BZ := 0.67

This is the distance from top of the J-weld, on the uphill side, to the bottom of the blind zone. Without UT data to verify this dimension, this value be iterated to determine the MINIMUM height above the top of the weld for which the blind zone can begin and yield an acceptable fracture mechanics solution.

BZ_length := 0.8

This value is based on the longest blind zone seen in the ANO-2 ICI nozzles. Both Waterford-3 and ANO-2 ICI nozzles have similar geometries above the top of the weld. Thus, a reasonable engineered assumption is that the largest blind zone for ANO-2 is assumed for the Waterford-3 ICI nozzles.

$$elev\_to\_mid\_BZ := Elev\_fea_2 + topweld\_to\_bottom\_BZ + \frac{BZ\_length}{2}$$

elev_to_mid_BZ = 5.315

bottom_of_BZ := $Elev\_fea_2$ + topweld_to_bottom_BZ

bottom_of_BZ = 4.875

top_of_BZ := $Elev\_fea_2$ + topweld_to_bottom_BZ + BZ_length

top_of_BZ = 5.755

For stress averaging and fracture mechanics purposes, the reference coordinate system--with a "0" elevation at the bottom of the nozzle, at the ID corner--must be converted into a new coordinate system with the top of the nozzle (nodal line 83301) as the new "0" elevation.. The positive direction along this new coordinate system will be towards nodal line 81101, which is the just below the top of the weld. This modification facilitates a fracture mechanics model more ammenable to the surface flaw loop structure previously developed in Reference 6.

The following iterative loop converts the five (5) through-wall stress components--ID, 25% tw (QT), 50% tw (MD), 75% tw (TQ), and OD--and the associated elevation, initially given in the DEI FEA model, into the "new" coordinate system, referenced from the top of the nozzle where it meets the reactor vessel head.

$$
\begin{aligned}
\text{Conv} := \;& n \leftarrow 20 \\
& \text{Top} \leftarrow \text{Elev\_fea}_n \\
& j \leftarrow n \\
& i \leftarrow 0 \\
& \text{while } j \geq 0 \\
& \quad \text{Elev\_conv}_i \leftarrow \text{Top} - \text{Elev\_fea}_j \\
& \quad \text{ID\_stress}_i \leftarrow \text{ID\_stress\_fea}_j \\
& \quad \text{QT\_stress}_i \leftarrow \text{QT\_stress\_fea}_j \\
& \quad \text{MD\_stress}_i \leftarrow \text{MD\_stress\_fea}_j \\
& \quad \text{TQ\_stress}_i \leftarrow \text{TQ\_stress\_fea}_j \\
& \quad \text{OD\_stress}_i \leftarrow \text{OD\_stress\_fea}_j \\
& \quad \text{output}_{(i,0)} \leftarrow \text{Elev\_conv}_i \\
& \quad \text{output}_{(i,1)} \leftarrow \text{ID\_stress}_i \\
& \quad \text{output}_{(i,2)} \leftarrow \text{QT\_stress}_i \\
& \quad \text{output}_{(i,3)} \leftarrow \text{MD\_stress}_i \\
& \quad \text{output}_{(i,4)} \leftarrow \text{TQ\_stress}_i \\
& \quad \text{output}_{(i,5)} \leftarrow \text{OD\_stress}_i \\
& \quad j \leftarrow j - 1 \\
& \quad i \leftarrow i + 1 \\
& \text{output}
\end{aligned}
$$

$Elev := Conv^{\langle 0 \rangle}$

$ID\_stress := Conv^{\langle 1 \rangle}$

$QT\_stress := Conv^{\langle 2 \rangle}$

$MD\_stress := Conv^{\langle 3 \rangle}$

$TQ\_stress := Conv^{\langle 4 \rangle}$

$OD\_stress := Conv^{\langle 5 \rangle}$

$Elev_i$ =	ID_stress_i =	QT_stress_i =	MD_stress_i =	TQ_stress_i =	OD_stress_i =
0	18.311	15.38	12.983	10.759	8.539
1.235	19.876	16.176	13.009	10.038	7.179
2.325	21.213	17.311	13.126	9.525	6.042
3.289	21.55	18.466	13.362	9.158	5.143
4.141	21.742	19.395	13.664	8.987	4.508
4.893	21.792	20.133	13.976	8.964	4.177
5.557	21.667	20.4	14.263	9.1	4.15
6.144	21.408	20.378	14.437	9.275	4.33
6.663	20.976	20.149	14.467	9.428	4.629
7.121	20.331	19.55	13.998	9.088	4.422
7.526	19.527	18.517	12.761	7.898	3.319
7.883	18.876	17.269	11.236	6.243	1.578
8.199	18.383	15.071	8.65	3.277	-1.652
8.478	18.722	14.133	7.28	0.963	-4.004
8.725	23.668	21.543	14.53	5.734	0.01
8.942	29.82	28.465	21.515	10.551	3.714
9.135	34.079	32.268	24.632	11.934	5.354
9.305	37.068	33.351	25.957	16.947	6.333
9.535	39.763	38.158	34.368	27.002	41.729
9.651	42.799	39.703	41.445	40.722	51.289
9.767	43.347	41.64	43.666	50.638	59.979

The five arrays given above include the elevation measured from the top of the ICI nozzle from the FEA model down to the top of the J-weld and the corresponding hoop stresses in the modified coordinate system (MCS).

Additional Geometry in Modified Coordinate System

The top of the J-groove weld in the MCS is equal to entry 18 in the "Elev" array:

$Top\_Jweld := Elev_{18}$

$Top\_Jweld = 9.535$

The location of the top of the UT blind zone (BZ) in the MCS (as measured from the ID surface) is

$BZ\_top := Top\_Jweld - (topweld\_to\_bottom\_BZ + BZ\_length)$

$BZ\_top = 7.985$

The midpoint of the BZ in the MCS is

$$BZ\_mid := BZ\_top + \frac{BZ\_length}{2}$$

$BZ\_mid = 8.425$

The bottom of the BZ in the MCS is

$BZ\_bottom := BZ\_top + BZ\_length$

$BZ\_bottom = 8.865$

The location of the actual counterbore (from design drawings) in the MCS:

$cbore\_elev := Top\_Jweld - 1.377$

$cbore\_elev = 8.158$

From the MCS, the stress distribution from elevation 0 (the top of the ICI nozzle where it intersects the RV head) to the top of the weld is graphically shown below.

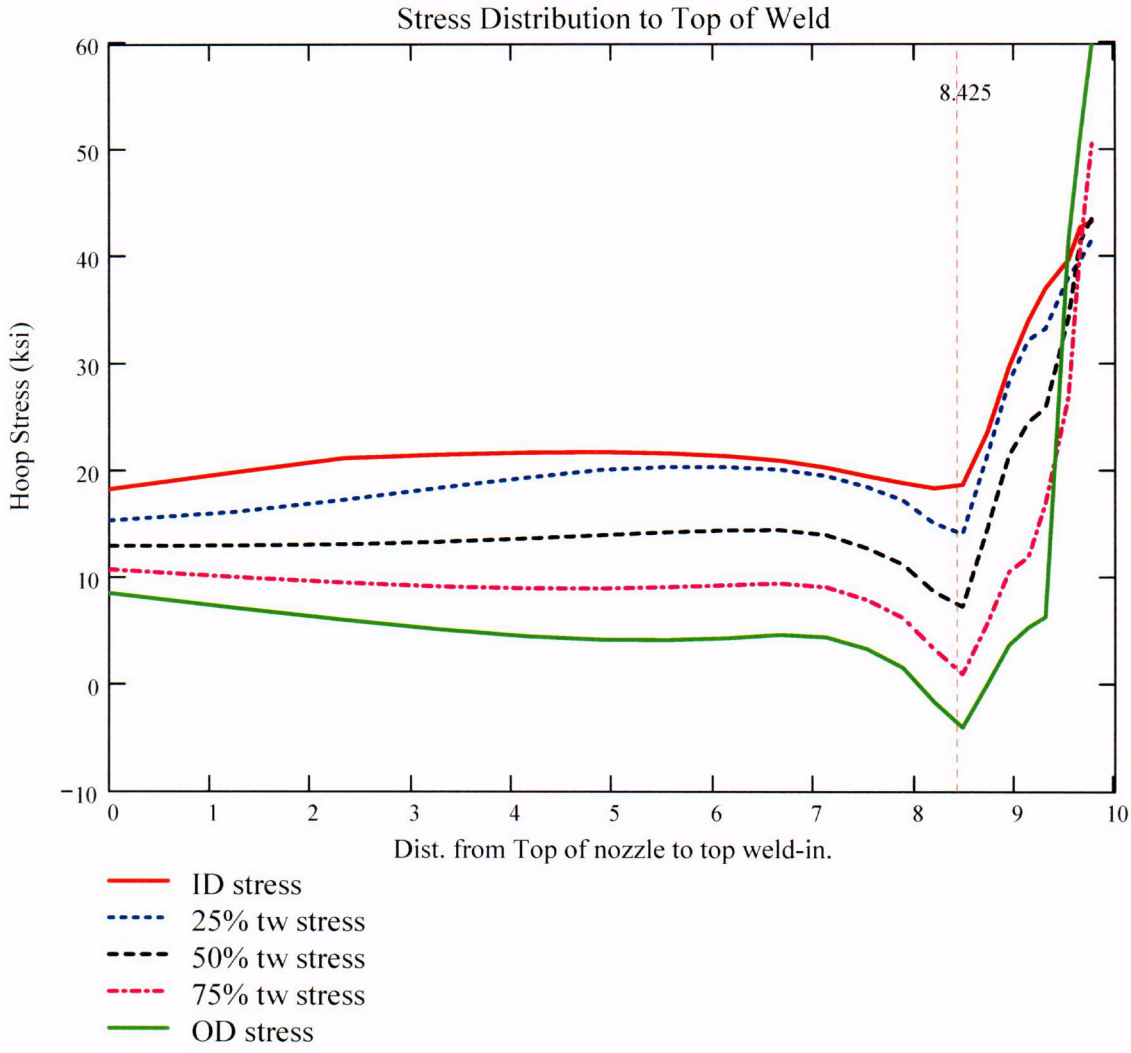

For the ID surface flaw model, the reference point is the location along the axis of the nozzle used to locate the flaw. For this analysis, the reference point is considered at the mid-height of the blind zone.

$Ref_{Point} := BZ\_mid$

C14

To place the flaw with respect to the reference point, the flaw tips and center can be located as follows:

1) The Upper "c- tip" located at the reference point (Enter 1)
2) The Center of the flaw at the reference point (Enter 2)
3) The lower "c- tip" located at the reference point (Enter 3).

$Val := 2$

The Input Below is the point below the blind zone region where stresses will be considered for curve-fitting. This point is taken as the top of the weld, since the stress distribution changes drastically within the weld region Enter this dimension or variable below.

$Elev_{Strs.Dist} := Elev_{20}$ The elevation to the point of maximum stress to consider (Axial distance from elevation 0 in the MCS).

ICI Nozzle Geometry Input Data:

$od := 5.563 - 0.001$ Tube OD, in inches (The value from Ref. 3, is 5.563" +0.00/-0.001)

$id1 := 4.625 + 0.01$ Maximum Tube ID above counterbore, in inches (The value from Ref. 3 is 4.625" +/- 0.010")

$id2 := 4.750 + 0.01$ Maximum Tube ID below counterbore, in inches (The value from Ref. 3 is 4.750" +/- 0.010")

$t1 := \frac{(od - id1)}{2}$ Minmum wall thickness above the counterbore, in inches

$t1 = 0.4635$

$t2 := \frac{(od - id2)}{2}$ Minimum wall thickness below the counterbore, in inches

$t2 = 0.401$

$R_o := \frac{od}{2}$ $R_o = 2.781$

$R_{id1} := \frac{id1}{2}$ $R_{id1} = 2.3175$

$R_{id2} := \frac{id2}{2}$ $R_{id2} = 2.38$

$R_{m1} := R_{id1} + \frac{t1}{2}$ $R_{m1} = 2.54925$

$R_{m2} := R_{id2} + \frac{t2}{2}$ $R_{m2} = 2.5805$

$R_t := \frac{R_{m2}}{t2}$ $R_t = 6.43516$

$\frac{R_o}{t2} = 6.93516$

Flaw Geometry Input Data:

A postulated flaw could exist in the **0.88"** UT Blindzone that occurs **0.67"** above the top of the J-weld at the uphill (180°) location. The flaw length (c) and depth (a) constitute the input parameters. This flaw represents an internal surface crack in a cylinder, as described in Reference 9.

$AR_0 := 10$ The flaw length-to-depth aspect ratio. This is a ratio common to ASME Section XI, and one sufficient to promote flaw growth through the thickness.

$t2 \cdot .10 = 0.0401$

$L_0 := 0.4$ Initial Flaw Length of an ID surface flaw in the counterbore region, in inches. The length was based on a sufficiently long flaw (10-to-1 aspect ratio) with enough depth into the thickness (10%) to precipitate growth in both the depth and length directions. Half the flaw length (0.2 inch) was placed the below the mid-height of the blind zone, while the other half was placed above the mid-height.

$a_0 := \frac{0.4}{AR_0}$ Initial Flaw Depth of the ID surface flaw in the blind zone above the top of the weld on the uphill side. The minimum detectable depth of a surface flaw from UT demonstrations [Ref. 12] was 8% throughwall. This flaw is 10% throughwall.

$a_0 = 0.04$

$c_0 := \frac{L}{2}$ The half flaw length used in the fracture mechanics model

Additional Input Data:

$P_{Int} := 2.235$ Design Operating Pressure (internal) [Ref. 4]

$Years := 40$ Number of Operating Years

$I_{lim} := 8000$ Iteration limit for Crack Growth loop

$T := 604$ Operating Temperature for the head, in °F. Reference 5b gives a value of 601°F after the Extended Power Uprate (EPU), and 604°F currently. Thus, the temperature of the head will be taken as 604°F.

$\alpha_{0c} := 2.67 \cdot 10^{-12}$ Constant in MRP-55 PWSCC Model for I-600 Wrought @ 617 deg. F [Ref. 10]

$Q_g := 31.0$ Thermal activation Energy for Crack Growth {MRP) [Ref. 10]

$T_{ref} := 617$ Reference Temperature for normalizing Data deg. F [Ref. 10]

$Tim_{opr} := 365.2422 \cdot 24 \cdot Years$ Numer of operating hours in a year

$CF_{inhr} := 1.417 \cdot 10^{5}$ Correction factor to convert meters per second to inches per hour

$$C_{blk} := \frac{Tim_{opr}}{I_{lim}}$$ Calculation block size for the crack growth iteration loop

$C_{blk} = 43.82906$

$$Prnt_{blk} := \left| \frac{I_{lim}}{50} \right|$$

$$C_{01} := e^{\left[\frac{-Q_g}{1.103 \cdot 10^{-3}} \cdot \left(\frac{1}{T+459.67} - \frac{1}{T_{ref}+459.67} \right) \right]} \cdot \alpha_{0c}$$ Temperature Correction for Coefficient Alpha from EPRI MRP-55, Revision 1 [Ref. 10]

$C_0 := 1.0 C_{01}$ 75 th percentile from MRP-55 Revision 1 [Ref. 10]

The flaw model used for a postulated flaw within the counterbore region on the uphill side of the ICI nozzle is an internal surface flaw in a cylinder, subject to an arbitrary stress distribution.

To allow for a "moving average" of through-thickness stress values as the flaw extends along the length of the ICI ID surface, the length from the bottom tip of the of the initial flaw in the blind zone to the stress distribution upper limit--$Elev_{Strs.Dist}$--is broken into 20 equal segments. Note that due to the MCS used, with a 0 elevation occurring at the TOP of the nozzle, the term "U_{Tip}" (implying the upper tip of the flaw) is actually the physical bottom tip of the flaw, closer to the top of the weld. U_{Tip} is the term used in Reference 6 for the CEDM nozzles, and thus it will continue to be used in the ICI nozzle evaluation.

$$FL_{Cntr} := \begin{cases} Ref_{Point} - c_0 & \text{if } Val = 1 \\ Ref_{Point} & \text{if } Val = 2 \\ Ref_{Point} + c_0 & \text{otherwise} \end{cases}$$

Flaw center Location at the mid-point of the blind zone region

$$U_{Tip} := FL_{Cntr} + c_0$$

$$U_{Tip} = 8.625$$

$$Inc_{Strs.avg} := \frac{Elev_{Strs.Dist} - U_{Tip}}{20}$$

$$Inc_{Strs.avg} = 0.0571$$

$$Ref_{Point} = 8.425$$

No User Input is required beyond this Point

Regression of Through-Thickness Stresses as a Function of Axial Elevation

Because of the minor variation in stresses occuring at the top of the nozzle where it intersects the reactor head and the need to accurately curve fit stresses in the region of interest in the BZ, the entire range of stresses is not appropriate to curve fit. To accomodate an area below and above the BZ region, the first two data points in each of the elevation and stress arrays were removed from consideration in the curve fitting equations. This is a reasonable assumption, given that in the completely through-wall tensile stress field that exists in the nozzle above the top of the J-weld, a flaw centered in the BZ region is likely to grow through the thickness entirely (in addition to growth along the surface of the nozzle) rather than grow very long into an area close to the top of the head or below the top of the J-weld (i.e., elevation ranges not included in the stress polynomial curve fit). Initially, a **third (3rd)** order polynomial was chosen for axial stress regression. After regression, the stress at the mid-height of the blind zone (8.445 inches in the MCS) is checked.

Regression for ID stresses:

$k := 0..5$

$$ID\_elev\_cf := \begin{pmatrix} 7.883 \\ 8.199 \\ 8.478 \\ 8.725 \\ 8.942 \\ 9.135 \end{pmatrix} \qquad ID\_stress\_cf := \begin{pmatrix} 18.876 \\ 18.383 \\ 18.722 \\ 23.668 \\ 29.82 \\ 34.079 \end{pmatrix}$$

$R_{ID} := regress(ID\_elev\_cf, ID\_stress\_cf, 3)$

$$R_{ID} = \begin{pmatrix} 3 \\ 3 \\ 3 \\ 3578.38988 \\ -1136.79548 \\ 118.13463 \\ -3.95831 \end{pmatrix}$$

$z_{ID} := 7.883, 7.884..9.135$

$f_{ID}(z_{ID}) := interp(R_{ID}, ID\_elev\_cf, ID\_stress\_cf, z_{ID})$

$Elev_i$ =	ID_stress_i =
0	18.311
1.235	19.876
2.325	21.213
3.289	21.55
4.141	21.742
4.893	21.792
5.557	21.667
6.144	21.408
6.663	20.976
7.121	20.331
7.526	19.527
7.883	18.876
8.199	18.383
8.478	18.722
8.725	23.668
8.942	29.82
9.135	34.079
9.305	37.068
9.535	39.763
9.651	42.799
9.767	43.347

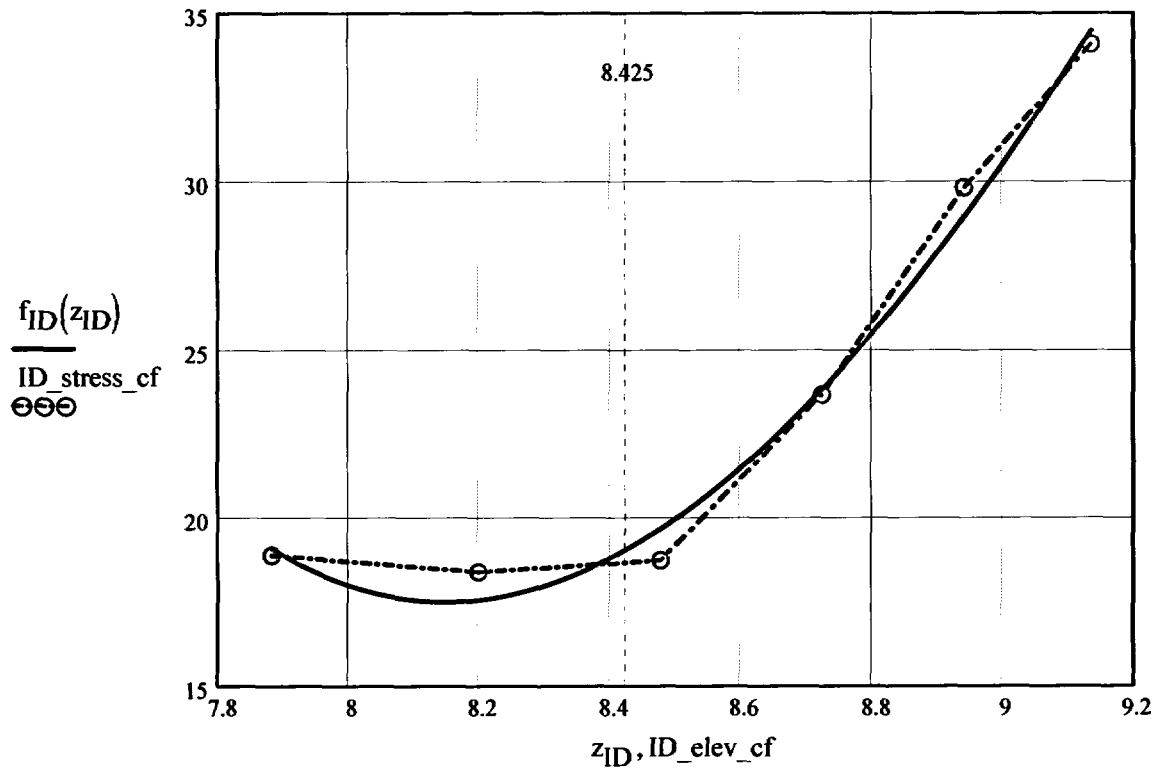

$f_{ID}(8.425) = 19.03958$

Regression for 25% throughwall stresses:

$$QT\_elev\_cf := \begin{pmatrix} 7.883 \\ 8.199 \\ 8.478 \\ 8.725 \\ 8.942 \\ 9.135 \end{pmatrix} \qquad QT\_stress\_cf := \begin{pmatrix} 17.269 \\ 15.071 \\ 14.133 \\ 21.543 \\ 28.465 \\ 32.268 \end{pmatrix}$$

$R_{QT} := \text{regress}(QT\_elev\_cf, QT\_stress\_cf, 3)$

$z_{QT} := 7.883, 7.884 .. 9.135$

$$R_{QT} = \begin{pmatrix} 3 \\ 3 \\ 3 \\ 10745.64054 \\ -3630.8401 \\ 406.73522 \\ -15.0681 \end{pmatrix}$$

$f_{QT}(z_{QT}) := \text{interp}(R_{QT}, QT\_elev\_cf, QT\_stress\_cf, z_{QT})$

$Elev_i =$	$QT\_stress_i =$
0	15.38
1.235	16.176
2.325	17.311
3.289	18.466
4.141	19.395
4.893	20.133
5.557	20.4
6.144	20.378
6.663	20.149
7.121	19.55
7.526	18.517
7.883	17.269
8.199	15.071
8.478	14.133
8.725	21.543
8.942	28.465
9.135	32.268
9.305	33.351
9.535	38.158
9.651	39.703
9.767	41.64

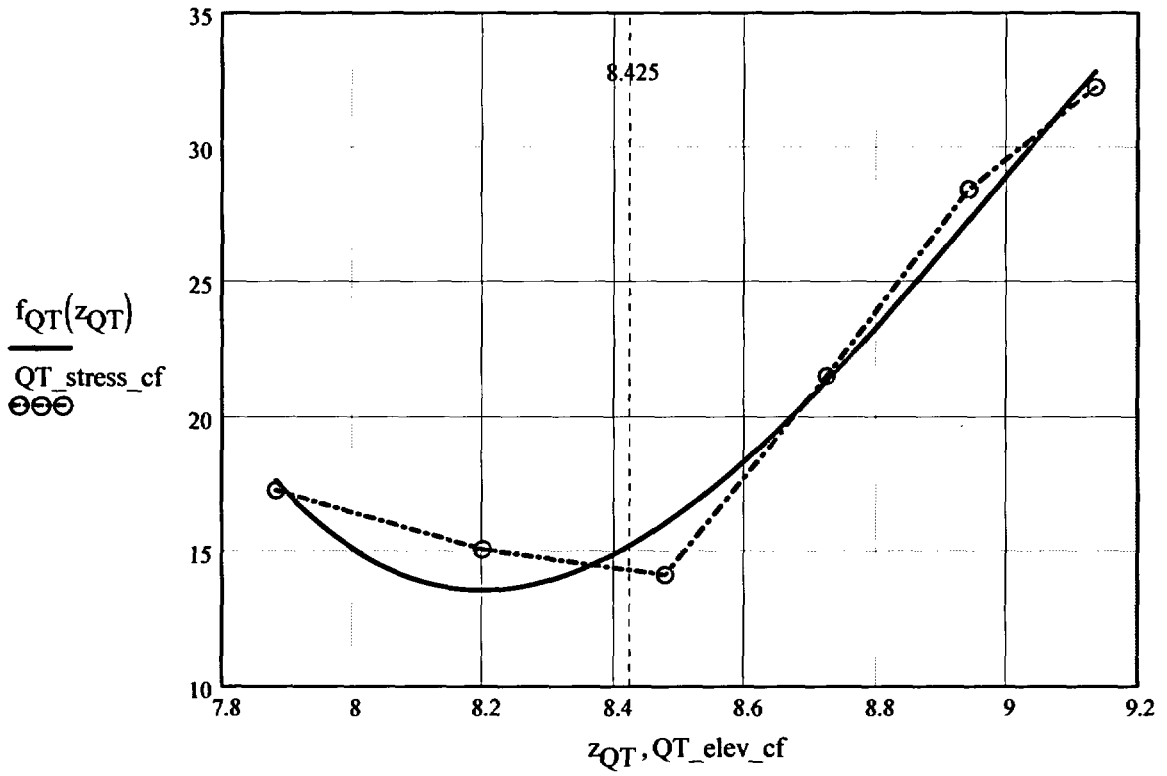

$f_{QT}(8.425) = 15.22949$

Regression for 50% throughwall stresses:

$$MD\_elev\_cf := \begin{pmatrix} 7.883 \\ 8.199 \\ 8.478 \\ 8.725 \\ 8.942 \\ 9.135 \end{pmatrix} \qquad MD\_stress\_cf := \begin{pmatrix} 11.236 \\ 8.65 \\ 7.28 \\ 14.53 \\ 21.515 \\ 24.632 \end{pmatrix}$$

$R_{MD} := regress(MD\_elev\_cf, MD\_stress\_cf, 3)$

$z_{MD} := 7.883, 7.884 .. 9.135$

$$R_{MD} = \begin{pmatrix} 3 \\ 3 \\ 3 \\ 11819.16519 \\ -4010.84838 \\ 451.35824 \\ -16.8173 \end{pmatrix}$$

$f_{MD}(z_{MD}) := interp(R_{MD}, MD\_elev\_cf, MD\_stress\_cf, z_{MD})$

$Elev_i$ =	MD_stress_i =
0	12.983
1.235	13.009
2.325	13.126
3.289	13.362
4.141	13.664
4.893	13.976
5.557	14.263
6.144	14.437
6.663	14.467
7.121	13.998
7.526	12.761
7.883	11.236
8.199	8.65
8.478	7.28
8.725	14.53
8.942	21.515
9.135	24.632
9.305	25.957
9.535	34.368
9.651	41.445
9.767	43.666

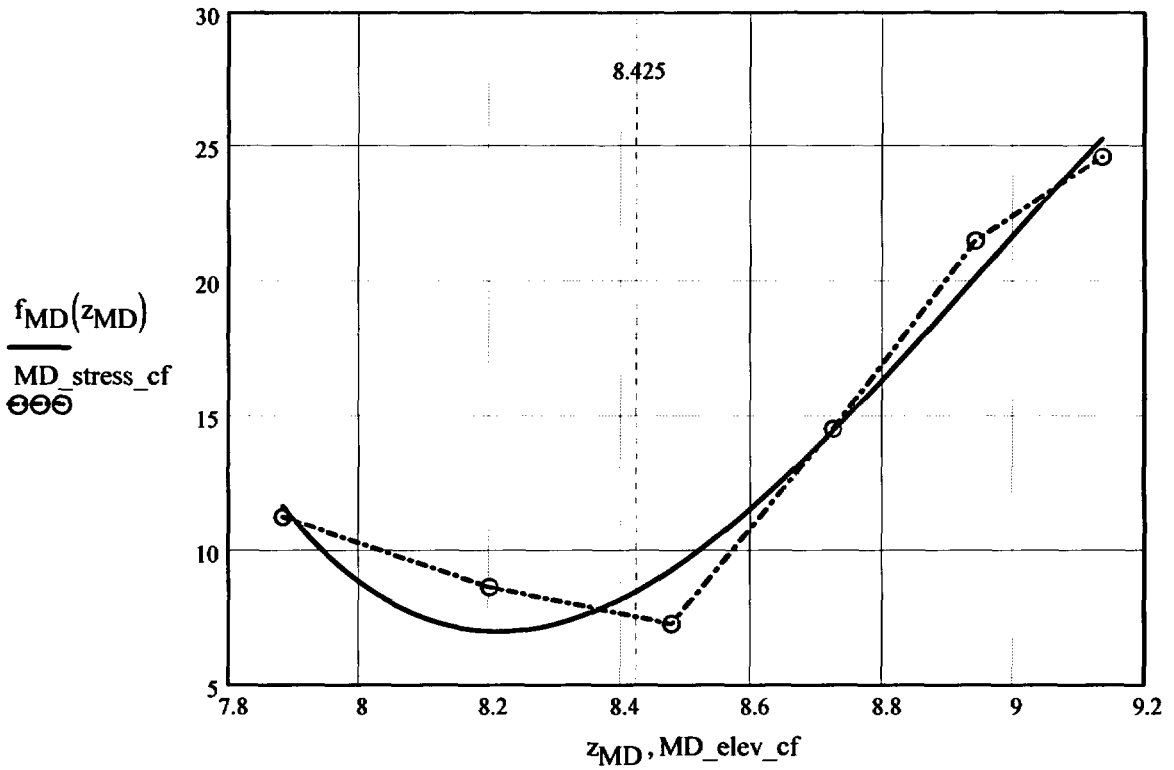

$f_{MD}(8.425) = 8.51122$

Regression for 75% throughwall stresses:

$$TQ\_elev\_cf := \begin{pmatrix} 7.883 \\ 8.199 \\ 8.478 \\ 8.725 \\ 8.942 \\ 9.135 \end{pmatrix} \qquad TQ\_stress\_cf := \begin{pmatrix} 6.243 \\ 3.277 \\ 0.963 \\ 5.734 \\ 10.551 \\ 11.934 \end{pmatrix}$$

$R_{TQ} := regress(TQ\_elev\_cf, TQ\_stress\_cf, 3)$

$z_{TQ} := 7.883, 7.884 .. 9.135$

$$R_{TQ} = \begin{pmatrix} 3 \\ 3 \\ 3 \\ 9313.45524 \\ -3159.012 \\ 355.56516 \\ -13.2686 \end{pmatrix}$$

$f_{TQ}(z_{TQ}) := \text{interp}(R_{TQ}, TQ\_elev\_cf, TQ\_stress\_cf, z_{TQ})$

$Elev_i$ =	TQ_stress_i =
0	10.759
1.235	10.038
2.325	9.525
3.289	9.158
4.141	8.987
4.893	8.964
5.557	9.1
6.144	9.275
6.663	9.428
7.121	9.088
7.526	7.898
7.883	6.243
8.199	3.277
8.478	0.963
8.725	5.734
8.942	10.551
9.135	11.934
9.305	16.947
9.535	27.002
9.651	40.722
9.767	50.638

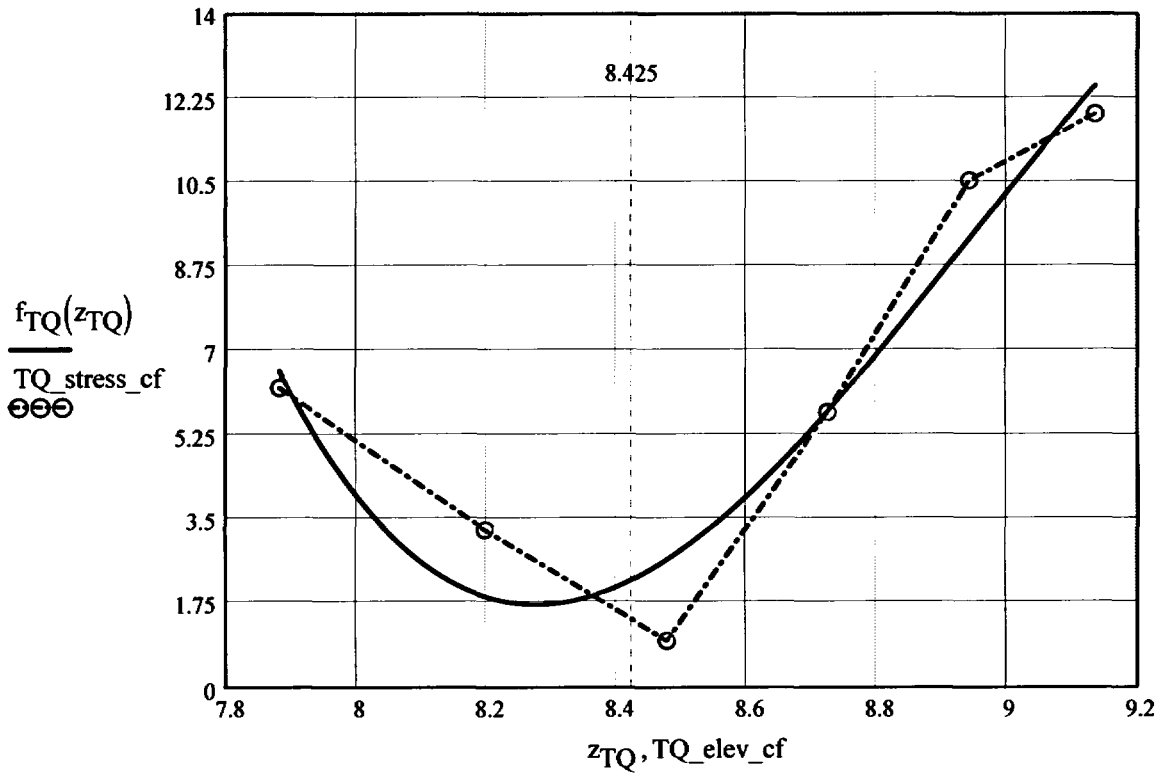

$f_{TQ}(8.425) = 2.2362$

Regression for OD stresses:

$kk := 0..5$

$$OD\_elev\_cf := \begin{pmatrix} 7.883 \\ 8.199 \\ 8.478 \\ 8.725 \\ 8.942 \\ 9.135 \end{pmatrix} \qquad OD\_stress\_cf := \begin{pmatrix} 1.578 \\ -1.652 \\ -4.004 \\ 0.01 \\ 3.714 \\ 5.354 \end{pmatrix}$$

$R_{OD} := regress(OD\_elev\_cf, OD\_stress\_cf, 3)$

$z_{OD} := 7.883, 7.884 .. 9.135$

$$R_{OD} = \begin{pmatrix} 3 \\ 3 \\ 3 \\ 7570.62763 \\ -2550.59622 \\ 284.86761 \\ -10.54291 \end{pmatrix}$$

$f_{OD}(z_{OD}) := interp(R_{OD}, OD\_elev\_cf, OD\_stress\_cf, z_{OD})$

$Elev_i$ =	OD_stress_i =
0	8.539
1.235	7.179
2.325	6.042
3.289	5.143
4.141	4.508
4.893	4.177
5.557	4.15
6.144	4.33
6.663	4.629
7.121	4.422
7.526	3.319
7.883	1.578
8.199	-1.652
8.478	-4.004
8.725	0.01
8.942	3.714
9.135	5.354
9.305	6.333
9.535	41.729
9.651	51.289
9.767	59.979

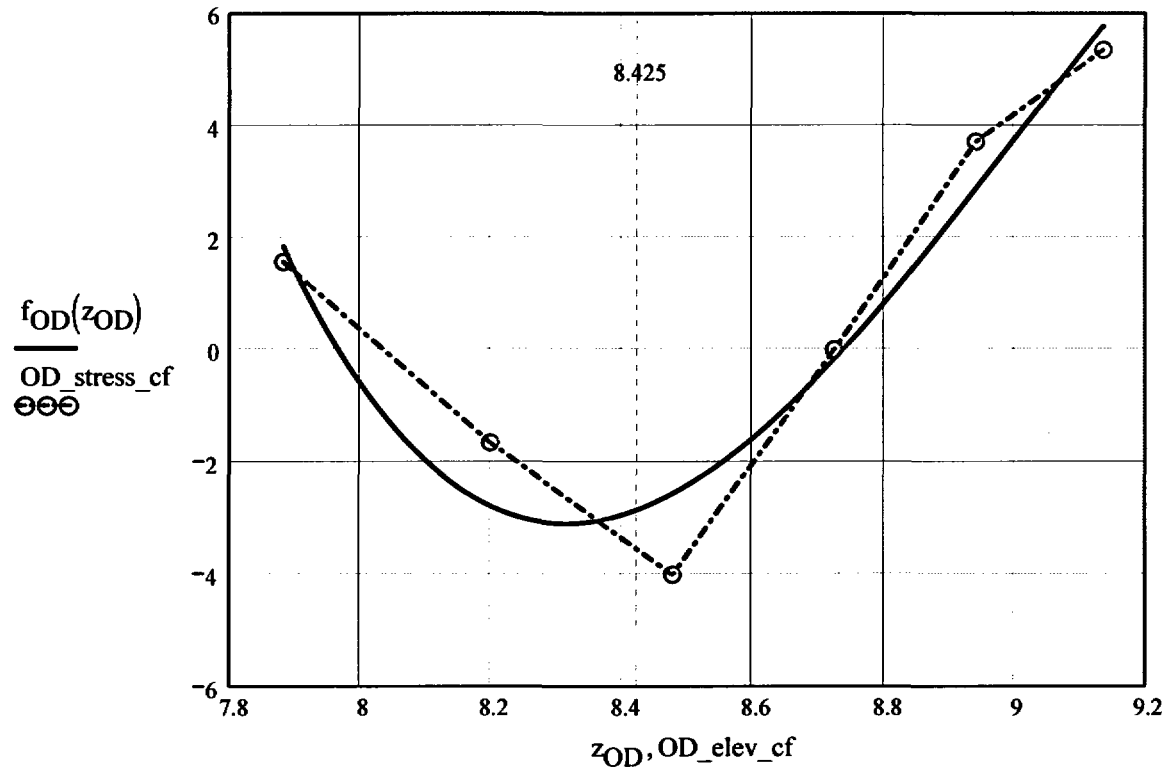

$f_{OD}(8.425) = -2.84902$

Calculation to develop Stress Profiles for Analysis

This analysis for the axial stress regression and the through-wall stress regression is the same as that used for the CEDM Nozzles (in Ref. 6); that is, the axial stresses are fit with a third-order polynomial.

$N := 20$ *Number of locations for stress profiles*

$Loc_0 := FL_{Cntr} - L$

$FL_{Cntr} = 8.425$

$L = 0.4$

$j := 1..N + 3$

$$Incr_j := \begin{cases} c_0 & \text{if } i < 4 \\ Inc_{Strs.avg} & \text{otherwise} \end{cases}$$

$Loc_i := Loc_{i-1} + Incr_i$

$SID_i := R_{ID_3} + R_{ID_4} \cdot Loc_i + R_{ID_5} \cdot (Loc_i)^2 + R_{ID_6} \cdot (Loc_i)^3$

$SQT_i := R_{QT_3} + R_{QT_4} \cdot Loc_i + R_{QT_5} \cdot (Loc_i)^2 + R_{QT_6} \cdot (Loc_i)^3$

$SMD_i := R_{MD_3} + R_{MD_4} \cdot Loc_i + R_{MD_5} \cdot (Loc_i)^2 + R_{MD_6} \cdot (Loc_i)^3$

$STQ_i := R_{TQ_3} + R_{TQ_4} \cdot Loc_i + R_{TQ_5} \cdot (Loc_i)^2 + R_{TQ_6} \cdot (Loc_i)^3$

$SOD_i := R_{OD_3} + R_{OD_4} \cdot Loc_i + R_{OD_5} \cdot (Loc_i)^2 + R_{OD_6} \cdot (Loc_i)^3$

$j := 1..N$

$$S_{id_j} := \begin{cases} \dfrac{SID_j + SID_{j+1} + SID_{j+2}}{3} & \text{if } j = 1 \\ \dfrac{S_{id_{j-1}} \cdot (j+1) + SID_{j+2}}{j+2} & \text{otherwise} \end{cases}$$

$$S_{qt_j} := \begin{cases} \dfrac{SQT_j + SQT_{j+1} + SQT_{j+2}}{3} & \text{if } j = 1 \\ \dfrac{S_{qt_{(j-1)}} \cdot (j+1) + SQT_{j+2}}{j+2} & \text{otherwise} \end{cases}$$

$$S_{md_j} := \begin{cases} \dfrac{SMD_j + SMD_{j+1} + SMD_{j+2}}{3} & \text{if } j = 1 \\ \dfrac{S_{md_{j-1}} \cdot (j+1) + SMD_{j+2}}{j+2} & \text{otherwise} \end{cases}$$

$$S_{tq_j} := \begin{cases} \dfrac{STQ_j + STQ_{j+1} + STQ_{j+2}}{3} & \text{if } j = 1 \\ \dfrac{S_{tq_{j-1}} \cdot (j+1) + STQ_{j+2}}{j+2} & \text{otherwise} \end{cases}$$

$$S_{od_j} := \begin{cases} \dfrac{SOD_j + SOD_{j+1} + SOD_{j+2}}{3} & \text{if } j = 1 \\ \dfrac{S_{od_{j-1}} \cdot (j+1) + SOD_{j+2}}{j+2} & \text{otherwise} \end{cases}$$

Through-Wall Stress Distribution for ID Flaws (i.e. ID to OD Stress distribution)

$u_0 := 0.000$ $u_1 := 0.25$ $u_2 := 0.50$ $u_3 := 0.75$ $u_4 := 1.00$

$$Y := \text{stack}(u_0, u_1, u_2, u_3, u_4)$$

$SIG_1 := \text{stack}(S_{id_1}, S_{qt_1}, S_{md_1}, S_{tq_1}, S_{od_1})$ $SIG_2 := \text{stack}(S_{id_2}, S_{qt_2}, S_{md_2}, S_{tq_2}, S_{od_2})$

$SIG_3 := \text{stack}(S_{id_3}, S_{qt_3}, S_{md_3}, S_{tq_3}, S_{od_3})$ $SIG_4 := \text{stack}(S_{id_4}, S_{qt_4}, S_{md_4}, S_{tq_4}, S_{od_4})$

$SIG_5 := \text{stack}(S_{id_5}, S_{qt_5}, S_{md_5}, S_{tq_5}, S_{od_5})$ $SIG_6 := \text{stack}(S_{id_6}, S_{qt_6}, S_{md_6}, S_{tq_6}, S_{od_6})$

$SIG_7 := \text{stack}(S_{id_7}, S_{qt_7}, S_{md_7}, S_{tq_7}, S_{od_7})$ $SIG_8 := \text{stack}(S_{id_8}, S_{qt_8}, S_{md_8}, S_{tq_8}, S_{od_8})$

$SIG_9 := \text{stack}(S_{id_9}, S_{qt_9}, S_{md_9}, S_{tq_9}, S_{od_9})$ $SIG_{10} := \text{stack}(S_{id_{10}}, S_{qt_{10}}, S_{md_{10}}, S_{tq_{10}}, S_{od_{10}})$

$SIG_{11} := \text{stack}(S_{id_{11}}, S_{qt_{11}}, S_{md_{11}}, S_{tq_{11}}, S_{od_{11}})$ $SIG_{12} := \text{stack}(S_{id_{12}}, S_{qt_{12}}, S_{md_{12}}, S_{tq_{12}}, S_{od_{12}})$

$SIG_{13} := \text{stack}(S_{id_{13}}, S_{qt_{13}}, S_{md_{13}}, S_{tq_{13}}, S_{od_{13}})$ $SIG_{14} := \text{stack}(S_{id_{14}}, S_{qt_{14}}, S_{md_{14}}, S_{tq_{14}}, S_{od_{14}})$

$SIG_{15} := \text{stack}(S_{id_{15}}, S_{qt_{15}}, S_{md_{15}}, S_{tq_{15}}, S_{od_{15}})$ $SIG_{16} := \text{stack}(S_{id_{16}}, S_{qt_{16}}, S_{md_{16}}, S_{tq_{16}}, S_{od_{16}})$

$SIG_{17} := \text{stack}(S_{id_{17}}, S_{qt_{17}}, S_{md_{17}}, S_{tq_{17}}, S_{od_{17}})$ $SIG_{18} := \text{stack}(S_{id_{18}}, S_{qt_{18}}, S_{md_{18}}, S_{tq_{18}}, S_{od_{18}})$

$SIG_{19} := \text{stack}(S_{id_{19}}, S_{qt_{19}}, S_{md_{19}}, S_{tq_{19}}, S_{od_{19}})$ $SIG_{20} := \text{stack}(S_{id_{20}}, S_{qt_{20}}, S_{md_{20}}, S_{tq_{20}}, S_{od_{20}})$

Regression of Through-Wall Stress distribution to Obtain Stress Coefficients Using a Third Order Polynomial

$IDRG_1 := regress(Y, SIG_1, 3)$

$IDRG_2 := regress(Y, SIG_2, 3)$

$IDRG_3 := regress(Y, SIG_3, 3)$

$IDRG_4 := regress(Y, SIG_4, 3)$

$IDRG_5 := regress(Y, SIG_5, 3)$

$IDRG_6 := regress(Y, SIG_6, 3)$

$IDRG_7 := regress(Y, SIG_7, 3)$

$IDRG_8 := regress(Y, SIG_8, 3)$

$IDRG_9 := regress(Y, SIG_9, 3)$

$IDRG_{10} := regress(Y, SIG_{10}, 3)$

$IDRG_{11} := regress(Y, SIG_{11}, 3)$

$IDRG_{12} := regress(Y, SIG_{12}, 3)$

$IDRG_{13} := regress(Y, SIG_{13}, 3)$

$IDRG_{14} := regress(Y, SIG_{14}, 3)$

$IDRG_{15} := regress(Y, SIG_{15}, 3)$

$IDRG_{16} := regress(Y, SIG_{16}, 3)$

$IDRG_{17} := regress(Y, SIG_{17}, 3)$

$IDRG_{18} := regress(Y, SIG_{18}, 3)$

$IDRG_{19} := regress(Y, SIG_{19}, 3)$

$IDRG_{20} := regress(Y, SIG_{20}, 3)$

Stress Distribution in the tube. ***Stress influence coefficients obtained from thrid-order polynomial curve fit to the throughwall stress distribution***

Data Files for Flaw Shape Factors from NASA SC04 Model [Ref. 9]

{NO INPUT Required}

Mettu Raju Newman Sivakumar Forman Solution of ID Part throughwall Flaw in Cyinder

Jsb :=

	0	1	2
0	1.000	0.200	0.000
1	1.000	0.200	0.200
2	1.000	0.200	0.500
3	1.000	0.200	0.800
4	1.000	0.200	1.000
5	1.000	0.400	0.000
6	1.000	0.400	0.200
7	1.000	0.400	0.500
8	1.000	0.400	0.800
9	1.000	0.400	1.000
10	1.000	1.000	0.000
11	1.000	1.000	0.200
12	1.000	1.000	0.500
13	1.000	1.000	0.800
14	1.000	1.000	1.000
15	2.000	0.200	0.000
16	2.000	0.200	0.200
17	2.000	0.200	0.500
18	2.000	0.200	0.800
19	2.000	0.200	1.000
20	2.000	0.400	0.000
21	2.000	0.400	0.200
22	2.000	0.400	0.500
23	2.000	0.400	0.800
24	2.000	0.400	1.000
25	2.000	1.000	0.000
26	2.000	1.000	0.200
27	2.000	1.000	0.500
28	2.000	1.000	0.800
29	2.000	1.000	1.000
30	4.000	0.200	0.000
31	4.000	0.200	0.200
32	4.000	0.200	0.500
33	4.000	0.200	0.800
34	4.000	0.200	1.000
35	4.000	0.400	0.000
36	4.000	0.400	0.200

37	4.000	0.400	0.500
38	4.000	0.400	0.800
39	4.000	0.400	1.000
40	4.000	1.000	0.000
41	4.000	1.000	0.200
42	4.000	1.000	0.500
43	4.000	1.000	0.800
44	4.000	1.000	1.000
45	10.000	0.200	0.000
46	10.000	0.200	0.200
47	10.000	0.200	0.500
48	10.000	0.200	0.800
49	10.000	0.200	1.000
50	10.000	0.400	0.000
51	10.000	0.400	0.200
52	10.000	0.400	0.500
53	10.000	0.400	0.800
54	10.000	0.400	1.000
55	10.000	1.000	0.000
56	10.000	1.000	0.200
57	10.000	1.000	0.500
58	10.000	1.000	0.800
59	10.000	1.000	1.000
60	300.000	0.200	0.000
61	300.000	0.200	0.200
62	300.000	0.200	0.500
63	300.000	0.200	0.800
64	300.000	0.200	1.000
65	300.000	0.400	0.000
66	300.000	0.400	0.200
67	300.000	0.400	0.500
68	300.000	0.400	0.800
69	300.000	0.400	1.000
70	300.000	1.000	0.000
71	300.000	1.000	0.200
72	300.000	1.000	0.500
73	300.000	1.000	0.800
74	300.000	1.000	1.000

Sambi :=

	0	1	2	3	4	5	6	7

0	1.076	0.693	0.531	0.434	0.608	0.083	0.023	0.009
1	1.056	0.647	0.495	0.408	0.615	0.085	0.027	0.013
2	1.395	0.767	0.557	0.446	0.871	0.171	0.069	0.038
3	2.53	1.174	0.772	0.58	1.554	0.363	0.155	0.085
4	3.846	1.615	0.995	0.716	2.277	0.544	0.233	0.127
5	1.051	0.689	0.536	0.444	0.74	0.112	0.035	0.015
6	1.011	0.646	0.504	0.421	0.745	0.119	0.041	0.02
7	1.149	0.694	0.529	0.435	0.916	0.181	0.073	0.04
8	1.6	0.889	0.642	0.51	1.334	0.307	0.132	0.073
9	2.087	1.093	0.761	0.589	1.752	0.421	0.183	0.101
10	0.992	0.704	0.534	0.506	1.044	0.169	0.064	0.032
11	0.987	0.701	0.554	0.491	1.08	0.182	0.067	0.034
12	1.01	0.709	0.577	0.493	1.116	0.2	0.078	0.041
13	1.07	0.73	0.623	0.523	1.132	0.218	0.095	0.051
14	1.128	0.75	0.675	0.556	1.131	0.229	0.11	0.06
15	1.049	0.673	0.519	0.427	0.6	0.078	0.021	0.008
16	1.091	0.661	0.502	0.413	0.614	0.083	0.025	0.012
17	1.384	0.764	0.556	0.446	0.817	0.15	0.058	0.031
18	2.059	1.033	0.708	0.545	1.3	0.291	0.123	0.067
19	2.739	1.301	0.858	0.643	1.783	0.421	0.18	0.099
20	1.075	0.674	0.527	0.436	0.73	0.072	0.044	0.021
21	1.045	0.659	0.511	0.425	0.76	0.122	0.043	0.021
22	1.16	0.71	0.536	0.441	0.919	0.197	0.064	0.034
23	1.51	0.854	0.623	0.498	1.231	0.271	0.114	0.062
24	1.876	0.995	0.71	0.555	1.519	0.317	0.161	0.089
25	1.037	0.732	0.594	0.505	1.132	0.192	0.07	0.035
26	1.003	0.707	0.577	0.493	1.113	0.19	0.071	0.036
27	1.023	0.714	0.58	0.495	1.155	0.207	0.08	0.042
28	1.129	0.774	0.619	0.521	1.286	0.247	0.098	0.052
29	1.242	0.84	0.661	0.549	1.416	0.285	0.115	0.061
30	1.003	0.649	0.511	0.43	0.577	0.07	0.015	0.005
31	1.097	0.666	0.511	0.426	0.606	0.079	0.023	0.01
32	1.405	0.776	0.567	0.46	0.797	0.141	0.054	0.028
33	1.959	0.996	0.692	0.542	1.201	0.262	0.108	0.059
34	2.461	1.197	0.808	0.619	1.586	0.37	0.154	0.085
35	1.024	0.668	0.528	0.451	0.737	0.11	0.033	0.015
36	1.057	0.666	0.52	0.439	0.77	0.123	0.042	0.021
37	1.193	0.715	0.545	0.454	0.924	0.174	0.068	0.036
38	1.443	0.828	0.614	0.509	1.219	0.263	0.109	0.059
39	1.665	0.934	0.681	0.565	1.487	0.339	0.143	0.078
40	1.005	0.72	0.597	0.518	1.119	0.188	0.068	0.034
41	1.009	0.713	0.588	0.511	1.128	0.194	0.072	0.037
42	1.041	0.726	0.594	0.515	1.191	0.214	0.082	0.043

43	1.105	0.768	0.623	0.536	1.316	0.248	0.097	0.05
44	1.162	0.81	0.653	0.558	1.428	0.277	0.109	0.055
45	0.973	0.635	0.499	0.446	0.579	0.07	0.016	0.005
46	1.115	0.673	0.514	0.438	0.607	0.079	0.023	0.01
47	1.427	0.783	0.571	0.462	0.791	0.138	0.052	0.027
48	1.872	0.96	0.671	0.529	1.179	0.253	0.104	0.056
49	2.23	1.108	0.757	0.594	1.548	0.356	0.149	0.081
50	0.992	0.656	0.52	0.443	0.733	0.109	0.032	0.014
51	1.072	0.672	0.523	0.441	0.777	0.125	0.043	0.021
52	1.217	0.723	0.549	0.456	0.936	0.176	0.069	0.036
53	1.393	0.806	0.601	0.493	1.219	0.259	0.106	0.056
54	1.521	0.875	0.647	0.528	1.469	0.328	0.135	0.071
55	0.994	0.715	0.59	0.518	1.114	0.187	0.068	0.035
56	1.015	0.715	0.588	0.512	1.14	0.197	0.074	0.038
57	1.05	0.729	0.596	0.515	1.219	0.221	0.085	0.044
58	1.09	0.76	0.618	0.532	1.348	0.255	0.099	0.051
59	1.118	0.788	0.639	0.55	1.456	0.282	0.109	0.056
60	0.936	0.62	0.486	0.405	0.582	0.068	0.015	0.005
61	1.145	0.681	0.514	0.42	0.613	0.081	0.024	0.011
62	1.459	0.79	0.569	0.454	0.79	0.138	0.051	0.026
63	1.774	0.917	0.641	0.501	1.148	0.239	0.096	0.051
64	1.974	1.008	0.696	0.537	1.482	0.328	0.134	0.07
65	0.982	0.651	0.512	0.427	0.721	0.103	0.031	0.013
66	1.095	0.677	0.52	0.431	0.782	0.127	0.045	0.022
67	1.244	0.727	0.546	0.446	0.946	0.18	0.071	0.037
68	1.37	0.791	0.585	0.473	1.201	0.253	0.102	0.054
69	1.438	0.838	0.618	0.496	1.413	0.31	0.126	0.066

$\underset{\sim}{W} := Jsb^{\langle 0 \rangle}$ $\quad X := Jsb^{\langle 1 \rangle}$ $\quad Y := Jsb^{\langle 2 \rangle}$

$a_U := Sambi^{\langle 0 \rangle}$ $\quad a_L := Sambi^{\langle 1 \rangle}$ $\quad a_Q := Sambi^{\langle 2 \rangle}$ $\quad a_C := Sambi^{\langle 3 \rangle}$

$c_U := Sambi^{\langle 4 \rangle}$ $\quad c_L := Sambi^{\langle 5 \rangle}$ $\quad c_Q := Sambi^{\langle 6 \rangle}$ $\quad c_C := Sambi^{\langle 7 \rangle}$

$$n := \begin{cases} 3 & \text{if } R_t \le 4.0 \\ 2 & \text{otherwise} \end{cases}$$

"a-Tip" Uniform Term

$M_{aU} := \text{augment}(W, X, Y) \qquad V_{aU} := a_U \qquad R_{aU} := \text{regress}(M_{aU}, V_{aU}, n)$

$$f_{aU}(W, X, Y) := \text{interp}\left[R_{aU}, M_{aU}, V_{aU}, \begin{pmatrix} W \\ X \\ Y \end{pmatrix}\right]$$

$f_{aU}(4, .4, .8) = 1.7089$ *Check Calculation*

Linear Term

$M_{aL} := \text{augment}(W, X, Y) \qquad V_{aL} := a_L \qquad R_{aL} := \text{regress}(M_{aL}, V_{aL}, n)$

$$f_{aL}(W, X, Y) := \text{interp}\left[R_{aL}, M_{aL}, V_{aL}, \begin{pmatrix} W \\ X \\ Y \end{pmatrix}\right]$$

$f_{aL}(4, .4, .8) = 0.93393$ *Check Calculation*

Quadratic Term

$M_{aQ} := \text{augment}(W, X, Y) \qquad V_{aQ} := a_Q \qquad R_{aQ} := \text{regress}(M_{aQ}, V_{aQ}, n)$

$$f_{aQ}(W,X,Y) := \text{interp}\left[R_{aQ}, M_{aQ}, V_{aQ}, \begin{pmatrix} W \\ X \\ Y \end{pmatrix}\right]$$

$f_{aQ}(4,.4,.8) = 0.67668$ *Check Calculation*

Cubic Term

$M_{aC} := \text{augment}(W,X,Y)$ $V_{aC} := a_C$ $R_{aC} := \text{regress}(M_{aC}, V_{aC}, n)$

$$f_{aC}(W,X,Y) := \text{interp}\left[R_{aC}, M_{aC}, V_{aC}, \begin{pmatrix} W \\ X \\ Y \end{pmatrix}\right]$$

$f_{aC}(4,.4,.8) = 0.54151$ *Check Calculation*

"C" Tip Coefficients

Uniform Term

$M_{cU} := \text{augment}(W,X,Y)$ $V_{cU} := c_U$ $R_{cU} := \text{regress}(M_{cU}, V_{cU}, n)$

$$f_{cU}(W,X,Y) := \text{interp}\left[R_{cU}, M_{cU}, V_{cU}, \begin{pmatrix} W \\ X \\ Y \end{pmatrix}\right]$$

$f_{cU}(4,.4,.8) = 1.31015$ *Check Calculation*

Linear Term

$M_{cL} := \text{augment}(W,X,Y)$ $V_{cL} := c_L$ $R_{cL} := \text{regress}(M_{cL}, V_{cL}, n)$

$$f_{cL}(W,X,Y) := \text{interp}\left[R_{cL}, M_{cL}, V_{cL}, \begin{pmatrix} W \\ X \\ Y \end{pmatrix}\right]$$

$f_{cL}(2,.4,.8) = 0.28509$ *Check Calculation*

Quadratic Term

$M_{cQ} := \text{augment}(W,X,Y)$ $V_{cQ} := c_Q$ $R_{cQ} := \text{regress}(M_{cQ}, V_{cQ}, n)$

$$f_{cQ}(W,X,Y) := \text{interp}\left[R_{cQ}, M_{cQ}, V_{cQ}, \begin{pmatrix} W \\ X \\ Y \end{pmatrix}\right]$$

$f_{cQ}(4,.4,.8) = 0.11797$ *Check Calculation*

Cubic Term

$M_{cC} := \text{augment}(W,X,Y)$ $V_{cC} := c_C$ $R_{cC} := \text{regress}(M_{cC}, V_{cC}, n)$

$$f_{cC}(W,X,Y) := \text{interp}\left[R_{cC}, M_{cC}, V_{cC}, \begin{pmatrix} W \\ X \\ Y \end{pmatrix}\right]$$

$f_{cC}(4,.4,.8) = 0.06384$ *Check Calculation*

Calculations : Recursive calculations to estimate flaw growth

Recursive Loop for Calculation of PWSCC Crack Growth

$$
\begin{aligned}
CGR_{sambi} := \;& j \leftarrow 0 \\
& a_0 \leftarrow a_0 \\
& c_0 \leftarrow c_0 \\
& t \leftarrow t2 \\
& NCB_0 \leftarrow C_{blk} \\
& \text{while } j \le I_{lim} \\
& \quad \sigma_0 \leftarrow \begin{cases}
IDRG1_3 & \text{if } c_j \le c_0 \\
IDRG2_3 & \text{if } c_0 < c_j \le c_0 + Inc_{Strs.avg} \\
IDRG3_3 & \text{if } c_0 + Inc_{Strs.avg} < c_j \le c_0 + 2 \cdot Inc_{Strs.avg} \\
IDRG4_3 & \text{if } c_0 + 2 \cdot Inc_{Strs.avg} < c_j \le c_0 + 3 \cdot Inc_{Strs.avg} \\
IDRG5_3 & \text{if } c_0 + 3 \cdot Inc_{Strs.avg} < c_j \le c_0 + 4 \cdot Inc_{Strs.avg} \\
IDRG6_3 & \text{if } c_0 + 4 \cdot Inc_{Strs.avg} < c_j \le c_0 + 5 \cdot Inc_{Strs.avg} \\
IDRG7_3 & \text{if } c_0 + 5 \cdot Inc_{Strs.avg} < c_j \le c_0 + 6 \cdot Inc_{Strs.avg} \\
IDRG8_3 & \text{if } c_0 + 6 \cdot Inc_{Strs.avg} < c_j \le c_0 + 7 \cdot Inc_{Strs.avg} \\
IDRG9_3 & \text{if } c_0 + 7 \cdot Inc_{Strs.avg} < c_j \le c_0 + 8 \cdot Inc_{Strs.avg} \\
IDRG10_3 & \text{if } c_0 + 8 \cdot Inc_{Strs.avg} < c_j \le c_0 + 9 \cdot Inc_{Strs.avg} \\
IDRG11_3 & \text{if } c_0 + 9 \cdot Inc_{Strs.avg} < c_j \le c_0 + 10 \cdot Inc_{Strs.avg} \\
IDRG12_3 & \text{if } c_0 + 10 \cdot Inc_{Strs.avg} < c_j \le c_0 + 11 \cdot Inc_{Strs.avg} \\
IDRG13_3 & \text{if } c_0 + 11 \cdot Inc_{Strs.avg} < c_j \le c_0 + 12 \cdot Inc_{Strs.avg} \\
IDRG14_3 & \text{if } c_0 + 12 \cdot Inc_{Strs.avg} < c_j \le c_0 + 13 \cdot Inc_{Strs.avg} \\
IDRG15_3 & \text{if } c_0 + 13 \cdot Inc_{Strs.avg} < c_j \le c_0 + 14 \cdot Inc_{Strs.avg}
\end{cases}
\end{aligned}
$$

$$
\begin{array}{l}
\left|\begin{array}{ll}
IDRG16_3 & \text{if } c_0 + 14\cdot Inc_{Strs.avg} < c_j \le c_0 + 15\cdot Inc_{Strs.avg} \\
IDRG17_3 & \text{if } c_0 + 15\cdot Inc_{Strs.avg} < c_j \le c_0 + 16\cdot Inc_{Strs.avg} \\
IDRG18_3 & \text{if } c_0 + 16\cdot Inc_{Strs.avg} < c_j \le c_0 + 17\cdot Inc_{Strs.avg} \\
IDRG19_3 & \text{if } c_0 + 17\cdot Inc_{Strs.avg} < c_j \le c_0 + 18\cdot Inc_{Strs.avg} \\
IDRG20_3 & \text{otherwise}
\end{array}\right. \\
\sigma_1 \leftarrow \left|\begin{array}{ll}
IDRG1_4 & \text{if } c_j \le c_0 \\
IDRG2_4 & \text{if } c_0 < c_j \le c_0 + Inc_{Strs.avg} \\
IDRG3_4 & \text{if } c_0 + Inc_{Strs.avg} < c_j \le c_0 + 2\cdot Inc_{Strs.avg} \\
IDRG4_4 & \text{if } c_0 + 2\cdot Inc_{Strs.avg} < c_j \le c_0 + 3\cdot Inc_{Strs.avg} \\
IDRG5_4 & \text{if } c_0 + 3\cdot Inc_{Strs.avg} < c_j \le c_0 + 4\cdot Inc_{Strs.avg} \\
IDRG6_4 & \text{if } c_0 + 4\cdot Inc_{Strs.avg} < c_j \le c_0 + 5\cdot Inc_{Strs.avg} \\
IDRG7_4 & \text{if } c_0 + 5\cdot Inc_{Strs.avg} < c_j \le c_0 + 6\cdot Inc_{Strs.avg} \\
IDRG8_4 & \text{if } c_0 + 6\cdot Inc_{Strs.avg} < c_j \le c_0 + 7\cdot Inc_{Strs.avg} \\
IDRG9_4 & \text{if } c_0 + 7\cdot Inc_{Strs.avg} < c_j \le c_0 + 8\cdot Inc_{Strs.avg} \\
IDRG10_4 & \text{if } c_0 + 8\cdot Inc_{Strs.avg} < c_j \le c_0 + 9\cdot Inc_{Strs.avg} \\
IDRG11_4 & \text{if } c_0 + 9\cdot Inc_{Strs.avg} < c_j \le c_0 + 10\cdot Inc_{Strs.avg} \\
IDRG12_4 & \text{if } c_0 + 10\cdot Inc_{Strs.avg} < c_j \le c_0 + 11\cdot Inc_{Strs.avg} \\
IDRG13_4 & \text{if } c_0 + 11\cdot Inc_{Strs.avg} < c_j \le c_0 + 12\cdot Inc_{Strs.avg} \\
IDRG14_4 & \text{if } c_0 + 12\cdot Inc_{Strs.avg} < c_j \le c_0 + 13\cdot Inc_{Strs.avg} \\
IDRG15_4 & \text{if } c_0 + 13\cdot Inc_{Strs.avg} < c_j \le c_0 + 14\cdot Inc_{Strs.avg} \\
IDRG16_4 & \text{if } c_0 + 14\cdot Inc_{Strs.avg} < c_j \le c_0 + 15\cdot Inc_{Strs.avg} \\
IDRG17 & \text{if } c_0 + 15\cdot Inc_{Strs.avg} < c_j \le c_0 + 16\cdot Inc_{Strs.avg}
\end{array}\right.
\end{array}
$$

IDRG_{18_4} if $c_0 + 16 \cdot \mathrm{Inc}_{\mathrm{Strs.avg}} < c_j \le c_0 + 17 \cdot \mathrm{Inc}_{\mathrm{Strs.avg}}$

IDRG_{19_4} if $c_0 + 17 \cdot \mathrm{Inc}_{\mathrm{Strs.avg}} < c_j \le c_0 + 18 \cdot \mathrm{Inc}_{\mathrm{Strs.avg}}$

IDRG_{20_4} otherwise

$\sigma_2 \leftarrow$ IDRG_{1_5} if $c_j \le c_0$

IDRG_{2_5} if $c_0 < c_j \le c_0 + \mathrm{Inc}_{\mathrm{Strs.avg}}$

IDRG_{3_5} if $c_0 + \mathrm{Inc}_{\mathrm{Strs.avg}} < c_j \le c_0 + 2 \cdot \mathrm{Inc}_{\mathrm{Strs.avg}}$

IDRG_{4_5} if $c_0 + 2 \cdot \mathrm{Inc}_{\mathrm{Strs.avg}} < c_j \le c_0 + 3 \cdot \mathrm{Inc}_{\mathrm{Strs.avg}}$

IDRG_{5_5} if $c_0 + 3 \cdot \mathrm{Inc}_{\mathrm{Strs.avg}} < c_j \le c_0 + 4 \cdot \mathrm{Inc}_{\mathrm{Strs.avg}}$

IDRG_{6_5} if $c_0 + 4 \cdot \mathrm{Inc}_{\mathrm{Strs.avg}} < c_j \le c_0 + 5 \cdot \mathrm{Inc}_{\mathrm{Strs.avg}}$

IDRG_{7_5} if $c_0 + 5 \cdot \mathrm{Inc}_{\mathrm{Strs.avg}} < c_j \le c_0 + 6 \cdot \mathrm{Inc}_{\mathrm{Strs.avg}}$

IDRG_{8_5} if $c_0 + 6 \cdot \mathrm{Inc}_{\mathrm{Strs.avg}} < c_j \le c_0 + 7 \cdot \mathrm{Inc}_{\mathrm{Strs.avg}}$

IDRG_{9_5} if $c_0 + 7 \cdot \mathrm{Inc}_{\mathrm{Strs.avg}} < c_j \le c_0 + 8 \cdot \mathrm{Inc}_{\mathrm{Strs.avg}}$

IDRG_{10_5} if $c_0 + 8 \cdot \mathrm{Inc}_{\mathrm{Strs.avg}} < c_j \le c_0 + 9 \cdot \mathrm{Inc}_{\mathrm{Strs.avg}}$

IDRG_{11_5} if $c_0 + 9 \cdot \mathrm{Inc}_{\mathrm{Strs.avg}} < c_j \le c_0 + 10 \cdot \mathrm{Inc}_{\mathrm{Strs.avg}}$

IDRG_{12_5} if $c_0 + 10 \cdot \mathrm{Inc}_{\mathrm{Strs.avg}} < c_j \le c_0 + 11 \cdot \mathrm{Inc}_{\mathrm{Strs.avg}}$

IDRG_{13_5} if $c_0 + 11 \cdot \mathrm{Inc}_{\mathrm{Strs.avg}} < c_j \le c_0 + 12 \cdot \mathrm{Inc}_{\mathrm{Strs.avg}}$

IDRG_{14_5} if $c_0 + 12 \cdot \mathrm{Inc}_{\mathrm{Strs.avg}} < c_j \le c_0 + 13 \cdot \mathrm{Inc}_{\mathrm{Strs.avg}}$

IDRG_{15_5} if $c_0 + 13 \cdot \mathrm{Inc}_{\mathrm{Strs.avg}} < c_j \le c_0 + 14 \cdot \mathrm{Inc}_{\mathrm{Strs.avg}}$

IDRG_{16_5} if $c_0 + 14 \cdot \mathrm{Inc}_{\mathrm{Strs.avg}} < c_j \le c_0 + 15 \cdot \mathrm{Inc}_{\mathrm{Strs.avg}}$

IDRG_{17_5} if $c_0 + 15 \cdot \mathrm{Inc}_{\mathrm{Strs.avg}} < c_j \le c_0 + 16 \cdot \mathrm{Inc}_{\mathrm{Strs.avg}}$

IDRG_{18_5} if $c_0 + 16 \cdot \mathrm{Inc}_{\mathrm{Strs.avg}} < c_j \le c_0 + 17 \cdot \mathrm{Inc}_{\mathrm{Strs.avg}}$

$$
\begin{cases}
\begin{cases}
\begin{cases}
IDRG19_5 & \text{if } c_0 + 17\cdot Inc_{Strs.avg} < c_j \le c_0 + 18\cdot Inc_{Strs.avg} \\
IDRG20_5 & \text{otherwise}
\end{cases} \\
\sigma_3 \leftarrow \begin{cases}
IDRG1_6 & \text{if } c_j \le c_0 \\
IDRG2_6 & \text{if } c_0 < c_j \le c_0 + Inc_{Strs.avg} \\
IDRG3_6 & \text{if } c_0 + Inc_{Strs.avg} < c_j \le c_0 + 2\cdot Inc_{Strs.avg} \\
IDRG4_6 & \text{if } c_0 + 2\cdot Inc_{Strs.avg} < c_j \le c_0 + 3\cdot Inc_{Strs.avg} \\
IDRG5_6 & \text{if } c_0 + 3\cdot Inc_{Strs.avg} < c_j \le c_0 + 4\cdot Inc_{Strs.avg} \\
IDRG6_6 & \text{if } c_0 + 4\cdot Inc_{Strs.avg} < c_j \le c_0 + 5\cdot Inc_{Strs.avg} \\
IDRG7_6 & \text{if } c_0 + 5\cdot Inc_{Strs.avg} < c_j \le c_0 + 6\cdot Inc_{Strs.avg} \\
IDRG8_6 & \text{if } c_0 + 6\cdot Inc_{Strs.avg} < c_j \le c_0 + 7\cdot Inc_{Strs.avg} \\
IDRG9_6 & \text{if } c_0 + 7\cdot Inc_{Strs.avg} < c_j \le c_0 + 8\cdot Inc_{Strs.avg} \\
IDRG10_6 & \text{if } c_0 + 8\cdot Inc_{Strs.avg} < c_j \le c_0 + 9\cdot Inc_{Strs.avg} \\
IDRG11_6 & \text{if } c_0 + 9\cdot Inc_{Strs.avg} < c_j \le c_0 + 10\cdot Inc_{Strs.avg} \\
IDRG12_6 & \text{if } c_0 + 10\cdot Inc_{Strs.avg} < c_j \le c_0 + 11\cdot Inc_{Strs.avg} \\
IDRG13_6 & \text{if } c_0 + 11\cdot Inc_{Strs.avg} < c_j \le c_0 + 12\cdot Inc_{Strs.avg} \\
IDRG14_6 & \text{if } c_0 + 12\cdot Inc_{Strs.avg} < c_j \le c_0 + 13\cdot Inc_{Strs.avg} \\
IDRG15_6 & \text{if } c_0 + 13\cdot Inc_{Strs.avg} < c_j \le c_0 + 14\cdot Inc_{Strs.avg} \\
IDRG16_6 & \text{if } c_0 + 14\cdot Inc_{Strs.avg} < c_j \le c_0 + 15\cdot Inc_{Strs.avg} \\
IDRG17_6 & \text{if } c_0 + 15\cdot Inc_{Strs.avg} < c_j \le c_0 + 16\cdot Inc_{Strs.avg} \\
IDRG18_6 & \text{if } c_0 + 16\cdot Inc_{Strs.avg} < c_j \le c_0 + 17\cdot Inc_{Strs.avg} \\
IDRG19_6 & \text{if } c_0 + 17\cdot Inc_{Strs.avg} < c_j \le c_0 + 18\cdot Inc_{Strs.avg}
\end{cases}
\end{cases}
$$

$$\left|\begin{array}{l} \text{IDRG}_{20_6} \text{ otherwise} \end{array}\right.$$

$$\xi_0 \leftarrow \sigma_0$$

$$\xi_1 \leftarrow \sigma_0 + \sigma_1 \cdot \left(\frac{0.25 \cdot a_j}{t}\right) + \sigma_2 \cdot \left(\frac{0.25 \cdot a_j}{t}\right)^2 + \sigma_3 \cdot \left(\frac{0.25 \cdot a_j}{t}\right)^3$$

$$\xi_2 \leftarrow \sigma_0 + \sigma_1 \cdot \left(\frac{0.5 \cdot a_j}{t}\right) + \sigma_2 \cdot \left(\frac{0.5 \cdot a_j}{t}\right)^2 + \sigma_3 \cdot \left(\frac{0.5 \cdot a_j}{t}\right)^3$$

$$\xi_3 \leftarrow \sigma_0 + \sigma_1 \cdot \left(\frac{0.75 \cdot a_j}{t}\right) + \sigma_2 \cdot \left(\frac{0.75 \cdot a_j}{t}\right)^2 + \sigma_3 \cdot \left(\frac{0.75 \cdot a_j}{t}\right)^3$$

$$\xi_4 \leftarrow \sigma_0 + \sigma_1 \cdot \left(\frac{1.0 \cdot a_j}{t}\right) + \sigma_2 \cdot \left(\frac{1.0 \cdot a_j}{t}\right)^2 + \sigma_3 \cdot \left(\frac{1.0 \cdot a_j}{t}\right)^3$$

$$x_0 \leftarrow 0.0$$

$$x_1 \leftarrow 0.25$$

$$x_2 \leftarrow 0.5$$

$$x_3 \leftarrow 0.75$$

$$x_4 \leftarrow 1.0$$

$$X \leftarrow \text{stack}(x_0, x_1, x_2, x_3, x_4)$$

$$ST \leftarrow \text{stack}(\xi_0, \xi_1, \xi_2, \xi_3, \xi_4)$$

$$RG \leftarrow \text{regress}(X, ST, 3)$$

$$\sigma_{00} \leftarrow RG_3 + P_{Int}$$

$$\sigma_{10} \leftarrow RG_4$$

$$\sigma_{20} \leftarrow RG_5$$

$$\sigma_{30} \leftarrow RG_6$$

$$AR_j \leftarrow \frac{a_j}{c_j}$$

$$AT_j \leftarrow \frac{a_j}{t}$$

$$G_{au_i} \leftarrow f_{aU}(R_t, AR_j, AT_j)$$

$$G_{al_j} \leftarrow f_{aL}(R_t, AR_j, AT_j)$$

$$G_{aq_j} \leftarrow f_{aQ}(R_t, AR_j, AT_j)$$

$$G_{ac_j} \leftarrow f_{aC}(R_t, AR_j, AT_j)$$

$$G_{cu_j} \leftarrow f_{cU}(R_t, AR_j, AT_j)$$

$$G_{cl_j} \leftarrow f_{cL}(R_t, AR_j, AT_j)$$

$$G_{cq_j} \leftarrow f_{cQ}(R_t, AR_j, AT_j)$$

$$G_{cc_j} \leftarrow f_{cC}(R_t, AR_j, AT_j)$$

$$Q_j \leftarrow \begin{cases} 1 + 1.464 \cdot \left(\frac{a_j}{c_j}\right)^{1.65} & \text{if } c_j \geq a_j \\ 1 + 1.464 \cdot \left(\frac{c_j}{a_j}\right)^{1.65} & \text{otherwise} \end{cases}$$

$$K_{a_j} \leftarrow \left(\frac{\pi \cdot a_j}{Q_j}\right)^{0.5} \cdot \left(\sigma_{00} \cdot G_{au_j} + \sigma_{10} \cdot G_{al_j} + \sigma_{20} \cdot G_{aq_j} + \sigma_{30} \cdot G_{ac_j}\right)$$

$$K_{c_j} \leftarrow \left(\frac{\pi \cdot c_j}{Q_j}\right)^{0.5} \cdot \left(\sigma_{00} \cdot G_{cu_j} + \sigma_{10} \cdot G_{cl_j} + \sigma_{20} \cdot G_{cq_j} + \sigma_{30} \cdot G_{cc_j}\right)$$

$$K_{\alpha_j} \leftarrow K_{a_j} \cdot 1.099$$

$$K_{\gamma_j} \leftarrow K_{c_j} \cdot 1.099$$

$$K_{\alpha_j} \leftarrow \begin{cases} 9.0 & \text{if } K_{\alpha_j} \leq 9.0 \\ K_{\alpha_j} & \text{otherwise} \end{cases}$$

$$K_{\gamma_j} \leftarrow \begin{cases} 9.0 & \text{if } K_{\gamma_j} \leq 9.0 \\ K_{\gamma_j} & \text{otherwise} \end{cases}$$

$$D_{a_j} \leftarrow C_0 \cdot \left(K_{\alpha_j} - 9.0\right)^{1.16}$$

$$D_{ag_i} \leftarrow \left| D_{a_i} \cdot CF_{inhr} \cdot C_{blk} \quad \text{if } K_{\alpha_i} < 80.0 \right.$$

$$\left| \begin{array}{l} \left| \begin{array}{ll} D_{c_j} \cdot CF_{inhr} \cdot C_{blk} & \text{if } K_{\gamma_j} < 80.0 \\ 4 \cdot 10^{-10} \cdot CF_{inhr} \cdot C_{blk} & \text{otherwise} \end{array} \right. \\ D_{c_j} \leftarrow C_0 \cdot \left(K_{\gamma_j} - 9.0 \right)^{1.16} \\ D_{cg_j} \leftarrow \left| \begin{array}{ll} D_{c_j} \cdot CF_{inhr} \cdot C_{blk} & \text{if } K_{\gamma_j} < 80.0 \\ 4 \cdot 10^{-10} \cdot CF_{inhr} \cdot C_{blk} & \text{otherwise} \end{array} \right. \\ output_{(j,0)} \leftarrow j \\ output_{(j,1)} \leftarrow a_j \\ output_{(j,2)} \leftarrow c_j - c_0 \\ output_{(j,3)} \leftarrow D_{ag_j} \\ output_{(j,4)} \leftarrow D_{cg_j} \\ output_{(j,5)} \leftarrow K_{a_j} \\ output_{(j,6)} \leftarrow K_{c_j} \\ output_{(j,7)} \leftarrow \frac{NCB_j}{365 \cdot 24} \\ output_{(j,8)} \leftarrow G_{au_j} \\ output_{(j,9)} \leftarrow G_{al_j} \\ output_{(j,10)} \leftarrow G_{aq_j} \\ output_{(j,11)} \leftarrow G_{ac_j} \\ output_{(j,12)} \leftarrow G_{cu_j} \\ output_{(j,13)} \leftarrow G_{cl_j} \\ output_{(j,14)} \leftarrow G_{cq_j} \\ output_{(j,15)} \leftarrow G_{cc_j} \\ j \leftarrow j + 1 \\ a_j \leftarrow a_{j-1} + D_{ag_{i-1}} \end{array} \right.$$

$$c_j \leftarrow c_{j-1} + D_{cg_{j-1}}$$

$$a_j \leftarrow \begin{cases} t & \text{if } a_j \geq t \\ a_j & \text{otherwise} \end{cases}$$

$$NCB_j \leftarrow NCB_{j-1} + C_{blk}$$

output

$k := 0 .. I_{lim}$

The curve below shows the flaw growth through-wall and the operating time (in years) it takes for the initial flaw in the blind zone to go through-wall.

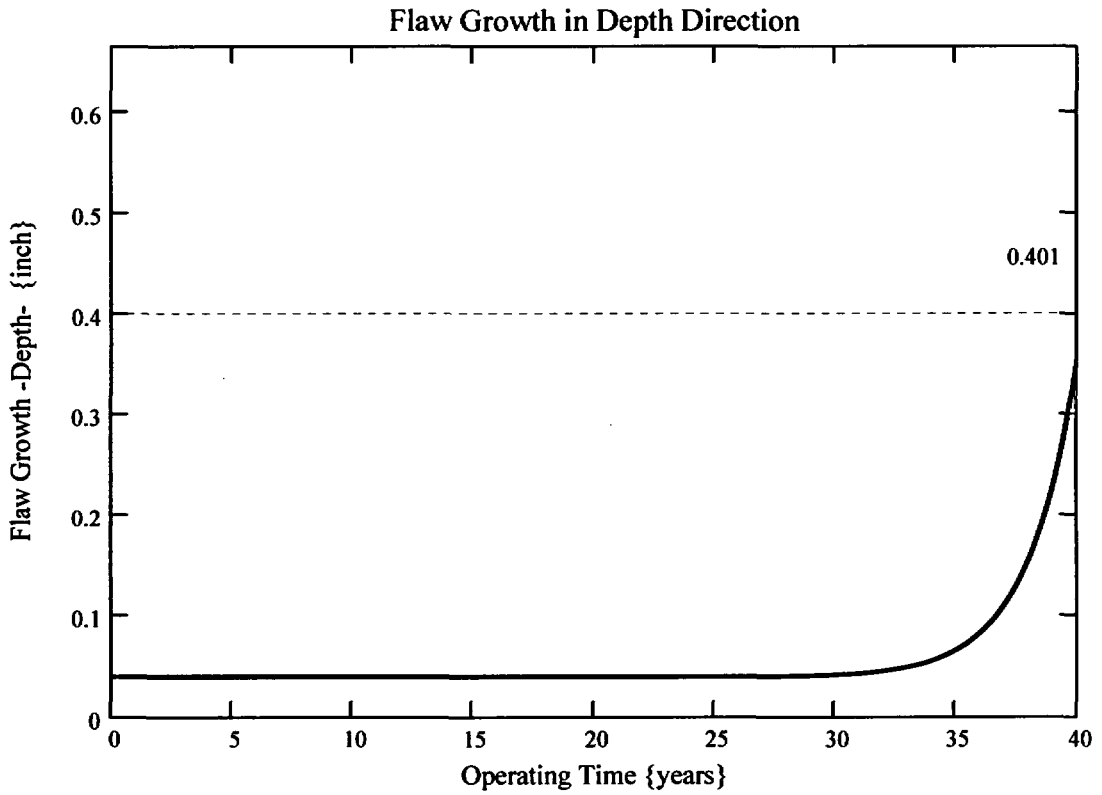

The propagation length for the ICI nozzles is defined as the length for which the initial flaw in the blind zone would extend out of the blind zone and grow to a detectable flaw. Reference 12 gives the minimum detectable flaw size of 4 mm (0.16) in length; thus, 0.16 inch was considered as this minimum detectable flaw length. This dimension is added to the end of the blind zone.

$$\text{Prop\_Length} := \frac{\text{BZ\_length}}{2} - c_0 + 0.16$$

$$\text{Prop\_Length} = 0.4$$

This implies that a flaw initially within the blindzone must grow 0.3 inch to become detectable via UT.

The curve below shows the flaw growth along the length of the ICI nozzle and the operating time (in years) it takes to reach the Prop_Length value defined above.

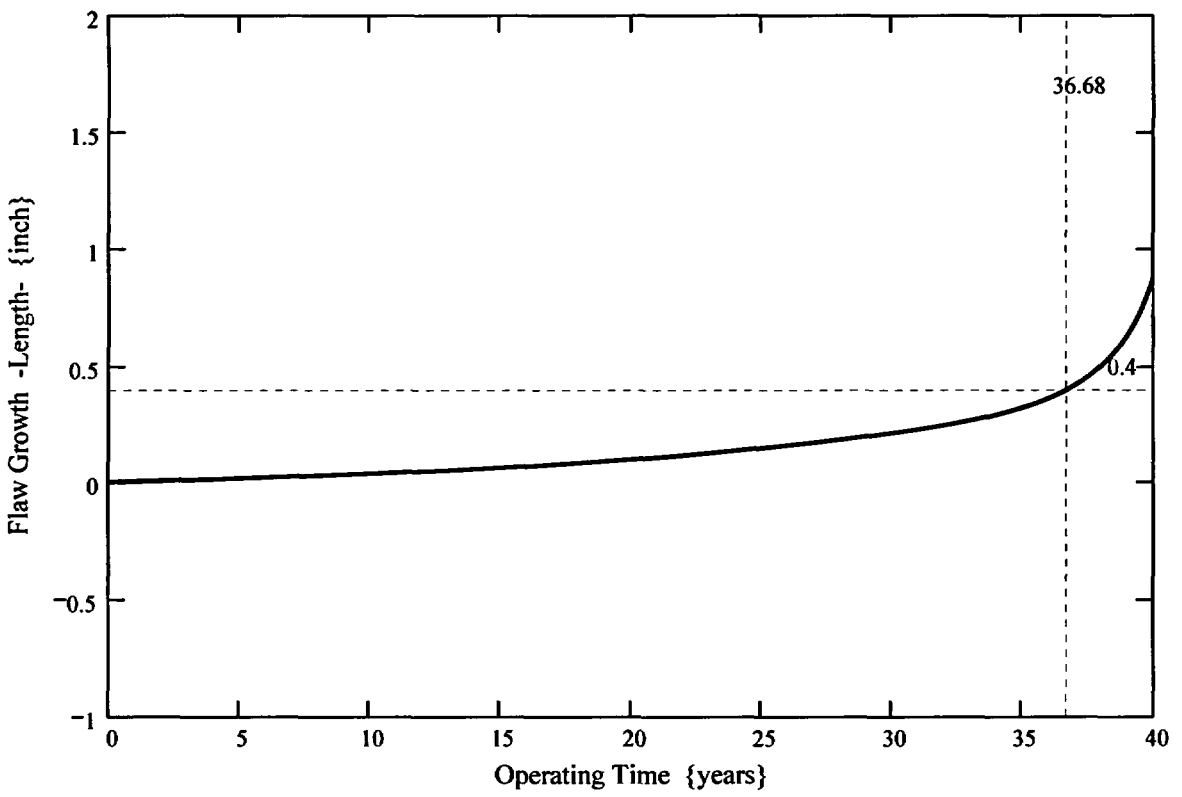

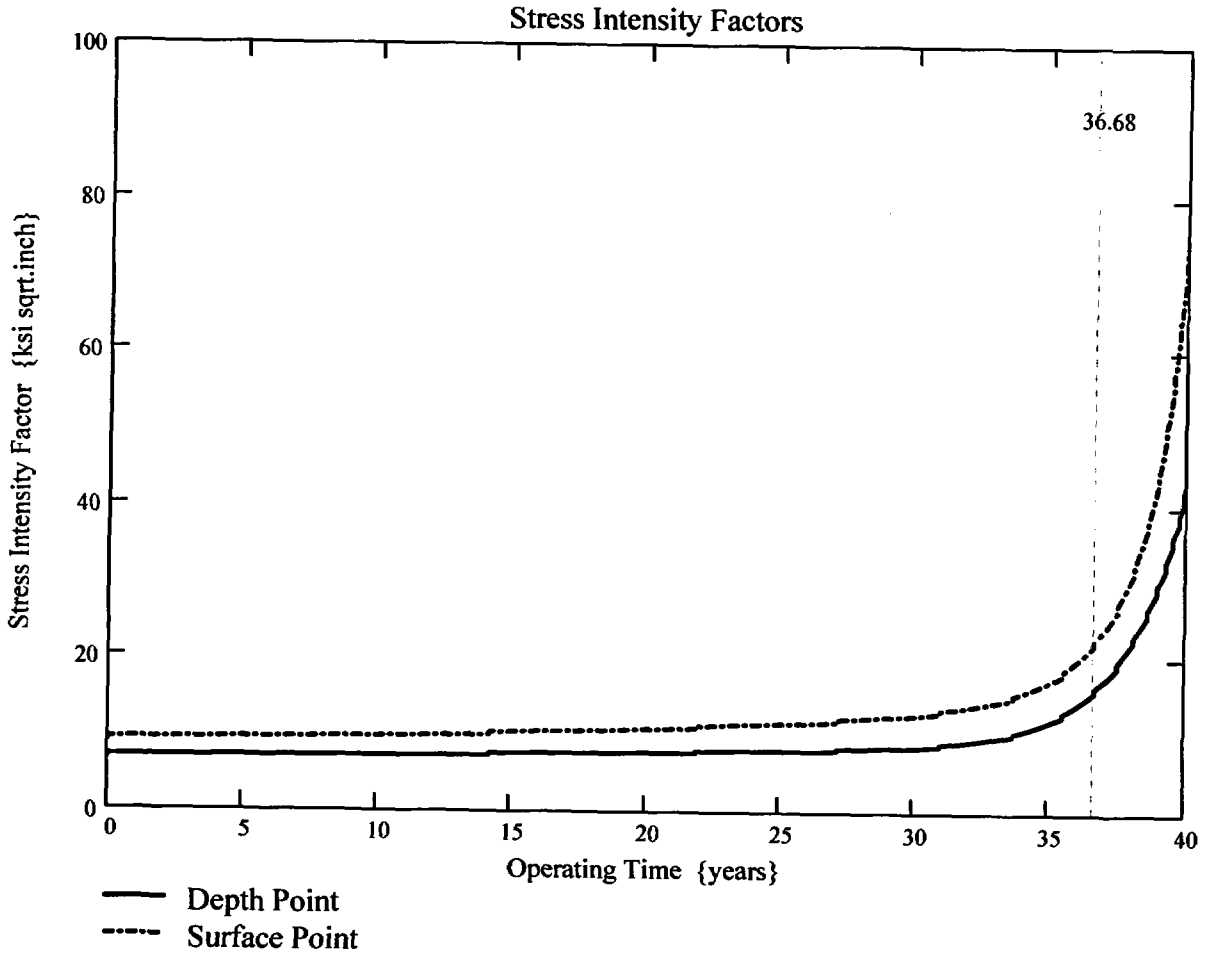
Stress Intensity Factors
100
80
60
40
20
0
36.68
Stress Intensity Factor {ksi sqrt.inch}
0
5
10
15
20
25
30
35
40
Operating Time {years}
Depth Point
Surface Point

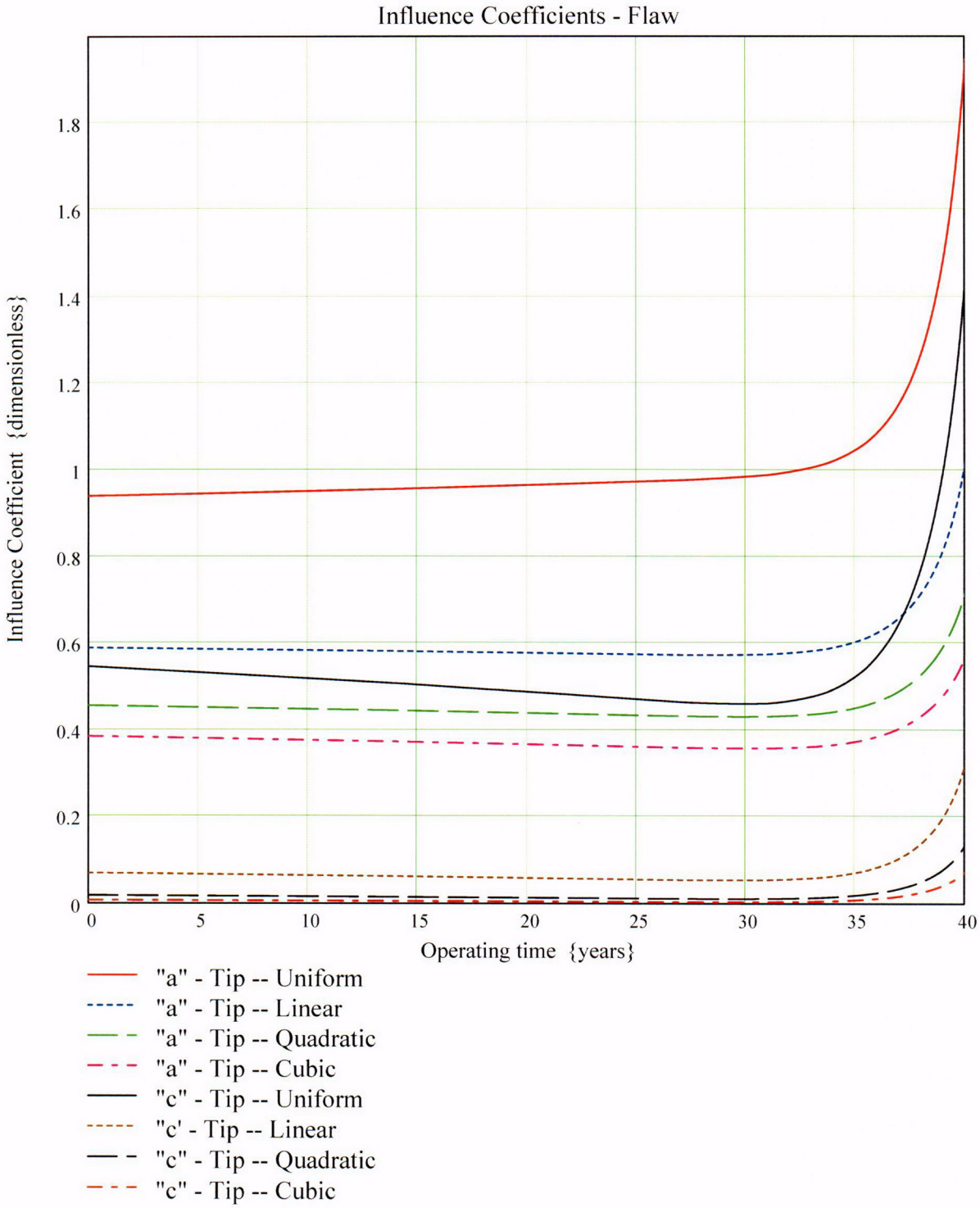
Influence Coefficients - Flaw
Influence Coefficient {dimensionless}
1.8
1.6
1.4
1.2
1
0.8
0.6
0.4
0.2
0
0
5
10
15
20
25
30
35
40
Operating time {years}
"a" - Tip -- Uniform
"a" - Tip -- Linear
"a" - Tip -- Quadratic
"a" - Tip -- Cubic
"c" - Tip -- Uniform
"c' - Tip -- Linear
"c" - Tip -- Quadratic
"c" - Tip -- Cubic

Waterford Steam Electric Station Unit 3

Primary Water Stress Corrosion Crack Growth Analysis for an ICI ID Surface Flaw Uphill (180°), in the Blind Zone above the Top of the J-Groove Weld
Developed by Central Engineering Programs, Entergy Operations Inc.

Flaw Case 3: 25% Through-Wall Flaw with a 4-to-1 Flaw Length-to-Depth Aspect Ratio, Located at the Center of the Blind Zone

Calculation Basis: MRP 75 th Percentile and Flaw Face Pressurized

Mean Radius -to- Thickness Ratio:- "R_m/t" -- between 1.0 and 300.0

Note : ***The Metric form of the equation from EPRI MRP was used 55-Rev. 1*** *. A correction factor is applied in the determination of the crack extension to convert the units of meters per second to the value in inches per hour .*

ID Surface Flaw

User Input:

The Dominion Engineering Inc. (DEI) finite element model nodal elevations and hoop stresses for the uphill side (180° azimuth) of the ICI nozzle are brought into the Mathcad worksheet from data supplied in Reference 8d. The data are composed of the nodal elevations (in inches), along with the ID, 25% through-wall (tw), 50% tw, 75% tw, and OD hoop stresses, beginning two nodal lines below (nodal line 81101) the top of the weld (nodal line 81301) and extending to the top of the nozzle in the FEA model (nodal line 83301), which is at the point where the nozzle intersects the reactor vessel head.

The DEI FEA data has elevation referenced from the bottom of the ICI nozzle. The elevations of the node points in the DEI FEA model, beginning below the top of the weld, at nodal line 81101, and the corresponding hoop stresses are as follows:

Note the following terms used throughout this evaluation:

ID-inside diameter of ICI nozzle
QT-25% tw position
MD-50% tw, or mid-wall, position
TQ-75% tw position
OD-outside diameter of ICI nozzle

$i := 0..20$

Node_line :=	Elev_fea :=	ID_stress_fea :=	QT_stress_fea :=
81101	3.973	43.347	41.640
81201	4.089	42.799	39.703
81301	4.205	39.763	38.158
81401	4.435	37.068	33.351
81501	4.605	34.079	32.268
81601	4.798	29.820	28.465
81701	5.015	23.668	21.543
81801	5.262	18.722	14.133
81901	5.541	18.383	15.071
82001	5.857	18.876	17.269
82101	6.214	19.527	18.517
82201	6.619	20.331	19.550
82301	7.077	20.976	20.149
82401	7.596	21.408	20.378
82501	8.183	21.667	20.400
82601	8.847	21.792	20.133
82701	9.599	21.742	19.395
82801	10.451	21.550	18.466
82901	11.415	21.213	17.311
83001	12.505	19.876	16.176
83101	13.740	18.311	15.380
83201	15.138	16.442	14.525
83301	18.057	12.330	12.146

$$MD\_stress\_fea := \begin{pmatrix} 43.666 \\ 41.445 \\ 34.368 \\ 25.957 \\ 24.632 \\ 21.515 \\ 14.530 \\ 7.280 \\ 8.650 \\ 11.236 \\ 12.761 \\ 13.998 \\ 14.467 \\ 14.437 \\ 14.263 \\ 13.976 \\ 13.664 \\ 13.362 \\ 13.126 \\ 13.009 \\ 12.983 \\ 12.960 \\ 12.033 \end{pmatrix}$$

$$TQ\_stress\_fea := \begin{pmatrix} 50.638 \\ 40.722 \\ 27.002 \\ 16.947 \\ 11.934 \\ 10.551 \\ 5.734 \\ 0.963 \\ 3.277 \\ 6.243 \\ 7.898 \\ 9.088 \\ 9.428 \\ 9.275 \\ 9.100 \\ 8.964 \\ 8.987 \\ 9.158 \\ 9.525 \\ 10.038 \\ 10.759 \\ 11.508 \\ 11.987 \end{pmatrix}$$

$$OD\_stress\_fea := \begin{pmatrix} 59.979 \\ 51.289 \\ 41.729 \\ 6.333 \\ 5.354 \\ 3.714 \\ 0.010 \\ -4.004 \\ -1.652 \\ 1.578 \\ 3.319 \\ 4.422 \\ 4.629 \\ 4.330 \\ 4.150 \\ 4.177 \\ 4.508 \\ 5.143 \\ 6.042 \\ 7.179 \\ 8.539 \\ 10.066 \\ 11.973 \end{pmatrix}$$

Blind Zone and Counterbore Reference dimensions:

From design drawings (Ref. 3) and the design details of Attachment 1, the following dimensions are used to locate the counterbore bottom and blind zone locations (bottom, top, and middle) as referenced from the nodal coordinates of the DEI FEA model.

Actual_cbore_bottom_elev := $Elev\_fea_2$ + 1.01

Actual_cbore_bottom_elev = 5.215

Primary Assumptions on blind zone dimensions:

topweld_to_bottom_BZ := 0.67

This is the distance from top of the J-weld, on the uphill side, to the bottom of the blind zone. Without UT data to verify this dimension, this value be iterated to determine the MINIMUM height above the top of the weld for which the blind zone can begin and yield an acceptable fracture mechanics solution.

BZ_length := 0.8

This value is based on the longest blind zone seen in the ANO-2 ICI nozzles. Both Waterford-3 and ANO-2 ICI nozzles have similar geometries above the top of the weld. Thus, a reasonable engineered assumption is that the largest blind zone for ANO-2 is assumed for the Waterford-3 ICI nozzles.

$$elev\_to\_mid\_BZ := Elev\_fea_2 + topweld\_to\_bottom\_BZ + \frac{BZ\_length}{2}$$

elev_to_mid_BZ = 5.315

bottom_of_BZ := $Elev\_fea_2$ + topweld_to_bottom_BZ

bottom_of_BZ = 4.875

top_of_BZ := $Elev\_fea_2$ + topweld_to_bottom_BZ + BZ_length

top_of_BZ = 5.755

For stress averaging and fracture mechanics purposes, the reference coordinate system--with a "0" elevation at the bottom of the nozzle, at the ID corner--must be converted into a new coordinate system with the top of the nozzle (nodal line 83301) as the new "0" elevation.. The positive direction along this new coordinate system will be towards nodal line 81101, which is the just below the top of the weld. This modification facilitates a fracture mechanics model more ammenable to the surface flaw loop structure previously developed in Reference 6.

The following iterative loop converts the five (5) through-wall stress components--ID, 25% tw (QT), 50% tw (MD), 75% tw (TQ), and OD--and the associated elevation, initially given in the DEI FEA model, into the "new" coordinate system, referenced from the top of the nozzle where it meets the reactor vessel head.

$$
\begin{aligned}
\text{Conv} := \;& n \leftarrow 20 \\
& \text{Top} \leftarrow \text{Elev\_fea}_n \\
& j \leftarrow n \\
& i \leftarrow 0 \\
& \text{while } j \geq 0 \\
& \quad \text{Elev\_conv}_i \leftarrow \text{Top} - \text{Elev\_fea}_j \\
& \quad \text{ID\_stress}_i \leftarrow \text{ID\_stress\_fea}_j \\
& \quad \text{QT\_stress}_i \leftarrow \text{QT\_stress\_fea}_j \\
& \quad \text{MD\_stress}_i \leftarrow \text{MD\_stress\_fea}_j \\
& \quad \text{TQ\_stress}_i \leftarrow \text{TQ\_stress\_fea}_j \\
& \quad \text{OD\_stress}_i \leftarrow \text{OD\_stress\_fea}_j \\
& \quad \text{output}_{(i,0)} \leftarrow \text{Elev\_conv}_i \\
& \quad \text{output}_{(i,1)} \leftarrow \text{ID\_stress}_i \\
& \quad \text{output}_{(i,2)} \leftarrow \text{QT\_stress}_i \\
& \quad \text{output}_{(i,3)} \leftarrow \text{MD\_stress}_i \\
& \quad \text{output}_{(i,4)} \leftarrow \text{TQ\_stress}_i \\
& \quad \text{output}_{(i,5)} \leftarrow \text{OD\_stress}_i \\
& \quad j \leftarrow j - 1 \\
& \quad i \leftarrow i + 1 \\
& \text{output}
\end{aligned}
$$

$Elev := Conv^{\langle 0 \rangle}$

$ID\_stress := Conv^{\langle 1 \rangle}$

$QT\_stress := Conv^{\langle 2 \rangle}$

$MD\_stress := Conv^{\langle 3 \rangle}$

$TQ\_stress := Conv^{\langle 4 \rangle}$

$OD\_stress := Conv^{\langle 5 \rangle}$

$Elev_i$ =	ID_stress_i =	QT_stress_i =	MD_stress_i =	TQ_stress_i =	OD_stress_i =
0	18.311	15.38	12.983	10.759	8.539
1.235	19.876	16.176	13.009	10.038	7.179
2.325	21.213	17.311	13.126	9.525	6.042
3.289	21.55	18.466	13.362	9.158	5.143
4.141	21.742	19.395	13.664	8.987	4.508
4.893	21.792	20.133	13.976	8.964	4.177
5.557	21.667	20.4	14.263	9.1	4.15
6.144	21.408	20.378	14.437	9.275	4.33
6.663	20.976	20.149	14.467	9.428	4.629
7.121	20.331	19.55	13.998	9.088	4.422
7.526	19.527	18.517	12.761	7.898	3.319
7.883	18.876	17.269	11.236	6.243	1.578
8.199	18.383	15.071	8.65	3.277	-1.652
8.478	18.722	14.133	7.28	0.963	-4.004
8.725	23.668	21.543	14.53	5.734	0.01
8.942	29.82	28.465	21.515	10.551	3.714
9.135	34.079	32.268	24.632	11.934	5.354
9.305	37.068	33.351	25.957	16.947	6.333
9.535	39.763	38.158	34.368	27.002	41.729
9.651	42.799	39.703	41.445	40.722	51.289
9.767	43.347	41.64	43.666	50.638	59.979

The five arrays given above include the elevation measured from the top of the ICI nozzle from the FEA model down to the top of the J-weld and the corresponding hoop stresses in the modified coordinate system (MCS).

Additional Geometry in Modified Coordinate System

The top of the J-groove weld in the MCS is equal to entry 18 in the "Elev" array:

$Top\_Jweld := Elev_{18}$

$Top\_Jweld = 9.535$

The location of the top of the UT blind zone (BZ) in the MCS (as measured from the ID surface) is

$BZ\_top := Top\_Jweld - (topweld\_to\_bottom\_BZ + BZ\_length)$

$BZ\_top = 7.985$

The midpoint of the BZ in the MCS is

$$BZ\_mid := BZ\_top + \frac{BZ\_length}{2}$$

$BZ\_mid = 8.425$

The bottom of the BZ in the MCS is

$BZ\_bottom := BZ\_top + BZ\_length$

$BZ\_bottom = 8.865$

The location of the actual counterbore (from design drawings) in the MCS:

$cbore\_elev := Top\_Jweld - 1.377$

$cbore\_elev = 8.158$

From the MCS, the stress distribution from elevation 0 (the top of the ICI nozzle where it intersects the RV head) to the top of the weld is graphically shown below.

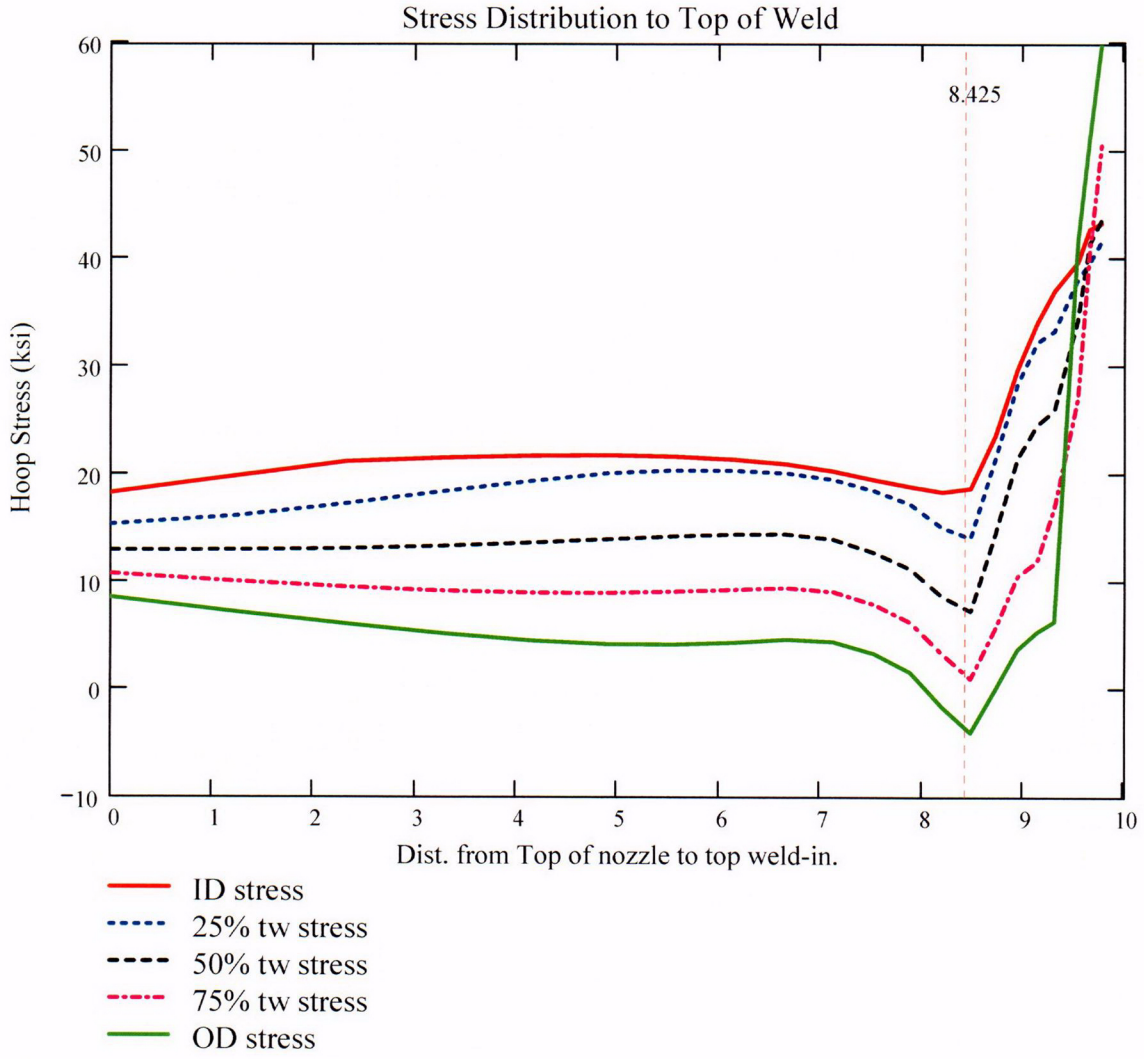

For the ID surface flaw model, the reference point is the location along the axis of the nozzle used to locate the flaw. For this analysis, the reference point is considered at the mid-height of the blind zone.

$Ref_{Point} := BZ\_mid$

To place the flaw with respect to the reference point, the flaw tips and center can be located as follows:

1) The Upper "c- tip" located at the reference point (Enter 1)
2) The Center of the flaw at the reference point (Enter 2)
3) The lower "c- tip" located at the reference point (Enter 3).

Val := 2

The Input Below is the point below the blind zone region where stresses will be considered for curve-fitting. This point is taken as the top of the weld, since the stress distribution changes drastically within the weld region Enter this dimension or variable below.

$Elev_{Strs.Dist} := Elev_{20}$ The elevation to the point of maximum stress to consider (Axial distance from elevation 0 in the MCS).

ICI Nozzle Geometry Input Data:

od := 5.563 − 0.001 Tube OD, in inches (The value from Ref. 3, is 5.563" +0.00/-0.001)

id1 := 4.625 + 0.01 Maximum Tube ID above counterbore, in inches (The value from Ref. 3 is 4.625" +/- 0.010")

id2 := 4.750 + 0.01 Maximum Tube ID below counterbore, in inches (The value from Ref. 3 is 4.750" +/- 0.010")

$t1 := \frac{(od - id1)}{2}$

Minmum wall thickness above the counterbore, in inches

t1 = 0.4635

$t2 := \frac{(od - id2)}{2}$

Minimum wall thickness below the counterbore, in inches

t2 = 0.401

$R_o := \frac{od}{2}$ $R_o = 2.781$

$R_{id1} := \frac{id1}{2}$ $R_{id1} = 2.3175$

$R_{id2} := \frac{id2}{2}$ $\quad R_{id2} = 2.38$

$R_{m1} := R_{id1} + \frac{t1}{2}$ $\quad R_{m1} = 2.54925$

$R_{m2} := R_{id2} + \frac{t2}{2}$ $\quad R_{m2} = 2.5805$

$R_t := \frac{R_{m2}}{t2}$ $\quad R_t = 6.43516$

$\frac{R_o}{t2} = 6.93516$

Flaw Geometry Input Data:

A postulated flaw could exist in the **0.88"** UT Blindzone that occurs **0.67"** above the top of the J-weld at the uphill (180°) location. The flaw length (c) and depth (a) constitute the input parameters. This flaw represents an internal surface crack in a cylinder, as described in Reference 9.

$AR_0 := 4$

$t2 \cdot .25 = 0.10025$

The flaw length-to-depth aspect ratio. This ratio (4-to-1) is potentially more conducive for through-wall growth than the 6-to-1 ratio used in ASME Section XI, and one sufficient to promote flaw growth through the thickness.

$a_0 := 0.1$

Initial Flaw Depth of the ID surface flaw in the blind zone above the top of the weld on the uphill side. The minimum detectable depth of a surface flaw from UT demonstrations [Ref. 12] was 8% throughwall. Conservatively, a 25% throughwall flaw is assumed. This flaw is sufficiently deep to see the stress field developed through the thickness.

$L := a_0 \cdot AR_0$

$L = 0.4$

Initial Flaw Length of an ID surface flaw in the counterbore region, in inches. The length was determined by assuming a 4-to-1 flaw length-to-depth aspect ratio. Half the flaw length (0.2 inch) was placed the below the mid-height of the blind zone, while the other half was placed above the mid-height.

$c_0 := \frac{L}{2}$

The half flaw length used in the fracture mechanics model

Additional Input Data:

$P_{Int} := 2.235$ Design Operating Pressure (internal) [Ref. 4]

$Years := 40$ Number of Operating Years

$I_{lim} := 8000$ Iteration limit for Crack Growth loop

$T := 604$ Operating Temperature for the head, in °F. Reference 5b gives a value of 601°F after the Extended Power Uprate (EPU), and 604°F currently. Thus, the temperature of the head will be taken as 604°F.

$\alpha_{0c} := 2.67 \cdot 10^{-12}$ Constant in MRP-55 PWSCC Model for I-600 Wrought @ 617 deg. F [Ref. 9]

$Q_g := 31.0$ Thermal activation Energy for Crack Growth {MRP) [Ref. 9]

$T_{ref} := 617$ Reference Temperature for normalizing Data deg. F [Ref. 9]

$Tim_{opr} := 365.2422 \cdot 24 \cdot Years$ Numer of operating hours in a year

$CF_{inhr} := 1.417 \cdot 10^{5}$ Correction factor to convert meters per second to inches per hour

$$C_{blk} := \frac{Tim_{opr}}{I_{lim}}$$ Calculation block size for the crack growth iteration loop

$C_{blk} = 43.82906$

$$Prnt_{blk} := \left| \frac{I_{lim}}{50} \right|$$

$$C_{01} := e^{\left[\frac{-Q_g}{1.103 \cdot 10^{-3}} \cdot \left(\frac{1}{T+459.67} - \frac{1}{T_{ref}+459.67} \right) \right] \cdot \alpha_{0c}}$$ Temperature Correction for Coefficient Alpha from EPRI MRP-55, Revision 1 [Ref. 10]

$C_0 := 1.0 C_{01}$ 75 th percentile from MRP-55 Revision 1 [Ref. 10]

The flaw model used for a postulated flaw within the counterbore region on the uphill side of the ICI nozzle is an internal surface flaw in a cylinder, subject to an arbitrary stress distribution.

To allow for a "moving average" of through-thickness stress values as the flaw extends along the length of the ICI ID surface, the length from the bottom tip of the of the initial flaw in the blind zone to the stress distribution upper limit--$Elev_{Strs.Dist}$--is broken into 20 equal segments. Note that due to the MCS used, with a 0 elevation occurring at the TOP of the nozzle, the term "U_{Tip}" (implying the upper tip of the flaw) is actually the physical bottom tip of the flaw, closer to the top of the weld. U_{Tip} is the term used in Reference 6 for the CEDM nozzles, and thus it will continue to be used in the ICI nozzle evaluation.

$$FL_{Cntr} := \begin{cases} Ref_{Point} - c_0 & \text{if } Val = 1 \\ Ref_{Point} & \text{if } Val = 2 \\ Ref_{Point} + c_0 & \text{otherwise} \end{cases}$$

Flaw center Location at the mid-point of the blind zone region

$$U_{Tip} := FL_{Cntr} + c_0$$

$$U_{Tip} = 8.625$$

$$Inc_{Strs.avg} := \frac{Elev_{Strs.Dist} - U_{Tip}}{20}$$

$$Inc_{Strs.avg} = 0.0571$$

$$Ref_{Point} = 8.425$$

No User Input is required beyond this Point

Regression of Through-Thickness Stresses as a Function of Axial Elevation

Because of the minor variation in stresses occuring at the top of the nozzle where it intersects the reactor head and the need to accurately curve fit stresses in the region of interest in the BZ, the entire range of stresses is not appropriate to curve fit. To accomodate an area below and above the BZ region, the first two data points in each of the elevation and stress arrays were removed from consideration in the curve fitting equations. This is a reasonable assumption, given that in the completely through-wall tensile stress field that exists in the nozzle above the top of the J-weld, a flaw centered in the BZ region is likely to grow through the thickness entirely (in addition to growth along the surface of the nozzle) rather than grow very long into an area close to the top of the head or below the top of the J-weld (i.e., elevation ranges not included in the stress polynomial curve fit). Initially, a **third (3rd)** order polynomial was chosen for axial stress regression. After regression, the stress at the mid-height of the blind zone (8.425 inches in the MCS) is checked.

Regression for ID stresses:

$k := 0..5$

$$ID\_elev\_cf := \begin{pmatrix} 7.883 \\ 8.199 \\ 8.478 \\ 8.725 \\ 8.942 \\ 9.135 \end{pmatrix} \qquad ID\_stress\_cf := \begin{pmatrix} 18.876 \\ 18.383 \\ 18.722 \\ 23.668 \\ 29.82 \\ 34.079 \end{pmatrix}$$

$R_{ID} := regress(ID\_elev\_cf, ID\_stress\_cf, 3)$

$$R_{ID} = \begin{pmatrix} 3 \\ 3 \\ 3 \\ 3578.38988 \\ -1136.79548 \\ 118.13463 \\ -3.95831 \end{pmatrix}$$

$z_{ID} := 7.883, 7.884.. 9.135$

$f_{ID}(z_{ID}) := interp(R_{ID}, ID\_elev\_cf, ID\_stress\_cf, z_{ID})$

$Elev_i$ =	ID_stress_i =
0	18.311
1.235	19.876
2.325	21.213
3.289	21.55
4.141	21.742
4.893	21.792
5.557	21.667
6.144	21.408
6.663	20.976
7.121	20.331
7.526	19.527
7.883	18.876
8.199	18.383
8.478	18.722
8.725	23.668
8.942	29.82
9.135	34.079
9.305	37.068
9.535	39.763
9.651	42.799
9.767	43.347

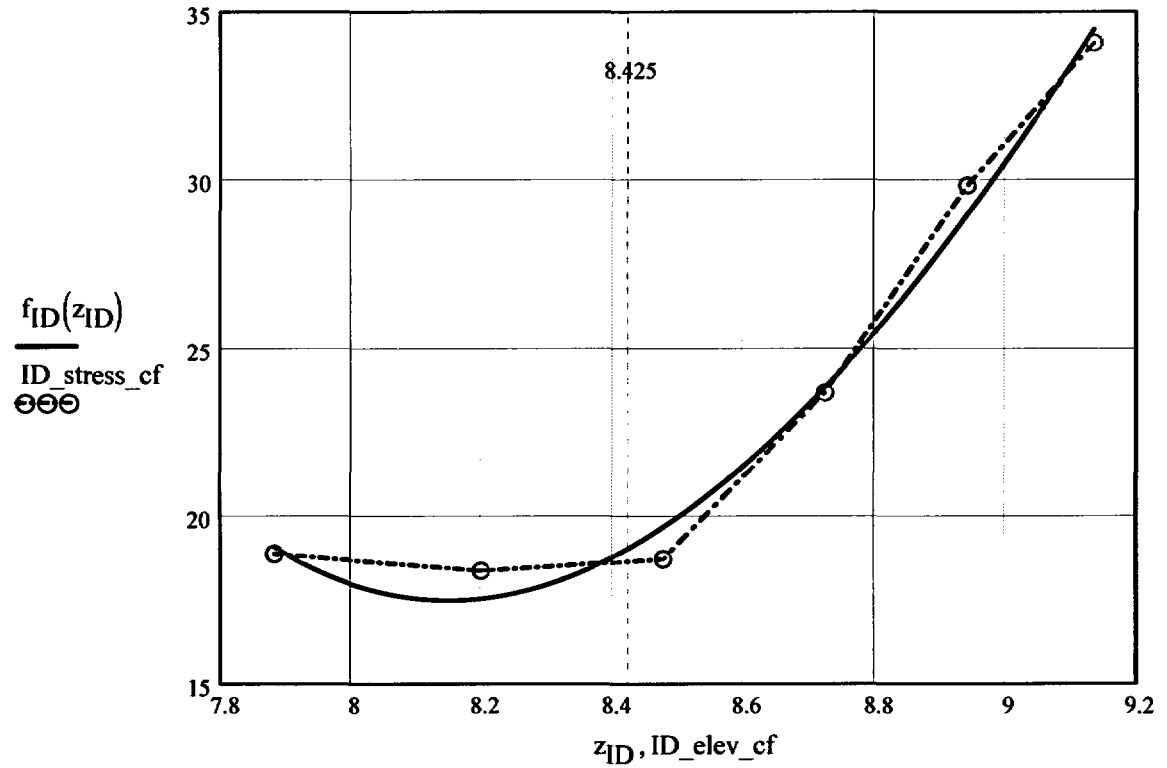

$f_{ID}(8.425) = 19.03958$

Regression for 25% throughwall stresses:

$$QT\_elev\_cf := \begin{pmatrix} 7.883 \\ 8.199 \\ 8.478 \\ 8.725 \\ 8.942 \\ 9.135 \end{pmatrix} \qquad QT\_stress\_cf := \begin{pmatrix} 17.269 \\ 15.071 \\ 14.133 \\ 21.543 \\ 28.465 \\ 32.268 \end{pmatrix}$$

$$R_{QT} := \text{regress}(QT\_elev\_cf, QT\_stress\_cf, 3)$$

$$z_{QT} := 7.883, 7.884 .. 9.135$$

$$R_{QT} = \begin{pmatrix} 3 \\ 3 \\ 3 \\ 10745.64054 \\ -3630.8401 \\ 406.73522 \\ -15.0681 \end{pmatrix}$$

$$f_{QT}(z_{QT}) := \text{interp}(R_{QT}, QT\_elev\_cf, QT\_stress\_cf, z_{QT})$$

$Elev_i$ =	QT_stress_i =
0	15.38
1.235	16.176
2.325	17.311
3.289	18.466
4.141	19.395
4.893	20.133
5.557	20.4
6.144	20.378
6.663	20.149
7.121	19.55
7.526	18.517
7.883	17.269
8.199	15.071
8.478	14.133
8.725	21.543
8.942	28.465
9.135	32.268
9.305	33.351
9.535	38.158
9.651	39.703
9.767	41.64

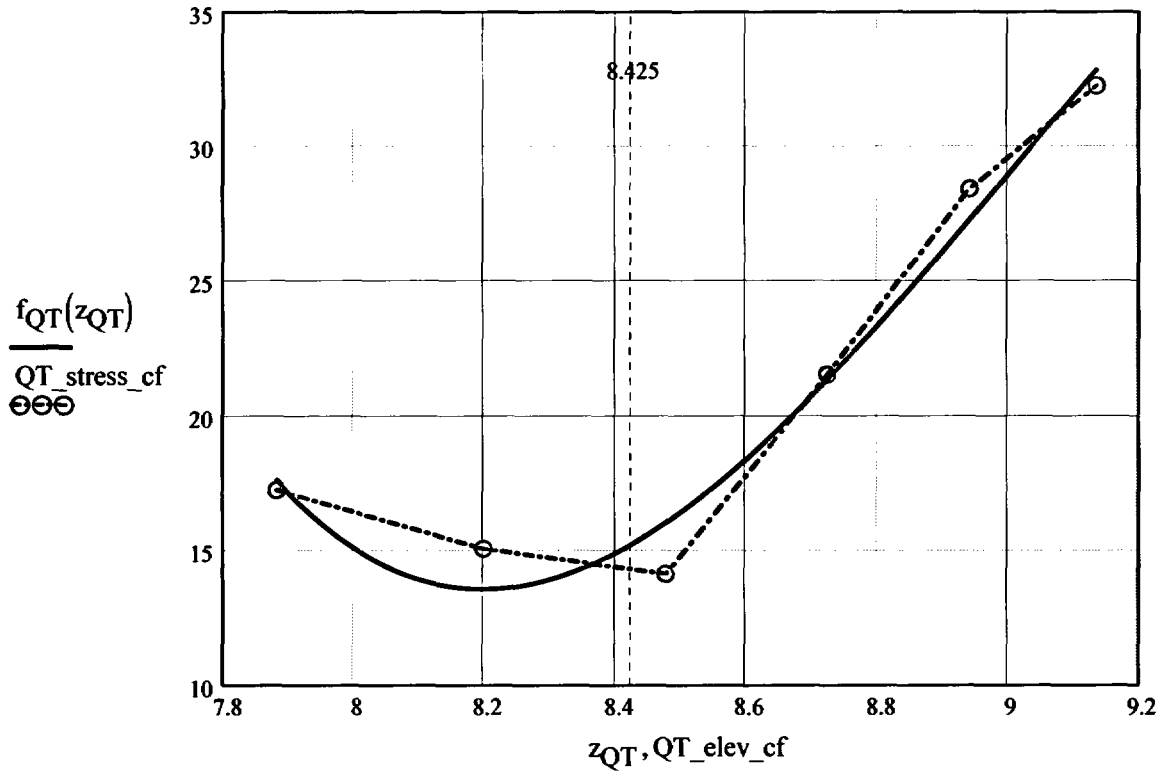

$f_{QT}(8.425) = 15.22949$

Regression for 50% throughwall stresses:

$$MD\_elev\_cf := \begin{pmatrix} 7.883 \\ 8.199 \\ 8.478 \\ 8.725 \\ 8.942 \\ 9.135 \end{pmatrix} \qquad MD\_stress\_cf := \begin{pmatrix} 11.236 \\ 8.65 \\ 7.28 \\ 14.53 \\ 21.515 \\ 24.632 \end{pmatrix}$$

$R_{MD} := regress(MD\_elev\_cf, MD\_stress\_cf, 3)$

$z_{MD} := 7.883, 7.884 .. 9.135$

$$R_{MD} = \begin{pmatrix} 3 \\ 3 \\ 3 \\ 11819.16519 \\ -4010.84838 \\ 451.35824 \\ -16.8173 \end{pmatrix}$$

$f_{MD}(z_{MD}) := interp(R_{MD}, MD\_elev\_cf, MD\_stress\_cf, z_{MD})$

$Elev_i$ =	MD_stress_i =
0	12.983
1.235	13.009
2.325	13.126
3.289	13.362
4.141	13.664
4.893	13.976
5.557	14.263
6.144	14.437
6.663	14.467
7.121	13.998
7.526	12.761
7.883	11.236
8.199	8.65
8.478	7.28
8.725	14.53
8.942	21.515
9.135	24.632
9.305	25.957
9.535	34.368
9.651	41.445
9.767	43.666

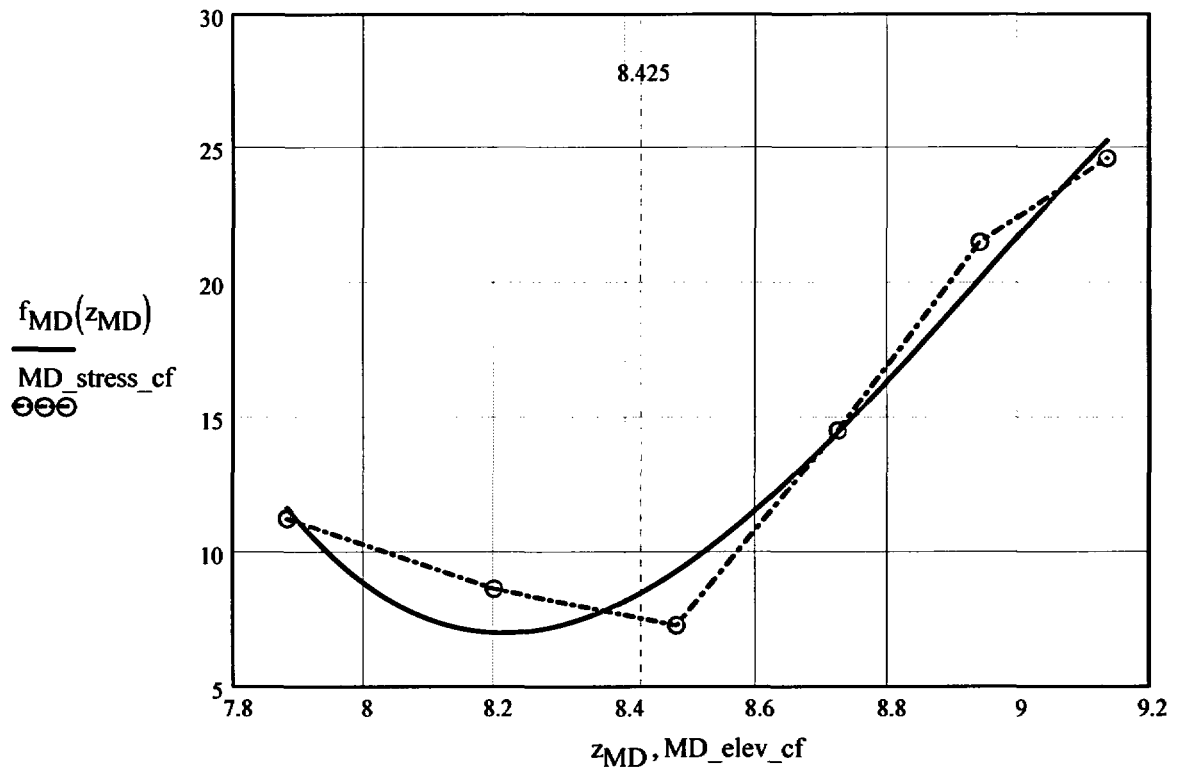

$f_{MD}(8.425) = 8.51122$

Regression for 75% throughwall stresses:

$$TQ\_elev\_cf := \begin{pmatrix} 7.883 \\ 8.199 \\ 8.478 \\ 8.725 \\ 8.942 \\ 9.135 \end{pmatrix} \qquad TQ\_stress\_cf := \begin{pmatrix} 6.243 \\ 3.277 \\ 0.963 \\ 5.734 \\ 10.551 \\ 11.934 \end{pmatrix}$$

$R_{TQ} := regress(TQ\_elev\_cf, TQ\_stress\_cf, 3)$

$z_{TQ} := 7.883, 7.884 .. 9.135$

$$R_{TQ} = \begin{pmatrix} 3 \\ 3 \\ 3 \\ 9313.45524 \\ -3159.012 \\ 355.56516 \\ -13.2686 \end{pmatrix}$$

$f_{TQ}(z_{TQ}) := \text{interp}(R_{TQ}, TQ\_elev\_cf, TQ\_stress\_cf, z_{TQ})$

$Elev_i =$	$TQ\_stress_i =$
0	10.759
1.235	10.038
2.325	9.525
3.289	9.158
4.141	8.987
4.893	8.964
5.557	9.1
6.144	9.275
6.663	9.428
7.121	9.088
7.526	7.898
7.883	6.243
8.199	3.277
8.478	0.963
8.725	5.734
8.942	10.551
9.135	11.934
9.305	16.947
9.535	27.002
9.651	40.722
9.767	50.638

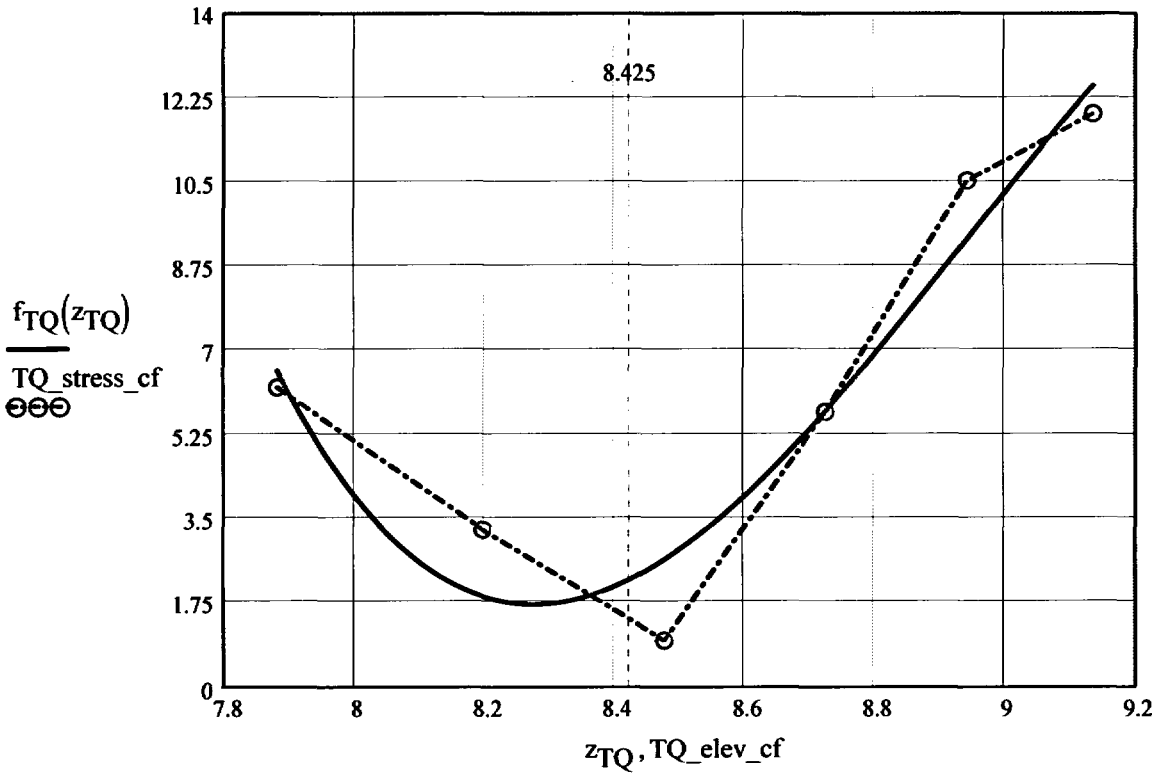

$f_{TQ}(8.425) = 2.2362$

Regression for OD stresses:

$kk := 0..5$

$$OD\_elev\_cf := \begin{pmatrix} 7.883 \\ 8.199 \\ 8.478 \\ 8.725 \\ 8.942 \\ 9.135 \end{pmatrix} \qquad OD\_stress\_cf := \begin{pmatrix} 1.578 \\ -1.652 \\ -4.004 \\ 0.01 \\ 3.714 \\ 5.354 \end{pmatrix}$$

$R_{OD} := regress(OD\_elev\_cf, OD\_stress\_cf, 3)$

$z_{OD} := 7.883, 7.884 .. 9.135$

$$R_{OD} = \begin{pmatrix} 3 \\ 3 \\ 3 \\ 7570.62763 \\ -2550.59622 \\ 284.86761 \\ -10.54291 \end{pmatrix}$$

$f_{OD}(z_{OD}) := interp(R_{OD}, OD\_elev\_cf, OD\_stress\_cf, z_{OD})$

$Elev_i$ =	OD_stress_i =
0	8.539
1.235	7.179
2.325	6.042
3.289	5.143
4.141	4.508
4.893	4.177
5.557	4.15
6.144	4.33
6.663	4.629
7.121	4.422
7.526	3.319
7.883	1.578
8.199	-1.652
8.478	-4.004
8.725	0.01
8.942	3.714
9.135	5.354
9.305	6.333
9.535	41.729
9.651	51.289
9.767	59.979

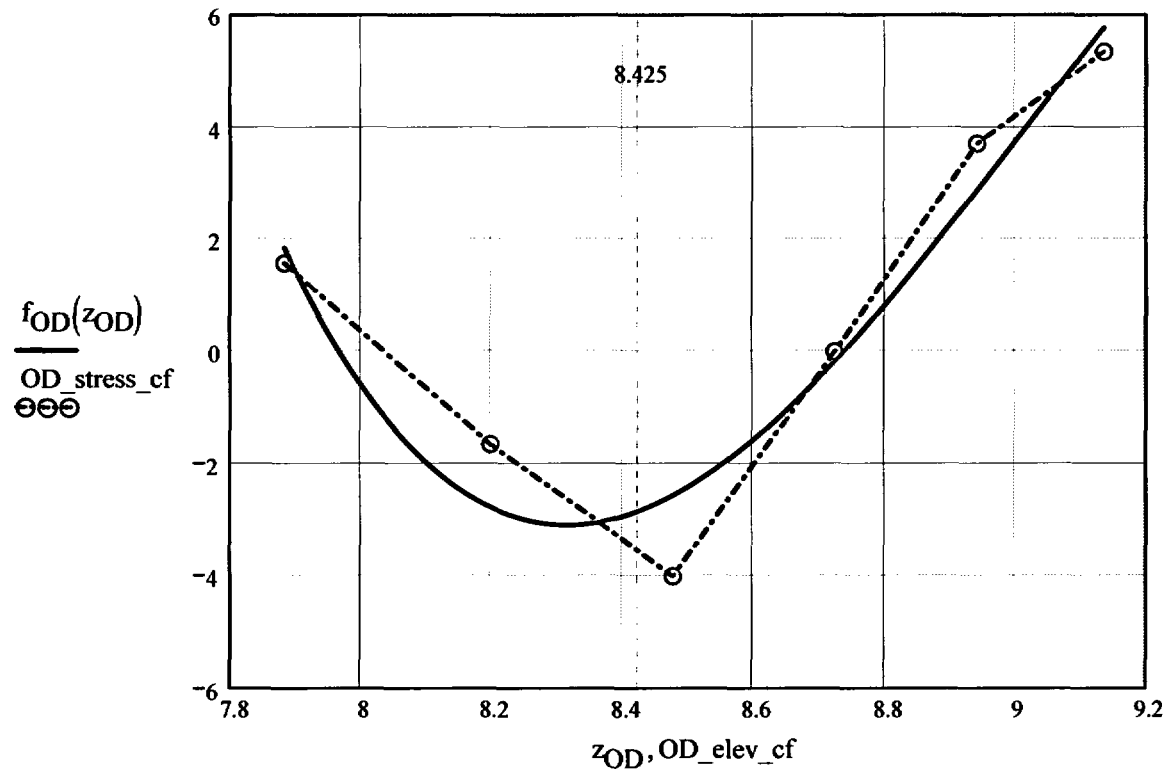

$f_{OD}(8.425) = -2.84902$

Calculation to develop Stress Profiles for Analysis

This analysis for the axial stress regression and the through-wall stress regression is the same as that used for the CEDM Nozzles (in Ref. 6); that is, the axial stresses are fit with a third-order polynomial.

$N := 20$ *Number of locations for stress profiles*

$Loc_0 := FL_{Cntr} - L$

$FL_{Cntr} = 8.425$

$L = 0.4$

$j := 1..N+3$

$$Incr_i := \begin{cases} c_0 & \text{if } i < 4 \\ Inc_{Strs.avg} & \text{otherwise} \end{cases}$$

$Loc_i := Loc_{i-1} + Incr_i$

$SID_i := R_{ID_3} + R_{ID_4} \cdot Loc_i + R_{ID_5} \cdot (Loc_i)^2 + R_{ID_6} \cdot (Loc_i)^3$

$SQT_i := R_{QT_3} + R_{QT_4} \cdot Loc_i + R_{QT_5} \cdot (Loc_i)^2 + R_{QT_6} \cdot (Loc_i)^3$

$SMD_i := R_{MD_3} + R_{MD_4} \cdot Loc_i + R_{MD_5} \cdot (Loc_i)^2 + R_{MD_6} \cdot (Loc_i)^3$

$STQ_i := R_{TQ_3} + R_{TQ_4} \cdot Loc_i + R_{TQ_5} \cdot (Loc_i)^2 + R_{TQ_6} \cdot (Loc_i)^3$

$SOD_i := R_{OD_3} + R_{OD_4} \cdot Loc_i + R_{OD_5} \cdot (Loc_i)^2 + R_{OD_6} \cdot (Loc_i)^3$

$j := 1..N$

$$S_{id_j} := \begin{cases} \dfrac{SID_j + SID_{j+1} + SID_{j+2}}{3} & \text{if } j = 1 \\ \dfrac{S_{id_{j-1}} \cdot (j+1) + SID_{j+2}}{j+2} & \text{otherwise} \end{cases}$$

$$S_{qt_j} := \begin{cases} \dfrac{SQT_j + SQT_{j+1} + SQT_{j+2}}{3} & \text{if } j = 1 \\ \dfrac{S_{qt_{(j-1)}} \cdot (j+1) + SQT_{j+2}}{j+2} & \text{otherwise} \end{cases}$$

$$S_{md_j} := \begin{cases} \dfrac{SMD_j + SMD_{j+1} + SMD_{j+2}}{3} & \text{if } j = 1 \\ \dfrac{S_{md_{j-1}} \cdot (j+1) + SMD_{j+2}}{j+2} & \text{otherwise} \end{cases}$$

$$S_{tq_j} := \begin{cases} \dfrac{STQ_j + STQ_{j+1} + STQ_{j+2}}{3} & \text{if } j = 1 \\ \dfrac{S_{tq_{j-1}} \cdot (j+1) + STQ_{j+2}}{j+2} & \text{otherwise} \end{cases}$$

$$S_{od_j} := \begin{cases} \dfrac{SOD_j + SOD_{j+1} + SOD_{j+2}}{3} & \text{if } j = 1 \\ \dfrac{S_{od_{j-1}} \cdot (j+1) + SOD_{j+2}}{j+2} & \text{otherwise} \end{cases}$$

Through-Wall Stress Distribution for ID Flaws (i.e. ID to OD Stress distribution)

$u_0 := 0.000$ $u_1 := 0.25$ $u_2 := 0.50$ $u_3 := 0.75$ $u_4 := 1.00$

$$Y := \text{stack}(u_0, u_1, u_2, u_3, u_4)$$

$SIG_1 := \text{stack}(S_{id_1}, S_{qt_1}, S_{md_1}, S_{tq_1}, S_{od_1})$ $SIG_2 := \text{stack}(S_{id_2}, S_{qt_2}, S_{md_2}, S_{tq_2}, S_{od_2})$

$SIG_3 := \text{stack}(S_{id_3}, S_{qt_3}, S_{md_3}, S_{tq_3}, S_{od_3})$ $SIG_4 := \text{stack}(S_{id_4}, S_{qt_4}, S_{md_4}, S_{tq_4}, S_{od_4})$

$SIG_5 := \text{stack}(S_{id_5}, S_{qt_5}, S_{md_5}, S_{tq_5}, S_{od_5})$ $SIG_6 := \text{stack}(S_{id_6}, S_{qt_6}, S_{md_6}, S_{tq_6}, S_{od_6})$

$SIG_7 := \text{stack}(S_{id_7}, S_{qt_7}, S_{md_7}, S_{tq_7}, S_{od_7})$ $SIG_8 := \text{stack}(S_{id_8}, S_{qt_8}, S_{md_8}, S_{tq_8}, S_{od_8})$

$SIG_9 := \text{stack}(S_{id_9}, S_{qt_9}, S_{md_9}, S_{tq_9}, S_{od_9})$ $SIG_{10} := \text{stack}(S_{id_{10}}, S_{qt_{10}}, S_{md_{10}}, S_{tq_{10}}, S_{od_{10}})$

$SIG_{11} := \text{stack}(S_{id_{11}}, S_{qt_{11}}, S_{md_{11}}, S_{tq_{11}}, S_{od_{11}})$ $SIG_{12} := \text{stack}(S_{id_{12}}, S_{qt_{12}}, S_{md_{12}}, S_{tq_{12}}, S_{od_{12}})$

$SIG_{13} := \text{stack}(S_{id_{13}}, S_{qt_{13}}, S_{md_{13}}, S_{tq_{13}}, S_{od_{13}})$ $SIG_{14} := \text{stack}(S_{id_{14}}, S_{qt_{14}}, S_{md_{14}}, S_{tq_{14}}, S_{od_{14}})$

$SIG_{15} := \text{stack}(S_{id_{15}}, S_{qt_{15}}, S_{md_{15}}, S_{tq_{15}}, S_{od_{15}})$ $SIG_{16} := \text{stack}(S_{id_{16}}, S_{qt_{16}}, S_{md_{16}}, S_{tq_{16}}, S_{od_{16}})$

$SIG_{17} := \text{stack}(S_{id_{17}}, S_{qt_{17}}, S_{md_{17}}, S_{tq_{17}}, S_{od_{17}})$ $SIG_{18} := \text{stack}(S_{id_{18}}, S_{qt_{18}}, S_{md_{18}}, S_{tq_{18}}, S_{od_{18}})$

$SIG_{19} := \text{stack}(S_{id_{19}}, S_{qt_{19}}, S_{md_{19}}, S_{tq_{19}}, S_{od_{19}})$ $SIG_{20} := \text{stack}(S_{id_{20}}, S_{qt_{20}}, S_{md_{20}}, S_{tq_{20}}, S_{od_{20}})$

Regression of Through-Wall Stress distribution to Obtain Stress Coefficients Using a Third Order Polynomial

$IDRG_1 := regress(Y, SIG_1, 3)$

$IDRG_2 := regress(Y, SIG_2, 3)$

$IDRG_3 := regress(Y, SIG_3, 3)$

$IDRG_4 := regress(Y, SIG_4, 3)$

$IDRG_5 := regress(Y, SIG_5, 3)$

$IDRG_6 := regress(Y, SIG_6, 3)$

$IDRG_7 := regress(Y, SIG_7, 3)$

$IDRG_8 := regress(Y, SIG_8, 3)$

$IDRG_9 := regress(Y, SIG_9, 3)$

$IDRG_{10} := regress(Y, SIG_{10}, 3)$

$IDRG_{11} := regress(Y, SIG_{11}, 3)$

$IDRG_{12} := regress(Y, SIG_{12}, 3)$

$IDRG_{13} := regress(Y, SIG_{13}, 3)$

$IDRG_{14} := regress(Y, SIG_{14}, 3)$

$IDRG_{15} := regress(Y, SIG_{15}, 3)$

$IDRG_{16} := regress(Y, SIG_{16}, 3)$

$IDRG_{17} := regress(Y, SIG_{17}, 3)$

$IDRG_{18} := regress(Y, SIG_{18}, 3)$

$IDRG_{19} := regress(Y, SIG_{19}, 3)$

$IDRG_{20} := regress(Y, SIG_{20}, 3)$

Stress Distribution in the tube. ***Stress influence coefficients obtained from thrid-order polynomial curve fit to the throughwall stress distribution***

Data Files for Flaw Shape Factors from NASA SC04 Model [Ref. 9]

{NO INPUT Required}

Mettu Raju Newman Sivakumar Forman Solution of ID Part throughwall Flaw in Cyinder

Jsb :=

	0	1	2
0	1.000	0.200	0.000
1	1.000	0.200	0.200
2	1.000	0.200	0.500
3	1.000	0.200	0.800
4	1.000	0.200	1.000
5	1.000	0.400	0.000
6	1.000	0.400	0.200
7	1.000	0.400	0.500
8	1.000	0.400	0.800
9	1.000	0.400	1.000
10	1.000	1.000	0.000
11	1.000	1.000	0.200
12	1.000	1.000	0.500
13	1.000	1.000	0.800
14	1.000	1.000	1.000
15	2.000	0.200	0.000
16	2.000	0.200	0.200
17	2.000	0.200	0.500
18	2.000	0.200	0.800
19	2.000	0.200	1.000
20	2.000	0.400	0.000
21	2.000	0.400	0.200
22	2.000	0.400	0.500
23	2.000	0.400	0.800
24	2.000	0.400	1.000
25	2.000	1.000	0.000
26	2.000	1.000	0.200
27	2.000	1.000	0.500
28	2.000	1.000	0.800
29	2.000	1.000	1.000
30	4.000	0.200	0.000
31	4.000	0.200	0.200
32	4.000	0.200	0.500
33	4.000	0.200	0.800
34	4.000	0.200	1.000
35	4.000	0.400	0.000
36	4.000	0.400	0.200

37	4.000	0.400	0.500
38	4.000	0.400	0.800
39	4.000	0.400	1.000
40	4.000	1.000	0.000
41	4.000	1.000	0.200
42	4.000	1.000	0.500
43	4.000	1.000	0.800
44	4.000	1.000	1.000
45	10.000	0.200	0.000
46	10.000	0.200	0.200
47	10.000	0.200	0.500
48	10.000	0.200	0.800
49	10.000	0.200	1.000
50	10.000	0.400	0.000
51	10.000	0.400	0.200
52	10.000	0.400	0.500
53	10.000	0.400	0.800
54	10.000	0.400	1.000
55	10.000	1.000	0.000
56	10.000	1.000	0.200
57	10.000	1.000	0.500
58	10.000	1.000	0.800
59	10.000	1.000	1.000
60	300.000	0.200	0.000
61	300.000	0.200	0.200
62	300.000	0.200	0.500
63	300.000	0.200	0.800
64	300.000	0.200	1.000
65	300.000	0.400	0.000
66	300.000	0.400	0.200
67	300.000	0.400	0.500
68	300.000	0.400	0.800
69	300.000	0.400	1.000
70	300.000	1.000	0.000
71	300.000	1.000	0.200
72	300.000	1.000	0.500
73	300.000	1.000	0.800
74	300.000	1.000	1.000

Sambi :=

	0	1	2	3	4	5	6	7

0	1.076	0.693	0.531	0.434	0.608	0.083	0.023	0.009
1	1.056	0.647	0.495	0.408	0.615	0.085	0.027	0.013
2	1.395	0.767	0.557	0.446	0.871	0.171	0.069	0.038
3	2.53	1.174	0.772	0.58	1.554	0.363	0.155	0.085
4	3.846	1.615	0.995	0.716	2.277	0.544	0.233	0.127
5	1.051	0.689	0.536	0.444	0.74	0.112	0.035	0.015
6	1.011	0.646	0.504	0.421	0.745	0.119	0.041	0.02
7	1.149	0.694	0.529	0.435	0.916	0.181	0.073	0.04
8	1.6	0.889	0.642	0.51	1.334	0.307	0.132	0.073
9	2.087	1.093	0.761	0.589	1.752	0.421	0.183	0.101
10	0.992	0.704	0.534	0.506	1.044	0.169	0.064	0.032
11	0.987	0.701	0.554	0.491	1.08	0.182	0.067	0.034
12	1.01	0.709	0.577	0.493	1.116	0.2	0.078	0.041
13	1.07	0.73	0.623	0.523	1.132	0.218	0.095	0.051
14	1.128	0.75	0.675	0.556	1.131	0.229	0.11	0.06
15	1.049	0.673	0.519	0.427	0.6	0.078	0.021	0.008
16	1.091	0.661	0.502	0.413	0.614	0.083	0.025	0.012
17	1.384	0.764	0.556	0.446	0.817	0.15	0.058	0.031
18	2.059	1.033	0.708	0.545	1.3	0.291	0.123	0.067
19	2.739	1.301	0.858	0.643	1.783	0.421	0.18	0.099
20	1.075	0.674	0.527	0.436	0.73	0.072	0.044	0.021
21	1.045	0.659	0.511	0.425	0.76	0.122	0.043	0.021
22	1.16	0.71	0.536	0.441	0.919	0.197	0.064	0.034
23	1.51	0.854	0.623	0.498	1.231	0.271	0.114	0.062
24	1.876	0.995	0.71	0.555	1.519	0.317	0.161	0.089
25	1.037	0.732	0.594	0.505	1.132	0.192	0.07	0.035
26	1.003	0.707	0.577	0.493	1.113	0.19	0.071	0.036
27	1.023	0.714	0.58	0.495	1.155	0.207	0.08	0.042
28	1.129	0.774	0.619	0.521	1.286	0.247	0.098	0.052
29	1.242	0.84	0.661	0.549	1.416	0.285	0.115	0.061
30	1.003	0.649	0.511	0.43	0.577	0.07	0.015	0.005
31	1.097	0.666	0.511	0.426	0.606	0.079	0.023	0.01
32	1.405	0.776	0.567	0.46	0.797	0.141	0.054	0.028
33	1.959	0.996	0.692	0.542	1.201	0.262	0.108	0.059
34	2.461	1.197	0.808	0.619	1.586	0.37	0.154	0.085
35	1.024	0.668	0.528	0.451	0.737	0.11	0.033	0.015
36	1.057	0.666	0.52	0.439	0.77	0.123	0.042	0.021
37	1.193	0.715	0.545	0.454	0.924	0.174	0.068	0.036
38	1.443	0.828	0.614	0.509	1.219	0.263	0.109	0.059
39	1.665	0.934	0.681	0.565	1.487	0.339	0.143	0.078
40	1.005	0.72	0.597	0.518	1.119	0.188	0.068	0.034
41	1.009	0.713	0.588	0.511	1.128	0.194	0.072	0.037
42	1.041	0.726	0.594	0.515	1.191	0.214	0.082	0.043

43	1.105	0.768	0.623	0.536	1.316	0.248	0.097	0.05
44	1.162	0.81	0.653	0.558	1.428	0.277	0.109	0.055
45	0.973	0.635	0.499	0.446	0.579	0.07	0.016	0.005
46	1.115	0.673	0.514	0.438	0.607	0.079	0.023	0.01
47	1.427	0.783	0.571	0.462	0.791	0.138	0.052	0.027
48	1.872	0.96	0.671	0.529	1.179	0.253	0.104	0.056
49	2.23	1.108	0.757	0.594	1.548	0.356	0.149	0.081
50	0.992	0.656	0.52	0.443	0.733	0.109	0.032	0.014
51	1.072	0.672	0.523	0.441	0.777	0.125	0.043	0.021
52	1.217	0.723	0.549	0.456	0.936	0.176	0.069	0.036
53	1.393	0.806	0.601	0.493	1.219	0.259	0.106	0.056
54	1.521	0.875	0.647	0.528	1.469	0.328	0.135	0.071
55	0.994	0.715	0.59	0.518	1.114	0.187	0.068	0.035
56	1.015	0.715	0.588	0.512	1.14	0.197	0.074	0.038
57	1.05	0.729	0.596	0.515	1.219	0.221	0.085	0.044
58	1.09	0.76	0.618	0.532	1.348	0.255	0.099	0.051
59	1.118	0.788	0.639	0.55	1.456	0.282	0.109	0.056
60	0.936	0.62	0.486	0.405	0.582	0.068	0.015	0.005
61	1.145	0.681	0.514	0.42	0.613	0.081	0.024	0.011
62	1.459	0.79	0.569	0.454	0.79	0.138	0.051	0.026
63	1.774	0.917	0.641	0.501	1.148	0.239	0.096	0.051
64	1.974	1.008	0.696	0.537	1.482	0.328	0.134	0.07
65	0.982	0.651	0.512	0.427	0.721	0.103	0.031	0.013
66	1.095	0.677	0.52	0.431	0.782	0.127	0.045	0.022
67	1.244	0.727	0.546	0.446	0.946	0.18	0.071	0.037
68	1.37	0.791	0.585	0.473	1.201	0.253	0.102	0.054
69	1.438	0.838	0.618	0.496	1.413	0.31	0.126	0.066

$W := Jsb^{\langle 0 \rangle}$ $X := Jsb^{\langle 1 \rangle}$ $Y := Jsb^{\langle 2 \rangle}$

$a_U := Sambi^{\langle 0 \rangle}$ $a_L := Sambi^{\langle 1 \rangle}$ $a_Q := Sambi^{\langle 2 \rangle}$ $a_C := Sambi^{\langle 3 \rangle}$

$c_U := Sambi^{\langle 4 \rangle}$ $c_L := Sambi^{\langle 5 \rangle}$ $c_Q := Sambi^{\langle 6 \rangle}$ $c_C := Sambi^{\langle 7 \rangle}$

$$n := \begin{cases} 3 & \text{if } R_t \le 4.0 \\ 2 & \text{otherwise} \end{cases}$$

"a-Tip" Uniform Term

$$M_{aU} := \text{augment}(W,X,Y) \qquad V_{aU} := a_U \qquad R_{aU} := \text{regress}(M_{aU}, V_{aU}, n)$$

$$f_{aU}(W,X,Y) := \text{interp}\left[R_{aU}, M_{aU}, V_{aU}, \begin{pmatrix} W \\ X \\ Y \end{pmatrix}\right]$$

$f_{aU}(4,.4,.8) = 1.7089$ *Check Calculation*

Linear Term

$$M_{aL} := \text{augment}(W,X,Y) \qquad V_{aL} := a_L \qquad R_{aL} := \text{regress}(M_{aL}, V_{aL}, n)$$

$$f_{aL}(W,X,Y) := \text{interp}\left[R_{aL}, M_{aL}, V_{aL}, \begin{pmatrix} W \\ X \\ Y \end{pmatrix}\right]$$

$f_{aL}(4,.4,.8) = 0.93393$ *Check Calculation*

Quadratic Term

$$M_{aQ} := \text{augment}(W,X,Y) \qquad V_{aQ} := a_Q \qquad R_{aQ} := \text{regress}(M_{aQ}, V_{aQ}, n)$$

$$f_{aQ}(W,X,Y) := \text{interp}\left[R_{aQ}, M_{aQ}, V_{aQ}, \begin{pmatrix} W \\ X \\ Y \end{pmatrix}\right]$$

$f_{aQ}(4,.4,.8) = 0.67668$ *Check Calculation*

Cubic Term

$M_{aC} := \text{augment}(W,X,Y)$ $V_{aC} := a_C$ $R_{aC} := \text{regress}(M_{aC}, V_{aC}, n)$

$$f_{aC}(W,X,Y) := \text{interp}\left[R_{aC}, M_{aC}, V_{aC}, \begin{pmatrix} W \\ X \\ Y \end{pmatrix}\right]$$

$f_{aC}(4,.4,.8) = 0.54151$ *Check Calculation*

"C" Tip Coefficients

Uniform Term

$M_{cU} := \text{augment}(W,X,Y)$ $V_{cU} := c_U$ $R_{cU} := \text{regress}(M_{cU}, V_{cU}, n)$

$$f_{cU}(W,X,Y) := \text{interp}\left[R_{cU}, M_{cU}, V_{cU}, \begin{pmatrix} W \\ X \\ Y \end{pmatrix}\right]$$

$f_{cU}(4,.4,.8) = 1.31015$ *Check Calculation*

Linear Term

$M_{cL} := \text{augment}(W,X,Y)$ $V_{cL} := c_L$ $R_{cL} := \text{regress}(M_{cL}, V_{cL}, n)$

$$f_{cL}(W,X,Y) := \text{interp}\left[R_{cL}, M_{cL}, V_{cL}, \begin{pmatrix} W \\ X \\ Y \end{pmatrix}\right]$$

$f_{cL}(2,.4,.8) = 0.28509$ *Check Calculation*

Quadratic Term

$M_{cQ} := \text{augment}(W,X,Y)$ $V_{cQ} := c_Q$ $R_{cQ} := \text{regress}(M_{cQ}, V_{cQ}, n)$

$$f_{cQ}(W,X,Y) := \text{interp}\left[R_{cQ}, M_{cQ}, V_{cQ}, \begin{pmatrix} W \\ X \\ Y \end{pmatrix}\right]$$

$f_{cQ}(4,.4,.8) = 0.11797$ *Check Calculation*

Cubic Term

$M_{cC} := \text{augment}(W,X,Y)$ $V_{cC} := c_C$ $R_{cC} := \text{regress}(M_{cC}, V_{cC}, n)$

$$f_{cC}(W,X,Y) := \text{interp}\left[R_{cC}, M_{cC}, V_{cC}, \begin{pmatrix} W \\ X \\ Y \end{pmatrix}\right]$$

$f_{cC}(4,.4,.8) = 0.06384$ *Check Calculation*

Calculations : Recursive calculations to estimate flaw growth

Recursive Loop for Calculation of PWSCC Crack Growth

$$
\begin{aligned}
CGR_{sambi} := \;& j \leftarrow 0 \\
& a_0 \leftarrow a_0 \\
& c_0 \leftarrow c_0 \\
& t \leftarrow t2 \\
& NCB_0 \leftarrow C_{blk} \\
& \text{while } j \le I_{lim} \\
& \quad \sigma_0 \leftarrow \begin{cases}
IDRG1_3 & \text{if } c_j \le c_0 \\
IDRG2_3 & \text{if } c_0 < c_j \le c_0 + Inc_{Strs.avg} \\
IDRG3_3 & \text{if } c_0 + Inc_{Strs.avg} < c_j \le c_0 + 2 \cdot Inc_{Strs.avg} \\
IDRG4_3 & \text{if } c_0 + 2 \cdot Inc_{Strs.avg} < c_j \le c_0 + 3 \cdot Inc_{Strs.avg} \\
IDRG5_3 & \text{if } c_0 + 3 \cdot Inc_{Strs.avg} < c_j \le c_0 + 4 \cdot Inc_{Strs.avg} \\
IDRG6_3 & \text{if } c_0 + 4 \cdot Inc_{Strs.avg} < c_j \le c_0 + 5 \cdot Inc_{Strs.avg} \\
IDRG7_3 & \text{if } c_0 + 5 \cdot Inc_{Strs.avg} < c_j \le c_0 + 6 \cdot Inc_{Strs.avg} \\
IDRG8_3 & \text{if } c_0 + 6 \cdot Inc_{Strs.avg} < c_j \le c_0 + 7 \cdot Inc_{Strs.avg} \\
IDRG9_3 & \text{if } c_0 + 7 \cdot Inc_{Strs.avg} < c_j \le c_0 + 8 \cdot Inc_{Strs.avg} \\
IDRG10_3 & \text{if } c_0 + 8 \cdot Inc_{Strs.avg} < c_j \le c_0 + 9 \cdot Inc_{Strs.avg} \\
IDRG11_3 & \text{if } c_0 + 9 \cdot Inc_{Strs.avg} < c_j \le c_0 + 10 \cdot Inc_{Strs.avg} \\
IDRG12_3 & \text{if } c_0 + 10 \cdot Inc_{Strs.avg} < c_j \le c_0 + 11 \cdot Inc_{Strs.avg} \\
IDRG13_3 & \text{if } c_0 + 11 \cdot Inc_{Strs.avg} < c_j \le c_0 + 12 \cdot Inc_{Strs.avg} \\
IDRG14_3 & \text{if } c_0 + 12 \cdot Inc_{Strs.avg} < c_j \le c_0 + 13 \cdot Inc_{Strs.avg} \\
IDRG15_3 & \text{if } c_0 + 13 \cdot Inc_{Strs.avg} < c_j \le c_0 + 14 \cdot Inc_{Strs.avg}
\end{cases}
\end{aligned}
$$

$$IDRG_{16_3} \text{ if } c_0 + 14 \cdot Inc_{Strs.avg} < c_j \le c_0 + 15 \cdot Inc_{Strs.avg}$$

$$IDRG_{17_3} \text{ if } c_0 + 15 \cdot Inc_{Strs.avg} < c_j \le c_0 + 16 \cdot Inc_{Strs.avg}$$

$$IDRG_{18_3} \text{ if } c_0 + 16 \cdot Inc_{Strs.avg} < c_j \le c_0 + 17 \cdot Inc_{Strs.avg}$$

$$IDRG_{19_3} \text{ if } c_0 + 17 \cdot Inc_{Strs.avg} < c_j \le c_0 + 18 \cdot Inc_{Strs.avg}$$

$$IDRG_{20_3} \text{ otherwise}$$

$$\sigma_1 \leftarrow IDRG_{1_4} \text{ if } c_j \le c_0$$

$$IDRG_{2_4} \text{ if } c_0 < c_j \le c_0 + Inc_{Strs.avg}$$

$$IDRG_{3_4} \text{ if } c_0 + Inc_{Strs.avg} < c_j \le c_0 + 2 \cdot Inc_{Strs.avg}$$

$$IDRG_{4_4} \text{ if } c_0 + 2 \cdot Inc_{Strs.avg} < c_j \le c_0 + 3 \cdot Inc_{Strs.avg}$$

$$IDRG_{5_4} \text{ if } c_0 + 3 \cdot Inc_{Strs.avg} < c_j \le c_0 + 4 \cdot Inc_{Strs.avg}$$

$$IDRG_{6_4} \text{ if } c_0 + 4 \cdot Inc_{Strs.avg} < c_j \le c_0 + 5 \cdot Inc_{Strs.avg}$$

$$IDRG_{7_4} \text{ if } c_0 + 5 \cdot Inc_{Strs.avg} < c_j \le c_0 + 6 \cdot Inc_{Strs.avg}$$

$$IDRG_{8_4} \text{ if } c_0 + 6 \cdot Inc_{Strs.avg} < c_j \le c_0 + 7 \cdot Inc_{Strs.avg}$$

$$IDRG_{9_4} \text{ if } c_0 + 7 \cdot Inc_{Strs.avg} < c_j \le c_0 + 8 \cdot Inc_{Strs.avg}$$

$$IDRG_{10_4} \text{ if } c_0 + 8 \cdot Inc_{Strs.avg} < c_j \le c_0 + 9 \cdot Inc_{Strs.avg}$$

$$IDRG_{11_4} \text{ if } c_0 + 9 \cdot Inc_{Strs.avg} < c_j \le c_0 + 10 \cdot Inc_{Strs.avg}$$

$$IDRG_{12_4} \text{ if } c_0 + 10 \cdot Inc_{Strs.avg} < c_j \le c_0 + 11 \cdot Inc_{Strs.avg}$$

$$IDRG_{13_4} \text{ if } c_0 + 11 \cdot Inc_{Strs.avg} < c_j \le c_0 + 12 \cdot Inc_{Strs.avg}$$

$$IDRG_{14_4} \text{ if } c_0 + 12 \cdot Inc_{Strs.avg} < c_j \le c_0 + 13 \cdot Inc_{Strs.avg}$$

$$IDRG_{15_4} \text{ if } c_0 + 13 \cdot Inc_{Strs.avg} < c_j \le c_0 + 14 \cdot Inc_{Strs.avg}$$

$$IDRG_{16_4} \text{ if } c_0 + 14 \cdot Inc_{Strs.avg} < c_j \le c_0 + 15 \cdot Inc_{Strs.avg}$$

$$IDRG_{17} \text{ if } c_0 + 15 \cdot Inc_{Strs.avg} < c_j \le c_0 + 16 \cdot Inc_{Strs.avg}$$

$IDRG_{17_4}$ if $c_0 + 15 \cdot Inc_{Strs.avg} < c_j \le c_0 + 16 \cdot Inc_{Strs.avg}$

$IDRG_{18_4}$ if $c_0 + 16 \cdot Inc_{Strs.avg} < c_j \le c_0 + 17 \cdot Inc_{Strs.avg}$

$IDRG_{19_4}$ if $c_0 + 17 \cdot Inc_{Strs.avg} < c_j \le c_0 + 18 \cdot Inc_{Strs.avg}$

$IDRG_{20_4}$ otherwise

$\sigma_2 \leftarrow$

$IDRG_{1_5}$ if $c_j \le c_0$

$IDRG_{2_5}$ if $c_0 < c_j \le c_0 + Inc_{Strs.avg}$

$IDRG_{3_5}$ if $c_0 + Inc_{Strs.avg} < c_j \le c_0 + 2 \cdot Inc_{Strs.avg}$

$IDRG_{4_5}$ if $c_0 + 2 \cdot Inc_{Strs.avg} < c_j \le c_0 + 3 \cdot Inc_{Strs.avg}$

$IDRG_{5_5}$ if $c_0 + 3 \cdot Inc_{Strs.avg} < c_j \le c_0 + 4 \cdot Inc_{Strs.avg}$

$IDRG_{6_5}$ if $c_0 + 4 \cdot Inc_{Strs.avg} < c_j \le c_0 + 5 \cdot Inc_{Strs.avg}$

$IDRG_{7_5}$ if $c_0 + 5 \cdot Inc_{Strs.avg} < c_j \le c_0 + 6 \cdot Inc_{Strs.avg}$

$IDRG_{8_5}$ if $c_0 + 6 \cdot Inc_{Strs.avg} < c_j \le c_0 + 7 \cdot Inc_{Strs.avg}$

$IDRG_{9_5}$ if $c_0 + 7 \cdot Inc_{Strs.avg} < c_j \le c_0 + 8 \cdot Inc_{Strs.avg}$

$IDRG_{10_5}$ if $c_0 + 8 \cdot Inc_{Strs.avg} < c_j \le c_0 + 9 \cdot Inc_{Strs.avg}$

$IDRG_{11_5}$ if $c_0 + 9 \cdot Inc_{Strs.avg} < c_j \le c_0 + 10 \cdot Inc_{Strs.avg}$

$IDRG_{12_5}$ if $c_0 + 10 \cdot Inc_{Strs.avg} < c_j \le c_0 + 11 \cdot Inc_{Strs.avg}$

$IDRG_{13_5}$ if $c_0 + 11 \cdot Inc_{Strs.avg} < c_j \le c_0 + 12 \cdot Inc_{Strs.avg}$

$IDRG_{14_5}$ if $c_0 + 12 \cdot Inc_{Strs.avg} < c_j \le c_0 + 13 \cdot Inc_{Strs.avg}$

$IDRG_{15_5}$ if $c_0 + 13 \cdot Inc_{Strs.avg} < c_j \le c_0 + 14 \cdot Inc_{Strs.avg}$

$IDRG_{16_5}$ if $c_0 + 14 \cdot Inc_{Strs.avg} < c_j \le c_0 + 15 \cdot Inc_{Strs.avg}$

$IDRG_{17_5}$ if $c_0 + 15 \cdot Inc_{Strs.avg} < c_j \le c_0 + 16 \cdot Inc_{Strs.avg}$

$IDRG_{18_5}$ if $c_0 + 16 \cdot Inc_{Strs.avg} < c_j \le c_0 + 17 \cdot Inc_{Strs.avg}$

$$\sigma_3 \leftarrow \begin{cases} IDRG_{19_5} & \text{if } c_0 + 17 \cdot Inc_{Strs.avg} < c_j \le c_0 + 18 \cdot Inc_{Strs.avg} \\ IDRG_{20_5} & \text{otherwise} \end{cases}$$

$$\sigma_3 \leftarrow \begin{cases} IDRG_{1_6} & \text{if } c_j \le c_0 \\ IDRG_{2_6} & \text{if } c_0 < c_j \le c_0 + Inc_{Strs.avg} \\ IDRG_{3_6} & \text{if } c_0 + Inc_{Strs.avg} < c_j \le c_0 + 2 \cdot Inc_{Strs.avg} \\ IDRG_{4_6} & \text{if } c_0 + 2 \cdot Inc_{Strs.avg} < c_j \le c_0 + 3 \cdot Inc_{Strs.avg} \\ IDRG_{5_6} & \text{if } c_0 + 3 \cdot Inc_{Strs.avg} < c_j \le c_0 + 4 \cdot Inc_{Strs.avg} \\ IDRG_{6_6} & \text{if } c_0 + 4 \cdot Inc_{Strs.avg} < c_j \le c_0 + 5 \cdot Inc_{Strs.avg} \\ IDRG_{7_6} & \text{if } c_0 + 5 \cdot Inc_{Strs.avg} < c_j \le c_0 + 6 \cdot Inc_{Strs.avg} \\ IDRG_{8_6} & \text{if } c_0 + 6 \cdot Inc_{Strs.avg} < c_j \le c_0 + 7 \cdot Inc_{Strs.avg} \\ IDRG_{9_6} & \text{if } c_0 + 7 \cdot Inc_{Strs.avg} < c_j \le c_0 + 8 \cdot Inc_{Strs.avg} \\ IDRG_{10_6} & \text{if } c_0 + 8 \cdot Inc_{Strs.avg} < c_j \le c_0 + 9 \cdot Inc_{Strs.avg} \\ IDRG_{11_6} & \text{if } c_0 + 9 \cdot Inc_{Strs.avg} < c_j \le c_0 + 10 \cdot Inc_{Strs.avg} \\ IDRG_{12_6} & \text{if } c_0 + 10 \cdot Inc_{Strs.avg} < c_j \le c_0 + 11 \cdot Inc_{Strs.avg} \\ IDRG_{13_6} & \text{if } c_0 + 11 \cdot Inc_{Strs.avg} < c_j \le c_0 + 12 \cdot Inc_{Strs.avg} \\ IDRG_{14_6} & \text{if } c_0 + 12 \cdot Inc_{Strs.avg} < c_j \le c_0 + 13 \cdot Inc_{Strs.avg} \\ IDRG_{15_6} & \text{if } c_0 + 13 \cdot Inc_{Strs.avg} < c_j \le c_0 + 14 \cdot Inc_{Strs.avg} \\ IDRG_{16_6} & \text{if } c_0 + 14 \cdot Inc_{Strs.avg} < c_j \le c_0 + 15 \cdot Inc_{Strs.avg} \\ IDRG_{17_6} & \text{if } c_0 + 15 \cdot Inc_{Strs.avg} < c_j \le c_0 + 16 \cdot Inc_{Strs.avg} \\ IDRG_{18_6} & \text{if } c_0 + 16 \cdot Inc_{Strs.avg} < c_j \le c_0 + 17 \cdot Inc_{Strs.avg} \\ IDRG_{19_6} & \text{if } c_0 + 17 \cdot Inc_{Strs.avg} < c_j \le c_0 + 18 \cdot Inc_{Strs.avg} \end{cases}$$

$$\left| \begin{array}{l} \left| IDRG_{20_6} \text{ otherwise} \right. \\ \xi_0 \leftarrow \sigma_0 \\ \xi_1 \leftarrow \sigma_0 + \sigma_1 \cdot \left(\frac{0.25 \cdot a_j}{t}\right) + \sigma_2 \cdot \left(\frac{0.25 \cdot a_j}{t}\right)^2 + \sigma_3 \cdot \left(\frac{0.25 \cdot a_j}{t}\right)^3 \\ \xi_2 \leftarrow \sigma_0 + \sigma_1 \cdot \left(\frac{0.5 \cdot a_j}{t}\right) + \sigma_2 \cdot \left(\frac{0.5 \cdot a_j}{t}\right)^2 + \sigma_3 \cdot \left(\frac{0.5 \cdot a_j}{t}\right)^3 \\ \xi_3 \leftarrow \sigma_0 + \sigma_1 \cdot \left(\frac{0.75 \cdot a_j}{t}\right) + \sigma_2 \cdot \left(\frac{0.75 \cdot a_j}{t}\right)^2 + \sigma_3 \cdot \left(\frac{0.75 \cdot a_j}{t}\right)^3 \\ \xi_4 \leftarrow \sigma_0 + \sigma_1 \cdot \left(\frac{1.0 \cdot a_j}{t}\right) + \sigma_2 \cdot \left(\frac{1.0 \cdot a_j}{t}\right)^2 + \sigma_3 \cdot \left(\frac{1.0 \cdot a_j}{t}\right)^3 \\ x_0 \leftarrow 0.0 \\ x_1 \leftarrow 0.25 \\ x_2 \leftarrow 0.5 \\ x_3 \leftarrow 0.75 \\ x_4 \leftarrow 1.0 \\ X \leftarrow \text{stack}(x_0, x_1, x_2, x_3, x_4) \\ ST \leftarrow \text{stack}(\xi_0, \xi_1, \xi_2, \xi_3, \xi_4) \\ RG \leftarrow \text{regress}(X, ST, 3) \\ \sigma_{00} \leftarrow RG_3 + P_{Int} \\ \sigma_{10} \leftarrow RG_4 \\ \sigma_{20} \leftarrow RG_5 \\ \sigma_{30} \leftarrow RG_6 \\ AR_j \leftarrow \frac{a_j}{c_j} \\ AT_j \leftarrow \frac{a_j}{t} \\ G_{au_i} \leftarrow f_{aU}(R_t, AR_j, AT_j) \end{array} \right.$$

$$G_{al_j} \leftarrow f_{aL}(R_t, AR_j, AT_j)$$

$$G_{aq_j} \leftarrow f_{aQ}(R_t, AR_j, AT_j)$$

$$G_{ac_j} \leftarrow f_{aC}(R_t, AR_j, AT_j)$$

$$G_{cu_j} \leftarrow f_{cU}(R_t, AR_j, AT_j)$$

$$G_{cl_j} \leftarrow f_{cL}(R_t, AR_j, AT_j)$$

$$G_{cq_j} \leftarrow f_{cQ}(R_t, AR_j, AT_j)$$

$$G_{cc_j} \leftarrow f_{cC}(R_t, AR_j, AT_j)$$

$$Q_j \leftarrow \begin{cases} 1 + 1.464 \cdot \left(\frac{a_j}{c_j}\right)^{1.65} & \text{if } c_j \geq a_j \\ 1 + 1.464 \cdot \left(\frac{c_j}{a_j}\right)^{1.65} & \text{otherwise} \end{cases}$$

$$K_{a_j} \leftarrow \left(\frac{\pi \cdot a_j}{Q_j}\right)^{0.5} \cdot \left(\sigma_{00} \cdot G_{au_j} + \sigma_{10} \cdot G_{al_j} + \sigma_{20} \cdot G_{aq_j} + \sigma_{30} \cdot G_{ac_j}\right)$$

$$K_{c_j} \leftarrow \left(\frac{\pi \cdot c_j}{Q_j}\right)^{0.5} \cdot \left(\sigma_{00} \cdot G_{cu_j} + \sigma_{10} \cdot G_{cl_j} + \sigma_{20} \cdot G_{cq_j} + \sigma_{30} \cdot G_{cc_j}\right)$$

$$K_{\alpha_j} \leftarrow K_{a_j} \cdot 1.099$$

$$K_{\gamma_j} \leftarrow K_{c_j} \cdot 1.099$$

$$K_{\alpha_j} \leftarrow \begin{cases} 9.0 & \text{if } K_{\alpha_j} \leq 9.0 \\ K_{\alpha_j} & \text{otherwise} \end{cases}$$

$$K_{\gamma_j} \leftarrow \begin{cases} 9.0 & \text{if } K_{\gamma_j} \leq 9.0 \\ K_{\gamma_j} & \text{otherwise} \end{cases}$$

$$D_{a_j} \leftarrow C_0 \cdot \left(K_{\alpha_j} - 9.0\right)^{1.16}$$

$$D_{ag_j} \leftarrow \begin{cases} D_{a_j} \cdot CF_{inhr} \cdot C_{blk} & \text{if } K_{\alpha_j} < 80.0 \end{cases}$$

$$D_{ag_j} \leftarrow \begin{cases} D_{c_j} \cdot CF_{inhr} \cdot C_{blk} & \text{if } K_{\gamma_j} < 80.0 \\ 4 \cdot 10^{-10} \cdot CF_{inhr} \cdot C_{blk} & \text{otherwise} \end{cases}$$

$$D_{c_j} \leftarrow C_0 \cdot \left(K_{\gamma_j} - 9.0\right)^{1.16}$$

$$D_{cg_j} \leftarrow \begin{cases} D_{c_j} \cdot CF_{inhr} \cdot C_{blk} & \text{if } K_{\gamma_j} < 80.0 \\ 4 \cdot 10^{-10} \cdot CF_{inhr} \cdot C_{blk} & \text{otherwise} \end{cases}$$

$output_{(j,0)} \leftarrow j$

$output_{(j,1)} \leftarrow a_j$

$output_{(j,2)} \leftarrow c_j - c_0$

$output_{(j,3)} \leftarrow D_{ag_j}$

$output_{(j,4)} \leftarrow D_{cg_j}$

$output_{(j,5)} \leftarrow K_{a_j}$

$output_{(j,6)} \leftarrow K_{c_j}$

$output_{(j,7)} \leftarrow \frac{NCB_j}{365 \cdot 24}$

$output_{(j,8)} \leftarrow G_{au_j}$

$output_{(j,9)} \leftarrow G_{al_j}$

$output_{(j,10)} \leftarrow G_{aq_j}$

$output_{(j,11)} \leftarrow G_{ac_j}$

$output_{(j,12)} \leftarrow G_{cu_j}$

$output_{(j,13)} \leftarrow G_{cl_j}$

$output_{(j,14)} \leftarrow G_{cq_j}$

$output_{(j,15)} \leftarrow G_{cc_j}$

$j \leftarrow j + 1$

$a_j \leftarrow a_{j-1} + D_{ag_{i-1}}$

$$c_j \leftarrow c_{j-1} + D_{cg_{j-1}}$$

$$a_j \leftarrow \begin{cases} t & \text{if } a_j \geq t \\ a_j & \text{otherwise} \end{cases}$$

$$NCB_j \leftarrow NCB_{j-1} + C_{blk}$$

output

$k := 0 .. I_{lim}$

The curve below shows the flaw growth through-wall and the operating time (in years) it takes for the initial flaw in the blind zone to go through-wall.

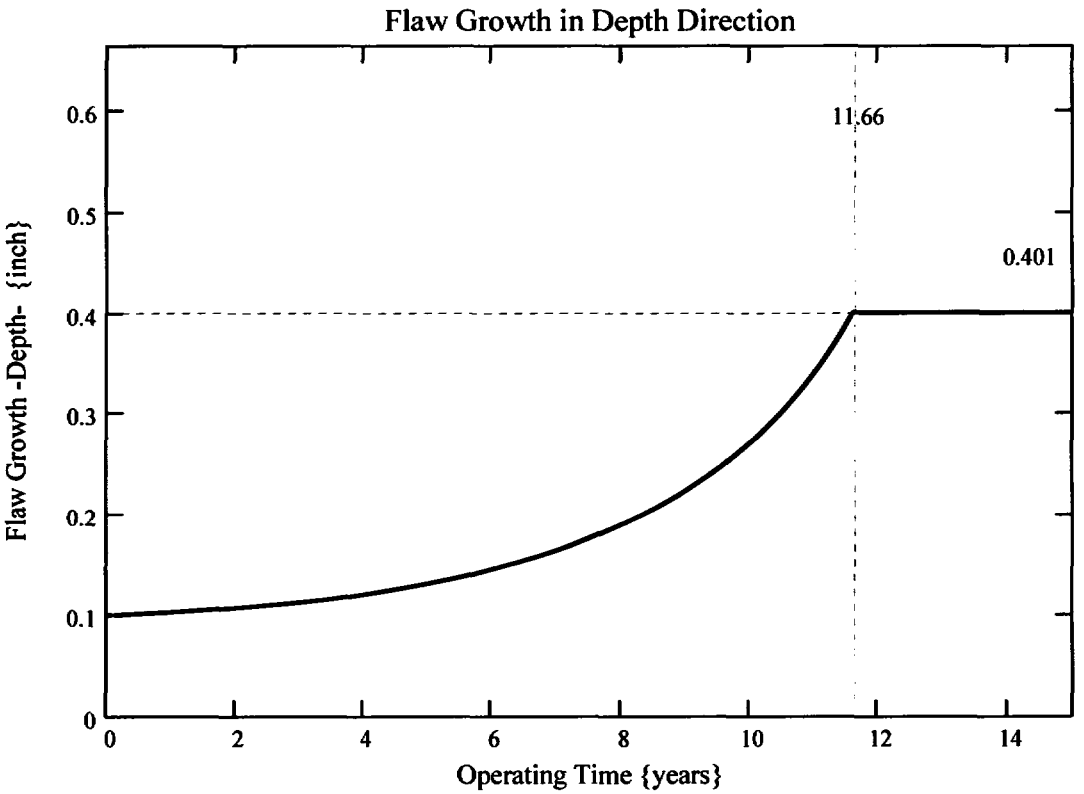

The propagation length for the ICI nozzles is defined as the length for which the initial flaw in the blind zone would extend out of the blind zone and grow to a detectable flaw. Reference 12 gives the minimum detectable flaw size of 4 mm (0.16) in length; thus, 0.16 inch was considered as this minimum detectable flaw length. This dimension is added to the end of the blind zone.

$$\text{Prop\_Length} := \frac{\text{BZ\_length}}{2} - c_0 + 0.16$$

$$\text{Prop\_Length} = 0.4$$

This implies that a flaw initially within the blindzone must grow 0.3 inch to become detectable via UT.

The curve below shows the flaw growth along the length of the ICI nozzle and the operating time (in years) it takes to reach the Prop_Length value defined above.

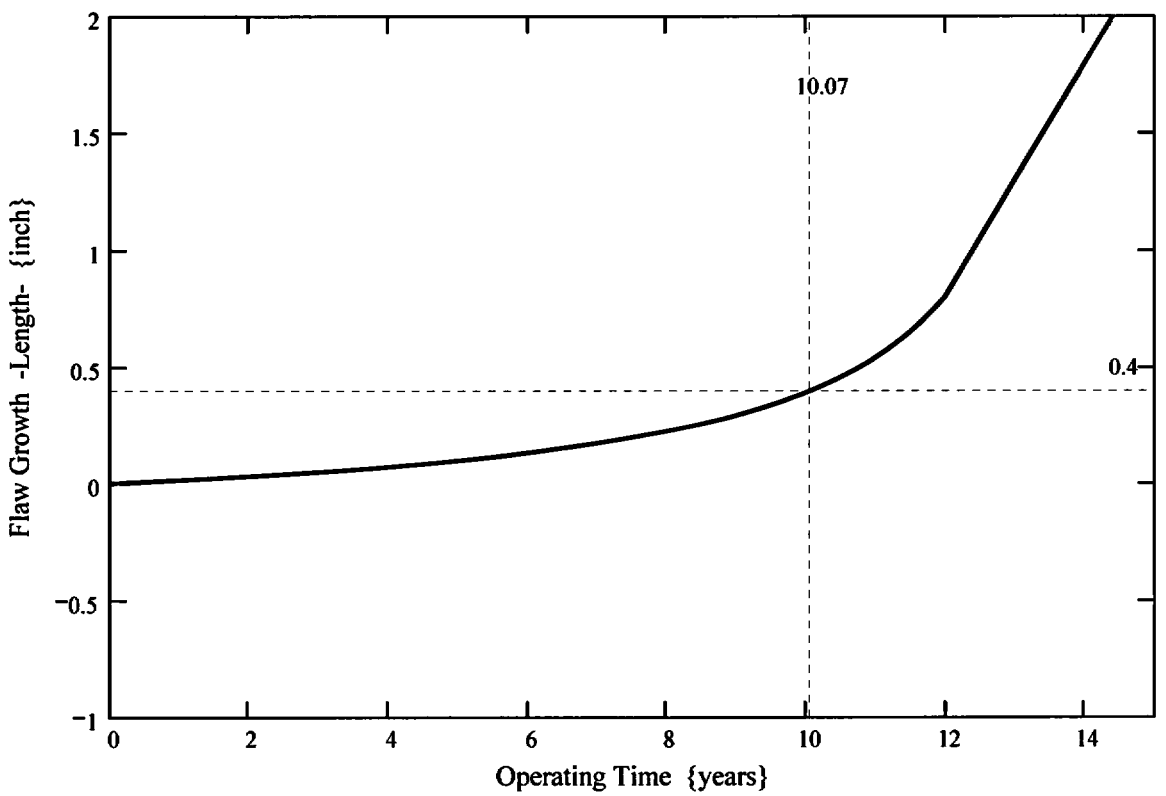

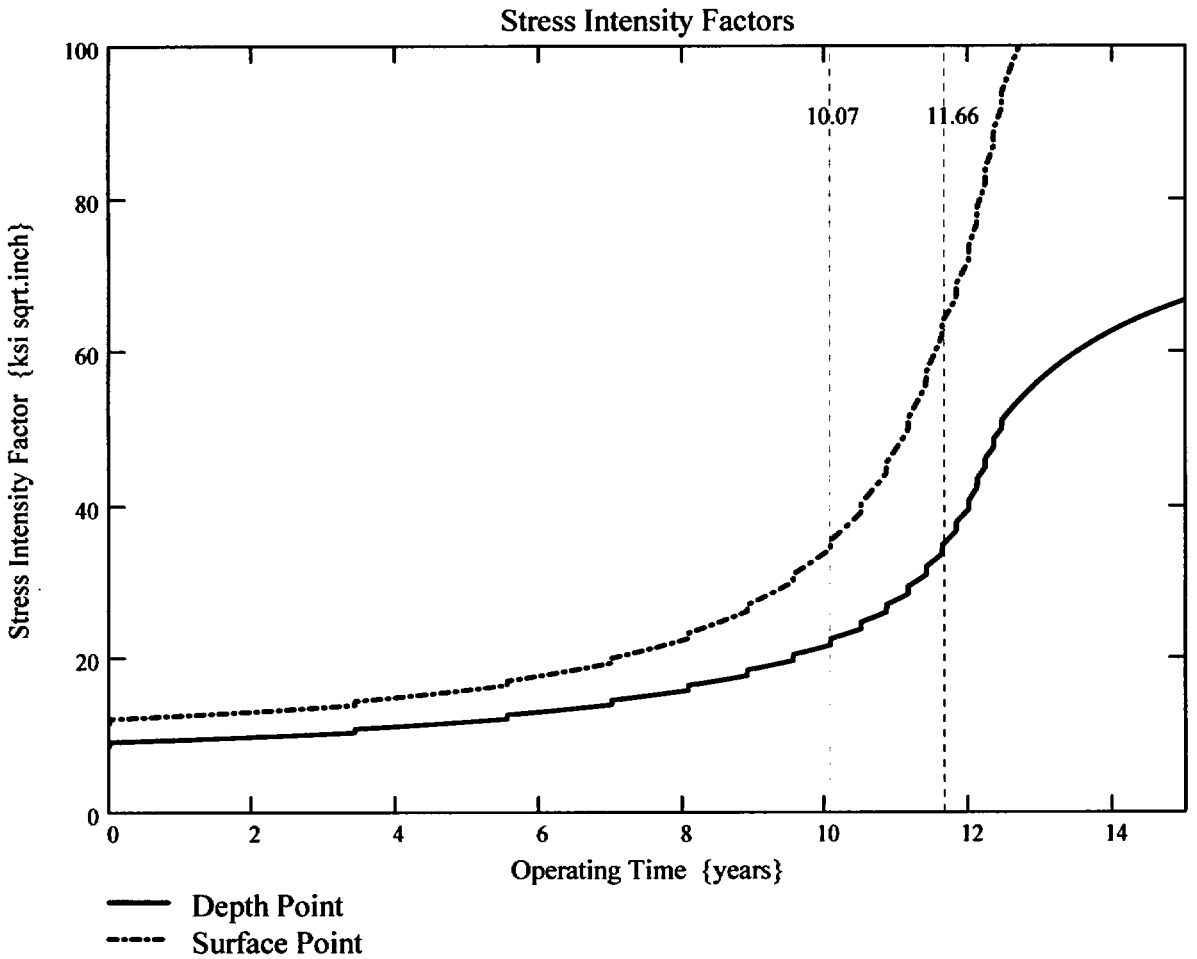
Stress Intensity Factors
100
80
60
40
20
0
Stress Intensity Factor {ksi sqrt.inch}
10.07
11.66
0
2
4
6
8
10
12
14
Operating Time {years}
Depth Point
Surface Point

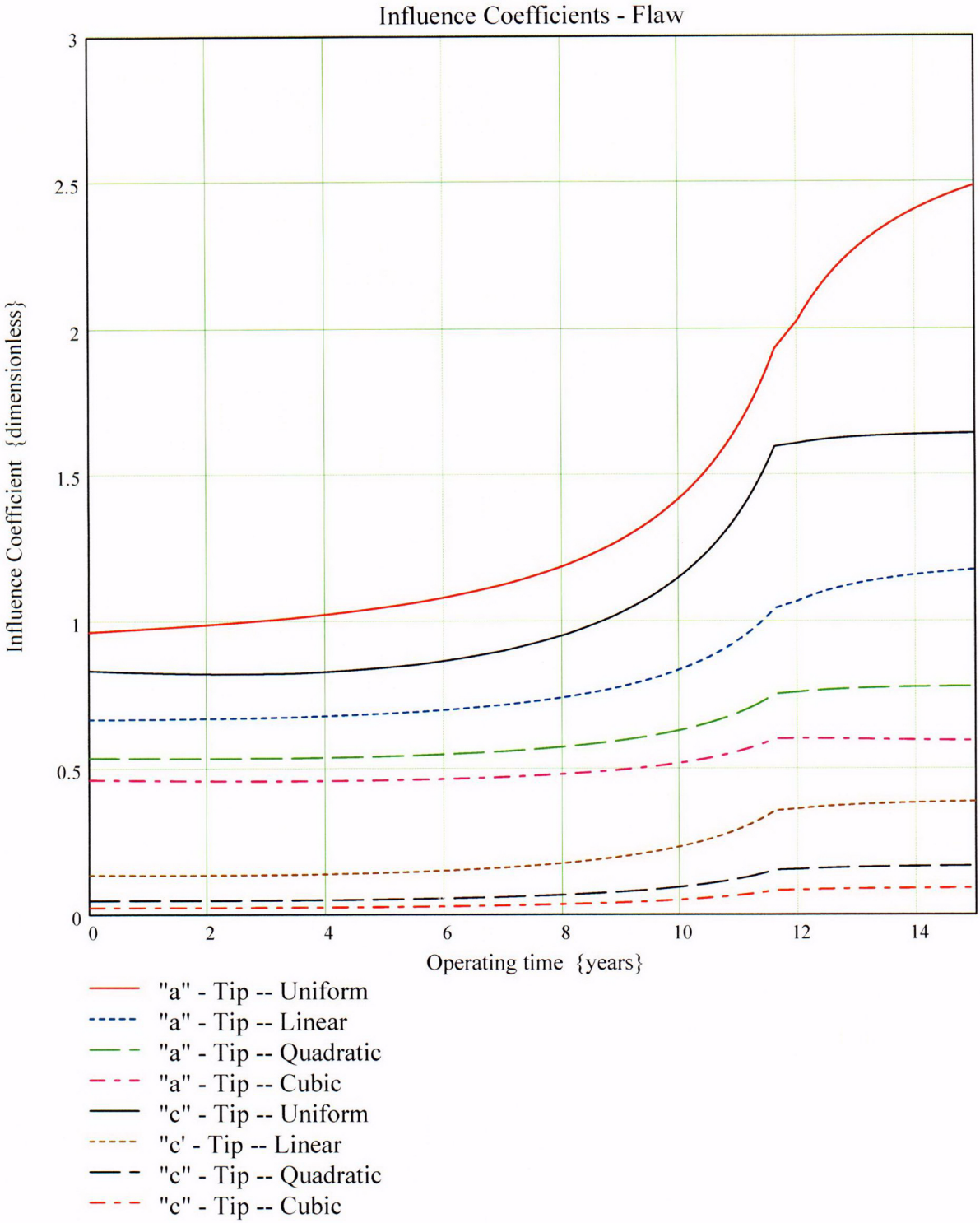
Influence Coefficients - Flaw
Influence Coefficient {dimensionless}
3
2.5
2
1.5
1
0.5
0
0
2
4
6
8
10
12
14
Operating time {years}
"a" - Tip -- Uniform
"a" - Tip -- Linear
"a" - Tip -- Quadratic
"a" - Tip -- Cubic
"c" - Tip -- Uniform
"c' - Tip -- Linear
"c" - Tip -- Quadratic
"c" - Tip -- Cubic

Waterford Steam Electric Station Unit 3

Primary Water Stress Corrosion Crack Growth Analysis for an ICI ID Surface Flaw Uphill (180°), in the Blind Zone above the Top of the J-Groove Weld
Developed by Central Engineering Programs, Entergy Operations Inc.

Flaw Case 4: Flaw Spanning the Full Length of the Blind Zone (0.88 Inch) with a 6-to-1 Aspect Ratio

Calculation Basis: MRP 75 th Percentile and Flaw Face Pressurized

Mean Radius -to- Thickness Ratio:- "R_m/t" – between 1.0 and 300.0

Note : ***The Metric form of the equation from EPRI MRP was used 55-Rev. 1*** *. A correction factor is applied in the determination of the crack extension to convert the units of meters per second to the value in inches per hour .*

ID Surface Flaw

User Input:

The Dominion Engineering Inc. (DEI) finite element model nodal elevations and hoop stresses for the uphill side (180° azimuth) of the ICI nozzle are brought into the Mathcad worksheet from data supplied in Reference 8d. The data are composed of the nodal elevations (in inches), along with the ID, 25% through-wall (tw), 50% tw, 75% tw, and OD hoop stresses, beginning two nodal lines below (nodal line 81101) the top of the weld (nodal line 81301) and extending to the top of the nozzle in the FEA model (nodal line 83301), which is at the point where the nozzle intersects the reactor vessel head.

The DEI FEA data has elevation referenced from the bottom of the ICI nozzle. The elevations of the node points in the DEI FEA model, beginning below the top of the weld, at nodal line 81101, and the corresponding hoop stresses are as follows:

Note the following terms used throughout this evaluation:

ID-inside diameter of ICI nozzle
QT-25% tw position
MD-50% tw, or mid-wall, position
TQ-75% tw position
OD-outside diameter of ICI nozzle

$i := 0..20$

Node_line :=	Elev_fea :=	ID_stress_fea :=	QT_stress_fea :=
81101	3.973	43.347	41.640
81201	4.089	42.799	39.703
81301	4.205	39.763	38.158
81401	4.435	37.068	33.351
81501	4.605	34.079	32.268
81601	4.798	29.820	28.465
81701	5.015	23.668	21.543
81801	5.262	18.722	14.133
81901	5.541	18.383	15.071
82001	5.857	18.876	17.269
82101	6.214	19.527	18.517
82201	6.619	20.331	19.550
82301	7.077	20.976	20.149
82401	7.596	21.408	20.378
82501	8.183	21.667	20.400
82601	8.847	21.792	20.133
82701	9.599	21.742	19.395
82801	10.451	21.550	18.466
82901	11.415	21.213	17.311
83001	12.505	19.876	16.176
83101	13.740	18.311	15.380
83201	15.138	16.442	14.525
83301	18.057	12.330	12.146

$$MD\_stress\_fea := \begin{pmatrix} 43.666 \\ 41.445 \\ 34.368 \\ 25.957 \\ 24.632 \\ 21.515 \\ 14.530 \\ 7.280 \\ 8.650 \\ 11.236 \\ 12.761 \\ 13.998 \\ 14.467 \\ 14.437 \\ 14.263 \\ 13.976 \\ 13.664 \\ 13.362 \\ 13.126 \\ 13.009 \\ 12.983 \\ 12.960 \\ 12.033 \end{pmatrix} \quad TQ\_stress\_fea := \begin{pmatrix} 50.638 \\ 40.722 \\ 27.002 \\ 16.947 \\ 11.934 \\ 10.551 \\ 5.734 \\ 0.963 \\ 3.277 \\ 6.243 \\ 7.898 \\ 9.088 \\ 9.428 \\ 9.275 \\ 9.100 \\ 8.964 \\ 8.987 \\ 9.158 \\ 9.525 \\ 10.038 \\ 10.759 \\ 11.508 \\ 11.987 \end{pmatrix} \quad OD\_stress\_fea := \begin{pmatrix} 59.979 \\ 51.289 \\ 41.729 \\ 6.333 \\ 5.354 \\ 3.714 \\ 0.010 \\ -4.004 \\ -1.652 \\ 1.578 \\ 3.319 \\ 4.422 \\ 4.629 \\ 4.330 \\ 4.150 \\ 4.177 \\ 4.508 \\ 5.143 \\ 6.042 \\ 7.179 \\ 8.539 \\ 10.066 \\ 11.973 \end{pmatrix}$$

Blind Zone and Counterbore Reference dimensions:

From design drawings (Ref. 3) and the design details of Attachment 1, the following dimensions are used to locate the counterbore bottom and blind zone locations (bottom, top, and middle) as referenced from the nodal coordinates of the DEI FEA model.

$Actual\_cbore\_bottom\_elev := Elev\_fea_2 + 1.01$

$Actual\_cbore\_bottom\_elev = 5.215$

Primary Assumptions on blind zone dimensions:

$topweld\_to\_bottom\_BZ := 0.67$ This is the distance from top of the J-weld, on the uphill side, to the bottom of the blind zone. Without UT data to verify this dimension, this value be iterated to determine the MINIMUM height above the top of the weld for which the blind zone can begin and yield an acceptable fracture mechanics solution.

$BZ\_length = 0.8$ This value is based on the longest blind zone seen in the ANO-2 ICI nozzles. Both Waterford-3 and ANO-2 ICI nozzles have similar geometries above the top of the weld. Thus, a reasonable engineered assumption is that the largest blind zone for ANO-2 is assumed for the Waterford-3 ICI nozzles.

$$elev\_to\_mid\_BZ := Elev\_fea_2 + topweld\_to\_bottom\_BZ + \frac{BZ\_length}{2}$$

$elev\_to\_mid\_BZ = 5.315$

$bottom\_of\_BZ := Elev\_fea_2 + topweld\_to\_bottom\_BZ$

$bottom\_of\_BZ = 4.875$

$top\_of\_BZ := Elev\_fea_2 + topweld\_to\_bottom\_BZ + BZ\_length$

$top\_of\_BZ = 5.755$

For stress averaging and fracture mechanics purposes, the reference coordinate system--with a "0" elevation at the bottom of the nozzle, at the ID corner--must be converted into a new coordinate system with the top of the nozzle (nodal line 83301) as the new "0" elevation.. The positive direction along this new coordinate system will be towards nodal line 81101, which is the just below the top of the weld. This modification facilitates a fracture mechanics model more ammenable to the surface flaw loop structure previously developed in Reference 6.

The following iterative loop converts the five (5) through-wall stress components--ID, 25% tw (QT), 50% tw (MD), 75% tw (TQ), and OD--and the associated elevation, initially given in the DEI FEA model, into the "new" coordinate system, referenced from the top of the nozzle where it meets the reactor vessel head.

$$
\begin{aligned}
\text{Conv} := \;& n \leftarrow 20 \\
& \text{Top} \leftarrow \text{Elev\_fea}_n \\
& j \leftarrow n \\
& i \leftarrow 0 \\
& \text{while } j \geq 0 \\
& \quad \text{Elev\_conv}_i \leftarrow \text{Top} - \text{Elev\_fea}_j \\
& \quad \text{ID\_stress}_i \leftarrow \text{ID\_stress\_fea}_j \\
& \quad \text{QT\_stress}_i \leftarrow \text{QT\_stress\_fea}_j \\
& \quad \text{MD\_stress}_i \leftarrow \text{MD\_stress\_fea}_j \\
& \quad \text{TQ\_stress}_i \leftarrow \text{TQ\_stress\_fea}_j \\
& \quad \text{OD\_stress}_i \leftarrow \text{OD\_stress\_fea}_j \\
& \quad \text{output}_{(i,0)} \leftarrow \text{Elev\_conv}_i \\
& \quad \text{output}_{(i,1)} \leftarrow \text{ID\_stress}_i \\
& \quad \text{output}_{(i,2)} \leftarrow \text{QT\_stress}_i \\
& \quad \text{output}_{(i,3)} \leftarrow \text{MD\_stress}_i \\
& \quad \text{output}_{(i,4)} \leftarrow \text{TQ\_stress}_i \\
& \quad \text{output}_{(i,5)} \leftarrow \text{OD\_stress}_i \\
& \quad j \leftarrow j - 1 \\
& \quad i \leftarrow i + 1 \\
& \text{output}
\end{aligned}
$$

$Elev := Conv^{\langle 0 \rangle}$

$ID\_stress := Conv^{\langle 1 \rangle}$

$QT\_stress := Conv^{\langle 2 \rangle}$

$MD\_stress := Conv^{\langle 3 \rangle}$

$TQ\_stress := Conv^{\langle 4 \rangle}$

$OD\_stress := Conv^{\langle 5 \rangle}$

$Elev_i$ =	ID_stress_i =	QT_stress_i =	MD_stress_i =	TQ_stress_i =	OD_stress_i =
0	18.311	15.38	12.983	10.759	8.539
1.235	19.876	16.176	13.009	10.038	7.179
2.325	21.213	17.311	13.126	9.525	6.042
3.289	21.55	18.466	13.362	9.158	5.143
4.141	21.742	19.395	13.664	8.987	4.508
4.893	21.792	20.133	13.976	8.964	4.177
5.557	21.667	20.4	14.263	9.1	4.15
6.144	21.408	20.378	14.437	9.275	4.33
6.663	20.976	20.149	14.467	9.428	4.629
7.121	20.331	19.55	13.998	9.088	4.422
7.526	19.527	18.517	12.761	7.898	3.319
7.883	18.876	17.269	11.236	6.243	1.578
8.199	18.383	15.071	8.65	3.277	-1.652
8.478	18.722	14.133	7.28	0.963	-4.004
8.725	23.668	21.543	14.53	5.734	0.01
8.942	29.82	28.465	21.515	10.551	3.714
9.135	34.079	32.268	24.632	11.934	5.354
9.305	37.068	33.351	25.957	16.947	6.333
9.535	39.763	38.158	34.368	27.002	41.729
9.651	42.799	39.703	41.445	40.722	51.289
9.767	43.347	41.64	43.666	50.638	59.979

The five arrays given above include the elevation measured from the top of the ICI nozzle from the FEA model down to the top of the J-weld and the corresponding hoop stresses in the modified coordinate system (MCS).

Additional Geometry in Modified Coordinate System

The top of the J-groove weld in the MCS is equal to entry 18 in the "Elev" array:

$Top\_Jweld := Elev_{18}$

$Top\_Jweld = 9.535$

The location of the top of the UT blind zone (BZ) in the MCS (as measured from the ID surface) is

$BZ\_top := Top\_Jweld - (topweld\_to\_bottom\_BZ + BZ\_length)$

$BZ\_top = 7.985$

The midpoint of the BZ in the MCS is

$$BZ\_mid := BZ\_top + \frac{BZ\_length}{2}$$

$BZ\_mid = 8.425$

The bottom of the BZ in the MCS is

$BZ\_bottom := BZ\_top + BZ\_length$

$BZ\_bottom = 8.865$

The location of the actual counterbore (from design drawings) in the MCS:

$cbore\_elev := Top\_Jweld - 1.377$

$cbore\_elev = 8.158$

From the MCS, the stress distribution from elevation 0 (the top of the ICI nozzle where it intersects the RV head) to the top of the weld is graphically shown below.

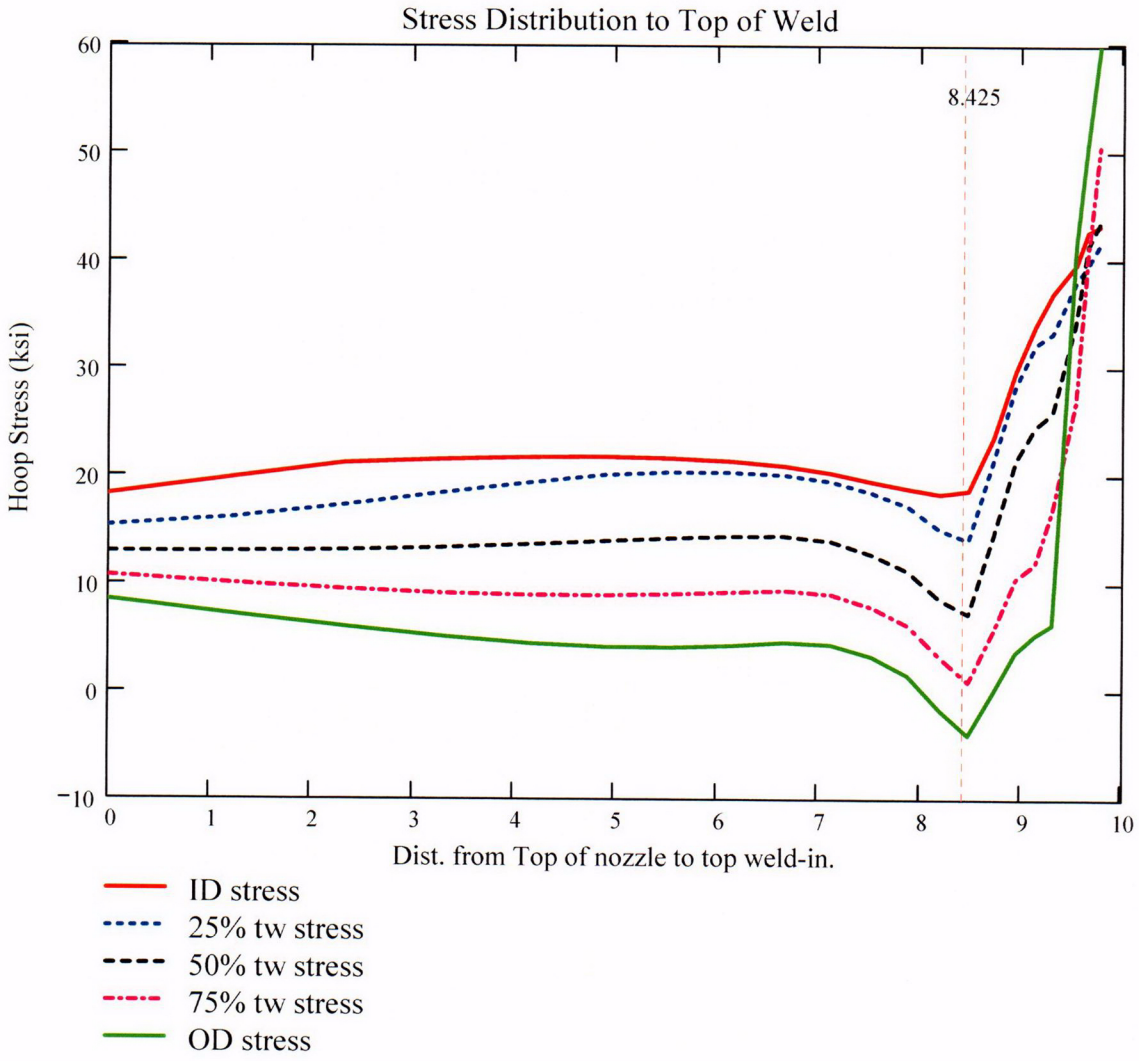

For the ID surface flaw model, the reference point is the location along the axis of the nozzle used to locate the flaw. For this analysis, the reference point is considered at the mid-height of the blind zone.

$Ref_{Point} := BZ\_mid$

To place the flaw with respect to the reference point, the flaw tips and center can be located as follows:

1) The Upper "c- tip" located at the reference point (Enter 1)
2) The Center of the flaw at the reference point (Enter 2)
3) The lower "c- tip" located at the reference point (Enter 3).

$Val := 2$

The Input Below is the point below the blind zone region where stresses will be considered for curve-fitting. This point is taken as the top of the weld, since the stress distribution changes drastically within the weld region Enter this dimension or variable below.

$Elev_{Strs.Dist} := Elev_{20}$ The elevation to the point of maximum stress to consider (Axial distance from elevation 0 in the MCS).

ICI Nozzle Geometry Input Data:

$od := 5.563 - 0.001$ Tube OD, in inches (The value from Ref. 3, is 5.563" +0.00/-0.001)

$id1 := 4.625 + 0.01$ Maximum Tube ID above counterbore, in inches (The value from Ref. 3 is 4.625" +/- 0.010")

$id2 := 4.750 + 0.01$ Maximum Tube ID below counterbore, in inches (The value from Ref. 3 is 4.750" +/- 0.010")

$t1 := \frac{(od - id1)}{2}$

Minmum wall thickness above the counterbore, in inches

$t1 = 0.4635$

$t2 := \frac{(od - id2)}{2}$

Minimum wall thickness below the counterbore, in inches

$t2 = 0.401$

$R_o := \frac{od}{2}$ $R_o = 2.781$

$R_{id1} := \frac{id1}{2}$ $R_{id1} = 2.3175$

$R_{id2} := \frac{id2}{2}$ $R_{id2} = 2.38$

$R_{m1} := R_{id1} + \frac{t1}{2}$ $R_{m1} = 2.54925$

$R_{m2} := R_{id2} + \frac{t2}{2}$ $R_{m2} = 2.5805$

$R_t := \frac{R_{m2}}{t2}$ $R_t = 6.43516$

$\frac{R_o}{t2} = 6.93516$

Flaw Geometry Input Data:

A postulated flaw could exist in the **0.88"** UT Blindzone that occurs **0.67"** above the top of the J-weld at the uphill (180°) location. The flaw length (c) and depth (a) constitute the input parameters. This flaw represents an internal surface crack in a cylinder, as described in Reference 9.

$AR_0 := 6$ The flaw length-to-depth aspect ratio. This is a ratio common to ASME Section XI, and one sufficient to promote flaw growth through the thickness.

$L := BZ\_length$ Initial Flaw Length of an ID surface flaw in the counterbore region, in inches. The length was set equal to the full length of the UT blind zone (0.88 inch). Flaw depth was based on a common length-to-depth aspect ratio of 6-to-1. Half the flaw length (0.44 inch) was placed the below the mid-height of the blind zone, while the other half was placed above the mid-height.

$L = 0.88$

$a_0 := \frac{L}{AR_0}$ Initial Flaw Depth of the ID surface flaw in the blind zone above the top of the weld on the uphill side. The minimum detectable depth of a surface flaw from UT demonstrations [Ref. 12] was 8% throughwall. This flaw equates to 36.58% through-wall. This flaw is sufficiently deep to see the stress field developed through the thickness.

$a_0 = 0.14667$

$t2 \cdot .36575 = 0.14667$

$c_0 := \frac{L}{2}$ The half flaw length used in the fracture mechanics model

Additional Input Data:

$P_{Int} := 2.235$ Design Operating Pressure (internal) [Ref. 4]

$Years := 40$ Number of Operating Years

$I_{lim} := 8000$ Iteration limit for Crack Growth loop

$T := 604$ Operating Temperature for the head, in °F. Reference 5b gives a value of 601°F after the Extended Power Uprate (EPU), and 604°F currently. Thus, the temperature of the head will be taken as 604°F.

$\alpha_{0c} := 2.67 \cdot 10^{-12}$ Constant in MRP-55 PWSCC Model for I-600 Wrought @ 617 deg. F [Ref. 10]

$Q_g := 31.0$ Thermal activation Energy for Crack Growth {MRP) [Ref. 10]

$T_{ref} := 617$ Reference Temperature for normalizing Data deg. F [Ref. 10]

$Tim_{opr} := 365.2422 \cdot 24 \cdot Years$ Numer of operating hours in a year

$CF_{inhr} := 1.417 \cdot 10^{5}$ Correction factor to convert meters per second to inches per hour

$$C_{blk} := \frac{Tim_{opr}}{I_{lim}}$$ Calculation block size for the crack growth iteration loop

$C_{blk} = 43.82906$

$$Prnt_{blk} := \left| \frac{I_{lim}}{50} \right|$$

$$C_{01} := e^{\left[\frac{-Q_g}{1.103 \cdot 10^{-3}} \cdot \left(\frac{1}{T+459.67} - \frac{1}{T_{ref}+459.67} \right) \right] \cdot \alpha_{0c}}$$ Temperature Correction for Coefficient Alpha from EPRI MRP-55, Revision 1 [Ref. 10]

$C_0 := 1.0 C_{01}$ 75 th percentile from MRP-55 Revision 1 [Ref. 10]

The flaw model used for a postulated flaw within the counterbore region on the uphill side of the ICI nozzle is an internal surface flaw in a cylinder, subject to an arbitrary stress distribution.

To allow for a "moving average" of through-thickness stress values as the flaw extends along the length of the ICI ID surface, the length from the bottom tip of the of the initial flaw in the blind zone to the stress distribution upper limit--$Elev_{Strs.Dist}$--is broken into 20 equal segments. Note that due to the MCS used, with a 0 elevation occurring at the TOP of the nozzle, the term "U_{Tip}" (implying the upper tip of the flaw) is actually the physical bottom tip of the flaw, closer to the top of the weld. U_{Tip} is the term used in Reference 6 for the CEDM nozzles, and thus it will continue to be used in the ICI nozzle evaluation.

$$FL_{Cntr} := \begin{cases} Ref_{Point} - c_0 & \text{if } Val = 1 \\ Ref_{Point} & \text{if } Val = 2 \\ Ref_{Point} + c_0 & \text{otherwise} \end{cases}$$

Flaw center Location at the mid-point of the blind zone region

$$U_{Tip} := FL_{Cntr} + c_0$$

$$U_{Tip} = 8.865$$

$$Inc_{Strs.avg} := \frac{Elev_{Strs.Dist} - U_{Tip}}{20}$$

$$Inc_{Strs.avg} = 0.0451$$

$$Ref_{Point} = 8.425$$

No User Input is required beyond this Point

Regression of Through-Thickness Stresses as a Function of Axial Elevation

Because of the minor variation in stresses occuring at the top of the nozzle where it intersects the reactor head and the need to accurately curve fit stresses in the region of interest in the BZ, the entire range of stresses is not appropriate to curve fit. To accomodate an area below and above the BZ region, the first two data points in each of the elevation and stress arrays were removed from consideration in the curve fitting equations. This is a reasonable assumption, given that in the completely through-wall tensile stress field that exists in the nozzle above the top of the J-weld, a flaw centered in the BZ region is likely to grow through the thickness entirely (in addition to growth along the surface of the nozzle) rather than grow very long into an area close to the top of the head or below the top of the J-weld (i.e., elevation ranges not included in the stress polynomial curve fit). Initially, a **third (3rd)** order polynomial was chosen for axial stress regression. After regression, the stress at the mid-height of the blind zone (8.445 inches in the MCS) is checked.

Regression for ID stresses:

$k := 0..5$

$$ID\_elev\_cf := \begin{pmatrix} 7.883 \\ 8.199 \\ 8.478 \\ 8.725 \\ 8.942 \\ 9.135 \end{pmatrix} \qquad ID\_stress\_cf := \begin{pmatrix} 18.876 \\ 18.383 \\ 18.722 \\ 23.668 \\ 29.82 \\ 34.079 \end{pmatrix}$$

$R_{ID} := regress(ID\_elev\_cf, ID\_stress\_cf, 3)$

$$R_{ID} = \begin{pmatrix} 3 \\ 3 \\ 3 \\ 3578.38988 \\ -1136.79548 \\ 118.13463 \\ -3.95831 \end{pmatrix}$$

$z_{ID} := 7.883, 7.884..9.135$

$f_{ID}(z_{ID}) := interp(R_{ID}, ID\_elev\_cf, ID\_stress\_cf, z_{ID})$

$Elev_i$ =	ID_stress_i =
0	18.311
1.235	19.876
2.325	21.213
3.289	21.55
4.141	21.742
4.893	21.792
5.557	21.667
6.144	21.408
6.663	20.976
7.121	20.331
7.526	19.527
7.883	18.876
8.199	18.383
8.478	18.722
8.725	23.668
8.942	29.82
9.135	34.079
9.305	37.068
9.535	39.763
9.651	42.799
9.767	43.347

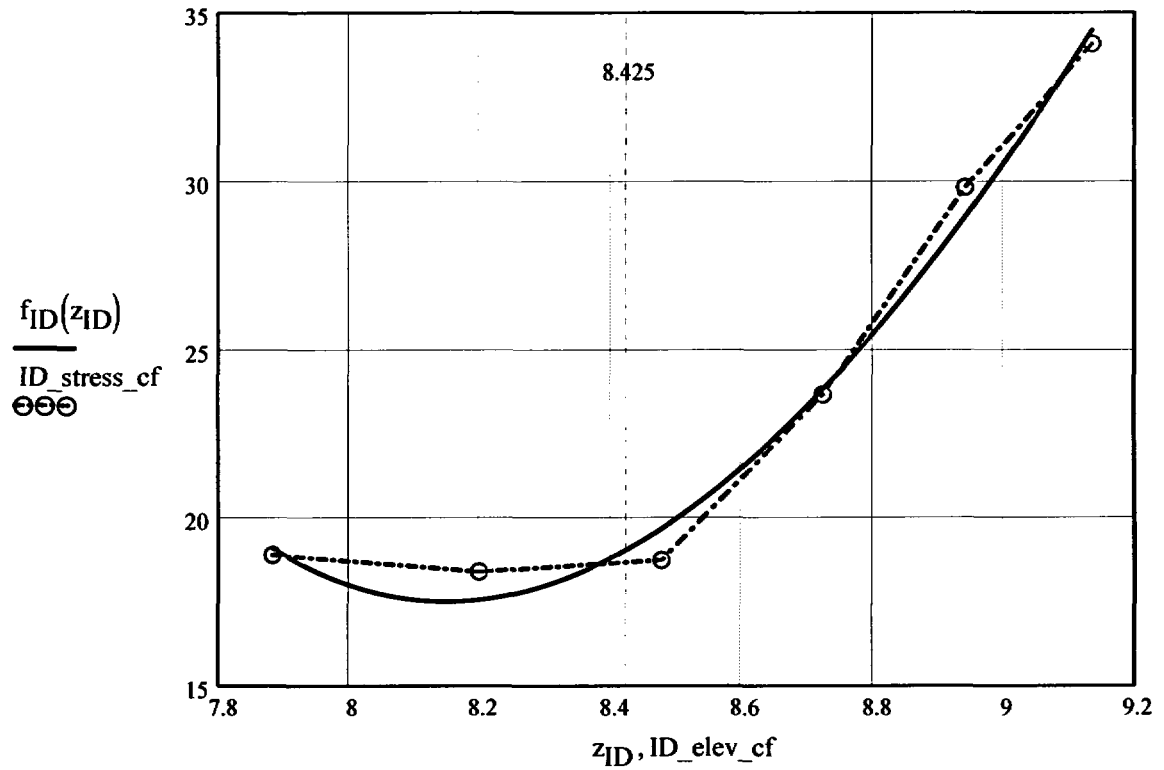

$f_{ID}(8.425) = 19.03958$

Regression for 25% throughwall stresses:

$$QT\_elev\_cf := \begin{pmatrix} 7.883 \\ 8.199 \\ 8.478 \\ 8.725 \\ 8.942 \\ 9.135 \end{pmatrix} \qquad QT\_stress\_cf := \begin{pmatrix} 17.269 \\ 15.071 \\ 14.133 \\ 21.543 \\ 28.465 \\ 32.268 \end{pmatrix}$$

$R_{QT} := regress(QT\_elev\_cf, QT\_stress\_cf, 3)$

$z_{QT} := 7.883, 7.884 .. 9.135$

$$R_{QT} = \begin{pmatrix} 3 \\ 3 \\ 3 \\ 10745.64054 \\ -3630.8401 \\ 406.73522 \\ -15.0681 \end{pmatrix}$$

$f_{QT}(z_{QT}) := interp(R_{QT}, QT\_elev\_cf, QT\_stress\_cf, z_{QT})$

$Elev_i =$	$QT\_stress_i =$
0	15.38
1.235	16.176
2.325	17.311
3.289	18.466
4.141	19.395
4.893	20.133
5.557	20.4
6.144	20.378
6.663	20.149
7.121	19.55
7.526	18.517
7.883	17.269
8.199	15.071
8.478	14.133
8.725	21.543
8.942	28.465
9.135	32.268
9.305	33.351
9.535	38.158
9.651	39.703
9.767	41.64

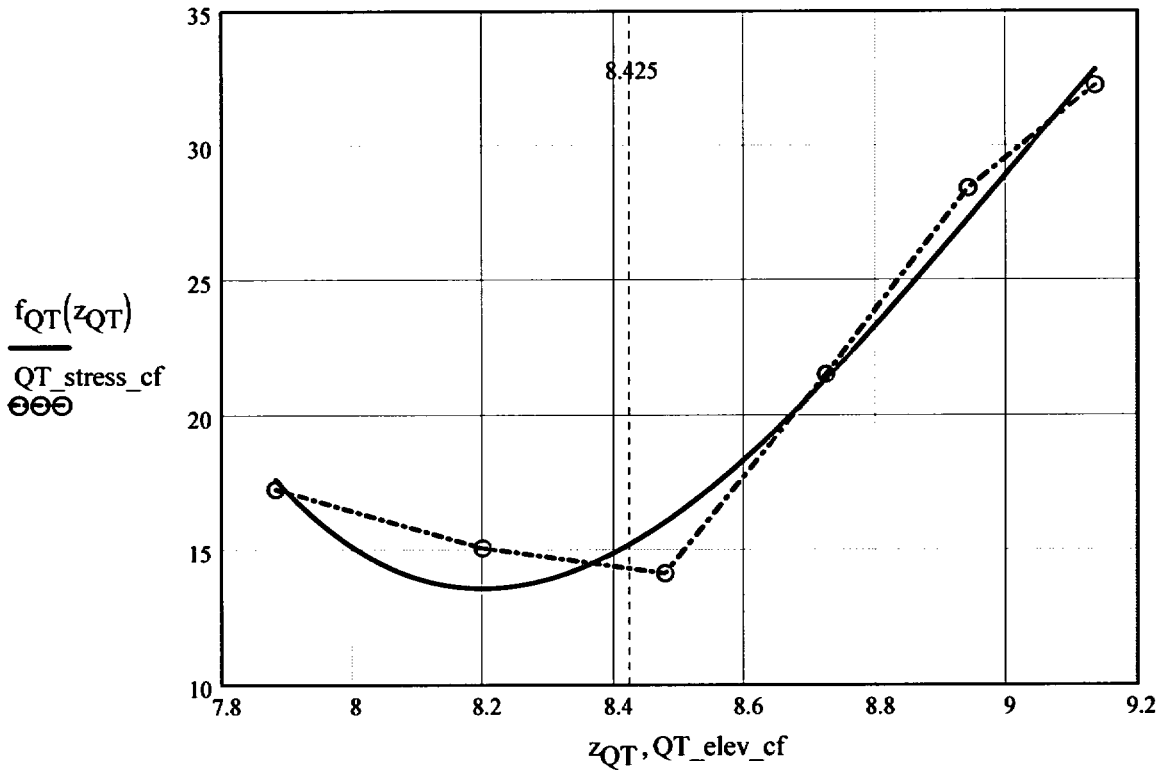

$f_{QT}(8.425) = 15.22949$

Regression for 50% throughwall stresses:

$$MD\_elev\_cf := \begin{pmatrix} 7.883 \\ 8.199 \\ 8.478 \\ 8.725 \\ 8.942 \\ 9.135 \end{pmatrix} \qquad MD\_stress\_cf := \begin{pmatrix} 11.236 \\ 8.65 \\ 7.28 \\ 14.53 \\ 21.515 \\ 24.632 \end{pmatrix}$$

$R_{MD} := regress(MD\_elev\_cf, MD\_stress\_cf, 3)$

$z_{MD} := 7.883, 7.884 .. 9.135$

$$R_{MD} = \begin{pmatrix} 3 \\ 3 \\ 3 \\ 11819.16519 \\ -4010.84838 \\ 451.35824 \\ -16.8173 \end{pmatrix}$$

$f_{MD}(z_{MD}) := interp(R_{MD}, MD\_elev\_cf, MD\_stress\_cf, z_{MD})$

$Elev_i$ =	MD_stress_i =
0	12.983
1.235	13.009
2.325	13.126
3.289	13.362
4.141	13.664
4.893	13.976
5.557	14.263
6.144	14.437
6.663	14.467
7.121	13.998
7.526	12.761
7.883	11.236
8.199	8.65
8.478	7.28
8.725	14.53
8.942	21.515
9.135	24.632
9.305	25.957
9.535	34.368
9.651	41.445
9.767	43.666

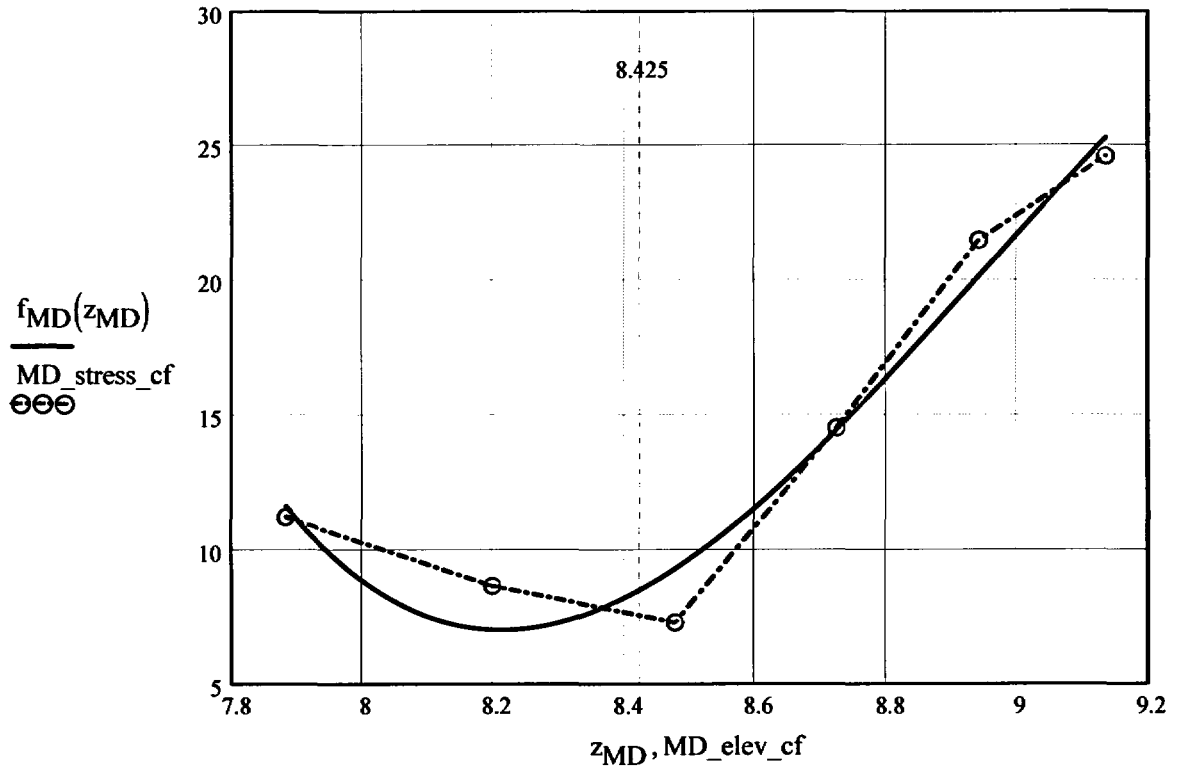

$f_{MD}(8.425) = 8.51122$

Regression for 75% throughwall stresses:

$$TQ\_elev\_cf := \begin{pmatrix} 7.883 \\ 8.199 \\ 8.478 \\ 8.725 \\ 8.942 \\ 9.135 \end{pmatrix} \qquad TQ\_stress\_cf := \begin{pmatrix} 6.243 \\ 3.277 \\ 0.963 \\ 5.734 \\ 10.551 \\ 11.934 \end{pmatrix}$$

$R_{TQ} := regress(TQ\_elev\_cf, TQ\_stress\_cf, 3)$

$z_{TQ} := 7.883, 7.884 .. 9.135$

$$R_{TQ} = \begin{pmatrix} 3 \\ 3 \\ 3 \\ 9313.45524 \\ -3159.012 \\ 355.56516 \\ -13.2686 \end{pmatrix}$$

$f_{TQ}(z_{TQ}) := \text{interp}(R_{TQ}, TQ\_elev\_cf, TQ\_stress\_cf, z_{TQ})$

$Elev_i =$	$TQ\_stress_i =$
0	10.759
1.235	10.038
2.325	9.525
3.289	9.158
4.141	8.987
4.893	8.964
5.557	9.1
6.144	9.275
6.663	9.428
7.121	9.088
7.526	7.898
7.883	6.243
8.199	3.277
8.478	0.963
8.725	5.734
8.942	10.551
9.135	11.934
9.305	16.947
9.535	27.002
9.651	40.722
9.767	50.638

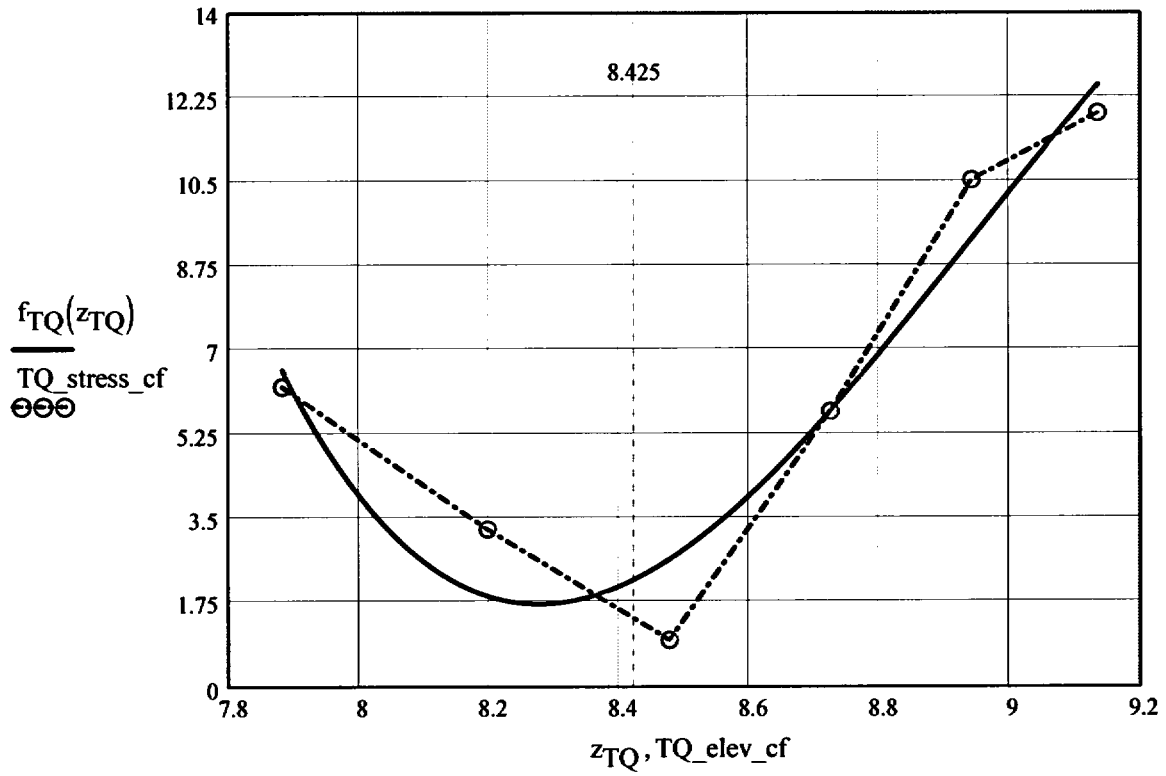

$f_{TQ}(8.425) = 2.2362$

Regression for OD stresses:

kk := 0 .. 5

$$OD\_elev\_cf := \begin{pmatrix} 7.883 \\ 8.199 \\ 8.478 \\ 8.725 \\ 8.942 \\ 9.135 \end{pmatrix} \qquad OD\_stress\_cf := \begin{pmatrix} 1.578 \\ -1.652 \\ -4.004 \\ 0.01 \\ 3.714 \\ 5.354 \end{pmatrix}$$

$R_{OD} := regress(OD\_elev\_cf, OD\_stress\_cf, 3)$

$z_{OD} := 7.883, 7.884 .. 9.135$

$$R_{OD} = \begin{pmatrix} 3 \\ 3 \\ 3 \\ 7570.62763 \\ -2550.59622 \\ 284.86761 \\ -10.54291 \end{pmatrix}$$

$f_{OD}(z_{OD}) := interp(R_{OD}, OD\_elev\_cf, OD\_stress\_cf, z_{OD})$

$Elev_i$ =	OD_stress_i =
0	8.539
1.235	7.179
2.325	6.042
3.289	5.143
4.141	4.508
4.893	4.177
5.557	4.15
6.144	4.33
6.663	4.629
7.121	4.422
7.526	3.319
7.883	1.578
8.199	-1.652
8.478	-4.004
8.725	0.01
8.942	3.714
9.135	5.354
9.305	6.333
9.535	41.729
9.651	51.289
9.767	59.979

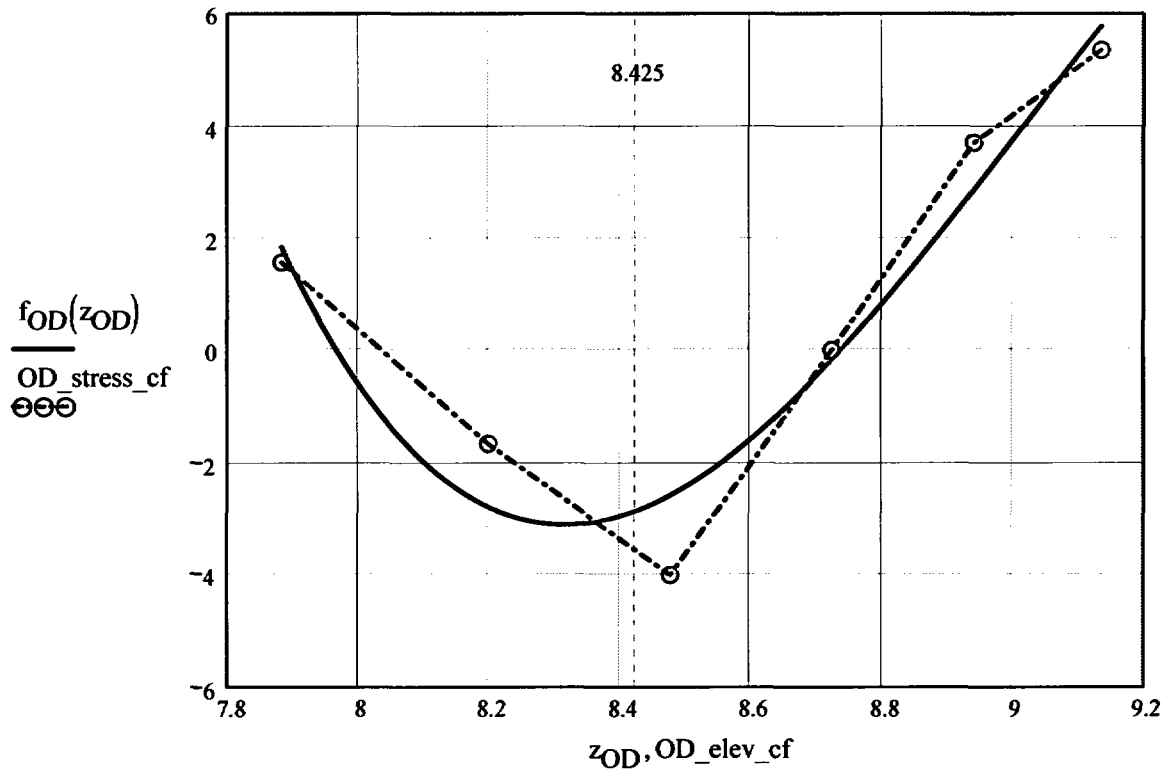

$f_{OD}(8.425) = -2.84902$

Calculation to develop Stress Profiles for Analysis

This analysis for the axial stress regression and the through-wall stress regression is the same as that used for the CEDM Nozzles (in Ref. 6); that is, the axial stresses are fit with a third-order polynomial.

$N := 20$ *Number of locations for stress profiles*

$Loc_0 := FL_{Cntr} - L$

$FL_{Cntr} = 8.425$

$L = 0.88$

$i := 1..N + 3$

$$Incr_i := \begin{cases} c_0 & \text{if } i < 4 \\ Inc_{Strs.avg} & \text{otherwise} \end{cases}$$

$Loc_i := Loc_{i-1} + Incr_i$

$SID_i := R_{ID_3} + R_{ID_4} \cdot Loc_i + R_{ID_5} \cdot (Loc_i)^2 + R_{ID_6} \cdot (Loc_i)^3$

$SQT_i := R_{QT_3} + R_{QT_4} \cdot Loc_i + R_{QT_5} \cdot (Loc_i)^2 + R_{QT_6} \cdot (Loc_i)^3$

$SMD_i := R_{MD_3} + R_{MD_4} \cdot Loc_i + R_{MD_5} \cdot (Loc_i)^2 + R_{MD_6} \cdot (Loc_i)^3$

$STQ_i := R_{TQ_3} + R_{TQ_4} \cdot Loc_i + R_{TQ_5} \cdot (Loc_i)^2 + R_{TQ_6} \cdot (Loc_i)^3$

$SOD_i := R_{OD_3} + R_{OD_4} \cdot Loc_i + R_{OD_5} \cdot (Loc_i)^2 + R_{OD_6} \cdot (Loc_i)^3$

$j := 1..N$

$$S_{id_j} := \begin{cases} \dfrac{SID_j + SID_{j+1} + SID_{j+2}}{3} & \text{if } j = 1 \\ \dfrac{S_{id_{j-1}} \cdot (j+1) + SID_{j+2}}{j+2} & \text{otherwise} \end{cases}$$

$$S_{qt_j} := \begin{cases} \dfrac{SQT_j + SQT_{j+1} + SQT_{j+2}}{3} & \text{if } j = 1 \\ \dfrac{S_{qt_{(j-1)}} \cdot (j+1) + SQT_{j+2}}{j+2} & \text{otherwise} \end{cases}$$

$$S_{md_j} := \begin{cases} \dfrac{SMD_j + SMD_{j+1} + SMD_{j+2}}{3} & \text{if } j = 1 \\ \dfrac{S_{md_{j-1}} \cdot (j+1) + SMD_{j+2}}{j+2} & \text{otherwise} \end{cases}$$

$$S_{tq_j} := \begin{cases} \dfrac{STQ_j + STQ_{j+1} + STQ_{j+2}}{3} & \text{if } j = 1 \\ \dfrac{S_{tq_{j-1}} \cdot (j+1) + STQ_{j+2}}{j+2} & \text{otherwise} \end{cases}$$

$$S_{od_j} := \begin{cases} \dfrac{SOD_j + SOD_{j+1} + SOD_{j+2}}{3} & \text{if } j = 1 \\ \dfrac{S_{od_{j-1}} \cdot (j+1) + SOD_{j+2}}{j+2} & \text{otherwise} \end{cases}$$

Through-Wall Stress Distribution for ID Flaws (i.e. ID to OD Stress distribution)

$u_0 := 0.000$ $u_1 := 0.25$ $u_2 := 0.50$ $u_3 := 0.75$ $u_4 := 1.00$

$$Y := \text{stack}(u_0, u_1, u_2, u_3, u_4)$$

$SIG_1 := \text{stack}(S_{id_1}, S_{qt_1}, S_{md_1}, S_{tq_1}, S_{od_1})$ $SIG_2 := \text{stack}(S_{id_2}, S_{qt_2}, S_{md_2}, S_{tq_2}, S_{od_2})$

$SIG_3 := \text{stack}(S_{id_3}, S_{qt_3}, S_{md_3}, S_{tq_3}, S_{od_3})$ $SIG_4 := \text{stack}(S_{id_4}, S_{qt_4}, S_{md_4}, S_{tq_4}, S_{od_4})$

$SIG_5 := \text{stack}(S_{id_5}, S_{qt_5}, S_{md_5}, S_{tq_5}, S_{od_5})$ $SIG_6 := \text{stack}(S_{id_6}, S_{qt_6}, S_{md_6}, S_{tq_6}, S_{od_6})$

$SIG_7 := \text{stack}(S_{id_7}, S_{qt_7}, S_{md_7}, S_{tq_7}, S_{od_7})$ $SIG_8 := \text{stack}(S_{id_8}, S_{qt_8}, S_{md_8}, S_{tq_8}, S_{od_8})$

$SIG_9 := \text{stack}(S_{id_9}, S_{qt_9}, S_{md_9}, S_{tq_9}, S_{od_9})$ $SIG_{10} := \text{stack}(S_{id_{10}}, S_{qt_{10}}, S_{md_{10}}, S_{tq_{10}}, S_{od_{10}})$

$SIG_{11} := \text{stack}(S_{id_{11}}, S_{qt_{11}}, S_{md_{11}}, S_{tq_{11}}, S_{od_{11}})$ $SIG_{12} := \text{stack}(S_{id_{12}}, S_{qt_{12}}, S_{md_{12}}, S_{tq_{12}}, S_{od_{12}})$

$SIG_{13} := \text{stack}(S_{id_{13}}, S_{qt_{13}}, S_{md_{13}}, S_{tq_{13}}, S_{od_{13}})$ $SIG_{14} := \text{stack}(S_{id_{14}}, S_{qt_{14}}, S_{md_{14}}, S_{tq_{14}}, S_{od_{14}})$

$SIG_{15} := \text{stack}(S_{id_{15}}, S_{qt_{15}}, S_{md_{15}}, S_{tq_{15}}, S_{od_{15}})$ $SIG_{16} := \text{stack}(S_{id_{16}}, S_{qt_{16}}, S_{md_{16}}, S_{tq_{16}}, S_{od_{16}})$

$SIG_{17} := \text{stack}(S_{id_{17}}, S_{qt_{17}}, S_{md_{17}}, S_{tq_{17}}, S_{od_{17}})$ $SIG_{18} := \text{stack}(S_{id_{18}}, S_{qt_{18}}, S_{md_{18}}, S_{tq_{18}}, S_{od_{18}})$

$SIG_{19} := \text{stack}(S_{id_{19}}, S_{qt_{19}}, S_{md_{19}}, S_{tq_{19}}, S_{od_{19}})$ $SIG_{20} := \text{stack}(S_{id_{20}}, S_{qt_{20}}, S_{md_{20}}, S_{tq_{20}}, S_{od_{20}})$

Regression of Through-Wall Stress distribution to Obtain Stress Coefficients Using a Third Order Polynomial

$IDRG_1 := regress(Y, SIG_1, 3)$

$IDRG_2 := regress(Y, SIG_2, 3)$

$IDRG_3 := regress(Y, SIG_3, 3)$

$IDRG_4 := regress(Y, SIG_4, 3)$

$IDRG_5 := regress(Y, SIG_5, 3)$

$IDRG_6 := regress(Y, SIG_6, 3)$

$IDRG_7 := regress(Y, SIG_7, 3)$

$IDRG_8 := regress(Y, SIG_8, 3)$

$IDRG_9 := regress(Y, SIG_9, 3)$

$IDRG_{10} := regress(Y, SIG_{10}, 3)$

$IDRG_{11} := regress(Y, SIG_{11}, 3)$

$IDRG_{12} := regress(Y, SIG_{12}, 3)$

$IDRG_{13} := regress(Y, SIG_{13}, 3)$

$IDRG_{14} := regress(Y, SIG_{14}, 3)$

$IDRG_{15} := regress(Y, SIG_{15}, 3)$

$IDRG_{16} := regress(Y, SIG_{16}, 3)$

$IDRG_{17} := regress(Y, SIG_{17}, 3)$

$IDRG_{18} := regress(Y, SIG_{18}, 3)$

$IDRG_{19} := regress(Y, SIG_{19}, 3)$

$IDRG_{20} := regress(Y, SIG_{20}, 3)$

Stress Distribution in the tube. ***Stress influence coefficients obtained from thrid-order polynomial curve fit to the throughwall stress distribution***

Data Files for Flaw Shape Factors from NASA SC04 Model [Ref. 9]

{NO INPUT Required}

Mettu Raju Newman Sivakumar Forman Solution of ID Part throughwall Flaw in Cyinder

Jsb :=

	0	1	2
0	1.000	0.200	0.000
1	1.000	0.200	0.200
2	1.000	0.200	0.500
3	1.000	0.200	0.800
4	1.000	0.200	1.000
5	1.000	0.400	0.000
6	1.000	0.400	0.200
7	1.000	0.400	0.500
8	1.000	0.400	0.800
9	1.000	0.400	1.000
10	1.000	1.000	0.000
11	1.000	1.000	0.200
12	1.000	1.000	0.500
13	1.000	1.000	0.800
14	1.000	1.000	1.000
15	2.000	0.200	0.000
16	2.000	0.200	0.200
17	2.000	0.200	0.500
18	2.000	0.200	0.800
19	2.000	0.200	1.000
20	2.000	0.400	0.000
21	2.000	0.400	0.200
22	2.000	0.400	0.500
23	2.000	0.400	0.800
24	2.000	0.400	1.000
25	2.000	1.000	0.000
26	2.000	1.000	0.200
27	2.000	1.000	0.500
28	2.000	1.000	0.800
29	2.000	1.000	1.000
30	4.000	0.200	0.000
31	4.000	0.200	0.200
32	4.000	0.200	0.500
33	4.000	0.200	0.800
34	4.000	0.200	1.000
35	4.000	0.400	0.000
36	4.000	0.400	0.200

37	4.000	0.400	0.500
38	4.000	0.400	0.800
39	4.000	0.400	1.000
40	4.000	1.000	0.000
41	4.000	1.000	0.200
42	4.000	1.000	0.500
43	4.000	1.000	0.800
44	4.000	1.000	1.000
45	10.000	0.200	0.000
46	10.000	0.200	0.200
47	10.000	0.200	0.500
48	10.000	0.200	0.800
49	10.000	0.200	1.000
50	10.000	0.400	0.000
51	10.000	0.400	0.200
52	10.000	0.400	0.500
53	10.000	0.400	0.800
54	10.000	0.400	1.000
55	10.000	1.000	0.000
56	10.000	1.000	0.200
57	10.000	1.000	0.500
58	10.000	1.000	0.800
59	10.000	1.000	1.000
60	300.000	0.200	0.000
61	300.000	0.200	0.200
62	300.000	0.200	0.500
63	300.000	0.200	0.800
64	300.000	0.200	1.000
65	300.000	0.400	0.000
66	300.000	0.400	0.200
67	300.000	0.400	0.500
68	300.000	0.400	0.800
69	300.000	0.400	1.000
70	300.000	1.000	0.000
71	300.000	1.000	0.200
72	300.000	1.000	0.500
73	300.000	1.000	0.800
74	300.000	1.000	1.000

Sambi :=

	0	1	2	3	4	5	6	7
0	1.076	0.693	0.531	0.434	0.608	0.083	0.023	0.009

0	1.076	0.693	0.531	0.434	0.608	0.083	0.023	0.009
1	1.056	0.647	0.495	0.408	0.615	0.085	0.027	0.013
2	1.395	0.767	0.557	0.446	0.871	0.171	0.069	0.038
3	2.53	1.174	0.772	0.58	1.554	0.363	0.155	0.085
4	3.846	1.615	0.995	0.716	2.277	0.544	0.233	0.127
5	1.051	0.689	0.536	0.444	0.74	0.112	0.035	0.015
6	1.011	0.646	0.504	0.421	0.745	0.119	0.041	0.02
7	1.149	0.694	0.529	0.435	0.916	0.181	0.073	0.04
8	1.6	0.889	0.642	0.51	1.334	0.307	0.132	0.073
9	2.087	1.093	0.761	0.589	1.752	0.421	0.183	0.101
10	0.992	0.704	0.534	0.506	1.044	0.169	0.064	0.032
11	0.987	0.701	0.554	0.491	1.08	0.182	0.067	0.034
12	1.01	0.709	0.577	0.493	1.116	0.2	0.078	0.041
13	1.07	0.73	0.623	0.523	1.132	0.218	0.095	0.051
14	1.128	0.75	0.675	0.556	1.131	0.229	0.11	0.06
15	1.049	0.673	0.519	0.427	0.6	0.078	0.021	0.008
16	1.091	0.661	0.502	0.413	0.614	0.083	0.025	0.012
17	1.384	0.764	0.556	0.446	0.817	0.15	0.058	0.031
18	2.059	1.033	0.708	0.545	1.3	0.291	0.123	0.067
19	2.739	1.301	0.858	0.643	1.783	0.421	0.18	0.099
20	1.075	0.674	0.527	0.436	0.73	0.072	0.044	0.021
21	1.045	0.659	0.511	0.425	0.76	0.122	0.043	0.021
22	1.16	0.71	0.536	0.441	0.919	0.197	0.064	0.034
23	1.51	0.854	0.623	0.498	1.231	0.271	0.114	0.062
24	1.876	0.995	0.71	0.555	1.519	0.317	0.161	0.089
25	1.037	0.732	0.594	0.505	1.132	0.192	0.07	0.035
26	1.003	0.707	0.577	0.493	1.113	0.19	0.071	0.036
27	1.023	0.714	0.58	0.495	1.155	0.207	0.08	0.042
28	1.129	0.774	0.619	0.521	1.286	0.247	0.098	0.052
29	1.242	0.84	0.661	0.549	1.416	0.285	0.115	0.061
30	1.003	0.649	0.511	0.43	0.577	0.07	0.015	0.005
31	1.097	0.666	0.511	0.426	0.606	0.079	0.023	0.01
32	1.405	0.776	0.567	0.46	0.797	0.141	0.054	0.028
33	1.959	0.996	0.692	0.542	1.201	0.262	0.108	0.059
34	2.461	1.197	0.808	0.619	1.586	0.37	0.154	0.085
35	1.024	0.668	0.528	0.451	0.737	0.11	0.033	0.015
36	1.057	0.666	0.52	0.439	0.77	0.123	0.042	0.021
37	1.193	0.715	0.545	0.454	0.924	0.174	0.068	0.036
38	1.443	0.828	0.614	0.509	1.219	0.263	0.109	0.059
39	1.665	0.934	0.681	0.565	1.487	0.339	0.143	0.078
40	1.005	0.72	0.597	0.518	1.119	0.188	0.068	0.034
41	1.009	0.713	0.588	0.511	1.128	0.194	0.072	0.037
42	1.041	0.726	0.594	0.515	1.191	0.214	0.082	0.043

43	1.105	0.768	0.623	0.536	1.316	0.248	0.097	0.05
44	1.162	0.81	0.653	0.558	1.428	0.277	0.109	0.055
45	0.973	0.635	0.499	0.446	0.579	0.07	0.016	0.005
46	1.115	0.673	0.514	0.438	0.607	0.079	0.023	0.01
47	1.427	0.783	0.571	0.462	0.791	0.138	0.052	0.027
48	1.872	0.96	0.671	0.529	1.179	0.253	0.104	0.056
49	2.23	1.108	0.757	0.594	1.548	0.356	0.149	0.081
50	0.992	0.656	0.52	0.443	0.733	0.109	0.032	0.014
51	1.072	0.672	0.523	0.441	0.777	0.125	0.043	0.021
52	1.217	0.723	0.549	0.456	0.936	0.176	0.069	0.036
53	1.393	0.806	0.601	0.493	1.219	0.259	0.106	0.056
54	1.521	0.875	0.647	0.528	1.469	0.328	0.135	0.071
55	0.994	0.715	0.59	0.518	1.114	0.187	0.068	0.035
56	1.015	0.715	0.588	0.512	1.14	0.197	0.074	0.038
57	1.05	0.729	0.596	0.515	1.219	0.221	0.085	0.044
58	1.09	0.76	0.618	0.532	1.348	0.255	0.099	0.051
59	1.118	0.788	0.639	0.55	1.456	0.282	0.109	0.056
60	0.936	0.62	0.486	0.405	0.582	0.068	0.015	0.005
61	1.145	0.681	0.514	0.42	0.613	0.081	0.024	0.011
62	1.459	0.79	0.569	0.454	0.79	0.138	0.051	0.026
63	1.774	0.917	0.641	0.501	1.148	0.239	0.096	0.051
64	1.974	1.008	0.696	0.537	1.482	0.328	0.134	0.07
65	0.982	0.651	0.512	0.427	0.721	0.103	0.031	0.013
66	1.095	0.677	0.52	0.431	0.782	0.127	0.045	0.022
67	1.244	0.727	0.546	0.446	0.946	0.18	0.071	0.037
68	1.37	0.791	0.585	0.473	1.201	0.253	0.102	0.054
69	1.438	0.838	0.618	0.496	1.413	0.31	0.126	0.066

$W := Jsb^{\langle 0 \rangle}$ $X := Jsb^{\langle 1 \rangle}$ $Y := Jsb^{\langle 2 \rangle}$

$a_U := Sambi^{\langle 0 \rangle}$ $a_L := Sambi^{\langle 1 \rangle}$ $a_Q := Sambi^{\langle 2 \rangle}$ $a_C := Sambi^{\langle 3 \rangle}$

$c_U := Sambi^{\langle 4 \rangle}$ $c_L := Sambi^{\langle 5 \rangle}$ $c_Q := Sambi^{\langle 6 \rangle}$ $c_C := Sambi^{\langle 7 \rangle}$

$$n := \begin{cases} 3 & \text{if } R_t \le 4.0 \\ 2 & \text{otherwise} \end{cases}$$

"a-Tip" Uniform Term

$M_{aU} := \text{augment}(W, X, Y) \qquad V_{aU} := a_U \qquad R_{aU} := \text{regress}(M_{aU}, V_{aU}, n)$

$$f_{aU}(W, X, Y) := \text{interp}\left[R_{aU}, M_{aU}, V_{aU}, \begin{pmatrix} W \\ X \\ Y \end{pmatrix}\right]$$

$f_{aU}(4, .4, .8) = 1.7089$ *Check Calculation*

Linear Term

$M_{aL} := \text{augment}(W, X, Y) \qquad V_{aL} := a_L \qquad R_{aL} := \text{regress}(M_{aL}, V_{aL}, n)$

$$f_{aL}(W, X, Y) := \text{interp}\left[R_{aL}, M_{aL}, V_{aL}, \begin{pmatrix} W \\ X \\ Y \end{pmatrix}\right]$$

$f_{aL}(4, .4, .8) = 0.93393$ *Check Calculation*

Quadratic Term

$M_{aQ} := \text{augment}(W, X, Y) \qquad V_{aQ} := a_Q \qquad R_{aQ} := \text{regress}(M_{aQ}, V_{aQ}, n)$

$$f_{aQ}(W, X, Y) := \text{interp}\left[R_{aQ}, M_{aQ}, V_{aQ}, \begin{pmatrix} W \\ X \\ Y \end{pmatrix}\right]$$

$f_{aQ}(4,.4,.8) = 0.67668$ *Check Calculation*

Cubic Term

$M_{aC} := \text{augment}(W,X,Y)$ $V_{aC} := a_C$ $R_{aC} := \text{regress}(M_{aC}, V_{aC}, n)$

$$f_{aC}(W,X,Y) := \text{interp}\left[R_{aC}, M_{aC}, V_{aC}, \begin{pmatrix} W \\ X \\ Y \end{pmatrix}\right]$$

$f_{aC}(4,.4,.8) = 0.54151$ *Check Calculation*

"C" Tip Coefficients

Uniform Term

$M_{cU} := \text{augment}(W,X,Y)$ $V_{cU} := c_U$ $R_{cU} := \text{regress}(M_{cU}, V_{cU}, n)$

$$f_{cU}(W,X,Y) := \text{interp}\left[R_{cU}, M_{cU}, V_{cU}, \begin{pmatrix} W \\ X \\ Y \end{pmatrix}\right]$$

$f_{cU}(4,.4,.8) = 1.31015$ *Check Calculation*

Linear Term

$M_{cL} := \text{augment}(W,X,Y)$ $V_{cL} := c_L$ $R_{cL} := \text{regress}(M_{cL}, V_{cL}, n)$

$$f_{cL}(W,X,Y) := \text{interp}\left[R_{cL}, M_{cL}, V_{cL}, \begin{pmatrix} W \\ X \\ Y \end{pmatrix}\right]$$

$f_{cL}(2,.4,.8) = 0.28509$ *Check Calculation*

Quadratic Term

$M_{cQ} := \text{augment}(W,X,Y)$ $V_{cQ} := c_Q$ $R_{cQ} := \text{regress}(M_{cQ}, V_{cQ}, n)$

$$f_{cQ}(W,X,Y) := \text{interp}\left[R_{cQ}, M_{cQ}, V_{cQ}, \begin{pmatrix} W \\ X \\ Y \end{pmatrix}\right]$$

$f_{cQ}(4,.4,.8) = 0.11797$ *Check Calculation*

Cubic Term

$M_{cC} := \text{augment}(W,X,Y)$ $V_{cC} := c_C$ $R_{cC} := \text{regress}(M_{cC}, V_{cC}, n)$

$$f_{cC}(W,X,Y) := \text{interp}\left[R_{cC}, M_{cC}, V_{cC}, \begin{pmatrix} W \\ X \\ Y \end{pmatrix}\right]$$

$f_{cC}(4,.4,.8) = 0.06384$ *Check Calculation*

Calculations : Recursive calculations to estimate flaw growth

Recursive Loop for Calculation of PWSCC Crack Growth

$$
\begin{aligned}
CGR_{sambi} := \;& j \leftarrow 0 \\
& a_0 \leftarrow a_0 \\
& c_0 \leftarrow c_0 \\
& t \leftarrow t2 \\
& NCB_0 \leftarrow C_{blk} \\
& \text{while } j \le I_{lim} \\
& \quad \sigma_0 \leftarrow \begin{cases}
IDRG1_3 & \text{if } c_j \le c_0 \\
IDRG2_3 & \text{if } c_0 < c_j \le c_0 + Inc_{Strs.avg} \\
IDRG3_3 & \text{if } c_0 + Inc_{Strs.avg} < c_j \le c_0 + 2 \cdot Inc_{Strs.avg} \\
IDRG4_3 & \text{if } c_0 + 2 \cdot Inc_{Strs.avg} < c_j \le c_0 + 3 \cdot Inc_{Strs.avg} \\
IDRG5_3 & \text{if } c_0 + 3 \cdot Inc_{Strs.avg} < c_j \le c_0 + 4 \cdot Inc_{Strs.avg} \\
IDRG6_3 & \text{if } c_0 + 4 \cdot Inc_{Strs.avg} < c_j \le c_0 + 5 \cdot Inc_{Strs.avg} \\
IDRG7_3 & \text{if } c_0 + 5 \cdot Inc_{Strs.avg} < c_j \le c_0 + 6 \cdot Inc_{Strs.avg} \\
IDRG8_3 & \text{if } c_0 + 6 \cdot Inc_{Strs.avg} < c_j \le c_0 + 7 \cdot Inc_{Strs.avg} \\
IDRG9_3 & \text{if } c_0 + 7 \cdot Inc_{Strs.avg} < c_j \le c_0 + 8 \cdot Inc_{Strs.avg} \\
IDRG10_3 & \text{if } c_0 + 8 \cdot Inc_{Strs.avg} < c_j \le c_0 + 9 \cdot Inc_{Strs.avg} \\
IDRG11_3 & \text{if } c_0 + 9 \cdot Inc_{Strs.avg} < c_j \le c_0 + 10 \cdot Inc_{Strs.avg} \\
IDRG12_3 & \text{if } c_0 + 10 \cdot Inc_{Strs.avg} < c_j \le c_0 + 11 \cdot Inc_{Strs.avg} \\
IDRG13_3 & \text{if } c_0 + 11 \cdot Inc_{Strs.avg} < c_j \le c_0 + 12 \cdot Inc_{Strs.avg} \\
IDRG14_3 & \text{if } c_0 + 12 \cdot Inc_{Strs.avg} < c_j \le c_0 + 13 \cdot Inc_{Strs.avg} \\
IDRG15_3 & \text{if } c_0 + 13 \cdot Inc_{Strs.avg} < c_j \le c_0 + 14 \cdot Inc_{Strs.avg} \\
IDRG16_3 & \text{if } c_0 + 14 \cdot Inc_{Strs.avg} < c_j \le c_0 + 15 \cdot Inc_{Strs.avg}
\end{cases}
\end{aligned}
$$

$$\begin{aligned}
&\mathrm{IDRG}_{17_3} \text{ if } c_0 + 15\cdot \mathrm{Inc}_{\mathrm{Strs.avg}} < c_j \le c_0 + 16\cdot \mathrm{Inc}_{\mathrm{Strs.avg}}\\
&\mathrm{IDRG}_{18_3} \text{ if } c_0 + 16\cdot \mathrm{Inc}_{\mathrm{Strs.avg}} < c_j \le c_0 + 17\cdot \mathrm{Inc}_{\mathrm{Strs.avg}}\\
&\mathrm{IDRG}_{19_3} \text{ if } c_0 + 17\cdot \mathrm{Inc}_{\mathrm{Strs.avg}} < c_j \le c_0 + 18\cdot \mathrm{Inc}_{\mathrm{Strs.avg}}\\
&\mathrm{IDRG}_{20_3} \text{ otherwise}
\end{aligned}$$

$$\sigma_1 \leftarrow \begin{aligned}
&\mathrm{IDRG}_{1_4} \text{ if } c_j \le c_0\\
&\mathrm{IDRG}_{2_4} \text{ if } c_0 < c_j \le c_0 + \mathrm{Inc}_{\mathrm{Strs.avg}}\\
&\mathrm{IDRG}_{3_4} \text{ if } c_0 + \mathrm{Inc}_{\mathrm{Strs.avg}} < c_j \le c_0 + 2\cdot \mathrm{Inc}_{\mathrm{Strs.avg}}\\
&\mathrm{IDRG}_{4_4} \text{ if } c_0 + 2\cdot \mathrm{Inc}_{\mathrm{Strs.avg}} < c_j \le c_0 + 3\cdot \mathrm{Inc}_{\mathrm{Strs.avg}}\\
&\mathrm{IDRG}_{5_4} \text{ if } c_0 + 3\cdot \mathrm{Inc}_{\mathrm{Strs.avg}} < c_j \le c_0 + 4\cdot \mathrm{Inc}_{\mathrm{Strs.avg}}\\
&\mathrm{IDRG}_{6_4} \text{ if } c_0 + 4\cdot \mathrm{Inc}_{\mathrm{Strs.avg}} < c_j \le c_0 + 5\cdot \mathrm{Inc}_{\mathrm{Strs.avg}}\\
&\mathrm{IDRG}_{7_4} \text{ if } c_0 + 5\cdot \mathrm{Inc}_{\mathrm{Strs.avg}} < c_j \le c_0 + 6\cdot \mathrm{Inc}_{\mathrm{Strs.avg}}\\
&\mathrm{IDRG}_{8_4} \text{ if } c_0 + 6\cdot \mathrm{Inc}_{\mathrm{Strs.avg}} < c_j \le c_0 + 7\cdot \mathrm{Inc}_{\mathrm{Strs.avg}}\\
&\mathrm{IDRG}_{9_4} \text{ if } c_0 + 7\cdot \mathrm{Inc}_{\mathrm{Strs.avg}} < c_j \le c_0 + 8\cdot \mathrm{Inc}_{\mathrm{Strs.avg}}\\
&\mathrm{IDRG}_{10_4} \text{ if } c_0 + 8\cdot \mathrm{Inc}_{\mathrm{Strs.avg}} < c_j \le c_0 + 9\cdot \mathrm{Inc}_{\mathrm{Strs.avg}}\\
&\mathrm{IDRG}_{11_4} \text{ if } c_0 + 9\cdot \mathrm{Inc}_{\mathrm{Strs.avg}} < c_j \le c_0 + 10\cdot \mathrm{Inc}_{\mathrm{Strs.avg}}\\
&\mathrm{IDRG}_{12_4} \text{ if } c_0 + 10\cdot \mathrm{Inc}_{\mathrm{Strs.avg}} < c_j \le c_0 + 11\cdot \mathrm{Inc}_{\mathrm{Strs.avg}}\\
&\mathrm{IDRG}_{13_4} \text{ if } c_0 + 11\cdot \mathrm{Inc}_{\mathrm{Strs.avg}} < c_j \le c_0 + 12\cdot \mathrm{Inc}_{\mathrm{Strs.avg}}\\
&\mathrm{IDRG}_{14_4} \text{ if } c_0 + 12\cdot \mathrm{Inc}_{\mathrm{Strs.avg}} < c_j \le c_0 + 13\cdot \mathrm{Inc}_{\mathrm{Strs.avg}}\\
&\mathrm{IDRG}_{15_4} \text{ if } c_0 + 13\cdot \mathrm{Inc}_{\mathrm{Strs.avg}} < c_j \le c_0 + 14\cdot \mathrm{Inc}_{\mathrm{Strs.avg}}\\
&\mathrm{IDRG}_{16_4} \text{ if } c_0 + 14\cdot \mathrm{Inc}_{\mathrm{Strs.avg}} < c_j \le c_0 + 15\cdot \mathrm{Inc}_{\mathrm{Strs.avg}}\\
&\mathrm{IDRG}_{17_4} \text{ if } c_0 + 15\cdot \mathrm{Inc}_{\mathrm{Strs.avg}} < c_j \le c_0 + 16\cdot \mathrm{Inc}_{\mathrm{Strs.avg}}
\end{aligned}$$

$$IDRG_{18_4} \text{ if } c_0 + 16 \cdot Inc_{Strs.avg} < c_j \le c_0 + 17 \cdot Inc_{Strs.avg}$$

$$IDRG_{19_4} \text{ if } c_0 + 17 \cdot Inc_{Strs.avg} < c_j \le c_0 + 18 \cdot Inc_{Strs.avg}$$

$$IDRG_{20_4} \text{ otherwise}$$

$$\sigma_2 \leftarrow IDRG_{1_5} \text{ if } c_j \le c_0$$

$$IDRG_{2_5} \text{ if } c_0 < c_j \le c_0 + Inc_{Strs.avg}$$

$$IDRG_{3_5} \text{ if } c_0 + Inc_{Strs.avg} < c_j \le c_0 + 2 \cdot Inc_{Strs.avg}$$

$$IDRG_{4_5} \text{ if } c_0 + 2 \cdot Inc_{Strs.avg} < c_j \le c_0 + 3 \cdot Inc_{Strs.avg}$$

$$IDRG_{5_5} \text{ if } c_0 + 3 \cdot Inc_{Strs.avg} < c_j \le c_0 + 4 \cdot Inc_{Strs.avg}$$

$$IDRG_{6_5} \text{ if } c_0 + 4 \cdot Inc_{Strs.avg} < c_j \le c_0 + 5 \cdot Inc_{Strs.avg}$$

$$IDRG_{7_5} \text{ if } c_0 + 5 \cdot Inc_{Strs.avg} < c_j \le c_0 + 6 \cdot Inc_{Strs.avg}$$

$$IDRG_{8_5} \text{ if } c_0 + 6 \cdot Inc_{Strs.avg} < c_j \le c_0 + 7 \cdot Inc_{Strs.avg}$$

$$IDRG_{9_5} \text{ if } c_0 + 7 \cdot Inc_{Strs.avg} < c_j \le c_0 + 8 \cdot Inc_{Strs.avg}$$

$$IDRG_{10_5} \text{ if } c_0 + 8 \cdot Inc_{Strs.avg} < c_j \le c_0 + 9 \cdot Inc_{Strs.avg}$$

$$IDRG_{11_5} \text{ if } c_0 + 9 \cdot Inc_{Strs.avg} < c_j \le c_0 + 10 \cdot Inc_{Strs.avg}$$

$$IDRG_{12_5} \text{ if } c_0 + 10 \cdot Inc_{Strs.avg} < c_j \le c_0 + 11 \cdot Inc_{Strs.avg}$$

$$IDRG_{13_5} \text{ if } c_0 + 11 \cdot Inc_{Strs.avg} < c_j \le c_0 + 12 \cdot Inc_{Strs.avg}$$

$$IDRG_{14_5} \text{ if } c_0 + 12 \cdot Inc_{Strs.avg} < c_j \le c_0 + 13 \cdot Inc_{Strs.avg}$$

$$IDRG_{15_5} \text{ if } c_0 + 13 \cdot Inc_{Strs.avg} < c_j \le c_0 + 14 \cdot Inc_{Strs.avg}$$

$$IDRG_{16_5} \text{ if } c_0 + 14 \cdot Inc_{Strs.avg} < c_j \le c_0 + 15 \cdot Inc_{Strs.avg}$$

$$IDRG_{17_5} \text{ if } c_0 + 15 \cdot Inc_{Strs.avg} < c_j \le c_0 + 16 \cdot Inc_{Strs.avg}$$

$$IDRG_{18_5} \text{ if } c_0 + 16 \cdot Inc_{Strs.avg} < c_j \le c_0 + 17 \cdot Inc_{Strs.avg}$$

$$\begin{array}{l} \quad \quad \quad \left| \begin{array}{ll} IDRG19_5 & \text{if } c_0 + 17 \cdot Inc_{Strs.avg} < c_j \le c_0 + 18 \cdot Inc_{Strs.avg} \\ IDRG20_5 & \text{otherwise} \end{array} \right. \\ \sigma_3 \leftarrow \left| \begin{array}{ll} IDRG1_6 & \text{if } c_j \le c_0 \\ IDRG2_6 & \text{if } c_0 < c_j \le c_0 + Inc_{Strs.avg} \\ IDRG3_6 & \text{if } c_0 + Inc_{Strs.avg} < c_j \le c_0 + 2 \cdot Inc_{Strs.avg} \\ IDRG4_6 & \text{if } c_0 + 2 \cdot Inc_{Strs.avg} < c_j \le c_0 + 3 \cdot Inc_{Strs.avg} \\ IDRG5_6 & \text{if } c_0 + 3 \cdot Inc_{Strs.avg} < c_j \le c_0 + 4 \cdot Inc_{Strs.avg} \\ IDRG6_6 & \text{if } c_0 + 4 \cdot Inc_{Strs.avg} < c_j \le c_0 + 5 \cdot Inc_{Strs.avg} \\ IDRG7_6 & \text{if } c_0 + 5 \cdot Inc_{Strs.avg} < c_j \le c_0 + 6 \cdot Inc_{Strs.avg} \\ IDRG8_6 & \text{if } c_0 + 6 \cdot Inc_{Strs.avg} < c_j \le c_0 + 7 \cdot Inc_{Strs.avg} \\ IDRG9_6 & \text{if } c_0 + 7 \cdot Inc_{Strs.avg} < c_j \le c_0 + 8 \cdot Inc_{Strs.avg} \\ IDRG10_6 & \text{if } c_0 + 8 \cdot Inc_{Strs.avg} < c_j \le c_0 + 9 \cdot Inc_{Strs.avg} \\ IDRG11_6 & \text{if } c_0 + 9 \cdot Inc_{Strs.avg} < c_j \le c_0 + 10 \cdot Inc_{Strs.avg} \\ IDRG12_6 & \text{if } c_0 + 10 \cdot Inc_{Strs.avg} < c_j \le c_0 + 11 \cdot Inc_{Strs.avg} \\ IDRG13_6 & \text{if } c_0 + 11 \cdot Inc_{Strs.avg} < c_j \le c_0 + 12 \cdot Inc_{Strs.avg} \\ IDRG14_6 & \text{if } c_0 + 12 \cdot Inc_{Strs.avg} < c_j \le c_0 + 13 \cdot Inc_{Strs.avg} \\ IDRG15_6 & \text{if } c_0 + 13 \cdot Inc_{Strs.avg} < c_j \le c_0 + 14 \cdot Inc_{Strs.avg} \\ IDRG16_6 & \text{if } c_0 + 14 \cdot Inc_{Strs.avg} < c_j \le c_0 + 15 \cdot Inc_{Strs.avg} \\ IDRG17_6 & \text{if } c_0 + 15 \cdot Inc_{Strs.avg} < c_j \le c_0 + 16 \cdot Inc_{Strs.avg} \\ IDRG18_6 & \text{if } c_0 + 16 \cdot Inc_{Strs.avg} < c_j \le c_0 + 17 \cdot Inc_{Strs.avg} \\ IDRG19_6 & \text{if } c_0 + 17 \cdot Inc_{Strs.avg} < c_j \le c_0 + 18 \cdot Inc_{Strs.avg} \\ IDRG20 & \text{otherwise} \end{array} \right. \end{array}$$

σ_6

$\xi_0 \leftarrow \sigma_0$

$\xi_1 \leftarrow \sigma_0 + \sigma_1 \cdot \left(\frac{0.25 \cdot a_j}{t}\right) + \sigma_2 \cdot \left(\frac{0.25 \cdot a_j}{t}\right)^2 + \sigma_3 \cdot \left(\frac{0.25 \cdot a_j}{t}\right)^3$

$\xi_2 \leftarrow \sigma_0 + \sigma_1 \cdot \left(\frac{0.5 \cdot a_j}{t}\right) + \sigma_2 \cdot \left(\frac{0.5 \cdot a_j}{t}\right)^2 + \sigma_3 \cdot \left(\frac{0.5 \cdot a_j}{t}\right)^3$

$\xi_3 \leftarrow \sigma_0 + \sigma_1 \cdot \left(\frac{0.75 \cdot a_j}{t}\right) + \sigma_2 \cdot \left(\frac{0.75 \cdot a_j}{t}\right)^2 + \sigma_3 \cdot \left(\frac{0.75 \cdot a_j}{t}\right)^3$

$\xi_4 \leftarrow \sigma_0 + \sigma_1 \cdot \left(\frac{1.0 \cdot a_j}{t}\right) + \sigma_2 \cdot \left(\frac{1.0 \cdot a_j}{t}\right)^2 + \sigma_3 \cdot \left(\frac{1.0 \cdot a_j}{t}\right)^3$

$x_0 \leftarrow 0.0$

$x_1 \leftarrow 0.25$

$x_2 \leftarrow 0.5$

$x_3 \leftarrow 0.75$

$x_4 \leftarrow 1.0$

$X \leftarrow \text{stack}(x_0, x_1, x_2, x_3, x_4)$

$ST \leftarrow \text{stack}(\xi_0, \xi_1, \xi_2, \xi_3, \xi_4)$

$RG \leftarrow \text{regress}(X, ST, 3)$

$\sigma_{00} \leftarrow RG_3 + P_{Int}$

$\sigma_{10} \leftarrow RG_4$

$\sigma_{20} \leftarrow RG_5$

$\sigma_{30} \leftarrow RG_6$

$AR_j \leftarrow \frac{a_j}{c_j}$

$AT_j \leftarrow \frac{a_j}{t}$

$G_{au_j} \leftarrow f_{aU}(R_t, AR_j, AT_j)$

$$G_{al_j} \leftarrow f_{aL}(R_t, AR_j, AT_j)$$

$$G_{aq_j} \leftarrow f_{aQ}(R_t, AR_j, AT_j)$$

$$G_{ac_j} \leftarrow f_{aC}(R_t, AR_j, AT_j)$$

$$G_{cu_j} \leftarrow f_{cU}(R_t, AR_j, AT_j)$$

$$G_{cl_j} \leftarrow f_{cL}(R_t, AR_j, AT_j)$$

$$G_{cq_j} \leftarrow f_{cQ}(R_t, AR_j, AT_j)$$

$$G_{cc_j} \leftarrow f_{cC}(R_t, AR_j, AT_j)$$

$$Q_j \leftarrow \begin{cases} 1 + 1.464 \cdot \left(\frac{a_j}{c_j}\right)^{1.65} & \text{if } c_j \geq a_j \\ 1 + 1.464 \cdot \left(\frac{c_j}{a_j}\right)^{1.65} & \text{otherwise} \end{cases}$$

$$K_{a_j} \leftarrow \left(\frac{\pi \cdot a_j}{Q_j}\right)^{0.5} \cdot \left(\sigma_{00} \cdot G_{au_j} + \sigma_{10} \cdot G_{al_j} + \sigma_{20} \cdot G_{aq_j} + \sigma_{30} \cdot G_{ac_j}\right)$$

$$K_{c_j} \leftarrow \left(\frac{\pi \cdot c_j}{Q_j}\right)^{0.5} \cdot \left(\sigma_{00} \cdot G_{cu_j} + \sigma_{10} \cdot G_{cl_j} + \sigma_{20} \cdot G_{cq_j} + \sigma_{30} \cdot G_{cc_j}\right)$$

$$K_{\alpha_j} \leftarrow K_{a_j} \cdot 1.099$$

$$K_{\gamma_j} \leftarrow K_{c_j} \cdot 1.099$$

$$K_{\alpha_j} \leftarrow \begin{cases} 9.0 & \text{if } K_{\alpha_j} \leq 9.0 \\ K_{\alpha_j} & \text{otherwise} \end{cases}$$

$$K_{\gamma_j} \leftarrow \begin{cases} 9.0 & \text{if } K_{\gamma_j} \leq 9.0 \\ K_{\gamma_j} & \text{otherwise} \end{cases}$$

$$D_{a_j} \leftarrow C_0 \cdot \left(K_{\alpha_j} - 9.0\right)^{1.16}$$

$$D_{ag_j} \leftarrow \begin{cases} D_{a_j} \cdot CF_{inhr} \cdot C_{blk} & \text{if } K_{\alpha_j} < 80.0 \end{cases}$$

$$\left| 4 \cdot 10^{-10} \cdot CF_{inhr} \cdot C_{blk} \quad \text{otherwise} \right.$$

$$D_{c_j} \leftarrow C_0 \cdot \left(K_{\gamma_j} - 9.0 \right)^{1.16}$$

$$D_{cg_j} \leftarrow \begin{cases} D_{c_j} \cdot CF_{inhr} \cdot C_{blk} & \text{if } K_{\gamma_j} < 80.0 \\ 4 \cdot 10^{-10} \cdot CF_{inhr} \cdot C_{blk} & \text{otherwise} \end{cases}$$

$$output_{(j,0)} \leftarrow j$$

$$output_{(j,1)} \leftarrow a_j$$

$$output_{(j,2)} \leftarrow c_j - c_0$$

$$output_{(j,3)} \leftarrow D_{ag_j}$$

$$output_{(j,4)} \leftarrow D_{cg_j}$$

$$output_{(j,5)} \leftarrow K_{a_j}$$

$$output_{(j,6)} \leftarrow K_{c_j}$$

$$output_{(j,7)} \leftarrow \frac{NCB_j}{365 \cdot 24}$$

$$output_{(j,8)} \leftarrow G_{au_j}$$

$$output_{(j,9)} \leftarrow G_{al_j}$$

$$output_{(j,10)} \leftarrow G_{aq_j}$$

$$output_{(j,11)} \leftarrow G_{ac_j}$$

$$output_{(j,12)} \leftarrow G_{cu_j}$$

$$output_{(j,13)} \leftarrow G_{cl_j}$$

$$output_{(j,14)} \leftarrow G_{cq_j}$$

$$output_{(j,15)} \leftarrow G_{cc_j}$$

$$j \leftarrow j + 1$$

$$a_j \leftarrow a_{j-1} + D_{ag_{j-1}}$$

$c_j \leftarrow c_{j-1} + D_{cg_{j-1}}$

$a_j \leftarrow \begin{cases} t & \text{if } a_j \geq t \\ a_j & \text{otherwise} \end{cases}$

$NCB_j \leftarrow NCB_{j-1} + C_{blk}$

output

$k := 0 .. I_{lim}$

The curve below shows the flaw growth through-wall and the operating time (in years) it takes for the initial flaw in the blind zone to go through-wall.

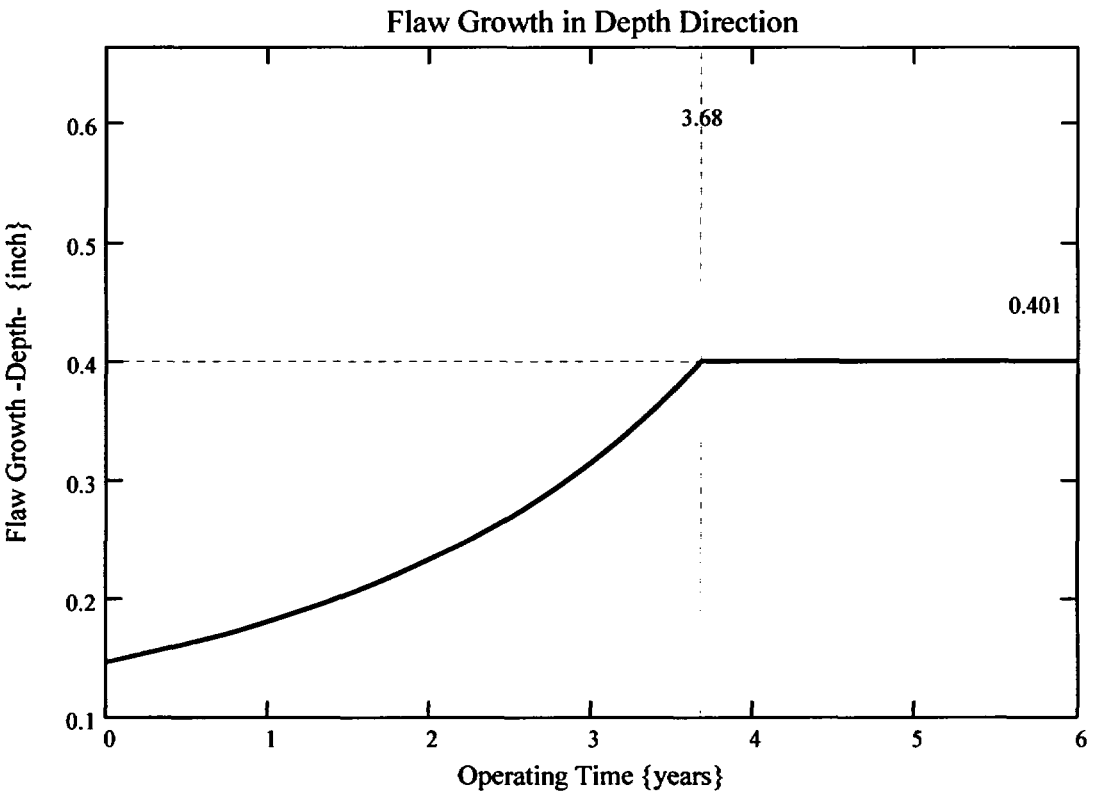

The propagation length for the ICI nozzles is defined as the length for which the initial flaw in the blind zone would extend out of the blind zone and grow to a detectable flaw. Reference 12 gives the minimum detectable flaw size of 4 mm (0.16) in length; thus, 0.16 inch was considered as this minimum detectable flaw length. This dimension is added to the end of the blind zone.

$$\text{Prop\_Length} := \frac{\text{BZ\_length}}{2} - c_0 + 0.16$$

$$\text{Prop\_Length} = 0.16$$

This implies that a flaw initially spanning the length of the blindzone must grow 0.16 inch to become detectable via UT.

The curve below shows the flaw growth along the length of the ICI nozzle and the operating time (in years) it takes to reach the Prop_Length value defined above.

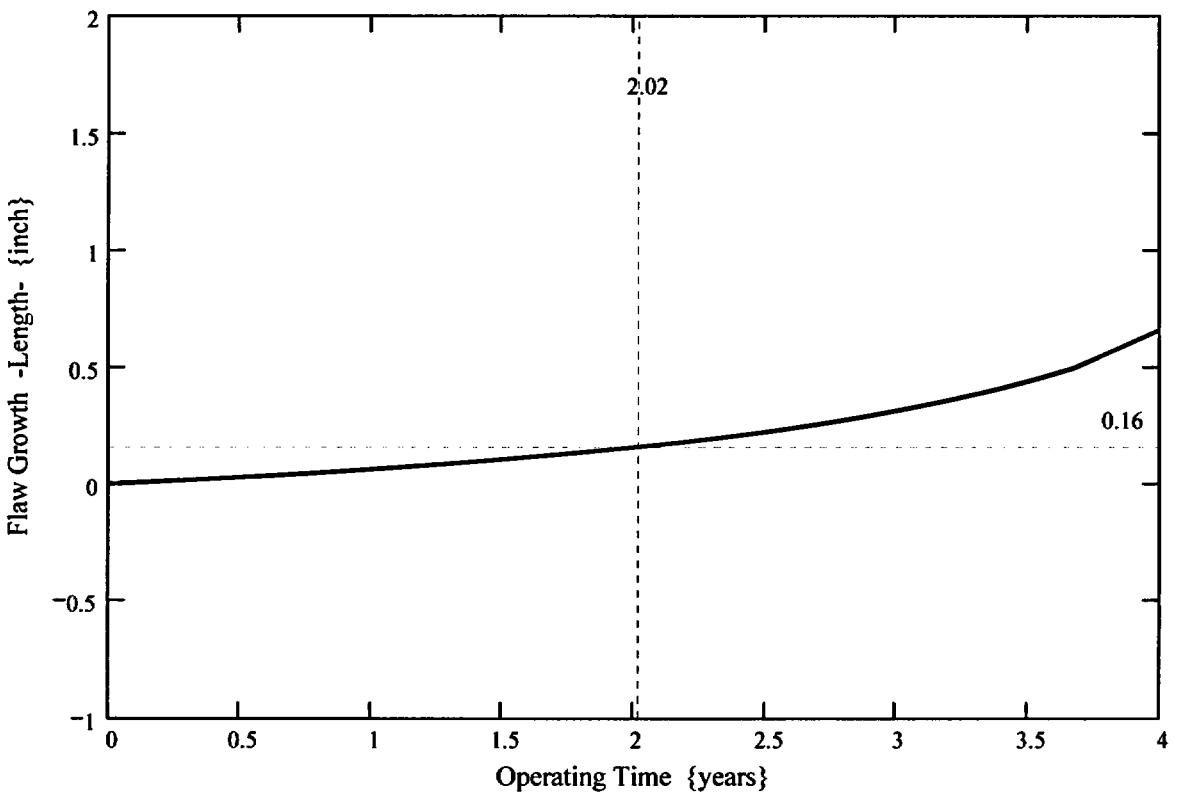

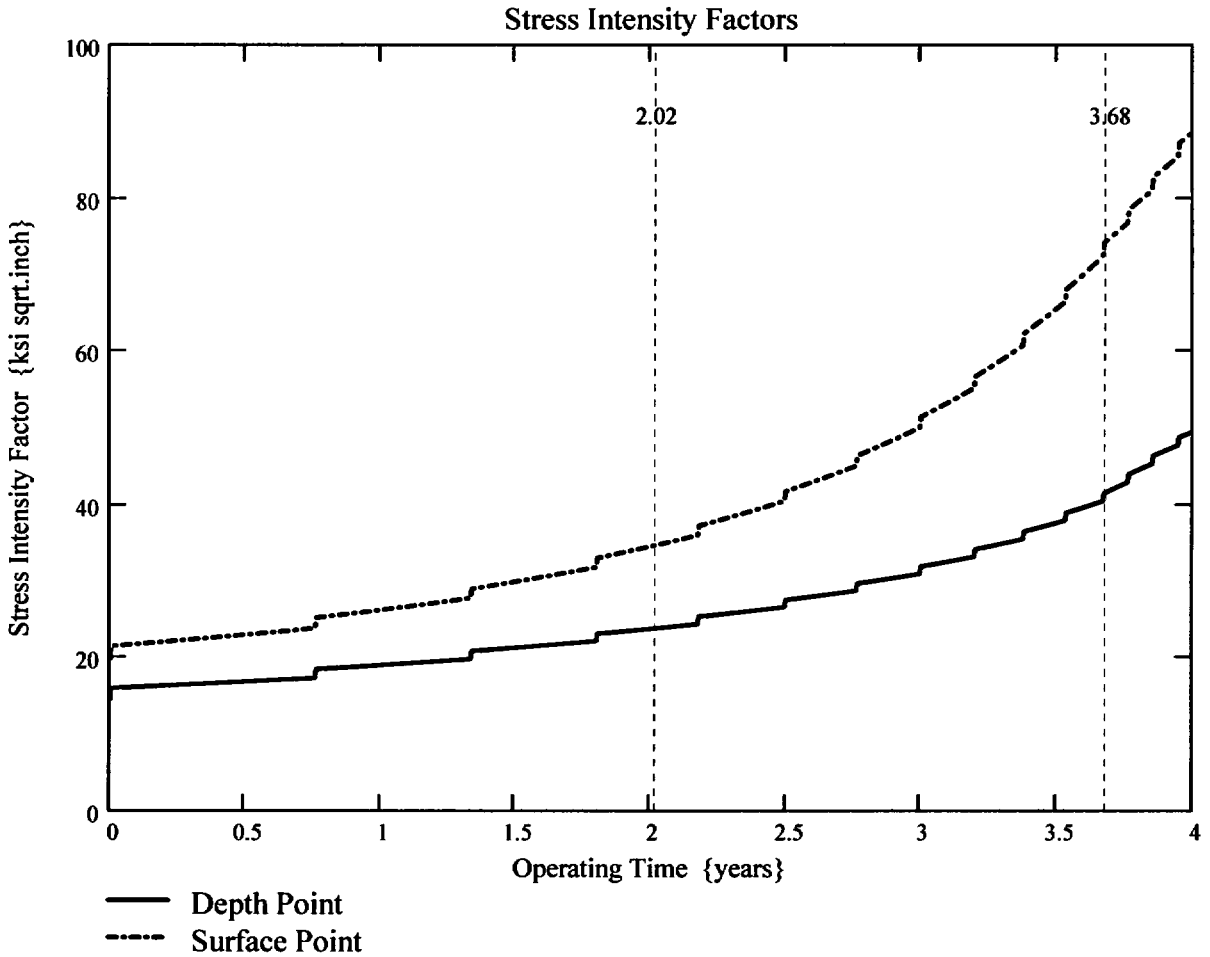
Stress Intensity Factors
100
80
60
40
20
0
Stress Intensity Factor {ksi sqrt.inch}
2.02
3.68
0
0.5
1
1.5
2
2.5
3
3.5
4
Operating Time {years}
Depth Point
Surface Point

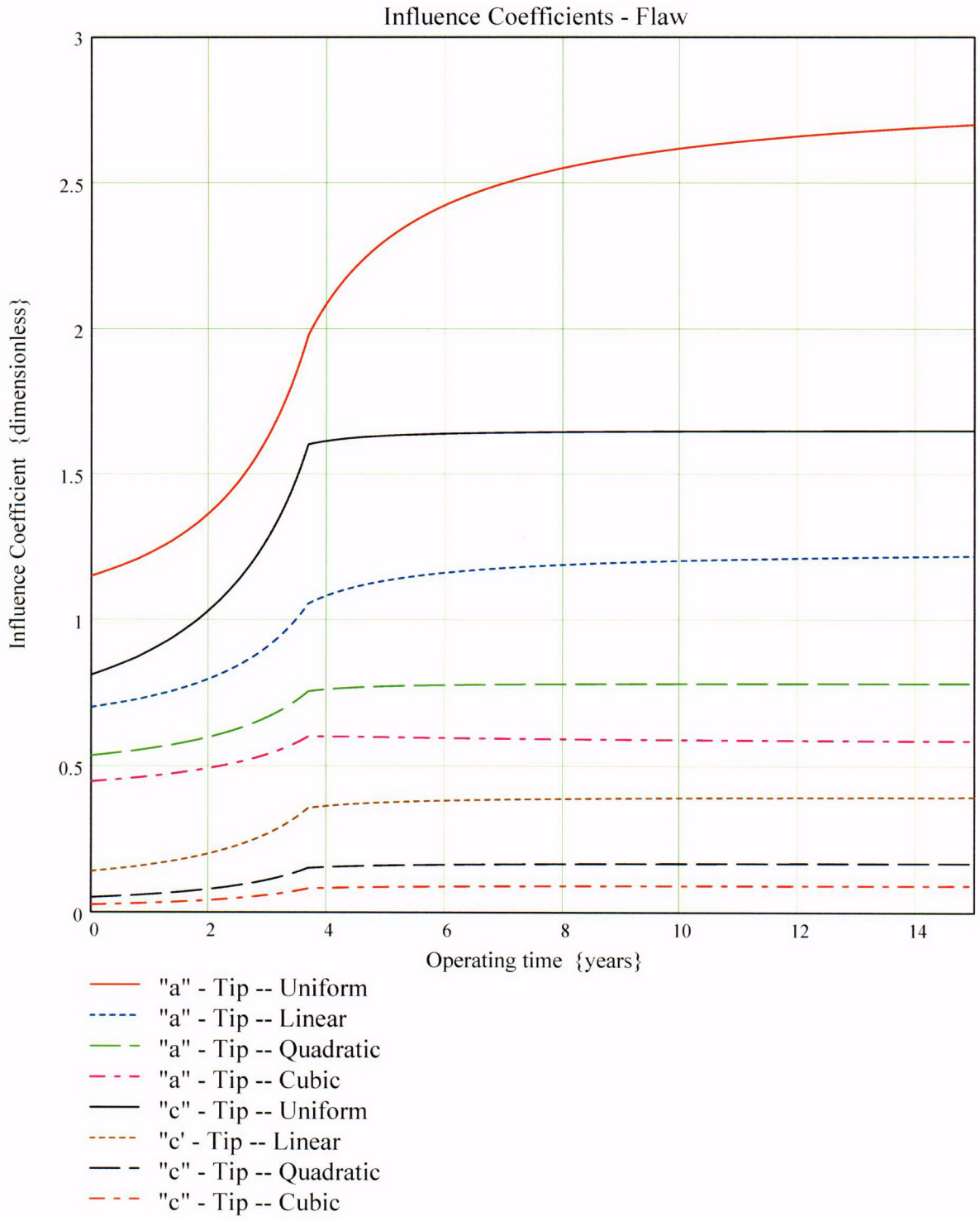
Influence Coefficients - Flaw
Influence Coefficient {dimensionless}
3
2.5
2
1.5
1
0.5
0
0
2
4
6
8
10
12
14
Operating time {years}
"a" - Tip -- Uniform
"a" - Tip -- Linear
"a" - Tip -- Quadratic
"a" - Tip -- Cubic
"c" - Tip -- Uniform
"c' - Tip -- Linear
"c" - Tip -- Quadratic
"c" - Tip -- Cubic

Determination of Circumferential Extent of Blind Zone and Computation of Axial Stress Distribution

The circumferential extent of the UT blind zone, centered on the uphill side (or 180° azimuth), is based on the height of the 0.88-inch long blind zone above the top of the weld. Fracture mechanics evaluations performed in Attachments 4 through 7 determined the minimum height of the blind zone above the top of the weld on the uphill side to be 0.67 inch. Using this dimension and the finite element nodal coordinate data contained in Attachment 3, the angular extent of the blind zone and the corresponding axial stress distributions can be calculated.

At the 180° azimuth, only 0.67 inch of material can be inspected (less than the 2.0 inches required by the NRC Order [Ref. 1]). Using the uphill "plane" of the nozzle as a reference coordinate system, the "0.00 inch" elevation occurs at the ID corner.

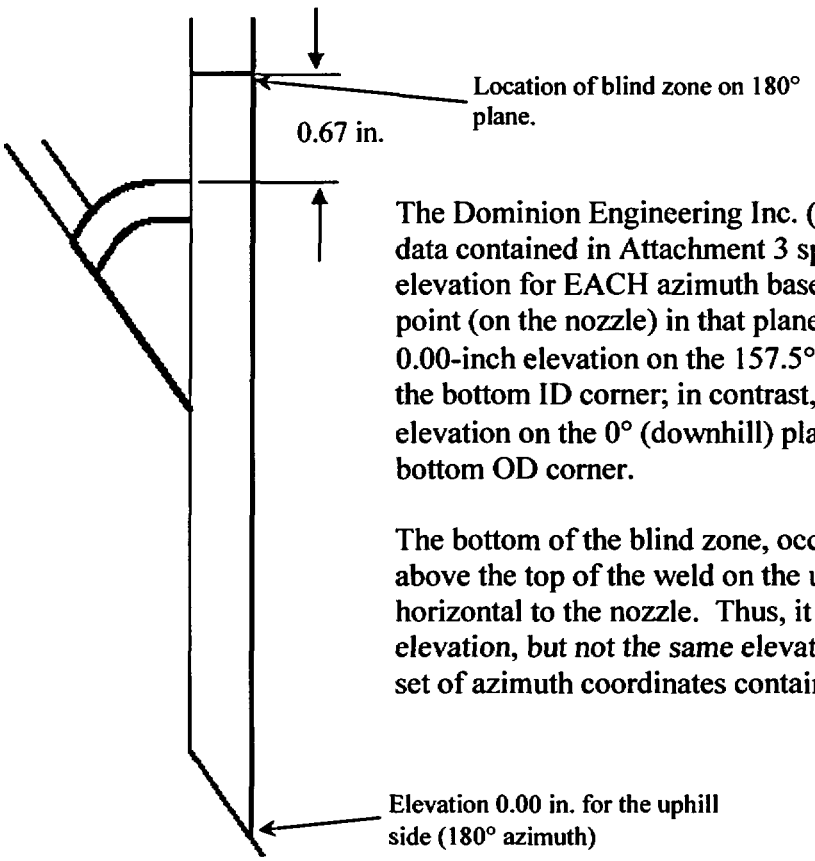

The Dominion Engineering Inc. (DEI) nodal coordinate data contained in Attachment 3 specifies a 0.00-inch elevation for EACH azimuth based on the lowest node point (on the nozzle) in that plane. For example, the 0.00-inch elevation on the 157.5° plane also occurs on the bottom ID corner; in contrast, the 0.00-inch elevation on the 0° (downhill) plane occurs at the bottom OD corner.

The bottom of the blind zone, occurring 0.67 inch above the top of the weld on the uphill side, is horizontal to the nozzle. Thus, it is at the same global elevation, but not the same elevation relative to each set of azimuth coordinates contained in Attachment 3.

The data provided by DEI below shows the elevation differentials needed to convert the height to the bottom of the blind zone in the reference coordinate system (on the uphill side) into the equivalent height in any other azimuthal plane.

From DEI:

"The following is a list of elevation differentials for the "zero point" elevations at all the circumferential planes relative to the "zero point" elevation for the uphill plane in the ICI nozzle model. All circumferential plane locations are for downhill = 0 degrees and uphill = 180 degrees.

Downhill	-7.4469
22.5 Degrees	-7.1411
45.0 Degrees	-6.2704
67.5 Degrees	-4.9672
Midplane	-3.4299
112.5 Degrees	-2.1174
135.0 Degrees	-1.0046
157.5 Degrees	-0.26109
Uphill	0.0000 "

180° azimuth (Uphill):

The top of the weld occurs at Node 81301, with an elevation of 4.205". The bottom of the blind zone occurs 0.67" above this node, at an elevation of 4.205" + 0.67" = 4.875"

The middle of the blind zone is at 4.875" + 0.88"/2 = 5.315"

The top of the blind zone is at 4.875" + 0.88" = 5.755"

From Attachment 3, nodal lines 81601 to 82001 cover the blind zone range from 4.875" to 5.755"

The maximum AXIAL stress magnitude in this nodal range is slightly less that 10 ksi at the ID at the bottom of the blind zone and rapidly becomes compressive through the thickness and toward the top of the blind zone. The curve-fits of the axial stress distributions shown in Figures 10 and 11 in the Engineering Report main body show a peak stress of approximately 4 ksi. This deviation is a resultant of fitting a large stress distribution. Since the actual ID maximum axial stress at the 180° azimuth in the blind zone region is less than 10 ksi, this discrepancy is considered inconsequential.

157.5° azimuth

The DEI information above shows the 0.00-inch elevation differential to be 0.26109 inch. To determine the blind zone dimensions in the 157.5° azimuth coordinate plane, this differential must be added to the blind zone dimensions at the 180° azimuth.

Bottom of blind zone: 4.875" + 0.26109" = 5.136"
Middle of blind zone: 5.315" + 0.26109" = 5.576"

Top of blind zone: 5.755" + 0.26109" = 6.016"

Height above the top of the weld at 157.5° = 0.67" + 0.26109" = 0.931" < 2.0"

From Attachment 3, nodal lines 71701 to 72101 cover the blind zone range from 5.136" to 6.016" on the 157.5° azimuthal plane.

The maximum AXIAL stress magnitude in this nodal range is 9 ksi at the ID at the bottom of the blind zone and rapidly becomes compressive through the thickness and axially toward the top of the blind zone.

135° azimuth

The DEI information above shows the 0.00-inch elevation differential to be 1.0046 inches. To determine the blind zone dimensions in the 135° azimuth coordinate plane, this differential must be added to the blind zone dimensions at the 180° azimuth.

Bottom of blind zone: 4.875" + 1.0046" = 5.88"
Middle of blind zone: 5.315" + 1.0046" =6.32"
Top of blind zone: 5.755" + 1.0046" = 6.76"

Height above the top of the weld at 135° = 0.67" + 1.0046" = 1.675" < 2.0"

From Attachment 3, nodal lines 62001 to 62301 cover the blind zone range from 5.88" to 6.76" on the 135° azimuthal plane.

The maximum AXIAL stress magnitude in this nodal range is 3 ksi on the OD at the top of the blind zone, becoming compressive through the thickness. All ID axial stresses within the blind zone are compressive.

112.5° azimuth

The DEI information above shows the 0.00-inch elevation differential to be 2.1174 inches. To determine the blind zone dimensions in the 135° azimuth coordinate plane, this differential must be added to the blind zone dimensions at the 180° azimuth.

Bottom of blind zone: 4.875" + 2.1174" = 6.992"
Middle of blind zone: 5.315" + 2.1174" =7.432"
Top of blind zone: 5.755" + 2.1174" = 7.872"

Height above the top of the weld at 112.5° = 0.67" + 2.1174" = 2.787" > 2.0"
Thus, at least 2.0 inches above the top of the weld, per the NRC Order, would be met at 112.5°.

From Attachment 3, nodal lines 52201 to 52501 cover the blind zone range from 6.992" to 7.872" on the 112.5° azimuthal plane.

Axial stresses are tensile through the thickness at the top of the blind zone, but the stress magnitude ranges from 0.3 ksi (on the ID) to 7 ksi (on the OD), below the 10 ksi stress, above which flaw initiation may occur. The very low tensile to compressive ID stresses preclude the existence of flaw initiation in the blind zone at the 112.5° azimuth.

ENCLOSURE 3

CNRO-2003-00042

LICENSEE-IDENTIFIED COMMITMENTS

LICENSEE-IDENTIFIED COMMITMENTS

COMMITMENT	TYPE (Check one)		SCHEDULED COMPLETION DATE
	ONE-TIME ACTION	CONTINUING COMPLIANCE	
1. Entergy will provide in the 60-day report for Waterford 3, as required by the Order, specific inspection information; i.e., extent of inspections and results of those inspections.	✓		60 days after startup from the next refueling outage
2. If the NRC staff finds that the crack-growth formula in MRP-55 is unacceptable, Entergy shall revise its analysis that justifies relaxation of the Order within 30 days after the NRC informs Entergy of an NRC-approved crack-growth formula.	✓		Within 30 days after the NRC informs Entergy of an NRC-approved crack-growth formula.
3. If Entergy's revised analysis (#2, above) shows that the crack growth acceptance criteria are exceeded prior to the end of Operating Cycle 13 (following the upcoming refueling outage), Entergy will, within 72 hours, submit to the NRC written justification for continued operation.	✓		Within 72 hours from completing the revised analysis in #2, above.
4. If the revised analysis (#2, above) shows that the crack growth acceptance criteria are exceeded during the subsequent operating cycle, Entergy shall, within 30 days, submit the revised analysis for NRC review.	✓		Within 30 days from completing the revised analysis in #2, above.
5. If the revised analysis (#2, above) shows that the crack growth acceptance criteria are not exceeded during either Operating Cycle 13 or the subsequent operating cycle, Entergy shall, within 30 days, submit a letter to the NRC confirming that its analysis has been revised.	✓		Within 30 days from completing the revised analysis in #2, above.
6. Any future crack-growth analyses performed for Operating Cycle 13 and future cycles for RPV head penetrations will be based on an acceptable crack growth rate formula.		✓	N/A